



THE UNIVERSITY OF QUEENSLAND
AUSTRALIA

**Parameterization of bottom spectral reflectance for shallow water
ocean color inversion models**

Martina Reichstetter

BSc. (Hons), MPhil

A thesis submitted for the degree of Doctor of Philosophy at

The University of Queensland in 2016

School of Geography, Planning and Environmental Management

Abstract

Satellite-based ocean color remote sensing has been extensively applied in monitoring deep ocean environments. Yet, ocean color products cannot be used to quantify water column properties with any degree of accuracy in shallow water environments because of bottom reflectance contamination. Currently, there are no operational ocean color algorithms that can correct for bottom reflectance contamination in optically shallow waters, where light reflected from the seafloor contributes to the water-leaving radiance. To improve the accuracy of ocean color products, it is essential to understand the impact of bottom reflectance on the retrieval of inherent optical properties (IOPs) of the water column. However, there is a lack of knowledge of the appropriate selection and parameterization of bottom reflectance inputs in shallow water inversion algorithms.

The aim of this research was to optimize bottom reflectance parameterization in shallow water inversion algorithms, and to assess the effects of the parameterization on the retrieval of IOPs. The research addressed the following three objectives, with investigations based in the Great Barrier Reef (GBR), Australia: (1) to assess the spectral separability and detectability of bottom reflectance in coral reef environments, (2) to test the sensitivity of bottom reflectance parameterization on the retrieval of IOPs using a Shallow Water Inversion Model (SWIM) and (3) to assess different approaches to create a spatially-resolved bottom reflectance map for shallow water areas, using different datasets.

To address research Objective 1, the spectral separability and detectability of bottom types at Moderate Resolution Imaging Spectroradiometer (MODIS) and Sea-Viewing Wide Field-of-View Sensor (SeaWiFS) bands were assessed. The results showed: (i) no significant contamination ($R_{\text{rscorr}} < 0.0005$) of bottom reflectance on the spectrally-averaged remote sensing reflectance signal at depths >19 m for the brightest spectral reflectance substrate (light sand) in clear reef waters; and (ii) bottom cover classes can be combined into two distinct groups, “light” and “dark”, based on the modeled surface reflectance signals. This research established that it is possible to improve parameterization of bottom reflectance and water column IOP retrievals in shallow water ocean color models for coral reef environments.

To address research Objective 2, the impact of bottom reflectance parameterization on IOP retrievals in SWIM was assessed. The results showed that there is no clear spatial pattern in mean IOP retrievals under different bottom reflectance scenarios. A GBR-wide assessment showed that retrieved IOP values vary considerably across the extent of the GBR and thus the differences in IOP retrievals due to bottom reflectance parameterization are also spatially variable. Water clarity was shown to further influence the differences in IOP retrievals between different bottom types. Analysis showed that most differences in SWIM IOP retrievals between sand and seagrass, as well as between sand and algae bottom reflectance scenarios are observed at depths above 20 m. The results also indicated that the magnitude of the bottom reflectance spectrum is not the only factor influencing the retrievals of IOPs, but also the spectral shape.

To address research Objective 3, four different methods to create spatially explicit bottom reflectance maps using two different available datasets were evaluated. Application of all generated bottom reflectance maps to IOP retrievals produced comparable results. It was determined that any one of these methods may be applied to create a bottom reflectance map suitable for use in the SWIM algorithm bottom reflectance parameterization, to improve IOP retrievals in optically shallow waters.

This thesis has successfully demonstrated that bottom reflectance parameterization can be optimized using only two bottom reflectance classes (“light” and “dark”). The sensitivity of IOP retrievals to bottom reflectance in the SWIM algorithm is variable across the large extent of the GBR. Different methods to produce optimized bottom reflectance maps for ocean color shallow water inversion models have been presented to ensure wide applicability to shallow water environments. In a practical context, the findings of this thesis will help improve bottom reflectance parameterization, and thus IOP retrievals, in shallow water ocean color inversion algorithms, such as SWIM.

Declaration by author

This thesis **is composed of my original work, and contains** no material previously published or written by another person except where due reference has been made in the text. I have clearly stated the contribution by others to jointly-authored works that I have included in my thesis.

I have clearly stated the contribution of others to my thesis as a whole, including statistical assistance, survey design, data analysis, significant technical procedures, professional editorial advice, and any other original research work used or reported in my thesis. The content of my thesis is the result of work I have carried out since the commencement of my research higher degree candidature and does not include a substantial part of work that has been submitted **to qualify for the award of any** other degree or diploma in any university or other tertiary institution. I have clearly stated which parts of my thesis, if any, have been submitted to qualify for another award.

I acknowledge that an electronic copy of my thesis must be lodged with the University Library and, subject to the policy and procedures of The University of Queensland, the thesis be made available for research and study in accordance with the Copyright Act 1968 unless a period of embargo has been approved by the Dean of the Graduate School.

I acknowledge that copyright of all material contained in my thesis resides with the copyright holder(s) of that material. Where appropriate I have obtained copyright permission from the copyright holder to reproduce material in this thesis.

Publications during candidature

Peer-reviewed papers:

REICHSTETTER, M., FEARNES, P. R. C. S., WEEKS, S. J., MCKINNA, L. I. W., ROELFSEMA, C. & FURNAS, M. 2015a. Bottom Reflectance in Ocean Color Satellite Remote Sensing for Coral Reef Environments. *Remote Sensing*, 7, 16756-16777.

MCKINNA, L. I. W., FEARNES, P. R. C., WEEKS, S. J., WERDELL, P. J., **REICHSTETTER, M.**, FRANZ, B. A., SHEA, D. M. & FELDMAN, G. C. 2015. A semianalytical ocean color inversion algorithm with explicit water column depth and substrate reflectance parameterization. *Journal of Geophysical Research: Oceans*, 120, 1741-1770.

Datasets:

REICHSTETTER, M., MCKINNA, L., FEARNES, P., WEEKS, S. J., ROELFSEMA, C. M. & FURNAS, M. 2015b. Seafloor brightness map of the Great Barrier Reef, Australia, derived from biodiversity data.

Publications included in this thesis

Publication citation – incorporated as Chapter 3.

REICHSTETTER, M., FEARN, P. R. C. S., WEEKS, S. J., MCKINNA, L. I. W., ROELFSEMA, C. & FURNAS, M. 2015a. Bottom Reflectance in Ocean Color Satellite Remote Sensing for Coral Reef Environments. *Remote Sensing*, 7, 16756-16777.

Contributor	Statement of contribution
Martina Reichstetter (Candidate)	Data processing (95%) Statistical analysis and interpretation of data (95%) Drafting and writing (100%)
Peter Fearn	Edited drafts of manuscript (35%) Statistical analysis and interpretation of data (5%)
Scarla Weeks	Edited drafts of manuscript (35%)
Lachlan McKinna	Edited drafts of manuscript (10%) Batch processing script (5%)
Chris Roelfsema	Edited drafts of manuscript (10%)
Miles Furnas	Edited drafts of manuscript (10%)

Contributions by others to the thesis

Dr. Lachlan McKinna processed the *in situ* IOP data included in Chapter 5. Dr. Scarla Weeks, Dr. Peter Fearn, Dr. Miles Furnas and Dr. Chris Roelfsema, through their advisory role, contributed to the research direction and research design as well as providing editing and revision of publication manuscripts and this thesis.

Statement of parts of the thesis submitted to qualify for the award of another degree

None.

Acknowledgements

Over the course of the past four years, while writing my Ph.D. thesis, I learned two things: first no research is ever really finished and second it takes a team of collaborative people to accomplish a sound research project. It is impossible to thank everyone who helped me during the duration of this project.

I was lucky to have a highly knowledgeable team of supervisors (Dr. Scarla Week, Dr. Peter Fearn, Dr. Chris Roelfsema, and Dr. Miles Furnas) that were willing to share their expertise freely with me and helped me edit many draft versions on tight time frames.

A special thank you to Dr. Peter Fearn who's intellectual heft is matched only by his genuinely good nature and down-to-earth humility. He is a teacher extraordinaire that has the gift of explaining things in simple to understand terms, which makes a PhD's life much easier. Many times when I was close to giving up, he was able to get me back on track in a short Skype call, with his motivating guidance and his clear and achievable approach to difficult research questions. Without his dedication and can-do attitude, and his willingness to let me research freely and independently I would not have completed this thesis.

I also like to thank Dr. Scarla Weeks who provided me with countless opportunities during my PhD journey, who advocated for me, and who always believed in my research and its importance. Not only did she made sure I stay on track, but also encouraged me endlessly to keep going and don't worry about all that can go wrong.

For me to undertake postgraduate study at PhD level research funding and scholarships were imperative and I would like to acknowledge the funding support from the following organizations, which made this project possible:

- Australian Research Council (ARC)
- The University of Queensland
- NASA- Ocean Biology Processing Group (OBPG)
- Great Barrier Reef Foundation

I like to thank Dr. Lachlan McKinna, for being a crucial technical, as well as practical advisor and collaborator. His help from fieldwork planning and sampling to computer coding and statistical analysis was crucial in the completion of my research project. His commitment to my research far exceeded his responsibilities as a project collaborator.

Thanks are also due to Marites Canto a friend and very knowledgeable research buddy. Tess has consistently reminded me that the daunting task of writing this thesis was indeed attainable and provided me with numerous lessons in computer programming.

I like to express my gratitude to my parents-in-law that spoiled my daughter with love and attention when I was busy working on my thesis. Without their support this thesis would not have been possible. I would like to thank my beloved parents for their encouragement throughout my life. You have taught me that anything is possible in life. Without this ingrained believe I most likely would not have undertaken the adventure of postgraduate research. You have also made the trip over the pond to come and spoil little Stella and made sure she is not missing out on anything, while I was busy writing up this thesis.

Deeply from my heart with love, I like to thank my husband, Steven, for his remarkable patience and also for the countless hours of daddy daycare to our beautiful daughter, Stella, during the months of writing. He was able to remind me that in the greater schemes of things, my research related problems and issues are not that significant.

Finally, to my beautiful, wondrous, daughter, Stella, I offer my immense gratitude for her unconditional love and her delightful diversions. Watching you discovering the world has taught me much about the process of learning and achieving, reminding me that all the falling over doesn't matter anymore once you walk.

Keywords

Optically shallow waters, remote sensing, geometric depth, benthic reflectance, Great Barrier Reef, inherent optical properties, remote sensing, satellite oceanography

Australian and New Zealand Standard Research Classifications (ANZSRC)

ANZSRC code: 090905 Photogrammetry and Remote Sensing 80%

ANZSRC code: 050206, Environmental Monitoring, 20%

Fields of Research (FoR) Classification

FoR code: 0909 Geomatic Engineering 60%

FoR code: 0502 Environmental Science and Management 40%

Table of Contents

CHAPTER 1 : INTRODUCTION AND SIGNIFICANCE OF THE RESEARCH	1
1.1 OVERVIEW	2
1.2 LIGHT IN WATER	4
1.3 OCEAN COLOR MODELING	7
1.4 BOTTOM REFLECTANCE IN REMOTE SENSING APPLICATIONS	11
1.4.1 BOTTOM REFLECTANCE IN OCEAN COLOR MODELING	11
1.4.2 SEAFLOOR COVER MAPPING	12
1.5 AIM OF THE PROJECT	17
1.6 CHAPTER SYNOPSIS	18
CHAPTER 2 : RESEARCH APPROACH AND STUDY SITE	20
2.1 OVERALL STUDY APPROACH	21
2.2 STUDY AREA	24
2.2.1 GBR BATHYMETRY	26
2.2.2 GBR SEAFLOOR COVER	27
2.3 MODELS	33
2.3.1 HYDROLIGHT	33
2.3.2 SHALLOW WATER INVERSION MODEL (SWIM)	34
CHAPTER 3 : BOTTOM REFLECTANCE IN OCEAN COLOR SATELLITE REMOTE SENSING FOR CORAL REEF ENVIRONMENTS	36
3.1 INTRODUCTION	37
3.2 DATA AND METHODS	40
3.2.1 METHODS OVERVIEW	40
3.2.2 BOTTOM REFLECTANCE DATASET	43
3.2.3 DATA ANALYSIS	46
3.3 RESULTS	49
3.3.1 CLUSTER ANALYSIS OF BOTTOM CLASSES AND SILHOUETTE PLOTS	49
3.3.2 CLUSTER ANALYSIS OF BOTTOM CLASSES FOR DIFFERENT IOP SCENARIOS	52
3.3.3 CLUSTER ANALYSIS AND INTERMEDIATE CLASSES	53
3.3.4 DETECTABILITY OF BOTTOM COVER	55
3.4 DISCUSSION	57
3.5 CONCLUSIONS	62

CHAPTER 4 : SENSITIVITY ANALYSIS OF BOTTOM REFLECTANCE PARAMETERIZATION IN SHALLOW WATER MODELS	64
4.1 INTRODUCTION	65
4.2 DATA AND METHODS	66
4.2.1 BOTTOM REFLECTANCE SCENARIOS	68
4.2.2 OVERVIEW AND SPATIAL ASSESSMENT OF THE SENSITIVITY OF IOP RETRIEVALS TO BOTTOM REFLECTANCE PARAMETERIZATION	70
4.2.3 TEMPORAL ASSESSMENT OF THE SENSITIVITY OF IOP RETRIEVALS TO BOTTOM REFLECTANCE PARAMETERIZATION	75
4.3 RESULTS	76
4.3.1 OVERALL SENSITIVITY OF IOP RETRIEVALS UNDER DIFFERENT BOTTOM REFLECTANCE SCENARIOS	76
4.3.2 SPATIAL SENSITIVITY OF IOP RETRIEVALS UNDER DIFFERENT BOTTOM REFLECTANCE SCENARIOS	80
4.1.1 TEMPORAL SENSITIVITY OF IOP RETRIEVALS UNDER DIFFERENT BOTTOM REFLECTANCE SCENARIOS	94
4.4 DISCUSSION	100
4.5 CONCLUSION AND RECOMMENDATION	105
CHAPTER 5 BOTTOM REFLECTANCE PARAMETERIZATION IN SHALLOW WATER OCEAN COLOR MODELS	107
5.1 INTRODUCTION	108
5.2 METHODS	111
5.2.1 STUDY AREA	113
5.2.2 MAPPING PROCESS	114
5.2.3 SWIM MODELING	123
5.2.4 FIELD DATA	123
5.2.5 COMPARISON OF IOP RETRIEVAL	125
5.2.6 COMPARISON OF IOP RETRIEVALS TO FIELD DATA	126
5.3 RESULTS	126
5.3.1 COMPARISON OF BOTTOM REFLECTANCE MAPS	126
5.3.2 COMPARISON OF IOP RETRIEVALS UNDER DIFFERENT BOTTOM REFLECTANCE SCENARIOS	131
5.4 DISCUSSION	136
5.5 CONCLUDING REMARKS	140
CHAPTER 6 : CONCLUSIONS, SIGNIFICANCE AND FUTURE RESEARCH	142
6.1 SUMMARY	143
6.2 MAIN FINDINGS AND OUTCOMES	144
6.3 LIMITATIONS AND FUTURE RESEARCH	145

6.4 CONTRIBUTION TO KNOWLEDGE	147
REFERENCES	148
APPENDIX A	163
APPENDIX B	167

List of Figures

FIGURE 1-1: SCHEMATIC DIAGRAM OF THE VARIOUS PROCESSES THAT CONTRIBUTE TO THE SIGNAL AS MEASURED BY A SATELLITE IN AN OPTICALLY SHALLOW WATER ENVIRONMENT, WHERE THE BOTTOM REFLECTANCE HAS A SIGNIFICANT EFFECT ON THE WATER-LEAVING RADIANCE (MODIFIED FROM ROELFSEMA C.M. (2010)).	5
FIGURE 1-2: MAIN MODEL APPROACHES IN OCEAN COLOR MODELING SHOWING THE INVERSE AND FORWARD MODELING PROCESSES (ADAPTED FROM SATHYENDRANATH (2000)).	8
FIGURE 2-2: MAP OF THE GREAT BARRIER REEF WITH THE GREEN LINE INDICATING THE BOUNDARIES OF THE GREAT BARRIER REEF MARINE PARK AREA, INCLUDING THE MAJOR REEF GROUPS (ADAPTED FROM (GBRMPA, 2002)).	25
FIGURE 2-3: GBR100 BATHYMETRY DATASET USED IN THIS THESIS (DATA FROM (BEAMAN, 2012)).	27
FIGURE 2-4: MAP OF THE PERCENTAGE DISTRIBUTION AND COVER OF ALCYONARIAN TYPE SOFT CORALS IN THE GREAT BARRIER REEF (FROM PITCHER, 2007).	29
FIGURE 2-5: MAP OF THE PERCENTAGE DISTRIBUTION AND COVER OF HARD CORALS (FROM PITCHER, 2007).	29
FIGURE 2-6: SEAGRASS DISTRIBUTION IN THE GBR (DATA FROM MCKENZIE ET AL., 2014B).	30
FIGURE 2-7: PERCENTAGE SAND (LEFT PANEL) AND PERCENTAGE CARBONATE SAND (RIGHT PANEL) DISTRIBUTION IN THE GREAT BARRIER REEF. THE WHITE AREAS ALONG THE EASTERN EDGE OF THE GBRWH AREA ARE IN DEEP WATERS (>100 M) AND DO NOT IMPACT SHALLOW WATER REMOTE SENSING.	32
FIGURE 2-8: MAP OF THE DISTRIBUTION OF NON-BIOTIC SEAFLOOR COVER TYPES IN THE GREAT BARRIER REEF SUMMARIZED AS A PERCENTAGE OF TRANSECT LENGTH AS OBSERVED BY TOWED VIDEO CAMERA (FROM PITCHER, 2007).	33
FIGURE 3-1: FLOWCHART SHOWING AN OVERVIEW OF THE INPUT VARIABLES FOR THE RADIATIVE TRANSFER MODELING FRAMEWORK USED TO CONDUCT A HIERARCHICAL ANALYSIS OF THE CLASS SPECTRAL SEPARABILITY OF COMMON BOTTOM TYPES. THE HYDROLIGHT MODEL SCENARIO SETUP IS FURTHER DESCRIBED IN TABLE 3-2.	40
FIGURE 3-2: MAP SHOWING SAMPLING LOCATIONS FOR THE FOUR INHERENT OPTICAL PROPERTY SCENARIOS USED: COASTAL, ESTUARINE, LAGOONAL AND REEF WATERS OF THE GREAT BARRIER REEF (ADAPTED FROM (BLONDEAU - PATISSIER ET AL., 2009)).	42
FIGURE 3-3: <i>IN SITU</i> REFLECTANCES FOR THE EIGHT PURE ENDMEMBER BOTTOM TYPES USED IN THIS STUDY. EACH LINE REPRESENTS A SUB-SAMPLE SPECTRUM FOR THE RESPECTIVE BOTTOM TYPE CATEGORY.	45
FIGURE 3-4: SILHOUETTE PLOTS FOR REEF WATERS AT 5 M GEOMETRIC DEPTH USING MODIS BANDS. EACH CLUSTER IS REPRESENTED BY A DIFFERENT COLOR (CLUSTER-1 (C1)-BLACK, CLUSTER-2 (C2)-GREY, CLUSTER-3 (C3)-GREEN, CLUSTER-4 (C4)-BLUE AND CLUSTER-5 (C5)-RED). THE CLUSTER STATISTICS REPRESENT THE NUMBER OF BOTTOM SPECTRA ASSIGNED TO EACH CLUSTER, FOLLOWED BY THE CLUSTER SILHOUETTE WIDTH. MISCLASSIFIED SPECTRA ARE COUNTED TOWARD THE CLUSTER THEY ARE ASSIGNED TO BUT REPRESENTED AS NEGATIVE, HENCE TO THE LEFT OF THE GRAPHICS.	50
FIGURE 3-5: SILHOUETTE PLOTS FOR REEF WATERS AT 5 M GEOMETRIC DEPTH AT SEAWIFS BANDS. EACH CLUSTER IS REPRESENTED BY A DIFFERENT COLOR (CLUSTER-1 (C1)-BLACK, CLUSTER-2 (C2)-GREY, CLUSTER-3 (C3)-GREEN, CLUSTER-4 (C4)-BLUE AND CLUSTER-5 (C5)-RED). THE CLUSTER STATISTICS REPRESENT THE NUMBER OF BOTTOM SPECTRA ASSIGNED TO EACH CLUSTER, FOLLOWED BY THE CLUSTER SILHOUETTE WIDTH. MISCLASSIFIED SPECTRA ARE COUNTED TOWARD THE CLUSTER THEY ARE ASSIGNED TO BUT REPRESENTED AS NEGATIVE, HENCE TO THE LEFT OF THE GRAPHICS.	51

FIGURE 3-6: MAXIMUM DEPTH OF DETECTABILITY FOR LIGHT SAND AND SEAGRASS UNDER FOUR DIFFERENT OPTICAL DOMAIN SCENARIOS: ESTUARINE, LAGOONAL, COASTAL AND REEF WATERS FOR DEPTHS ASSESSED BETWEEN 5 M AND 49 M.	56
FIGURE 3-7: WATER COLUMN-CORRECTED (A BLACK BOTTOM SCENARIO WAS SUBTRACTED FROM THE MODEL RUN), AVERAGE SURFACE REFLECTANCE SIGNALS FOR TWO EXTREMES OF SUBSTRATE BRIGHTNESS: LIGHT SAND (LEFT PANEL) AND SEAGRASS (RIGHT PANEL) FOR THE FOUR OPTICAL WATER PROPERTY SCENARIOS FOR SEAWiFS AND MODIS SENSORS. FOR LIGHT SAND, THE R_{RSCORR} VALUES FOR THE ESTUARINE AND COASTAL SCENARIOS ARE CLOSE TO ZERO EVEN AT SHALLOW DEPTHS, WHILE FOR SEAGRASS, R_{RSCORR} VALUES ARE CLOSE TO ZERO AT ALL DEPTHS FOR THE ESTUARINE, COASTAL AND LAGOONAL SCENARIOS.	57
FIGURE 4-1: FLOWCHART OF THE SENSITIVITY ANALYSIS APPROACH USED IN CHAPTER 4.....	67
FIGURE 4-2: SPECTRAL SIGNATURES USED TO GENERATE THE BOTTOM REFLECTANCE SCENARIOS IN THE SENSITIVITY ANALYSIS	69
FIGURE 4-3: TRUE COLOR IMAGE OF THE SELECTED MODIS SCENE 1 (03 DECEMBER 2005) PROCESSED USING SEADAS. THE SCENE SHOWS THE LIZARD ISLAND (BLUE) AND CAPRICORN BUNKER (RED) SUB-REGIONS USED FOR TIME SERIES ANALYSIS.	71
FIGURE 4-4: TRUE COLOR IMAGE OF THE SELECTED MODIS SCENE 2 (09 AUGUST 2009) PROCESSED USING SEADAS. THE SCENE SHOWS THE LIZARD ISLAND (BLUE) AND CAPRICORN BUNKER (RED) SUB-REGIONS USED FOR TIME SERIES ANALYSIS.	72
FIGURE 4-5: SHALLOW WATER BATHYMETRY FOR THE THREE SECTIONS OF THE GREAT BARRIER REEF, THE NORTHERN (TOP), CENTRAL (CENTER) AND SOUTHERN (BOTTOM).	74
FIGURE 4-6: REGION OF INTEREST (5 TO 25 M DEPTH) HISTOGRAM DISTRIBUTION FOR BACKSCATTER COEFFICIENT AT 443NM (BBP443) FOR SCENE 1, (03 DECEMBER 2005) (TOP), AND FOR SCENE 2, (09 AUGUST 2011) (BOTTOM) AND MEAN BBP443 VALUES FOR EACH BOTTOM SCENARIO.	78
FIGURE 4-7: REGION OF INTEREST (5 TO 25 M DEPTH) HISTOGRAM DISTRIBUTION FOR ABSORPTION COEFFICIENT AT 443NM (A443) FOR SCENE 1, (03 DECEMBER 2005) (TOP), AND FOR SCENE 2, (09 AUGUST 2011) (BOTTOM) AND MEAN A443 VALUES FOR EACH BOTTOM SCENARIO.	80
FIGURE 4-8: MEAN BACKSCATTER RETRIEVALS (BBP443) FOR SCENES 1 (03 DECEMBER 2005) AND 2 (09 AUGUST 2011) FOR THE NORTHERN, CENTRAL AND SOUTHERN GREAT BARRIER REEF UNDER DIFFERENT BOTTOM REFLECTANCE SCENARIOS AND DEPTH RANGES.	82
FIGURE 4-9: MEAN ABSORPTION RETRIEVALS (A443) FOR SCENES 1 (03 DECEMBER 2005) AND 2 (09 AUGUST 2011) FOR THE NORTHERN, CENTRAL AND SOUTHERN GREAT BARRIER REEF UNDER DIFFERENT BOTTOM REFLECTANCE SCENARIOS AND DEPTH RANGES.	85
FIGURE 4-10: RELATIVE DIFFERENCES IN ALGORITHM-DERIVED BBP443 BETWEEN THE BLACK AND WHITE BOTTOM SCENARIOS (1) SCENE 1 NORTHERN GBR (TOP-LEFT PANEL) (2) SCENE 2 NORTHERN GBR (TOP-RIGHT PANEL) (3) SCENE 1 CENTRAL GBR (CENTER-LEFT PANEL) (4) SCENE 2 CENTRAL GBR (CENTER-RIGHT PANEL) (5) SCENE 1 SOUTHERN GBR (BOTTOM-LEFT PANEL) (6) SCENE 2 SOUTHERN GBR (BOTTOM-RIGHT PANEL)	87
FIGURE 4-11: RELATIVE DIFFERENCES IN ALGORITHM-DERIVED BBP443 BETWEEN THE SAND AND SEAGRASS BOTTOM SCENARIOS (1) SCENE 1 NORTHERN GBR (TOP-LEFT PANEL) (2) SCENE 2 NORTHERN GBR (TOP-RIGHT PANEL) (3) SCENE 1 CENTRAL GBR (CENTER-LEFT PANEL) (4) SCENE 2 CENTRAL GBR (CENTER-RIGHT PANEL) (5) SCENE 1 SOUTHERN GBR (BOTTOM-LEFT PANEL) (6) SCENE 2 SOUTHERN GBR (BOTTOM-RIGHT PANEL)	88
FIGURE 4-12: RELATIVE DIFFERENCES IN ALGORITHM-DERIVED A443 BETWEEN THE BLACK AND WHITE BOTTOM SCENARIOS (1) SCENE 1 NORTHERN GBR (TOP-LEFT PANEL) (2) SCENE 2 NORTHERN GBR (TOP-RIGHT PANEL) (3) SCENE 1 CENTRAL GBR (CENTER-LEFT PANEL) (4) SCENE 2 CENTRAL GBR (CENTER-RIGHT PANEL) (5) SCENE 1 SOUTHERN GBR (BOTTOM-LEFT PANEL) (6) SCENE 2 SOUTHERN GBR (BOTTOM-RIGHT PANEL)	90

FIGURE 4-13: RELATIVE DIFFERENCES IN ALGORITHM-DERIVED A443 BETWEEN THE SEAGRASS AND SAND BOTTOM SCENARIOS (1) SCENE 1 NORTHERN GBR (TOP-LEFT PANEL) (2) SCENE 2 NORTHERN GBR (TOP-RIGHT PANEL) (3) SCENE 1 CENTRAL GBR (CENTER-LEFT PANEL) (4) SCENE 2 CENTRAL GBR (CENTER-RIGHT PANEL) (5) SCENE 1 SOUTHERN GBR (BOTTOM- LEFT PANEL) (6) SCENE 2 SOUTHERN GBR (BOTTOM-RIGHT PANEL)	91
FIGURE 4-14: RETRIEVED A443 FOR SCENE 1 (LEFT) AND SCENE 2 (RIGHT) USING THE SAND BOTTOM REFLECTANCE SCENARIO.	92
FIGURE 4-15: RETRIEVED BBP443 FOR SCENE 1 (LEFT) AND SCENE 2 (RIGHT) USING THE SAND BOTTOM REFLECTANCE SCENARIO	93
FIGURE 4-16: SECCHI DEPTH FOR SCENE 1 (LEFT) AND SCENE 2 (RIGHT) PROCESSED USING THE GBR-VALIDATED SECCHI DEPTH ALGORITHM (WEEKS ET AL., 2012)	94
FIGURE 4-17: 12 -MONTH TIME SERIES DIFFERENCES IN A443 RETRIEVALS FOR THE SESA AND BASA SCENARIOS FOR THE LIZARD ISLAND AND CAPRICORN BUNKER TEST REGIONS	96
FIGURE 4-18: 12 -MONTH TIME SERIES OF DIFFERENCES IN BBP443 RETRIEVALS FOR THE SESA AND BASA SCENARIOS FOR THE LIZARD ISLAND AND CAPRICORN BUNKER TEST REGIONS	98
FIGURE 4-19: YEARLY MEDIAN PERCENTAGE DIFFERENCES FROM 5 TO 25 M IN BBP443 (LEFT PANEL) AND A443 (RIGHT PANEL) FOR THE SESA AND BASA SCENARIOS IN THE CAPRICORN BUNKER GROUP (CB) AND THE LIZARD ISLAND AREA (LI)	100
FIGURE 5-1: FLOWCHART OF METHODS USED IN THIS STUDY	112
FIGURE 5-2: ATMOSPHERICALLY CORRECTED LANDSAT 8 (LC80910762014198LGN00) (17 JULY 2014) IMAGE FOR THE STUDY AREA: THE CAPRICORN BUNKER GROUP AND THE SOUTHERN GBR AND MAP OF THE GREAT BARRIER REEF WITH THE GREEN LINE ON THE GBR MAP INDICATES THE BOUNDARIES OF THE GREAT BARRIER REEF MARINE PARK AREA	113
FIGURE 5-3 LIGHT AND DARK SPECTRA USED IN THE SWIM BOTTOM REFLECTANCE PARAMETERIZATION.....	114
FIGURE 5-4: RGB LANDSAT 8 IMAGE (17 JULY 2014) AND SAMPLE POINTS MAP SHOWING THE 23 SITES SAMPLED DURING THE CRC SEABED BIODIVERSITY SURVEY IN THE STUDY REGION (DATA FROM: PITCHER, 2007).....	116
FIGURE 5-5: RGB LANDSAT 8 IMAGES USED TO GENERATE THE BOTTOM REFLECTANCE MAPS: IMAGE A (JULY 2013) (TOP LEFT PANEL), IMAGE B (JULY 2014) (TOP RIGHT PANEL), IMAGE C (AUGUST 2014) (BOTTOM LEFT PANEL) AND IMAGE D (JULY 2015) (BOTTOM RIGHT PANEL).....	119
FIGURE 5-6: RGB LANDSAT 8 IMAGE (17 JULY 2014) DISPLAYING THE FIELD DATA POINT USED IN THIS STUDY.....	124
FIGURE 5-7:DEPTH BINS USED TO DERIVE MEAN DAILY IOPS	125
FIGURE 5-8: MAPS OF PERCENTAGE LIGHT COVER AT ORIGINAL RESOLUTION USING THE FOLLOWING METHODS: LYZENGA CLASSIFIED (CL) (TOP LEFT), LYZENGA GRADED (LZ) (TOP RIGHT), BIODIVERSITY (BIO) (BOTTOM LEFT) AND THE BIERWIRTH APPROACH (BR) (BOTTOM RIGHT). THE WHITE PIXELS ARE NOT OF INTEREST TO THIS STUDY AND EITHER REPRESENT LAND OR DEEP AREAS.....	128
FIGURE 5-9: PAIRWISE PERCENTAGE DIFFERENCES IN LYZENGA GRADED LIGHT BOTTOM COVER MAPS BETWEEN THE FOUR LANDSAT 8 IMAGES: IMAGES, A (JULY 2013) AND B (JULY 2014) (TOP LEFT), B (JULY 2014) AND D (AUGUST 2015) (TOP RIGHT), A (JULY 2013) AND D (AUGUST 2015) (CENTER LEFT), B (JULY 2014) AND C (AUGUST 2014) (CENTER RIGHT), A (JULY 2013) AND C (AUGUST 2014) (BOTTOM LEFT), C (AUGUST 2014) AND D (AUGUST 2015) (BOTTOM RIGHT).....	130
FIGURE 5-10: SCATTERPLOTS DISPLAYING PAIRWISE COMPARISON (COLUMN TO ROW) BETWEEN MEAN DAILY SWIM-DERIVED A443 VALUES OF THE FOUR DIFFERENT BOTTOM REFLECTANCE MAPS (BR, CL, BIO AND LZ) FROM 1 JANUARY 2013 TO 31 DECEMBER 2013 GROUPED WITHIN THE FOLLOWING 5-METER DEPTH BINS: 5-10 M (TOP LEFT PANEL), 10-15 M (TOP RIGHT PANEL) 15-20 M (BOTTOM LEFT PANEL) AND 20-25 M (BOTTOM RIGHT PANEL).....	132

FIGURE 5-11: SCATTERPLOTS DISPLAYING PAIRWISE COMPARISON (COLUMN TO ROW) BETWEEN MEAN DAILY SWIM-DERIVED BBP443 VALUES OF THE FOUR DIFFERENT BOTTOM REFLECTANCE MAPS (BR, CL, BIO AND LZ) FROM 1 JANUARY 2013 TO 31 DECEMBER 2013 GROUPED WITHIN THE FOLLOWING 5-METER DEPTH BINS: 5–10 M (TOP LEFT PANEL), 10–15 M (TOP RIGHT PANEL) 15–20 M (BOTTOM LEFT PANEL) AND 20–25 M (BOTTOM RIGHT PANEL).....	134
---	-----

List of Tables

TABLE 3-1: ASSESSED BAND CENTER AND BANDWIDTHS (NM) USED FOR THE STATISTICAL ANALYSIS OF SPECTRAL SEPARABILITY AND DETECTABILITY OF BOTTOM TYPES.	39
TABLE 3-2: SEPARABILITY SCENARIO DESCRIPTION.	41
TABLE 3-3: OPTICALLY ACTIVE CONSTITUENT MATTER VALUES USED IN HYDROLIGHT 5 TO CALCULATE INHERENT OPTICAL PROPERTIES. VALUES ARE FROM (BLONDEAU - PATISSIER ET AL., 2009).....	43
TABLE 3-4: ASSESSED ENDMEMBER AND MIXED BOTTOM CLASSES, AND EXCLUDED MIXED BOTTOM CLASSES.	44
TABLE 3-5: AVERAGE SILHOUETTE WIDTHS BASED ON THE DIFFERENT CLUSTER CONFIGURATIONS, WHERE EACH CLUSTER REPRESENTS STATISTICALLY SIMILAR MODELED R_{rs} SPECTRA FOR THE FOUR OPTICAL WATER TYPES: REEF WATERS, LAGOONAL, COASTAL AND ESTUARINE.	52
TABLE 3-6: BOTTOM CLASS PARTITIONING FOR THE TWO-CLUSTER CONFIGURATION FOR MODIS BANDS. FOR EXAMPLE, RUBBLE: GREEN ALGAE (50:50) REFERS TO 50% RUBBLE AND 50% GREEN ALGAE MIXED LINEARLY TO CALCULATE THE BOTTOM SPECTRA FOR THAT CLASS.	54
TABLE 3-7: BOTTOM CLASS PARTITIONING FOR THE TWO-CLUSTER CONFIGURATION FOR SEAWIFS BANDS.	54
TABLE 4-1: TABLE OF BOTTOM REFLECTANCE SCENARIOS.....	68
TABLE 4-2: OPTICAL PARAMETERS DERIVED FROM THE SWIM ALGORITHM USING DIFFERENT BOTTOM REFLECTANCE SCENARIOS	70
TABLE 5-1: LIGHT AND DARK FEATURE CLASSIFICATION BASED ON THE CSIRO SEABED BIODIVERSITY.....	117
TABLE 5-2: LANDSAT 8 IMAGES USED FOR THE REMOTE-SENSING BASED BOTTOM REFLECTANCE MAPS.....	118
TABLE 5-3: MEAN K_d LEE VALUES USED IN THE BIERWIRTH ET AL. (1993) WATER COLUMN CORRECTION.....	122
TABLE 5-4: AVERAGE RETRIEVED IOP VALUES USING SWIM WITH DIFFERENT BOTTOM REFLECTANCE SCENARIOS, QAA AND <i>IN SITU</i> DATA.....	136
TABLE A- 1: MEAN RETRIEVED BBP443 UNDER DIFFERENT BOTTOM REFLECTANCE SCENARIOS AND GBR REGIONS FOR 2005 ...	163
TABLE A- 2: MEAN RETRIEVED BBP443 UNDER DIFFERENT BOTTOM REFLECTANCE SCENARIOS AND GBR REGIONS FOR 2011 ...	164
TABLE A- 3: MEAN RETRIEVED A443 UNDER DIFFERENT BOTTOM REFLECTANCE SCENARIOS AND GBR REGIONS FOR 2005.....	165
TABLE A- 4: MEAN RETRIEVED A443 UNDER DIFFERENT BOTTOM REFLECTANCE SCENARIOS AND GBR REGIONS FOR 2011.....	165
TABLE B- 1: DETAILED OF MATCH-UP <i>IN SITU</i> DATA USED IN THIS THESIS	167

List of Abbreviations

AOP	Apparent Optical Properties
ASTER	Advanced Space-borne Thermal Emission and Reflection Radiometer
AUV	Autonomous Underwater Vehicle
CDOM	Colored Dissolved Organic Matter
chl-a	Chlorophyll a
GBR	Great Barrier Reef
GBRWHA	Great Barrier Reef World Heritage Area
HE5	Hydrolight 5
HOPE	Hyperspectral Optimization Process Exemplar model
IOP	Inherent Optical Properties
L2gen	Level-2 Processing Code
LIDAR	Light Detection and Ranging
MANOVA	Multivariate Analysis of Variance
MERIS	Medium Resolution Imaging Spectrometer
MODIS	Moderate Resolution Imaging Spectroradiometer
MPA	Marine Protected Areas
MSL	Mean Sea Level
NASA	National Aeronautics and Space Administration
OLCI	Ocean Land Color Instrument
PACE	Pre-Aerosol Cloud and Ocean Ecosystem
ROI	Region of Interest
SAM	Spectral Angle Mapper
SAMBUCA	Semi-Analytical Model for Bathymetry, Un-mixing, and Concentration Assessment
SCM	Spectral Correlation Measure
SeaDAS	SeaWiFS Data Analysis System
SeaWiFS	Sea-Viewing Wide Field-of-View Sensor
SPOT	Satellite Pour l'Observation de la Terre
SRTM	Shuttle Radar Topographic Mission
SWIM	Shallow Water Inversion Model
TSS	Total Suspended Sediments

CHAPTER 1 : INTRODUCTION AND SIGNIFICANCE OF THE RESEARCH

This chapter provides the general context that motivated the research presented in the thesis.

1.1 Overview

Coral reefs are not only important ecologically, but also economically (Spurgeon, 1992). It is estimated that up to 500 million people rely to some degree on coral reefs for subsistence and income, through tourism, fisheries, coastal protection, living resources and sand transportation (Veron et al., 2009, Wilkinson, 2004). Oceanographic processes, climate change and anthropogenic influences, such as tourism and coastal development, all affect water quality and coral reef health (Moberg and Folke, 1999, Lovelock and Ellison, 2007, Walling, 2006). In recent years, concern for the health of coral reefs has grown, particularly reefs in coastal or nearshore areas; with declining water quality identified as one of the principal threats (Fabricius, 2005, De'ath and Fabricius, 2010, Mumby et al., 2004b).

In recognition of these environmental concerns, water quality monitoring is important for managing reef ecosystems. Assessing water quality or ecosystem health requires a compromise between the practicality of measuring the various indicators of interest and the requirements to sample spatial and temporal dynamics at appropriate scales (Udy et al., 2005). Remote sensing is frequently used to monitor environmental variables as indicators of reef health over large scales (Mumby et al., 2004b, Mumby et al., 2004a, Andréfouët et al., 2002, Beijbom et al., 2012, Lirman et al., 2007). Remote sensing is often described as the acquisition of information about an object without making physical contact with the object (Panigrahi, 2014).

Satellite remote sensing data can be acquired several times a day, and the spatial extent of a scene can cover areas from a few kilometers to several thousand kilometers, providing observation to terrain that otherwise may be inaccessible, where field data might be impossible or too cost intensive to collect (Campbell and Wynne, 2011). Remote sensing has great potential for improving management practices, providing the possibility of quick event-based analysis, as well as detection of long term trends, allowing for adaptive management outcomes (Mumby et al., 1999). Further, long term trends can be used for benchmarking regional water quality objectives to ensure optimal ecosystem health (Antoine et al., 2005). Also, management decisions often require up to date field data, which are in the case of the GBR, costly and time intensive to obtain, but readily available from satellite data.

Current outputs from remote sensing products include water quality parameters such as chlorophyll *a* concentration (*chl-a*), sediment concentration and water turbidity (Example: Weeks et al., 2012, O'Reilly et al., 1998, Stumpf and Pennock, 1989, Dekker, 1993). Many global physics-based algorithms have been developed to generate synoptic imagery and estimates of water column optical properties from remotely sensed data, but they have neglected the impact of light reflected from the bottom (Lee et al., 2002, Werdell et al., 2013). In optically shallow waters the algorithms need to account for the influence of light reflected from the bottom if they are to produce reliable estimates of water column properties (Barnes et al., 2013, McKinna et al., 2015). Very clear waters often characterize coral reef environments, thus light reflectance of the bottom becomes an issue. However this is often not the case in coastal systems that are relatively turbid (Reichstetter et al., 2015a).

Remote sensing has been extensively implemented in monitoring programs of terrestrial and deep ocean environments (Example: O'Reilly et al., 1998, Mélin et al., 2005, Zhao et al., 2005). Currently, there are no operational algorithms that can correct for bottom reflectance contamination in remote sensing products for optically shallow waters, where light reflected from the bottom of the ocean contaminates the remote sensing signal. Therefore, ocean color products of shallow water environments cannot be used with any degree of accuracy.

New advances in satellite technology and the globally recognized need for optically shallow water quality products have led to optically shallow water algorithm development and validation (Example: McKinna et al., 2015, Wettle and Brando, 2006, Carder et al., 2005, Dekker et al., 2011, Lee et al., 1998). One example is the Shallow Water Inversion Model (SWIM) (McKinna et al., 2015), recently developed to improve retrievals of inherent optical properties (IOPs) of the water column in shallow water environments. SWIM uses bathymetry and bottom reflectance as input parameters. The algorithm has been incorporated into NASA's SeaWiFS Data Analysis System (SeaDAS) processing code, L2gen (<http://oceancolor.gsfc.nasa.gov>), as an evaluation product available to the research community (McKinna et al., 2015).

The newly developed shallow water inversion model, SWIM, requires bottom reflectance input parameters. Little is known about the effect of bottom reflectance parameterization on IOP retrievals in shallow water inversion models. Yet, both the atmospheric and water column light interactions have been well researched (Example: Lee et al., 1998, Ackleson, 2003, Hu et al., 2000, Mobley and Mobley, 1994, Mobley et al., 1993, Mobley et al., 2002) and operational models to calculate these interactions have been developed and utilized.

To date, little research exists on optimal bottom reflectance parameterization and its effects on the retrievals of IOPs. This lack of knowledge of the impact of bottom reflectance parameterization in shallow water inversion models may lead to ambiguous estimations or uncertainties in IOP retrievals and to suboptimal characterization of the bottom reflectance input parameter. This thesis focuses on optimizing bottom reflectance parameterizations in shallow water inversion models for coral reef environments and assesses the effects of bottom reflectance parameterization on the retrievals of IOPs.

1.2 Light in water

Ocean color satellite remote sensing can be described as the acquisition and interpretation of visible range (400-700 nm) data of the ocean collected by satellite-based sensors (Mobley et al., 2010). Reflected sunlight is the most commonly measured parameter in the production of satellite remote sensing products (Campbell, 2002). The radiance measured by ocean color satellite sensors originates from sunlight which passes through the atmosphere and is absorbed, and scattered by constituents in the water column, such as phytoplankton cells and suspended organic and inorganic matter—affected in shallow waters by the seafloor—and is then transmitted back through the atmosphere to a satellite sensor (Sathyendranath, 2000) (see Figure 1–1).

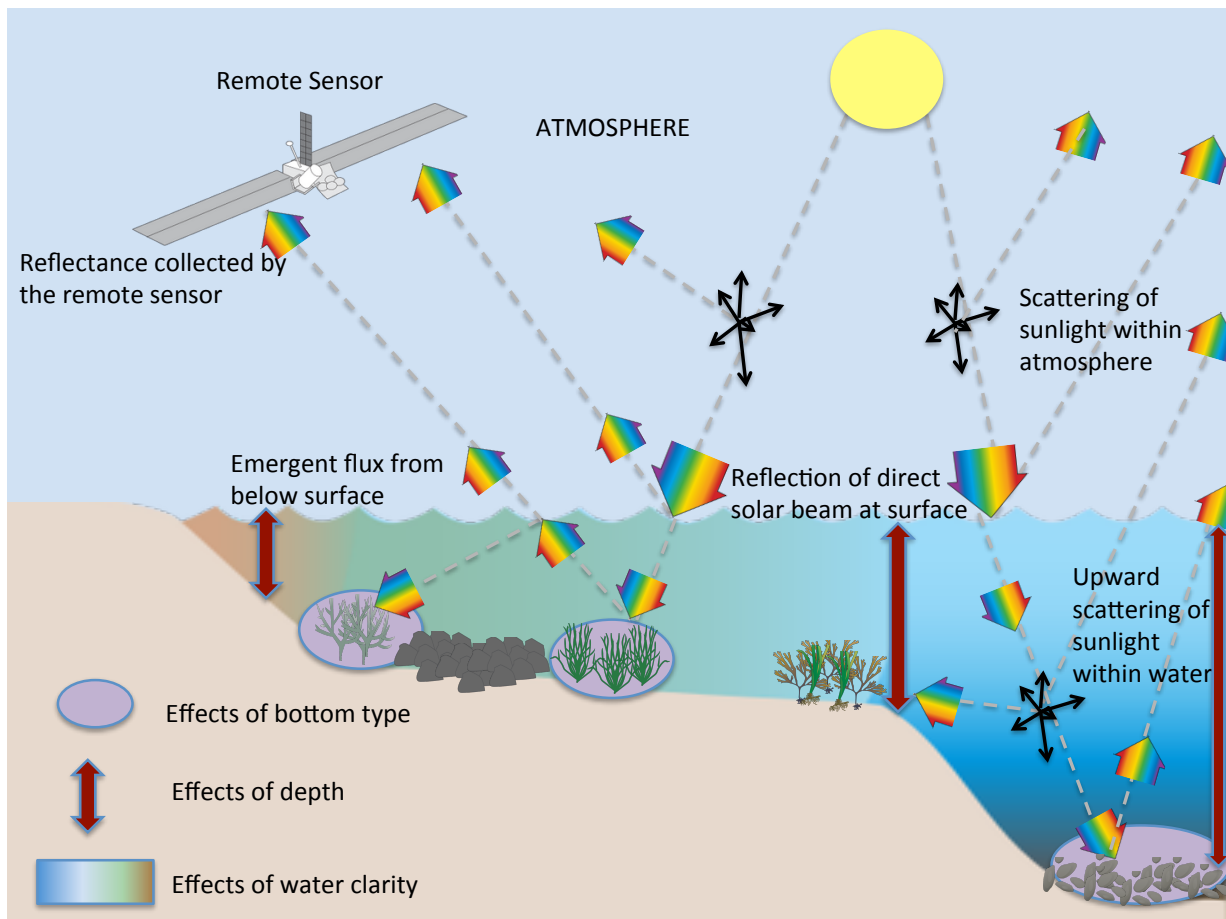


Figure 1-1: Schematic diagram of the various processes that contribute to the signal as measured by a satellite in an optically shallow water environment, where the bottom reflectance has a significant effect on the water-leaving radiance (modified from Roelfsema C.M. (2010)).

In ocean waters, light propagates through the water column, where it interacts with its constituents (Tzortziou et al., 2006, Doxaran et al., 2007). The water-leaving radiance contains information on optically active components, such as phytoplankton, non-living suspended particles and dissolved organic material, as well as seafloor cover (in shallow waters) (Jerlov, 1976, Perry, 2003). Hence, the light that leaves the ocean (the ocean color signal) carries information on ocean biology and biogeochemistry. The various optical constituents each affect the spectral nature of the light through preferential spectral absorption/reflection; thus, the spectral nature or color of the light is changed. It is the changes in the spectral nature, or the signature, that are employed in algorithms to determine the various ocean color products (Sathyendranath, 2000, Mobley et al., 2010, Mobley, 1994).

The optical signature for each constituent is unique and is defined by its inherent optical properties (IOPs) of absorption, backscattering and fluorescence (Kirk, 1994). IOPs describe everything there is to know about the bulk optical properties of a water body (Mobley et al., 2010, Mobley, 1994). Commonly used IOPs in ocean color remote sensing are the absorption coefficient (a) and the backscattering coefficient (b). Both absorption and backscattering can be expressed as a sum of contributions from individual constituents. The spectral absorption coefficient (a_{λ}) of natural waters is dependent on the number, size and kind of individual particles in the water column. The total absorption of natural waters can be expressed as:

$$a(\lambda) = a_w(\lambda) + a_{ph}(\lambda) + a_d(\lambda) + a_g(\lambda) \quad (1.1)$$

where a_w is the absorption of pure water, a_{ph} is the absorption of phytoplankton, a_d is the absorption of non-pigmented particulates and a_g is the absorption of colored dissolved organic matter (Kirk, 1994). The wavelength (λ) is written explicitly to reinforce the idea that each of these parameters varies spectrally.

The scattering coefficient (b) can be divided into two parts, forward scattering, b_f and backscattering b_b

$$b(\lambda) = b_f(\lambda) + b_b(\lambda) \quad (1.2)$$

The backscattering coefficient (b_b) can be further divided into contributions of pure water b_{bw} and particles b_{bp} and can be calculated as follows:

$$b_b(\lambda) = b_{bw}(\lambda) + b_{bp}(\lambda) \quad (1.3)$$

The particle backscattering (b_{bp}) is mostly due to phytoplankton and non-living particulates in the water column (Mobley, 1994). It is determined primarily by the concentration of particles, their shape, index of refraction and particle size distribution (Kirk, 1994). Particle backscattering (b_{bp}) is an important factor in the interpretation of remotely sensed signals, because it is directly proportional to the upwelling radiance.

To derive water quality products from water-leaving radiance, as measured by the satellite sensors, one needs to establish the relationships between the water-coloring constituents in the water column and the apparent optical properties (Mobley et al., 2010, Mobley, 1994, Sathyendranath, 2000).

It used to be difficult to collect *in situ* IOPs other than by using the beam attenuation coefficient (Mobley et al., 2010). Yet, it was comparatively easy to collect *in situ* measurements of radiometric variables such as the upwelling and downwelling irradiances. Therefore, apparent optical properties (AOPs) rather than IOPs were used to assess the bulk optical properties of a water body (Mobley et al., 2010). AOPs can provide information about a water body, such as the concentrations and types of the in-water constituents, from measurements of the light field and are associated with the ocean's color and clarity (Bissett et al., 2005, Mobley et al., 2010).

AOPs depend on two things: (I) the inherent optical properties (IOPs) of the system and (II) the light field in which they are measured (Kirk, 1994). The diffuse attenuation coefficient, K , the primary turbidity measures of the water column, is a commonly used AOP in the ocean color remote sensing community (Maritorena et al., 2002, Bricaud et al., 1998, Kirk, 1984). For example, K_d490 determines how visible light in the blue-green part (490 nm) of the electromagnetic spectrum penetrates the water column. K_d is directly related to the presence of scattering and absorbing constituents in the water column. The measured value of K_d is dependent on depth, sun angle and sky conditions (Kirk, 1994, Mobley et al., 2010).

1.3 Ocean color modeling

Ocean color remote sensing is often utilized to map the distribution of chlorophyll concentration, one of the most fundamental properties of ocean ecosystem functioning. Ocean color remote sensing products have also been applied to a number of other applications such as management of fisheries, detection of harmful algal blooms, as well as the discrimination of functional groups of phytoplankton (Platt, 2008).

Ocean color models are used to relate remote sensing data—radiance measured at the satellite—to biogeophysical properties, such as chlorophyll concentrations (Sathyendranath, 2000). Ocean color remote sensing models are generally categorized as: empirical, analytical or semi-analytical (Sathyendranath, 2000) (Figure 1–2).

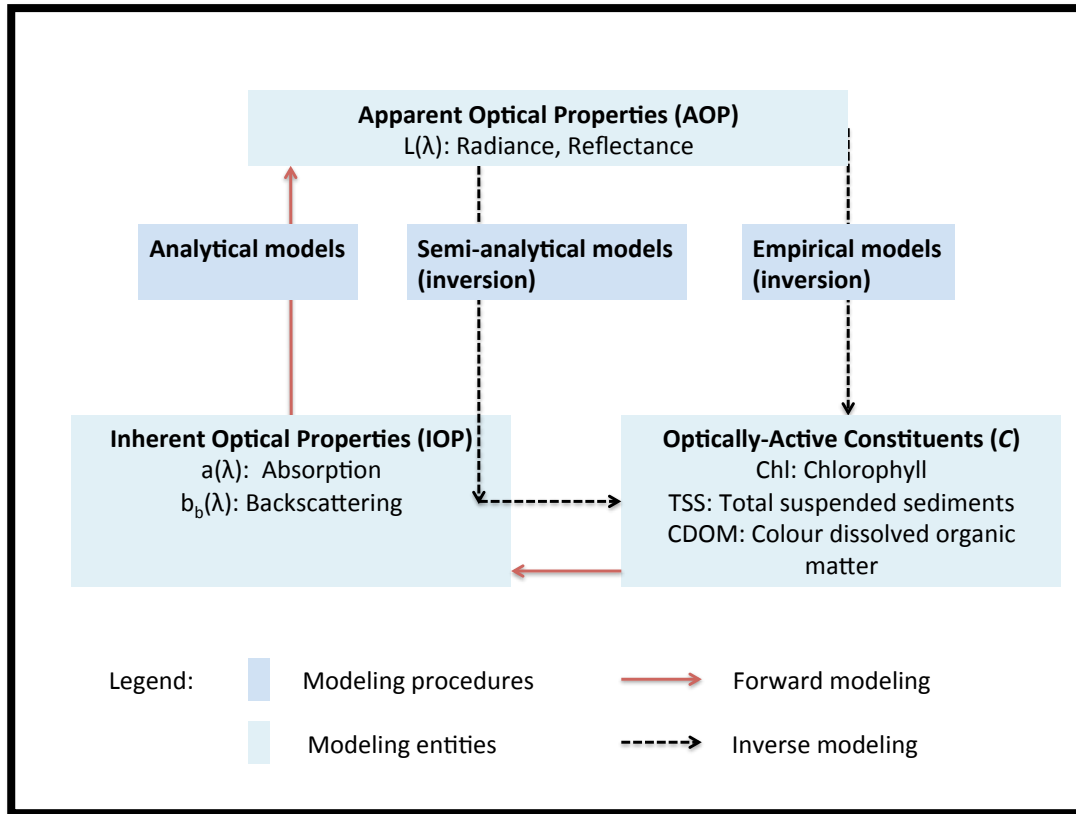


Figure 1-2: Main model approaches in ocean color modeling showing the inverse and forward modeling processes (adapted from Sathyendranath (2000))

Ocean color models can also be classified as forward and inverse models. Forward models use IOPs (absorption, backscattering coefficients) of *chl-a*, particles and absorbing materials to estimate AOPs, such as R_{rs} and K_d . On the other hand, inverse models use AOPs to derive optically-active constituents and IOPs (Sathyendranath, 2000) (Figure 1–2). For example, in this thesis I will use a forward modeling approach to derive R_{rs} from different substrate reflectances and IOPs to calculate the maximum depth at which a bottom reflectance signal still affects the remote sensing signal. But, I will use an inverse model to derive IOPs for the Great Barrier Reef (GBR) from MODIS (Moderate Resolution Imaging Spectroradiometer) data.

Analytical optical models in ocean color remote sensing are usually classified as forward models. Analytical optical approaches require the application of radiative transfer theory (Feng, 2004). Radiative transfer theory is based on the propagation of radiation through the atmosphere and water where it is affected by absorption, emission and scattering processes (Mobley et al., 2010).

Analytical optical models are more complex than empirical optical models due to the inclusion of light interactions between the source and sensor. Because of the model complexity, analytical optical models are frequently used by remote sensing specialists rather than by application scientists (Franklin, 2001). With the introduction of improved underwater spectrometers in the late 1990s, the development of analytical optical models has improved (Dekker et al., 2011). Also, a commercial software model, Hydrolight, now allows the user to simulate *in situ* spectra under different water column conditions to better understand light interactions in the ocean and therefore, to provide a better understanding of the basic theory of analytical models (Mobley and Sundman, 2008a).

Empirical and semi-analytical optical models are mostly classified as inverse models (Sathyendranath, 2000). Empirical optical approaches are based on statistical relationships between observational and/or experimental data, and remotely sensed data. Empirical optical models are widely used, especially in the open ocean, but do require extensive field calibration and thus, can be site specific (Leiper et al., 2009). Also, the ocean's water column properties are changing, both on regional and global scales. It is likely that models based on *in situ* data collected over the past decades are not replicable in the near future (Dierssen, 2010).

Semi-analytical or "quasi-analytical" models are based on the theory of light propagation through the water and the inclusion of some empirical approximations (Zoffoli et al., 2014). However, semi-analytical models do not rely on the fixed relationships between the empirical approximations and absorption or backscattering, that the empirical optical models are based on (Orcutt, 2013). Semi-analytical ocean color models can retrieve multiple ocean color properties simultaneously from a single water-leaving radiance spectrum, whereas empirical optical models usually only retrieve one parameter (Maritorena et al., 2002). Further, semi-analytical models use the retrieved IOPs to generate biochemical parameters, such as total suspended sediments and *chl-a*.

One of the most recent and widely accepted semi-analytical models for shallow water remote sensing was developed by Lee et al. (1998). In this model, the diffuse attenuation coefficients are explicitly expressed as functions of in-water absorption and backscattering (Lee et al., 1998). Lee et al. (2001) further developed Lee's inversion optimization approach to derive water column properties and water depth from hyperspectral data.

The later algorithm of Adler-Golden et al. (2005), that is based on the algorithm of Lee et al. (2001), assumes constant water column optical properties to retrieve coastal water properties and to estimate bathymetry of shallow waters. A recent study compared the absolute and relative accuracies, as well as computational efficiencies, of ocean color algorithms for optically shallow waters (Dekker et al., 2011). The study found that empirical models produced less accurate bathymetric retrievals than radiative-transfer-based models, but found all the tested inversion models produced reasonably accurate results of bathymetry, IOPs and bottom reflectance for waters shallower than 13 m. Locally parameterized models performed better, while none of the methods reviewed performed satisfactorily in all situations (Dekker et al., 2011).

Increased efforts are currently being made within the ocean color remote sensing community to develop tools to retrieve water clarity parameters for optically shallow waters (Dekker et al., 2011). Optically shallow waters are characterized as areas in which light reflected from the seafloor affects the water-leaving radiance signal (Lee et al., 1998). This can lead to errors in ocean color products of models developed for deep water, such as IOPs (Cannizzaro and Carder, 2006, Qin et al., 2007, Zhao et al., 2013). In recent years, methods to derive IOPs from optically shallow waters have been developed (McKinna et al., 2015, Brando et al., 2012, Barnes et al., 2014, Barnes et al., 2013). To date, only one of the developed methods, the Shallow Water Inversion Model (SWIM) (McKinna et al., 2015), explicitly uses bathymetry and benthic reflectance datasets to improve IOP retrievals. SWIM focuses on IOP retrievals. Most previous research in shallow water ocean color modeling focused on bathymetric retrieval and seafloor classification with little emphasis on the derived water column IOP values and geophysical products such as *chl*, and other water clarity measures (Brando et al., 2009, Dekker et al., 2011, Fearn et al., 2011, Goodman and Ustin, 2007, Hedley et al., 2009, Klonowski et al., 2007, Lee, 1999, Lesser and Mobley, 2007).

The recent inclusion of SWIM into the NASA SeaDAS L2gen processing code (<http://oceancolor.gsfc.nasa.gov>) marks a milestone in the application of semi-analytical models to retrieve IOPs. SWIM allows the user to specify bathymetry and bottom reflectance to improve IOP retrievals (McKinna et al., 2015). The SWIM model has been found to perform well in clear coral reef waters in the Great Barrier Reef, under the current default IOP model parameterizations using MODIS ocean color data (McKinna et al., 2015).

1.4 Bottom reflectance in remote sensing applications

1.4.1 Bottom reflectance in ocean color modeling

Bottom reflectance parameterization in ocean color shallow water models usually includes the spectral reflectance signature of common bottom classes, while the recently developed shallow water inversion model, SWIM, also includes the spatial distribution of each bottom class (McKinna et al., 2015). Adding a bottom reflectance parameter to a shallow water inversion model should improve IOP retrievals, as the influence of light reflected from the corresponding bottom type is included in the calculation of the IOPs. The parameterization of bottom reflectance in shallow water inversion models is usually based on the original Lee et al. (1998, 1999, 2001) approach, which is as follows:

$$P = B \cdot \rho(\lambda_0) \tag{1.4}$$

where P is the bottom reflectance, $\rho(\lambda_0)$ is the bottom reflectance spectrum normalized at wavelength λ_0 , and B is a scalar representing the magnitude of the bottom reflectance spectrum at the corresponding wavelength. B is the only variable that controls the contribution of the bottom reflectance to the water-leaving reflectance, because the spectral shape of the bottom cover type does not change. Lee's bottom reflectance parameterization was tested in shallow waters in Tampa Bay, Florida (Lee et al., 2001). The only bottom cover present in that study area was sand, yet, the model was adjusted to select either a sand or seagrass spectrum, based on a rough estimation of existing bottom reflectance (Lee et al., 2001).

Not all shallow water ocean color models use the same approach to parameterize bottom reflectance. For example, the shallow water inversion model, Semi-Analytical Model for Bathymetry, Un-mixing, and Concentration Assessment (SAMBUCA), searches

an inbuilt spectral library of bottom reflectance spectra to account for the diversity of seafloor cover (Wettle and Brando, 2006). For a model to search a spectral library to find the most appropriate combination of bottom reflectance spectra for each pixel in the satellite image increases the processing time substantially, limiting the application of such a model.

For example, the SAMBUCA model needed 1147 hours to process one scene of Lee Stocking Island, while another model, the Hyperspectral Optimization Process Exemplar model (HOPE), that has a more simple bottom reflectance configuration, required only 48 minutes to process the same image (Dekker et al., 2011).

The current version of the NASA SWIM model applied to the GBR uses a 2-bottom cover class approach, where the user can specify the spectral signature and proportion contribution of a bottom class, such as sand or seagrass to the two classes of “light” and “dark”. The current SWIM model for the GBR is parameterized as follows:

$$\rho_{net}(\lambda) = c_L \rho_L(\lambda) + c_D \rho_D(\lambda) \quad (1.5)$$

where $\rho_{net}(\lambda)$ is the net spectral reflectance per-pixel, C_L represents the relative proportion of “light bottom” cover with C_D representing the relative proportion of “dark bottom” cover (McKinna et al., 2015).

1.4.2 Seafloor cover mapping

Seabed mapping provides essential information to strengthen effective management of the marine environment by documenting the extent and distribution of particular seabed cover types and assessing the selection of Marine Protected Areas (MPAs). Seabed mapping and marine habitat mapping are loosely defined terms and can have different meanings based on their application. For example, seabed mapping may refer to bathymetry information or points representing occurrences of a single species or habitat across an area. In this thesis, the term bottom reflectance mapping will be used as a more general term to describe any activities involving mapping of the optical properties of the seabed.

Satellite imagery is frequently used for seafloor mapping (Example: Fearn et al., 2011, Goodman et al., 2013, Green et al., 1998, Joyce et al., 2004). Satellite images are composed of a matrix of image elements, or pixels, which are the smallest units of an image. The pixel defines the spatial resolution of an image representing the size of the surface area (i.e. km²) being measured on the ground, determined by the sensors' instantaneous field of view (IFOV) (Schowengerdt, 2006). Most reef structures such as different coral cover or algae patches are spatial structures (cm²-m²), but can cover larger spatial extents (>km²) (Pitcher, 2007).

Large shelf-scale ecosystems that contain a large number of coral reefs, such as the Great Barrier Reef are heterogeneous environments presenting several bottom types within one satellite pixel (Pitcher, 2007). Thus in moderate resolution sensors such as MODIS (1 km²) the pixel is usually a mix of substrate types. Thus, it is essential that shallow water inversion models account for the heterogeneity of bottom covers in shallow waters, where the seafloor is generally diverse.

There is an abundance of research published about mapping seafloor cover for biodiversity or habitat purposes, or for bathymetry (Example: Adler-Golden et al., 2005, Andréfouët et al., 2003, Casal et al., 2011, Goodman and Ustin, 2007, Fearn et al., 2011); however, not much has been reported about mapping the seafloor based on its optical properties. Yet, to correct for bottom contamination in satellite ocean color algorithms, the bottom cover has to be classified based on its optical properties. The most common methods of large-scale seafloor mapping are based on remote sensing techniques. Most recently, several studies have assessed the integration of LIDAR and hyperspectral data to generate maps of seafloor reflectance (Macon et al., 2008, Tuell et al., 2005, Tuell et al., 2010). Seafloor mapping on smaller scales (<100 m) often includes underwater video or photography. The emergence of the autonomous underwater vehicle (AUV) may make future large-scale habitat mapping based on underwater imagery possible (Fair et al., 2006). While there is a focus on creating substrate maps using remote sensing techniques, no studies known to the author have focused on converting biodiversity *in situ* datasets to optical seabed cover maps.

Remote sensing approaches for mapping seabed cover in coral reef systems started in the 1970s, using aerial photo interpretation (Hopley et al., 1978). In the 1980s, satellite data from the Landsat Multispectral Scanner (MSS) Thematic Mapper™ and Satellite

Pour l'Observation de la Terre (SPOT) sensors were used for broad habitat classifications (Jupp et al., 1985, Poiner et al., 1987). Over recent years, state of the art high spatial and high spectral resolution airborne data have been used for bottom mapping (Leiper et al., 2011). Spatially, they are classified into low (100-1000 m), moderate (10-100 m) and high (0.5–10 m) resolutions (Goodman et al., 2013)

Numerous satellite and airborne imaging sensors have been used for coral reef mapping. They are primarily categorized based on their spatial and spectral resolution. Spectrally, sensors are classified as multispectral, where imagery is produced by satellite sensors that measure reflected energy within several specific broad bands of the electromagnetic spectrum, or hyperspectral, that contain hundreds of narrow bands across the electromagnetic spectrum. When using hyperspectral sensors, finer spectral reflectance differences may be detected compared to those detected using multispectral sensors (Phinn et al., 2008, Kutser et al., 2003). However, the importance of spatial versus spectral resolution for coral reef mapping remains a challenge for researchers (Capolsini et al., 2003, Lee et al., 2007, Mumby and Edwards, 2002, Pulliza, 2004, Hochberg et al., 2003).

Multispectral resolution sensors with moderate spatial resolution, such as Landsat 5 Thematic Mapper TM, Landsat 7 Enhanced Thematic Mapper Plus (ETM+), SPOT and the Advanced Space-borne Thermal Emission and Reflection Radiometer (ASTER) have been used in coral reef research since the 1980s (Ahmad and Neil, 1994, Andréfouët et al., 2003, Andréfouët and Riegl, 2004, Capolsini et al., 2003, Dobson and Dustan, 2000, Mumby et al., 1998, Mumby et al., 1997, Purkis and Pasterkamp, 2004). Landsat imagery has been found to be the most successful for multi-spectral resolution remote sensing mapping, as its data records have now been available for more than 30 years, which makes trend analysis possible. Further, Landsat data also provide a cost-effective way to map coral reefs (Dobson and Dustan, 2000) especially since the Landsat archive is made freely accessible (Wulder et al., 2012). Nevertheless, these sensors are not able to distinguish between some coral reef benthos types, including live coral or macroalgae (Andréfouët et al., 2001). The recent introduction of multi-spectral sensors with high spatial resolution (approx. 0.5-10 m), such as IKONOS, Quickbird-2 and Worldview-2, has allowed researchers to map seafloor cover with higher descriptive resolutions than was possible with the moderate spatial resolution sensors, such as Landsat (Andréfouët et al.,

2003, Karpouzli et al., 2004, Mumby et al., 1998, Mumby et al., 1997, Mumby and Edwards, 2002, Tuell et al., 2010, Eugenio et al., 2015). Lee et al. (2007) assessed the most suitable spectral bands for remote sensing of aquatic environments. That study proposed more spectral bands than currently available on the MODIS sensor. In addition, it identified that a band between 551 and 667 nm on MODIS would be useful for remote sensing of suspended sediment and optically shallow waters.

Hedley et al. (2012) further assessed sensor limitations in optical remote sensing of coral reefs, concluding that bottom classes and sub-pixel mixing are the main limiting factors in the accuracy of bottom mapping classification using remote sensing. The study also found that current instrument noise levels are a minor factor in the discrimination of bottom cover.

Spectral libraries are used in some ocean color models to correct for the effects of bottom reflectance (Wettle and Brando, 2006) and in seafloor mapping. Spectral libraries of pure endmembers (single organisms, for example: sand, seagrass or algae) or cover types have been assessed in various studies (Andréfouët et al., 2001, Andréfouët and Riegl, 2004, Hochberg et al., 2004, Holden and LeDrew, 1998, Holden and Ledrew, 1999, Joyce et al., 2004, Kutser et al., 2003, Kutser et al., 2006, Leiper et al., 2009, Minghelli-Roman et al., 2002, Myers et al., 1999, Hochberg et al., 2003). These studies were predominantly based on *in situ* field spectrometry measurements of single cover classes (Leiper, 2011). For example, Hochberg et al. (2003) analyzed 13,100 *in situ* spectral reflectance signatures for shallow water environments in the Atlantic, Pacific and Indian Oceans. The authors identified 12 bottom types which showed unique spectral features: fleshy brown, green, and red algae; non-fleshy encrusting calcareous and turf algae; bleached, blue, and brown hermatypic coral; soft/gorgonian coral; seagrass; terrigenous mud; carbonate sand. Significant conclusions from this analysis were that the geographical location does not significantly influence spectral reflectance signatures. Spectral features are based on the unique suite of pigments of each bottom type and these pigment suites are the same in all the geographic regions (Hochberg et al., 2003).

Even though much research on spectral discrimination of bottom covers using *in situ* data has been conducted, no accepted criteria for spectral separability of bottom classes have been established (Hochberg et al., 2003). A number of studies demonstrate spectral discrimination of bottom cover types for individual datasets using a study specific

methodology (Kutser et al., 2003, Mumby et al., 2004b, Call et al., 2003, Hochberg et al., 2003). However, there are considerable differences between the spectral separability methods used, as well as between the results of spectral separability studies in coral reef systems. Some studies have used derivative analysis and multivariate techniques to analyze datasets of pure bottom cover spectral libraries (Holden and LeDrew, 1998, Pinnel et al., 2004, Hedley et al., 2012).

While those techniques may have produced discriminative criteria, they have failed to identify the underlying reason for the results, thus their application is limited (Hedley and Mumby, 2002). At large, studies that have used mixed endmember spectra have derived them using spectrum-matching and lookup table methods (Goodman and Ustin, 2007, Mobley et al., 2005). Further studies have assessed the spectral reflectance features and classification potential of coral reef benthos and bottom assemblages using *in situ* measurements, with limited success (Leiper et al., 2011, Hochberg et al., 2003). For example, Hochberg and Atkinson (2003) found that narrowband multispectral sensors overestimated coral cover by 11-15%, while broadband multispectral sensors overestimated coral cover by up to 103%. The task of translating *in situ* reflectance measurements to satellite imagery scale remains a challenge when mapping optical properties of seabed cover.

1.5 Aim of the project

At present, it is not clear how bottom reflectance parameterization will affect the retrievals of IOPs in shallow water inversion models or how to derive bottom reflectance parameters from available data sources. It is thus important to identify the optimal bottom reflectance parameterization, and its effects on the retrievals of IOPs in shallow water areas.

The overall aim of the project was to optimize bottom reflectance parameterizations in shallow water inversion models for coral reef environments and assess the effects of bottom reflectance parameterization on IOP retrievals.

The main objectives for the project are:

Objective 1: Assess the spectral separability and detectability of bottom reflectance in coral reef environments.

Objective 2: Test the sensitivity of bottom reflectance parameterization on the retrieval of IOPs using a shallow water inversion model (SWIM).

Objective 3: Assess and test different approaches to create a spatially explicit bottom reflectance map for areas deeper than 5 m, using different datasets.

1.6 Chapter synopsis

The thesis has been organized with the following structure:

Chapter 1—Overview of the project

This chapter provides the theoretical background and a review of the relevant literature that has preceded the research proposed in this thesis, as well as the aims of the project. I will discuss issues that are important for mapping spectral bottom reflectance and the current challenges faced by researchers. A significant gap in the current state of knowledge regarding the available bottom reflectance data and methods for assembling such data for use in ocean color algorithms is identified, based on a case study of the GBR.

Chapter 2—Research approach and study site

A brief overview of the research approach is given. The study site used throughout the thesis is introduced.

Chapter 3—An assessment of bottom reflectance contamination in satellite remote sensing

The methodology and results for the assessment of spectral reflectance characteristics for the use in shallow water ocean color algorithms are presented and discussed. The separability and detectability of bottom cover classes are assessed and discussed.

Chapter 4—Sensitivity analysis of bottom reflectance parameterization in the ocean color Shallow Water Inversion Model (SWIM): A case study of the Great Barrier Reef

A sensitivity analysis of bottom type parameterization on IOP retrievals using SWIM is presented. The bottom cover parameterization is assessed for the GBR region using single scene and time series analysis of retrieved IOP data.

Chapter 5—The development of spatially explicit bottom reflectance parameters for use in shallow water inversion models

Different approaches to building a bottom reflectance map are presented. The different datasets used for the bottom reflectance maps are discussed and results are presented in detail. The effects of different bottom cover maps on the retrieval of IOPs are discussed.

Chapter 6—Conclusion and recommendations

Conclusions and recommendations are made. The main outcomes and contributions in the context of the objectives as well as limitations and directions for future work are presented.

CHAPTER 2 : RESEARCH APPROACH AND STUDY SITE

Chapter 2 provides an overview of the research approach, and provides a summary of the study site. As this thesis has been structured to provide three standalone chapters (Chapters 3-5), further details about methods and datasets specific to these individual chapters are covered in their relevant sections.

2.1 Overall study approach

The study uses radiative transfer modeling and remote sensing approaches to gain an understanding of bottom reflectance parameterization in shallow water inversion models. Specifically, the study assesses bottom reflectance parameterization with SWIM using MODIS satellite data. Chapter 1 highlighted both the need for inclusion of bottom reflectance in shallow water inversion models and the current lack of understanding of the impact of bottom reflectance parameterization in ocean color shallow water models. These two conditions were the primary motivators for the researcher. To address the aims of the study, the research approach needed to include three stages: (i) the assessment of appropriate and efficient bottom categorization, (ii) the development of bottom reflectance parameters and (iii) testing of these parameters in SWIM.

To assess, develop and test the bottom reflectance parameterization in SWIM, four questions were addressed:

- (1) What spectral information is needed for bottom reflectance parameterization in ocean color shallow water models and how does it relate to bottom cover types?
- (2) How sensitive is SWIM to differences in bottom reflectance parameterization?
- (3) What types of data can we use to construct a spatially explicit bottom reflectance map for inclusion in shallow water inversion models?
- (4) How do different mapping approaches influence IOP retrievals?

To address the first question, the researcher used *in situ* spectral reflectance data and radiative transfer modeling to define distinct optical bottom cover classes that can be spectrally separated by MODIS and the Sea-Viewing Wide Field-of-View Sensor (SeaWiFS). While the thesis focuses on MODIS data, SeaWiFS was included in this thesis because it has a long time-series of historic data that are often used in ocean color trend analysis. The researcher also assessed the maximum depth at which the bottom reflectance contributes to the surface reflectance (R_{rs})—Chapter 3. The second question was addressed by conducting a sensitivity analysis on the retrieval of inherent optical properties (IOPs) using different bottom reflectance parameterizations in SWIM—Chapter 4.

The final two questions were addressed by using various bottom cover data to generate spatially explicit bottom reflectance maps and assess the modeled IOP retrievals—Chapter 5. The overall study design is shown schematically in Figure 2–1. More detail pertaining to each of the steps documented in Figure 2–1 is contained in Chapters 3-5.

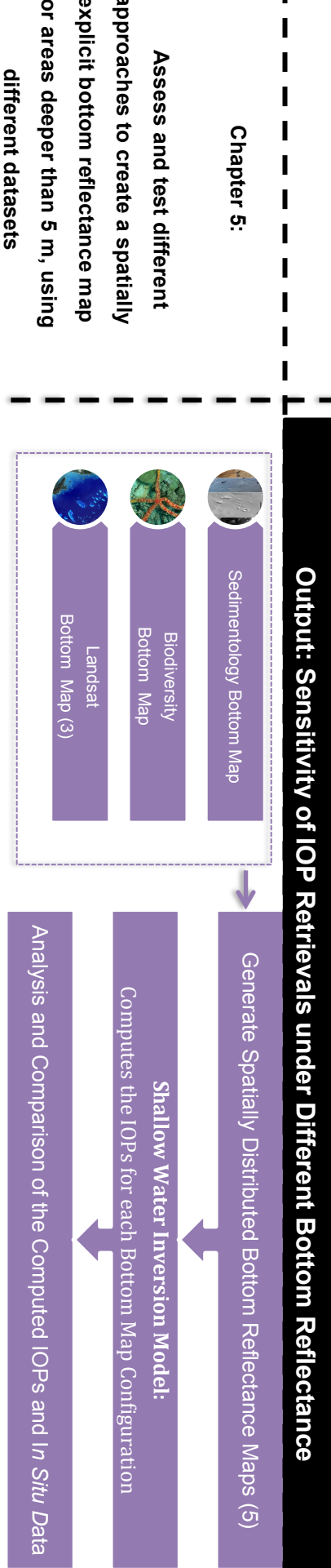
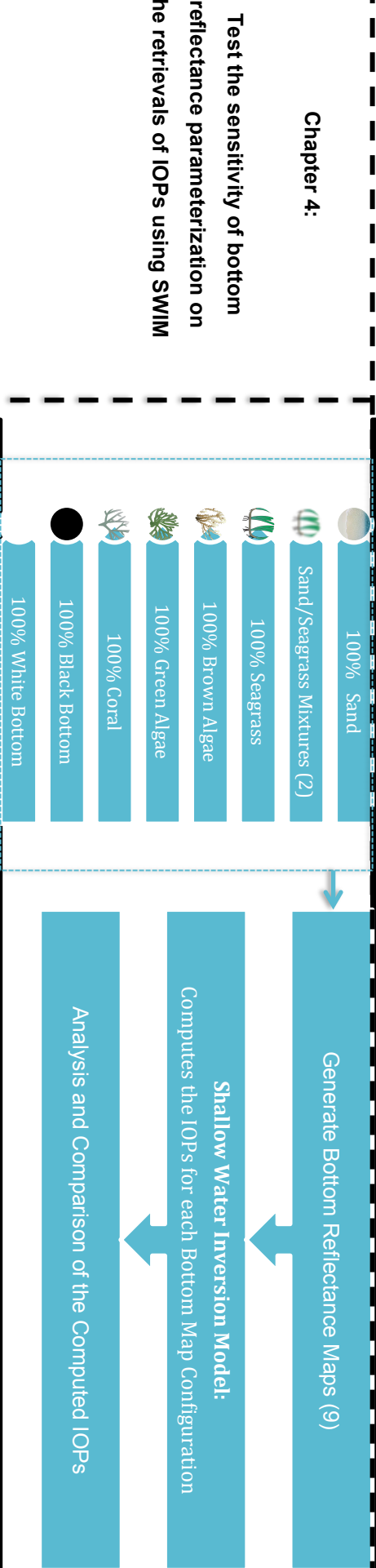
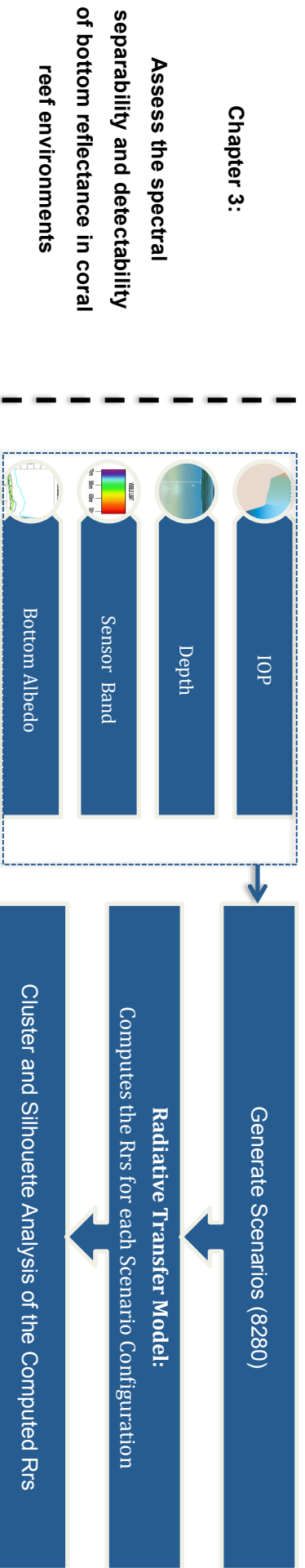


Figure 2-1: Flowchart illustrating the main components and linkages of the data and methods

2.2 Study area

The project focuses on a subset of the Great Barrier Reef (GBR) shelf system between 10°5'24"S and 25°00'00"S, and from the coastline to the continental shelf edge, as illustrated in Figure 2–2 (GBRMPA, 2002). The Great Barrier Reef World Heritage Area (GBRWHA) covers an area of approximately 346,000 km² (GBRMPA, 2014) consisting of 225,000 km² of shelf areas and approximately 120 000 km² of oceanic waters. It extends along 2300 km of the Queensland coastline from Torres Strait in the north almost to Fraser Island in the south. The GBR consists of a complex reef matrix of nearly 3000 separate coral reefs. About 36% of the GBR Marine Park consists of continental slope, with depths ranging from 150 to 2000 m, while 64% comprises the continental shelf, including the coral reefs, with depths ranging from <1 to 150 m. The continental shelf consists of inter-reef areas (25% of the Marine Park) and lagoons (33%). The vast majority of coral reefs are offshore with the inshore waters containing fewer reefs (Spalding et al., 2001).

The GBR includes an extensive system of coral reefs and inter-reef areas, thus remote sensing provides the only viable approach for synoptic monitoring of reef-wide environmental parameters, such as water quality. However, reef waters can be clear and relatively shallow (above 30 m) allowing bottom reflectance to interfere with the remote sensing signal recorded by satellite sensors. Carbonate sediments, in particular, are highly reflective (bright) and therefore are most likely to interfere with extraction of water column properties from ocean color data. The GBR has been widely researched and considerable data on GBR water quality exist (Example: Fabricius, 2005, Fabricius et al., 2013, Fabricius et al., 2014, Furnas and Mitchell, 2001, Furnas et al., 2005, Schaffelke et al., 2012, Schaffelke et al., 2005), providing a good case for developing and testing the SWIM algorithm. However, due to the large extent of the GBR, availability of detailed bottom cover data is a challenge. The following sections discuss the bathymetry and seafloor covers of the GBR used throughout this thesis.



Figure 2-2: Map of the Great Barrier Reef with the green line indicating the boundaries of the Great Barrier Reef Marine Park area, including the major reef groups (adapted from (GBRMPA, 2002))

2.2.1 GBR bathymetry

Bathymetry data is essential to this study. It is used in creating the bottom reflectance maps, as well as providing an input into the SWIM model. At present, two shelf-scale bathymetry data sets exist for the GBR, the Geoscience Australia bathymetry dataset (2009) and the gbr100 dataset (2010). Geoscience Australia and the Australian National Oceans Office have produced a high-quality 9 arc second (0.0025° or ~ 250 m at the equator) bathymetric grid for all Australian waters (92° E– 172° E and 8° S– 60° S), including the GBR. This bathymetry map is derived from bathymetric survey, seismic and sampling data collected between 1963 and 2009 (Whiteway, 2009).

The second bathymetry dataset used in this thesis, is the gbr100 dataset from the 3DGBR project (Beaman, 2012). The gbr100 dataset is a gridded digital elevation model based on WGS-84 and mean sea level (MSL) as the vertical datum (Beaman, 2012). This dataset was constructed from various data sources and includes multibeam and singlebeam acoustic soundings, Royal Australian Navy airborne Light Detecting and Ranging (LiDAR) data, Shuttle Radar Topographic Mission (SRTM) data and coastline data, and has a 100 m x 100 m resolution (Beaman, 2012). The gbr100 was chosen as the appropriate data set for this work because it is already included in the NASA SeaDAS processing code as an auxiliary database. Figure 2–3 shows the gbr100 bathymetry map of the study region.

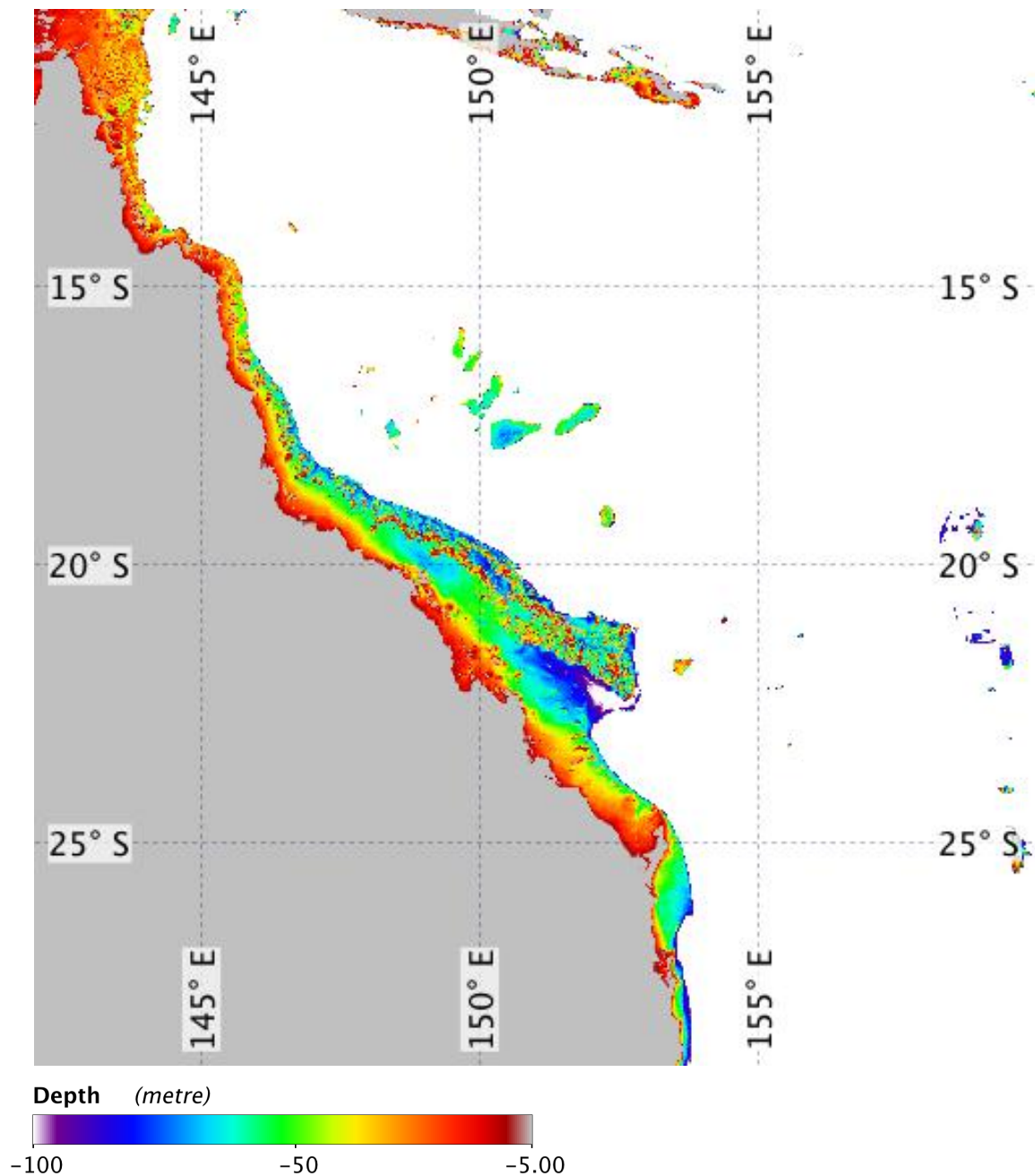


Figure 2-3: gbr100 bathymetry dataset used in this thesis (data from (Beaman, 2012))

2.2.2 GBR seafloor cover

Mapping the nature and spectral characteristics of the GBR seafloor and its biological cover is an essential step in developing reflectance parameterizations, which are useful in shallow water ocean color retrieval algorithms. Linking seafloor cover to improved IOP retrievals using shallow water inversion models requires accurate, spectrally and spatially detailed bottom cover datasets.

Due to the large spatial extent and remoteness of much of the GBR, detailed mapping of seafloor cover at the spatial resolution of ocean color sensors (250 m–1 km) is very limited. One of the most comprehensive sources of bottom cover distribution in the GBR is the biodiversity dataset by Pitcher (2007). The following sections describe the distribution of the main seafloor cover types observed in the GBR.

2.2.2.1 Biotic bottom cover

The GBR has approximately 3000 coral reefs (GBRMPA, 2009). Most bottom cover research focuses on very shallow areas (above 5 m) of these reefs, yet these areas are usually not of interest in ocean color data processing to retrieve water column properties (Example: Roelfsema et al., 2006). However, a wide range of biota also grows in inter-reefal areas at depths below 5 m. As examples, Figure 2–4 shows the occurrence of soft coral in the GBR shelf, while Figure 2–5 represents the occurrence of hard corals with a focus on inter-reefal areas, as recorded by Pitcher et al. (2007). Most soft and hard corals are located on the middle and outer shelf. A maximum of 30% coral cover was recorded for soft corals, as illustrated in Figure 2–4. A maximum of 20% coral cover was recorded for hard coral substratum, as displayed in Figure 2–5. However, these are point data and thus do not include complete spatial distribution. There are no comprehensive inter-reefal maps of coral distribution, known to the author. Pitcher et al. (2007) found that many types of reef organisms exist as part of “reef communities” growing on sections of hard substrate in inter-reefal areas. Attached forms, such as hard or soft corals, tend to be less abundant in open sandy areas (Example: GBR lagoon), and more abundant around areas of greater “surface reef” development. Thus, this thesis considers only a limited amount of the coral bottom cover in shallow water areas above 25 m.

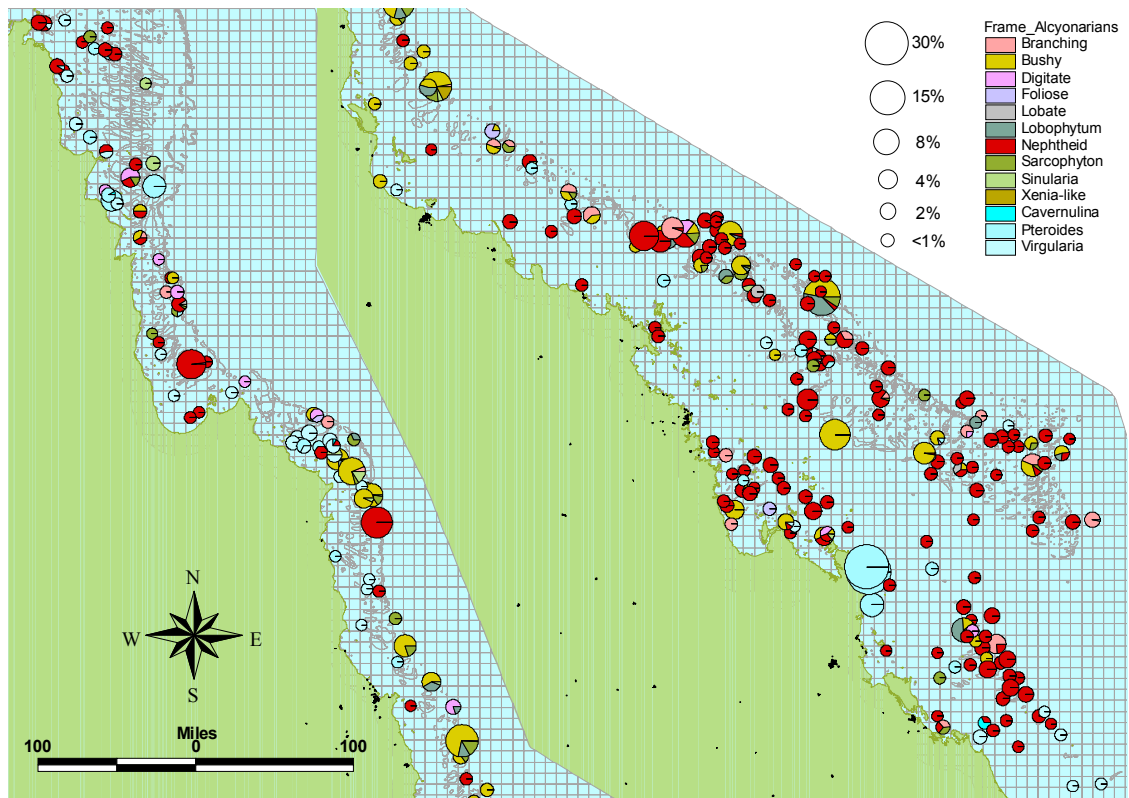


Figure 2-4: Map of the percentage distribution and cover of alcyonarian type soft corals in the Great Barrier Reef (from Pitcher, 2007).

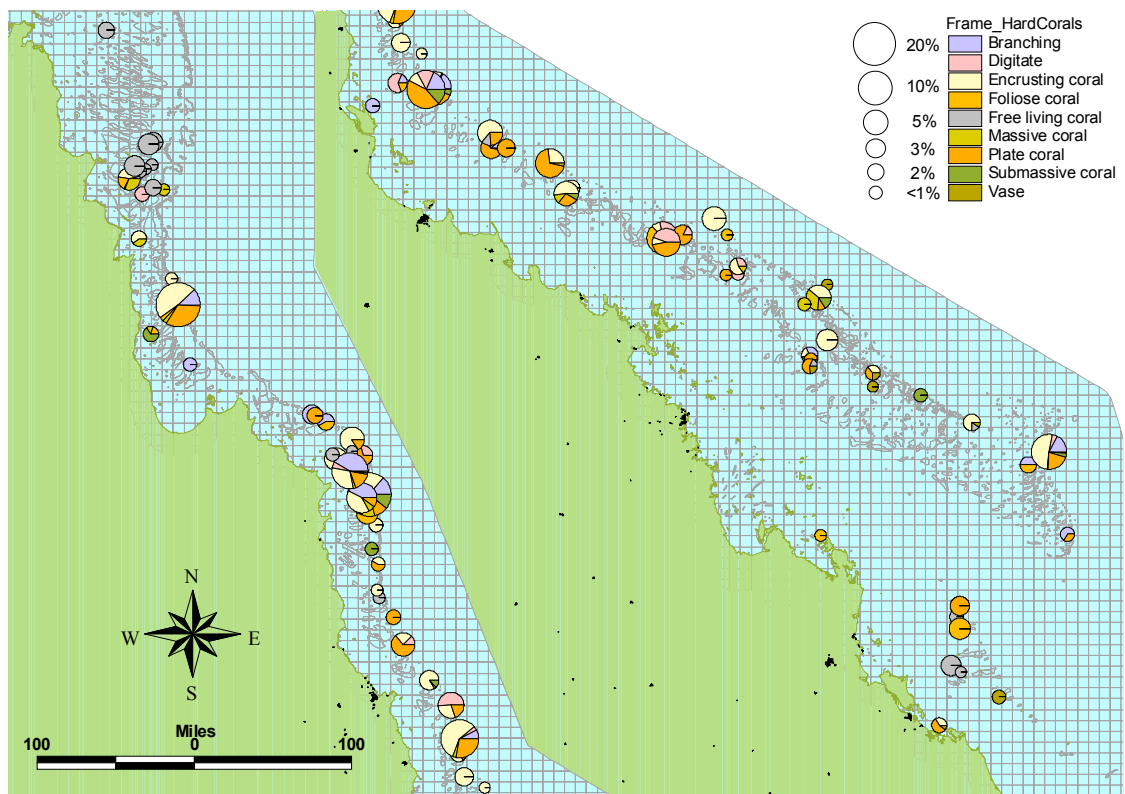


Figure 2-5: Map of the percentage distribution and cover of hard corals (from Pitcher, 2007).

Seagrasses are widely distributed across the GBR system. They occur in various habitats, such as rivers, inlets, coastal, reef, intertidal, sub-tidal and deep-water areas (Pitcher, 2007). McKenzie et al. (2014a) estimated the total area of shallow (water depth above -15 m) and deep (water depth below 15 m) seagrass cover at 3,063 km² and 31,778 km², respectively. Most seagrass mapping has been focused in shallower depths (above 15m). Figure 2–6 shows the seagrass distribution in the GBR, mapped mainly for shallower coastal areas McKenzie et al., 2014b. Yet, seagrasses have been found growing in waters up to 61 m deep in the GBR (Coles et al., 2009). However, the only *in situ* information about deeper inter-reefal seagrass spatial distribution known to the author is the biodiversity study by Pitcher (2007). The study found that there is a long band of mixed algae and patchy seagrass along the mid-shelf off Townsville. Further, Pitcher (2007) found that there is dense seagrass over much of the shelf in the Capricorn region, located in the southern GBR and around the Turtle Island Group, which is located in the central northern GBR (Pitcher, 2007).

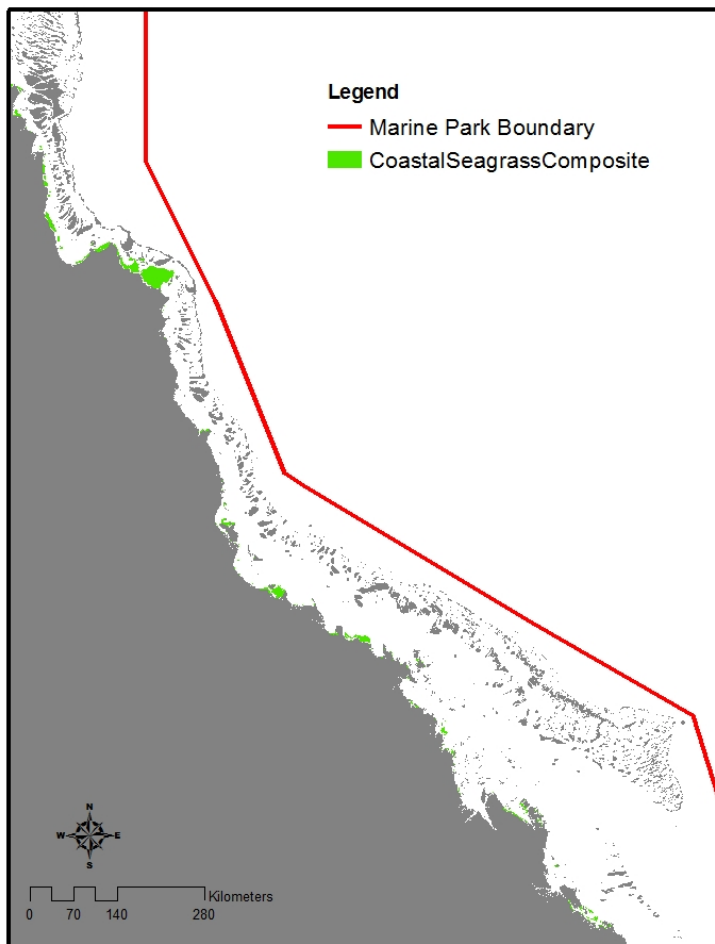


Figure 2-6: Seagrass distribution in the GBR (data from McKenzie et al., 2014b).

It is estimated that 600-700 species of benthic algae occur in the GBR, accounting for approximately one-third of the total macroalgal species recorded for the Australian continent (Diaz-Pulido et al., 2008). Despite this, the distribution and identification of macroalgae in the GBR system are still poorly resolved, with survey data often limited to gross characteristics (Examples: red, green and brown algae). The spatial distribution of benthic algae is highly variable, with occurrence and degree of cover varying between seasons (Diaz-Pulido et al., 2008). Pitcher et al., 2007 found that Halimeda algae are present in the northern GBR near Lizard Island, as well as in the central northern GBR, and the far northern GBR. Other types of algae can be found along some sections of the outer shelf in water up to 80-100 m deep (Pitcher, 2007). However, the lack of spatial information and the temporal variability of algae distribution in the GBR present an issue when mapping bottom cover for the input in SWIM. It is likely that annual and seasonal trends in algae cover can introduce errors in the parameterization of bottom reflectance in shallow water ocean color models and thus affect the retrievals of IOPs. In general, *in situ* information on biota in inter-reefal areas of interest for ocean color shallow water modelers is limited.

2.2.2.2 Non-biotic seafloor cover

Sand is the most broadly distributed sediment type in the GBR, covering 140,900 km²—more than 40% of the total 344,400 km² GBR Marine Park area (Mathews et al., 2007). Sand cover is spatially very variable across the GBR, but is generally higher on the outer shelf and in the south, while mud is more likely to occur in coastal areas (Mathews et al., 2007). Figure 2–7 (left panel) shows the percentage sand content distribution in the GBR. The same spatial variability of carbonate concentrations can be observed (Mathews et al., 2007). Carbonate is the dominant sediment type in the GBR, with high concentrations of above 60% covering 152,700 km²—nearly 45% of the total area (Mathews et al., 2007). Carbonate concentrations vary from approximately 20% near the coast to more than 80% on the middle and outer shelves (Mathews et al., 2007). Figure 2–7 (right panel) shows the percentage carbonate content in superficial sediments in the GBR. Carbonate sand is generally considered the brightest substrate (Reichstetter et al., 2015a) and therefore, has the greatest influence on the accuracy of IOP retrievals in shallow water environments.

Terrigenous sand originates from the land and is mainly found near the coast (Figure 2–7) (Scoffin and Tudhope, 1985), whereas carbonate sand is largely derived from corals and other calcifying organisms and is most abundant away from the coast, even though it can be found in most parts of the GBR (Scoffin and Tudhope, 1985).

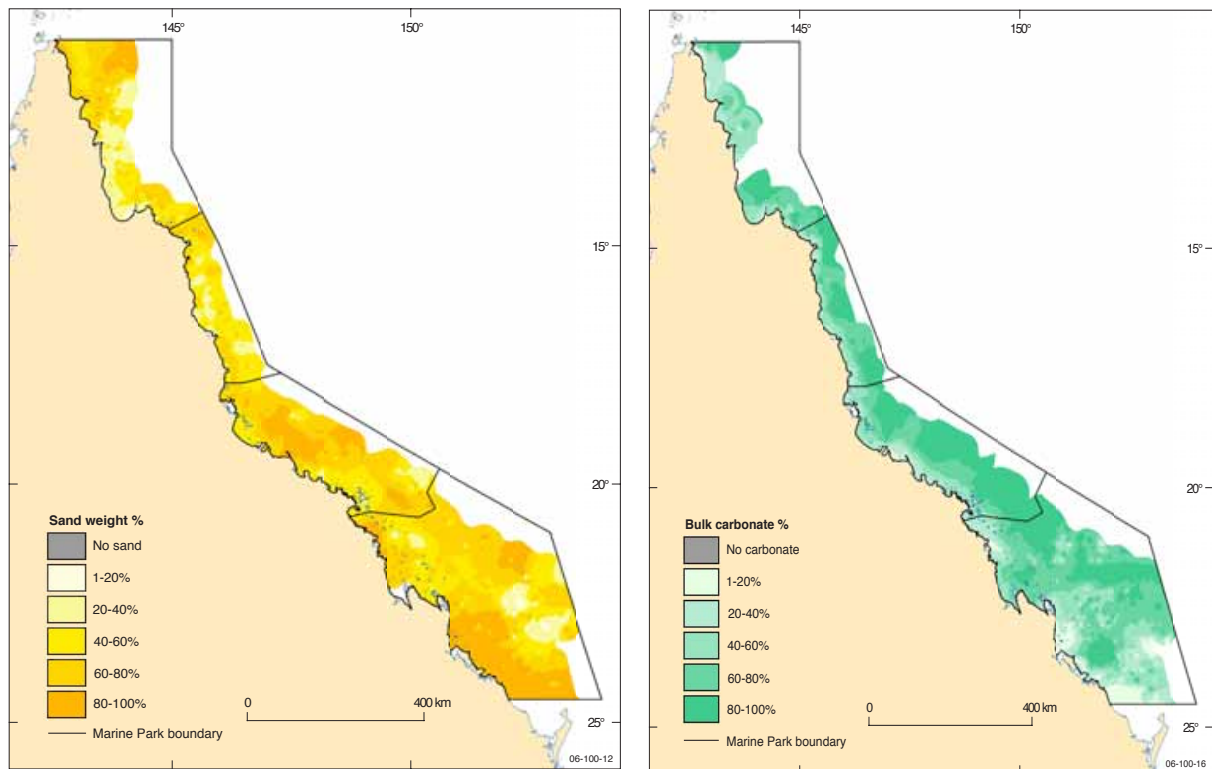


Figure 2-7: Percentage sand (left panel) and percentage carbonate sand (right panel) distribution in the Great Barrier Reef. The white areas along the eastern edge of the GBRWH area are in deep waters (>100 m) and do not impact shallow water remote sensing.

Figure 2–8 shows areas within the GBR where there is mostly hard or consolidated (rock) substratum recorded. Most of the rocky seafloor occurs on the outer shelf of the mid- and southern GBR (approximately 18-20°S). Rubble (5-50 mm) occurs mostly in the outer self and the coastal areas of the GBR, but is mainly recorded in the mid- and southern GBR.

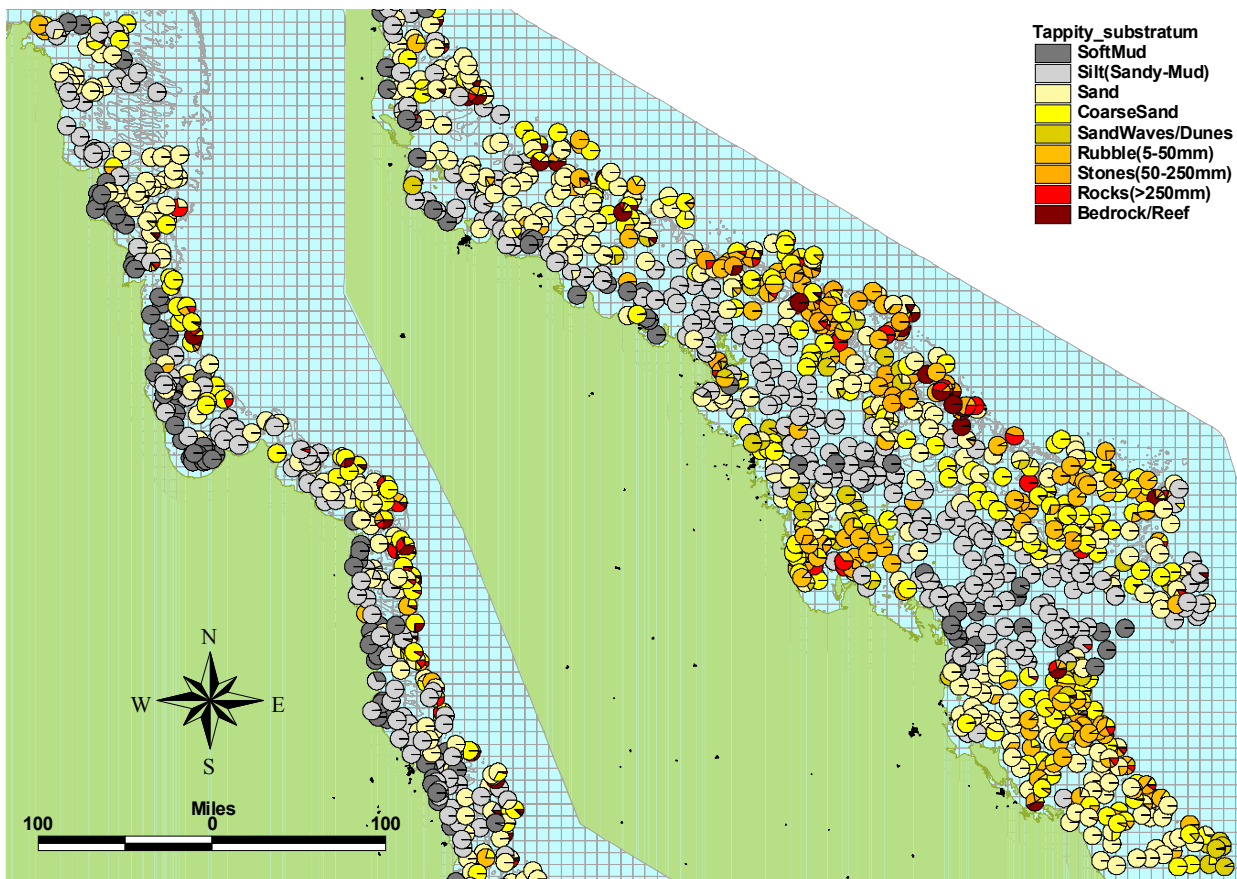


Figure 2-8: Map of the distribution of non-biotic seafloor cover types in the Great Barrier Reef summarized as a percentage of transect length as observed by towed video camera (from Pitcher, 2007).

2.3 Models

2.3.1 Hydrolight

Hydrolight is a commercial radiative transfer numerical model that computes radiance distributions and related quantities, such as irradiances, reflectances, diffuse attenuation functions and similar in a water body (Mobley and Sundman, 2008a). Hydrolight's inputs, such as water absorption and scattering properties, the sky conditions, and the bottom boundary conditions are highly adaptable and can be adjusted to user specifications (Mobley and Sundman, 2008a). For example, the user can choose to select a built-in bio-optical and sky model, or read in user-specific data, or write their own Fortran subroutines to define their input (Mobley and Sundman, 2008a). Hydrolight then solves the radiative transfer equation to calculate the in-water radiance as a function of water depth, direction, and wavelength. Other quantities of interest to this thesis, such as the water-leaving

radiance and remote-sensing reflectance, can also be computed using Hydrolight (Mobley and Sundman, 2008a). Detailed quantitative explanation of Hydrolight can be found in Mobley and Sundman (2008a).

2.3.2 Shallow water inversion model (SWIM)

SWIM is a semi-analytical ocean color model, which was developed specifically for IOP retrievals in shallow water. SWIM is constructed using the following three components: (i) a forward reflectance model, (ii) an inverse solution method and (iii) spectral IOP models (McKinna et al., 2015). The SWIM algorithm structure is similar to a general semi-analytical inversion model, but has a different forward reflection model (McKinna et al., 2015). The forward model analytically calculates the remote sensing reflectance, R_{rs}^{mod} (McKinna et al., 2015). A similarity matrix is then applied to compare R_{rs}^{mod} to R_{rs}^{obs} , the sensor observed spectra (McKinna et al., 2015). The IOP values returned when R_{rs}^{mod} best matches R_{rs}^{obs} . SWIM's forward model is based on Lee et al. (1998, 1999), (McKinna et al., 2015), however, within SWIM the bathymetry and seafloor reflectance values are given as input and thus result in the following forward model:

$$R_{rs}^{mod}(\lambda) = f(P, G, X) [sr^{-1}] \quad (2.1)$$

Where P is the magnitude of $a_{\phi}(443)$, G is the magnitude of $a_{gd}(443)$, and X is the magnitude of $b_{bp}(443)$. The scalar parameters P, G and X represent the magnitude of the IOPs, which are iteratively changed until the set convergence criteria is met, where the error between R_{rs}^{mod} and R_{rs}^{obs} is below the set threshold (McKinna et al., 2015). SWIM used the Levenberg-Marquardt optimization routine, to compare R_{rs}^{mod} and R_{rs}^{obs} and thus retrieve IOPs for a sensor –observed pixel (McKinna et al., 2015). For the simulations presented in this study SWIM's Levenberg-Marquardt error threshold was set to 1×10^{-6} . If the convergence criteria cannot be met the flag (PRODFAIL) is returned (McKinna et al., 2015).

The forward model within SWIM does use an input bathymetry dataset (McKinna et al., 2015). In this a spatially consistent gridded digital elevation model dataset as described in Section 2.2.1. Further, the SWIM forward model requires a seafloor reflectance map. Currently, the SWIM model is able to use two seafloor reflectance classes, which are classified as light and dark. Each class contains their own reflectance spectrum $\rho_L(\lambda)$ for

the light substrate class and $\rho_D(\lambda)$ for the dark substrate class. The net seafloor reflectance per pixel, $\rho_{net}(\lambda)$, is calculated using the following linear mixing model:

$$\rho_{net}(\lambda) = c_L \rho_L(\lambda) + c_D \rho_D(\lambda) \quad (2.2)$$

where c_L and c_D are the relative proportion of light and dark seafloor classes for a given pixel (McKinna et al., 2015). It is anticipated that SWIM will be able to include more substrate reflectance classes in the future (McKinna et al., 2015). Details of the seafloor reflectance maps used in this thesis can be found in the corresponding Chapters.

Including the bathymetry and seafloor reflectance maps as inputs in the model parameterization reduces two unknowns usually present in other semi-analytical ocean color models. The absorption and backscattering coefficients of optically-active constituent matter in the water column are calculated using the following spectral IOP models within SWIM:

$$a(\lambda) = a_w(\lambda) + a_\phi(\lambda) + a_{dg}(\lambda) \quad [m^{-1}] \quad (2.3)$$

$$b_b(\lambda) = b_{bw}(\lambda) + b_{bp}(\lambda) \quad [m^{-1}] \quad (2.4)$$

where the w , ϕ , p and dg are water itself, phytoplankton, particulate matter, colored dissolved and detrital matter, respectively (McKinna et al., 2015). The spectral IOP models in SWIM are parameterized the same as common semi-analytical ocean color models (McKinna et al., 2015).

CHAPTER 3 : BOTTOM REFLECTANCE IN OCEAN COLOR SATELLITE REMOTE SENSING FOR CORAL REEF ENVIRONMENTS

This chapter uses spectral signatures of common bottom types and radiative transfer modeling to assess bottom spectral separability and detectability at MODIS and SeaWiFS spectral bands. The results provide a basis for spectral signature selection and region of interest in ocean color shallow water models.

This chapter was published:

REICHSTETTER, M., FEARNES, P. R. C. S., WEEKS, S. J., MCKINNA, L. I. W., ROELFSEMA, C. & FURNAS, M. 2015a. Bottom Reflectance in Ocean Color Satellite Remote Sensing for Coral Reef Environments. *Remote Sensing*, 7, 16756-16777.

Main findings:

- No significant contamination ($R_{rs\text{corr}} < 0.0005$) was observed from bottom reflectance on the spectrally-averaged remote sensing reflectance signal at depths >19 m for the brightest spectral reflectance substrate (light sand) in clear reef waters.
- Bottom cover classes can be combined into two distinct groups, “light” and “dark”, based on the modeled surface reflectance signals.
- In Estuarine waters, low water clarity, bottom reflectance does not affect the remote sensing signal.

3.1 Introduction

Water clarity, or transparency, is an important characteristic of marine ecosystem health, affecting the primary resource (light) required by photosynthetic organisms. Ecosystems such as coral reefs and seagrass meadows are built by photosynthetic organisms, and are therefore highly sensitive to changes in water clarity (Fabricius, 2005). Recently, ocean color remote sensing techniques have complemented field sampling to monitor water clarity in coral reefs. Ocean color remote sensing allows large scale, synoptic water clarity monitoring where *in situ* physical sampling is difficult and costly (Weeks et al., 2012, Loisel et al., 2013). Satellite sensors provide spectral radiometric measurements of the color of the ocean that can be directly related to the relative concentrations of optically-active constituents, such as phytoplankton, dissolved organic matter or suspended particulate matter (Mobley et al., 2010).

Empirical and physics-based algorithms relate sensor-observed remote-sensing reflectance signals to *in situ* marine components. The radiative transfer problem of optically deep waters has been widely researched; with deep-water ocean color algorithms meeting NASA mission required accuracies for water-leaving radiance and chlorophyll-a retrievals, (Example: O'Reilly et al., 1998, Lee et al., 2002, Werdell and Bailey, 2005, Maritorena et al., 2002). On the other hand, deriving reliable ocean color products for optically shallow water masses, where light reflected from the seafloor contributes to the net water-leaving radiance, is more challenging and requires specialized algorithms. Water clarity monitoring of optically shallow waters using ocean color imagery data requires an understanding of the effects of bottom reflectance on the surface reflectance signal.

Initial efforts in the development of shallow water inversion algorithms focused primarily on the simultaneous retrieval of bathymetry and bottom cover. Less attention was given to the derivation of the inherent optical properties (IOPs) of the water column (Bierwirth et al., 1993, Dierssen et al., 2003, Louchard et al., 2002, Werdell and Roesler, 2003, Lee et al., 2010). More recently, effort has focused on the development of ocean color inversion algorithms for IOP retrievals in optically shallow waters (Wettle and Brando, 2006, Dekker et al., 2011, McKinna et al., 2015, Barnes et al., 2013).

One example is the newly developed Shallow Water Inversion Model (SWIM), currently implemented as an evaluation product in NASA's ocean color processing code, L2gen (McKinna et al., 2015). SWIM is based on the shallow water optical model of Lee et al. (1998); however, the SWIM algorithm does not retrieve water depth and bottom reflectance as free parameters. Instead, estimates of water column depth and benthic albedo (reflectance) are supplied to SWIM as ancillary data inputs. The current implementation of SWIM for the Great Barrier Reef (GBR), Australia, has been developed with the requirement of two specific regional input datasets, bathymetry and benthic albedo: Reliable bathymetry data at 100 m spatial resolution are available over the full extent of the GBR (Beaman, 2012). Prior to this study, an existing benthic biodiversity database (Pitcher, 2007) was used to derive the bottom reflectance signatures for a simple two-component "light" and "dark" reflectance map (Reichstetter et al., 2015b).

However, the optimal parameterization of bottom reflectance in shallow water inversion models is still not well constrained, particularly with respect to the spectral signature and number of required spectral classes. There remains a need to resolve spectral separability for current ocean color sensors to optimize bottom reflectance parameterization, and thus IOP retrievals in shallow water inversion models.

Quantifying the bottom reflectance contribution to the remote-sensing reflectance signals is challenging due to heterogeneous bottom cover and differences in spatial and spectral resolutions of common ocean color sensors. Current ocean color satellite sensors have limited capabilities to resolve bottom types or communities, such as sand, seagrass, algae or coral, due to the limited number and placement of their spectral bands (Lee et al., 2007). Most sensors have 6–15 spectral bands in the 400–1050 nm optical range, spatial pixel resolutions ranging from 250 m to 1.1 km and spatial swath extents of 1000s of kilometers. Whilst planned next generation satellite sensors with improved spectral and/or spatial resolution, such as the Pre-Aerosol Cloud and ocean Ecosystem (PACE) and the Ocean Land Color Instrument (OLCI) (Sentinel-3) missions (Malenovsky et al., 2012), may be able to better differentiate bottom cover spectral signatures, data acquisition from such sensors is still likely to be coarse, with pixels sizes of 300 m to 1 km in size.

Moderate resolution satellite sensors, such as the Moderate Resolution Imaging Spectroradiometer (MODIS), Medium Resolution Imaging Spectrometer (MERIS) and Sea-Viewing Wide Field-of-View Sensor (SeaWiFS), are currently used by the satellite remote sensing community due to ease of data accessibility and large spatial (global) and temporal (daily) coverage. Numerous previous studies have assessed the spectral separability of different bottom types based on pure endmembers (single organisms or substrate types) within a small area (<1 m²) (Andréfouët et al., 2001, Hochberg et al., 2004, Holden and LeDrew, 1998, Joyce et al., 2004, Kutser et al., 2006, Botha et al., 2013). Only a few such investigations, however, have assessed the impact of bottom type mixtures on the remote-sensing reflectance signal (Hedley et al., 2012, Leiper et al., 2011). Those studies have focused on higher spatial resolution sensors with pixel sizes of <50 m. Data from moderate resolution sensors are represented by 6 to 7 visible bands (Table 3–1) and relatively large pixel sizes (1 km × 1 km), which typically contain a mixture of bottom types in one pixel. Therefore, it is particularly important to assess the impact of mixed substrate pixels on their spectral separability, rather than analyzing single bottom covers.

The primary objective of this study therefore was to determine a reliable and efficient approach to select the optimal bottom cover spectral parameterization for shallow water inversion algorithms. Specifically, we have focused on shallow water inversion algorithms applied to moderate resolution ocean color remote sensing of coral reef environments by: (1) determining threshold depths at which the bottom reflectance signal of individual and mixed bottom types can contribute to the remote-sensing reflectance signal; and (2) determining the number of bottom spectral signatures required to accurately characterize bottom reflectance in shallow water inversion models. We applied the methodology to the MODIS and SeaWiFS spectral bands. Due to project restraints, MERIS data were not used in this study, however the methods are similarly applicable.

Table 3-1: Assessed band center and bandwidths (nm) used for the statistical analysis of spectral separability and detectability of bottom types.

Sensor	Band Center (Band Width) (units: nm)						
MODIS	412.5 (15)	443 (10)	488 (10)	531 (10)	551 (10)	667 (10)	677.5 (10)
SeaWiFS	412 (20)	443 (20)	490 (20)	510 (20)	555 (20)	670 (20)	

3.2 Data and methods

3.2.1 Methods overview

Radiative transfer modeling was used to determine the detectability and spectral separability of bottom cover classes through a variety of water column types. The radiative transfer model used, Hydrolight-Ecolight 5 (HE5) (Mobley and Sundman, 2008b), was parameterized based on combinations of IOPs, bottom reflectance, depth and sensor type. Output remote-sensing reflectances were then statistically analyzed to determine the detectability and spectral separability of bottom cover classes. The overall modeling approach is illustrated in Figure 3–1.

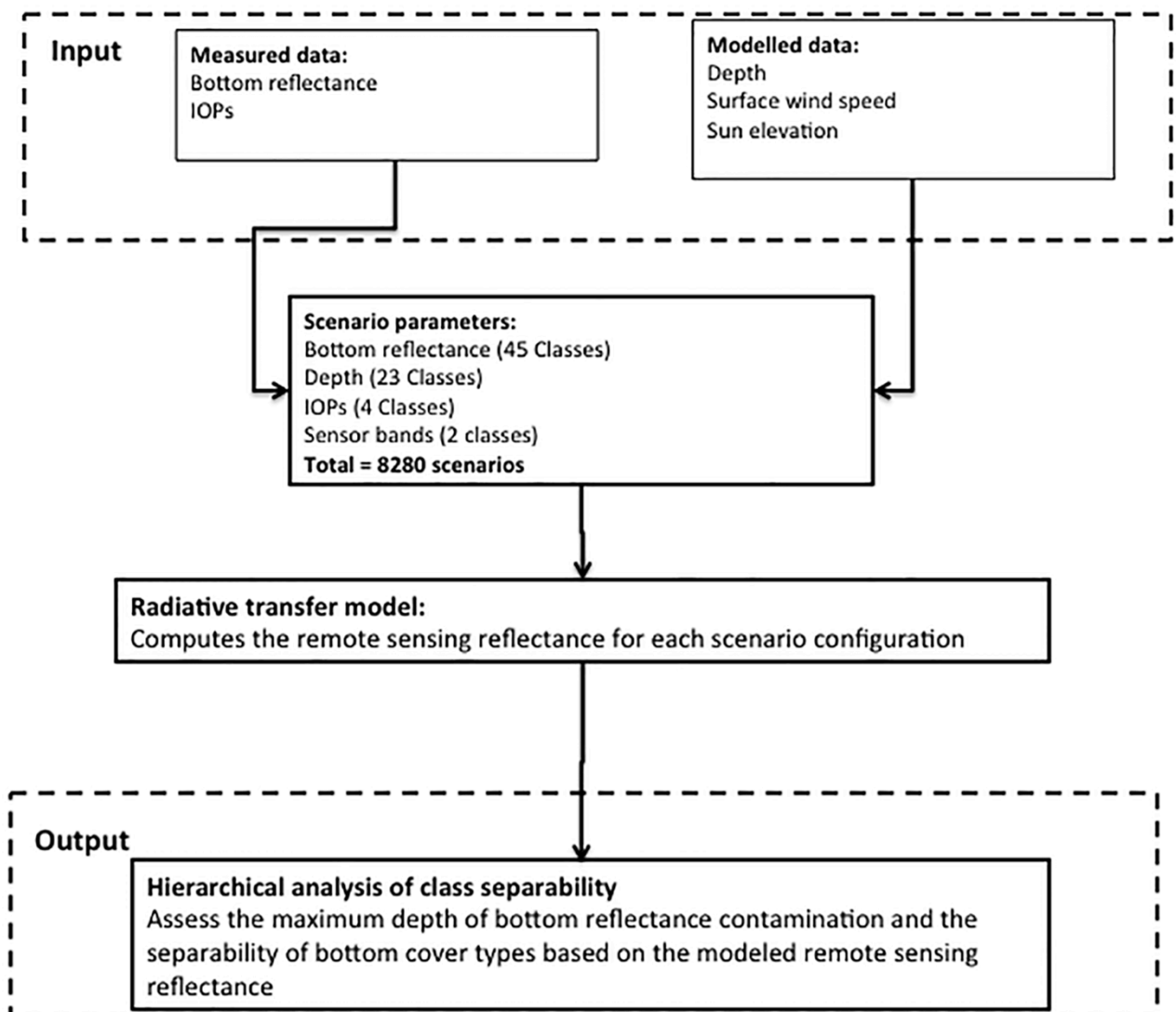


Figure 3-1: Flowchart showing an overview of the input variables for the radiative transfer modeling framework used to conduct a hierarchical analysis of the class spectral separability of common bottom types. The Hydrolight model scenario setup is further described in Table 3–2.

Table 3-2: Separability scenario description.

Input	Description
Bottom Classes (45 Classes)	
Light Sand (carbonate) Sand (largely terrigenous) Seagrass Rock Rubble Green Algae Brown Algae Live Coral	Eight endmember (pure bottom) classes were mixed with one another in 25% increments. We then selected 45 classes, eight pure endmember classes and 37 mixed classes. Each class was represented by five spectral reflectance signatures constructed as proportional linear mix from in situ data, except for the coral class, which had ten spectral signatures. A total of 230 bottom scenarios were tested (44 classes * 5 spectral signatures + 10 coral spectral signatures = 230 bottom cover scenarios). Spectra for the scenario classes were derived from existing sources [33–35].
Depth (23 Classes)	
5–49 m	The depth classes were in geometric depth, modeled in 2 m increments.
IOPs (4 Classes)	
Reef Waters (Dry Season) Coastal (Dry Season) Lagoonal (Dry Season) Estuarine (Wet Season)	The IOP parameters represent typical optically shallow water environments for the GBR, and were based on field data published in Blondeau-Patissier <i>et al.</i> [36]. As shown in Figure 2 below: “Reef Waters” were located on the outer shelf, within the reef matrix; “Coastal” data were from the inshore Whitsundays region; “Lagoonal” data were from shallow lagoonal stations in the Townsville region with no impact of any estuary or flood plume; “Estuarine” data were collected from the Mossman-Daintree region.
Sensors (2 Classes)	
MODIS SeaWiFS	The sensors were selected as commonly used in ocean color remote sensing.

The HE5 models spectral remote sensing reflectance (R_{rs}) based on user-specified geometric depth, spectral values of water column IOPs, and bottom reflectance. Here, HE5 was configured to calculate R_{rs} for the spectral bands of the SeaWiFS and MODIS sensors. We used built-in HE5 sensor spectral bands for MODIS and SeaWiFS, which include the sensor bands as well as some intermediate bands. For the statistical analysis of bottom type spectral separability and detectability, we only used the spectral bands listed in Table 3–1.

The R_{rs} values were calculated for each bottom class (i), IOP configuration (w) and specific sensor bands (W) at incremental depths (z) from 5 m to 49 m (see Table 3–2). A baseline model, where the bottom reflectance was set to zero (black/non-reflective), was used to calculate the water column contribution to the R_{rs} for each IOP, depth increment and sensor band combination.

Our study excluded depths shallower than 5 m, where benthic reflectance is likely to dominate the surface reflectance signal potentially causing sensor saturation. In these very shallow waters (<5 m), IOP retrievals are expected to be unreliable because the water column optical interactions contribute less to the remote-sensing reflectance than bottom reflectance. The deepest depth modeled, 49 m, was expected to be deep enough such that there would be no benthic reflectance contribution to the water-leaving signal.

To parameterize the spectral shape and magnitude of IOPs used in the HE5 simulations, the concentration of constituent matter (Chl and total suspended solids) and the spectral slope of the colored dissolved organic matter absorption coefficient were required. For this study, typical values for the four optical classes were based on *in situ* measurements in GBR waters, as reported by Blondeau - Patissier et al. (2009), with locations shown in Figure 3–2. Table 3–3 provides a summary of the constituent concentrations representative of the four optical scenarios used in our study. The built-in MODIS and SeaWiFS bands in HE5 were used to simulate the spectral R_{rs} signals for each scenario.

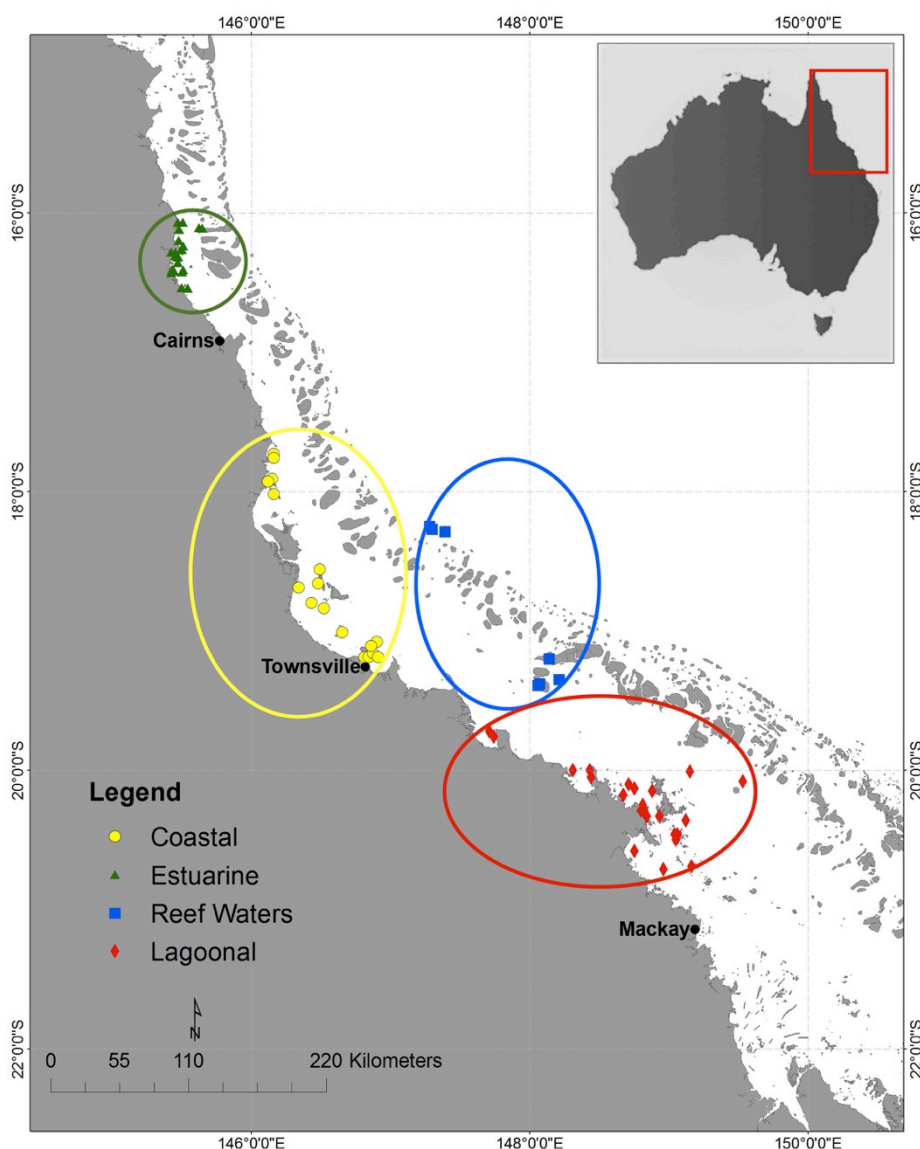


Figure 3-2: Map showing sampling locations for the four inherent optical property scenarios used: Coastal, Estuarine, Lagoonal and Reef Waters of the Great Barrier Reef (adapted from (Blondeau - Patissier et al., 2009)).

Table 3-3: Optically active constituent matter values used in Hydrolight 5 to calculate inherent optical properties. Values are from (Blondeau - Patissier et al., 2009).

Parameter	Abbreviation	Units	Estuarine	Lagoonal	Coastal	Reef
Chlorophyll concentration	Chl	mg·m ⁻³	3.165	0.441	0.7605	0.1345
Total Suspended Solids concentration	TSS	mg·L ⁻¹	11.63	3.65	6.35	1.4
Colored Dissolved Organic Matter Spectral Slope	S_{CDOM}	nm ⁻¹	0.016	0.0215	0.0185	0.0145

3.2.2 Bottom reflectance dataset

Our study used published datasets of *in situ* spectral reflectance signatures for selected biotic and abiotic coral reef features and communities from various global locations representative of coral reef environments. These environments included the GBR, Australia, Fiji, the Cook Islands and Belize (Roelfsema and Phinn, 2012, Roelfsema and Phinn, 2013, Hedley et al., 2012). The datasets comprised reflectance spectra of different bottom types obtained *in situ*, using a spectrometer in a custom-made underwater housing. All the bottom cover spectra were considered also representative of bottom cover classes occurring in the GBR. Eight endmember classes were selected: light sand (carbonate), darker (largely terrigenous) sand, rock, rubble, live coral, green algae, brown algae, and seagrass. These endmember classes were selected based on their frequency of occurrence in the GBR, and their potential spectral separability based on previous research (Kutser and Jupp, 2006, Hochberg et al., 2004, Hochberg et al., 2003, Leiper et al., 2011, Hedley et al., 2012, Hedley et al., 2004, Hedley and Mumby, 2002). The eight classes were then linearly mixed by percentage with each other in 25%:75%, 50%:50% and 75%:25% proportions, to provide a total of 84 mixed classes. The mixed bottom classes were calculated using two different bottom classes only (Table 3–4).

The following linear mixing method was applied:

$$M_i = \sum_{j=1}^n (R_{ij} \cdot F_j) \quad (3.1)$$

where $i = 1, \dots, m$ represents the number of bands, $j = 1, \dots, n$ is number of endmembers (for our study $n = 2$), M_i is the spectral reflectance of the i_{th} spectral band of a spectral mixture, R_{ij} is the spectral reflectance of the j^{th} component and F_j is the fraction coefficient of the j^{th} component.

A selection (47) of mixed bottom classes were then subjectively eliminated from further consideration because they are less common in shallow coral reef environments. For example, seagrass does not grow on coral or rock, and light sand does not generally occur in the same pixel as terrigenous sand. A total of 37 remaining mixed bottom classes were used in this study. Table 3–4 shows the assessed bottom classes, comprising eight endmember and 37 mixed classes, as well as mixed classes excluded from the study.

Table 3-4: Assessed endmember and mixed bottom classes, and excluded mixed bottom classes.

Assessed Endmembers (8 Classes)	
Coral (100)	Light sand (100)
Green algae (100)	Rock (100)
Brown algae (100)	Rubble (100)
Seagrass (100)	Sand (100)
Assessed Mixed Bottom Classes (37 Classes)	
Brown algae: Green algae (50:50, 25:75)	Sand: Coral (75:25)
Brown algae: Coral (50:50, 75:25)	Sand: Rock (50:50, 75:25)
Green algae: Coral (75:25)	Sand: Rubble (50:50, 75:25)
Light sand: Brown algae (50: 50, 75:25)	Sand: Brown algae (50:50, 75:25)
Light sand: Green algae (50: 50, 75:25)	Sand: Green algae (50:50, 75:25)
Light sand: Rock (50:50, 75:25)	Sand: Seagrass (50:50, 75:25)
Light sand: Rubble (50:50, 75:25)	Seagrass: Rubble (50:50, 75:25)
Light sand: Seagrass (50:50, 75:25)	Seagrass: Brown algae (75:25)
Light sand: Coral (75:25)	Seagrass: Green algae (75:25)
Rubble: Brown algae (50:50, 75:25)	Seagrass: Rock (75:25)
Rubble: Green algae (50:50, 75:25)	
Rubble: Coral (75:25)	
Excluded Bottom Classes (47)	
Brown algae: Green algae (25:75)	Rubble: Rock (50:50, 75:25, 25:75)
Brown algae: Coral (25:75)	Rock: Coral (50:50, 75:25, 25:75)
Coral: Seagrass (50:50, 75:25, 25:75)	Rock: Brown algae (50:50, 75:25, 25:75)
Green algae: Coral (50:50, 25:75)	Rock: Green algae (50:50, 75:25 , 25:75)
Light sand: Coral (50:50, 25:75)	Sand: Coral (50:50, 25:75)
Light sand: Brown algae (25:75)	Sand: Brown algae (25:75)
Light sand: Green algae (25:75)	Sand: Green algae (25:75)
Light sand: Rock (25:75)	Sand: Rock (25:75)
Light sand: Rubble (25:75)	Sand: Rubble (25:75)
Light sand: Seagrass (25:75)	Sand: Seagrass (25:75)
Light sand: Sand (50:50, 75:25, 25:75)	Seagrass: Rubble (25:75)
Rubble: Brown algae (25:75)	Seagrass: Brown algae (50:50, 25:75)
Rubble: Green algae (25:75)	Seagrass: Green algae (50:50, 25:75)
Rubble: Coral (50:50, 25:75)	Seagrass: Rock (50:50, 25:75)

The eight “pure” endmember classes were each represented by five field-measured spectra, except for the live coral class that was represented by ten field-measured spectra. The number of spectral signatures used was chosen based on data availability and quality for each endmember. For each mixed bottom class, five spectral signatures were calculated. The use of multiple sample spectra for each mixed and pure endmember class accounted for within-class variability. Figure 3–3 shows the “pure” endmember spectra used in this study, with light sand representing the brightest bottom cover, and green algae the darkest. In this study, we used seagrass to represent the darkest bottom cover as it is the most spatially distributed bottom cover in the GBR and hence most relevant to this study.

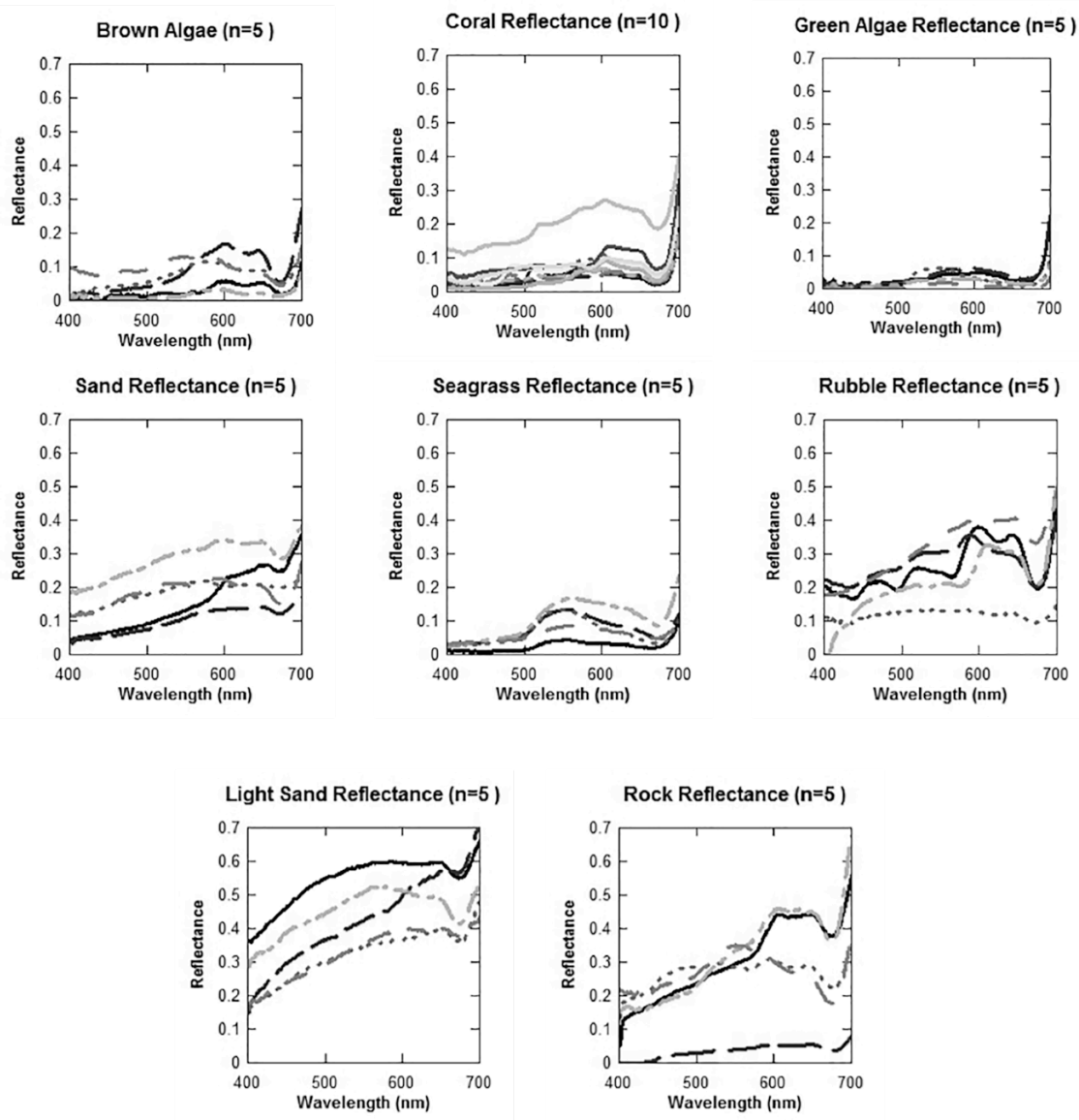


Figure 3-3: *In situ* reflectances for the eight pure endmember bottom types used in this study. Each line represents a sub-sample spectrum for the respective bottom type category.

3.2.3 Data analysis

HE5-modeled R_{rs} were used to determine: (1) bottom detectability, by calculating the difference between R_{rs} for a black bottom and R_{rs} for the substrate being tested; and (2) bottom separability, where separability was determined by cluster analysis of spectral characteristics of the substrate classes.

3.2.3.1 Maximum depth of bottom reflectance detectability

A water-column-only baseline scenario was simulated for each IOP and depth combination. This allowed us to ascertain the depth at which bottom reflectance becomes negligible in the R_{rs} signal. The water-column-only simulations were performed using a black bottom to represent a non-reflective seafloor. The resulting water-column-only remote-sensing reflectance spectra were then subtracted from R_{rs} modeled with a reflective seafloor, to give $R_{rs\text{corr}}$. We chose two reflective seafloors for this analysis: light sand and seagrass as representative of a light and a dark class, respectively, of the GBR shallow water environment. The band-averaged water column-corrected remote sensing reflectance, $R_{rs\text{corr},z,w}$ was calculated as follows:

$$R_{rs\text{corr},z,w} = \frac{\sum_{W=1}^n (|R_{rs\text{Albedo},z,w,W} - R_{rsB,z,w,W}|)}{n} \quad (3.2)$$

where $R_{rs\text{Albedo}}$ is the simulated remote sensing signal for the respective bottom type, light sand or seagrass, R_{rsB} is the modeled remote sensing reflectance using a black bottom, z is the water column depth, w is the IOP configuration, W is the sensor band, and n is the number of bands. We denoted the depth of maximum detectability (z_{max}) for each IOP scenario where the water column-corrected, band-averaged, absolute bottom reflectance signal was less than 0.0005 sr^{-1} or less than 2% of the maximum band-averaged, modeled R_{rs} (0.025 sr^{-1}). Assessment of the modeled data below this threshold showed uncorrelated noise, most likely due to bottom boundary conditions within Hydrolight and water column interaction.

3.2.3.2 Bottom cover separability

There are several approaches to compare and differentiate spectral signatures. Some of the most common are the Spectral Correlation Measure (SCM) (Gardner, 1986), the Spectral Angle Mapper (SAM) (Casal et al., 2011, Botha et al., 2013, Kutser and Jupp, 2006), spectral clustering (Kutser and Jupp, 2006), derivative analysis (Holden and LeDrew, 1998, Karpouzli et al., 2004), spectral mixture analysis (Van Der Meer, 1999, Goodman and Ustin, 2007) and linear discriminant analysis (Hedley et al., 2012). For this study, we were interested in both the absolute detectability of a bottom type and also the ability to spectrally distinguish one substrate type from another. For appropriate bottom reflectance parameterization, it was essential to know the number of different spectral classes and which spectral signatures were appropriate model inputs.

The similarity between pure endmember spectra and spectral mixtures, or between clusters of similar spectra, can be mathematically assessed using distance metrics such as the Euclidean distance, the spectral angle or the Mahalanobis distance (Sohn and Rebello, 2002). These metrics indicate which spectral features can be differentiated and/or identified by different satellite image processing methods. Here, a cluster analysis using the cosine dissimilarity (spectral angle) was used to quantitatively analyze the similarity and hierarchical clustering of our bottom reflectance spectra. The cosine similarity was used because it is widely accepted in the remote sensing research community for application in various disciplines (Kutser et al., 2006, Keshava, 2004, Kruse et al., 2003, Sohn et al., 1999, Lass et al., 2002, Sohn and Rebello, 2002). The cosine dissimilarity was calculated as follows:

$$S(x_i, x_j) = \cos^{-1} \frac{\sum_{k=1}^p x_{i,k} x_{j,k}}{\sqrt{\sum_{k=1}^p x_{i,k}^2} \sqrt{\sum_{k=1}^p x_{j,k}^2}} \quad (3.3)$$

where the cosine dissimilarity, S , is a metric based on the angle between two observations x_i and x_j , with p representing the number of spectral bands per observation. If the value for S is zero, the angle between the two modeled R_{rs} spectra is 90 degrees and they are dissimilar. If the value is one, the two modeled R_{rs} spectra have the same shape, but not necessarily the same magnitude.

This method provides a good estimate of spectral separability and has been used in a number of spectral classification studies, (Example: Casal et al., 2011, Kutser and Jupp, 2006). However, it is to be noted that the spectral angle is based on differences in spectral shape rather than magnitude.

First, the spectral angle algorithm was applied to the shallowest depth scenarios (5 m) to find the dissimilarity matrix based on each IOP and sensor combination for each of the 45 pure and mixed bottom classes. We only considered the shallowest depth as we expected the most separation between individual bottom classes here, hence providing the most detailed information for bottom reflectance parameterization. To account for possible within-class variability, the five (ten for live coral) spectral signatures per bottom class were analyzed as individual samples and not averaged for each class, providing a total of 230 sample spectra.

In a second step, agglomerative hierarchical clustering (Kaufman and Rousseeuw, 2009), was applied to the dissimilarity matrix to determine how many bottom sample spectra, as well as which spectra, could be differentiated. The agglomerative hierarchical clustering method is based on a series of fusions, where each bottom class spectrum (230) is considered as an individual cluster at the start. It then merges bottom spectra until all the substrate spectra belong to the same cluster. The clusters are merged based on the Ward's method (Batagelj, 1988), which calculates the total within-cluster variance.

Cluster accuracy, based on the modeled R_{rs} values, was interpreted using silhouette plots (Rousseeuw, 1987) to determine the optimal cluster configuration for each scenario set. A silhouette plot acts as a graphical means to identify how well each bottom type fits into the cluster to which it was assigned. Each cluster represents similarly modeled subsurface reflectance spectra. The silhouette plot allows one to compare how similar any one bottom class spectrum is to other bottom class spectra within its own cluster, as well as how close it is to bottom spectra in other clusters. In this study, the average silhouette width was used to select the appropriate number of clusters. The average silhouette width, also called the silhouette coefficient (SC), is a dimensionless measure quantifying the cluster structuring of the modeled remote sensing reflectance data. The silhouette width lies in the interval $(-1, 1)$.

Values near one mean that the bottom type spectrum is well placed in its cluster; values near zero mean that it is likely that the bottom spectrum might belong in some other cluster, while negative values mean that the bottom spectrum has been misclassified. Here, we used the silhouette width to determine how many bottom class spectra were distinguishable from each other. We compared the silhouette widths for different numbers of clusters, selecting the largest silhouette width to indicate the most appropriate number of clusters to use in the bottom reflectance parameterization.

3.3 Results

3.3.1 Cluster analysis of bottom classes and silhouette plots

Cluster analysis of modeled R_{rs} revealed that the most distinct spectral separation of the 230 modeled bottom cover spectra was achieved by separation into two clusters. These two clusters can be described as “light” and “dark”, with the light cluster mainly containing scenarios of light sand and light sand dominated mixtures, while the dark cluster consisted of the remaining bottom class spectra.

3.3.1.1 Results for MODIS spectral resolution

Figure 3–4 shows the silhouette plots for clustering of the modeled R_{rs} signals for 5 m deep Reef Waters at MODIS bands, with clusters visually separated by color from top-to-bottom. We present only the silhouette plots for the shallowest depth (5 m) where the sensors can differentiate spectral separation most distinctly. The number of spectra grouped into each cluster, as well as the mean cluster width, is indicated alongside each plot. We used the silhouette width to determine how many clusters optimally represented the different spectral classes. We compared the silhouette widths for different numbers of clusters and selected the largest silhouette widths as indicative of the most appropriate number of clusters (2–5) to use in the bottom reflectance map. The top-left silhouette plot in Figure 3–4, which displays the results for a two-cluster configuration, dark and light, (shaded black and grey, respectively), shows two distinct clusters for the 230 bottom sample spectra considered, with cluster silhouette average widths of 0.85 (123 spectra) and 0.69 (107 spectra). Only a few (5) bottom sample spectra were “misclassified” in this scenario, as shown by the negative tail at the base of the plot, indicating that they are outliers that cannot clearly be classified in the two-cluster structure (Note that misclassified bottom covers are still counted towards the respective cluster.)

The three-, four- and five-cluster results (top-right, bottom-left, and bottom-right, respectively in Figure 3–4) also clearly show two dominant clusters, with 123 of the 230 bottom sample spectra consistently grouped in Cluster 1 (C1) and between 107 and 90 bottom spectra grouped in Cluster 2 (C2). Only three to ten bottom spectra were assigned to each of the additional clusters, each with low average cluster widths (0.13 to 0.46), indicating poor separability.

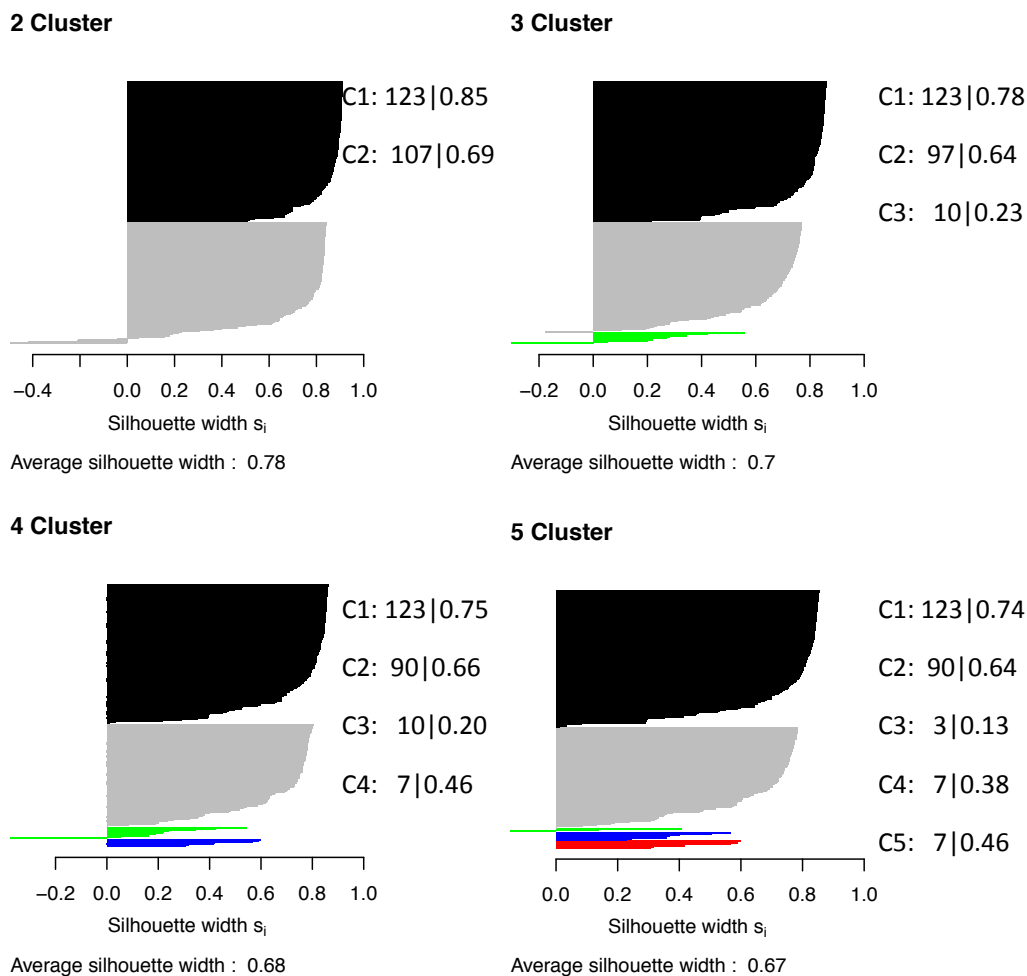


Figure 3-4: Silhouette plots for Reef Waters at 5 m geometric depth using MODIS bands. Each cluster is represented by a different color (Cluster-1 (C1)-Black, Cluster-2 (C2)-Grey, Cluster-3 (C3)-Green, Cluster-4 (C4)-Blue and Cluster-5 (C5)-Red). The cluster statistics represent the number of bottom spectra assigned to each cluster, followed by the cluster silhouette width. Misclassified spectra are counted toward the cluster they are assigned to but represented as negative, hence to the left of the graphics.

3.3.1.2 Results for SeaWiFS Spectral Resolution

Figure 3–5 shows the silhouette plots for the clustering of the modeled R_{rs} signals for 5 m deep Reef Waters, using SeaWiFS bands. The two-cluster configuration shows relatively high silhouette widths of 0.80 (130 spectra) and 0.77 (100 spectra) for the two clusters, C1 and C2, indicating strong within-cluster structures (Rousseeuw, 1987). The three, four and five clusters have lower silhouette widths for C3 to C5, ranging from 0.27 to 0.48. Overall, the cluster partitioning for the R_{rs} with SeaWiFS spectral resolution in 5 m deep clear Reef Waters were similar to those for R_{rs} with MODIS spectral resolution, namely that only two clusters presented a strong within-cluster structure. Any clusters beyond two resulted in silhouette widths less than 0.5, thus negligible or weak within-cluster structure was indicated (Rousseeuw, 1987). Further, these other clusters contained only a small number of bottom spectra (three to nine) compared to the two dominant clusters, as for the MODIS band results.

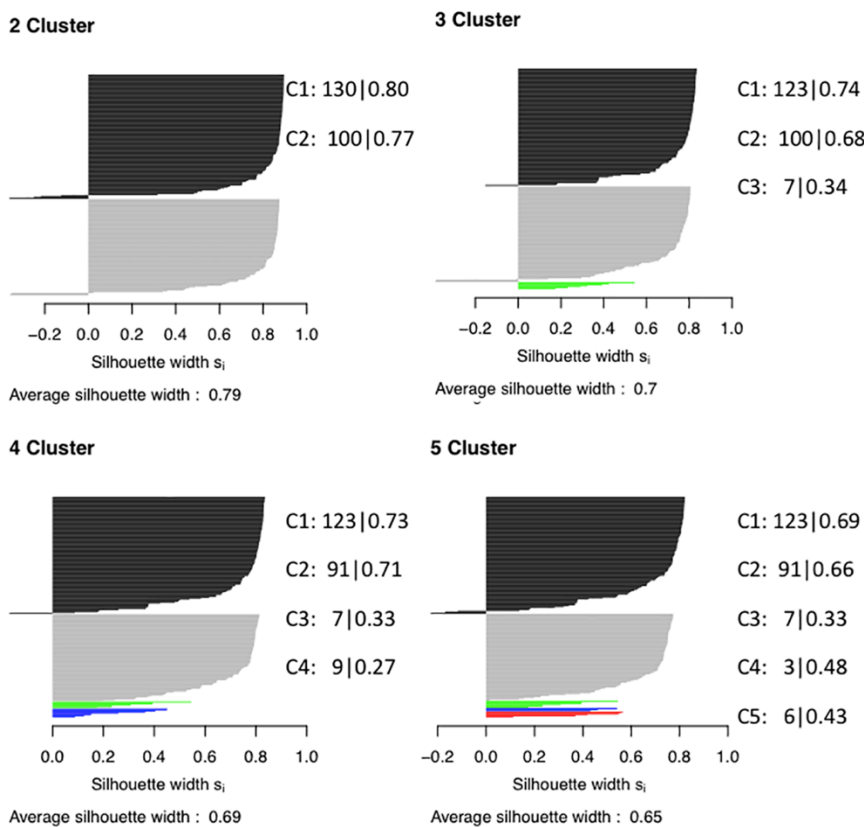


Figure 3-5: Silhouette plots for Reef Waters at 5 m geometric depth at SeaWiFS bands. Each cluster is represented by a different color (Cluster-1 (C1)-Black, Cluster-2 (C2)-Grey, Cluster-3 (C3)-Green, Cluster-4 (C4)-Blue and Cluster-5 (C5)-Red). The cluster statistics represent the number of bottom spectra assigned to each cluster, followed by the cluster silhouette width. Misclassified spectra are counted toward the cluster they are assigned to but represented as negative, hence to the left of the graphics.

3.3.2 Cluster analysis of bottom classes for different IOP scenarios

One may also consider the average width of all clusters in each analysis, and compare results for the different IOP scenarios. The average cluster width of all clusters is indicated underneath each cluster plot in Figures 3–4 and 3–5. The average silhouette widths are provided in Table 3–5 for each cluster configuration for each of the assessed IOP scenarios and satellite sensors at 5 m depth. With respect to MODIS bands, the average silhouette width was greatest for a two-cluster configuration for Reef Waters (0.78) and Lagoonal (0.76) IOP scenarios whereas, for the Coastal scenario, a three-cluster configuration resulted in the highest silhouette width (0.65). However, the two-cluster configuration was the only one that did not have any misclassified bottom spectra in the Coastal scenario. No bottom signal was detected at 5 m in Estuarine waters, thus no separation of bottom types resulted here. Examination of the individual silhouettes of each cluster showed that two clusters consistently contained the majority (>92%) of the bottom class spectra, with the remaining clusters containing only a few bottom spectra. For SeaWiFS, like MODIS bands, two clusters contained the majority (>93%) of the bottom classes and also had higher mean silhouette width values, indicating stronger within cluster agreement of the modeled remote sensing reflectances compared to the remaining clusters with much lower silhouette widths and therefore considered dissimilar.

Table 3-5: Average silhouette widths based on the different cluster configurations, where each cluster represents statistically similar modeled R_{rs} spectra for the four optical water types: Reef Waters, Lagoonal, Coastal and Estuarine.

Optical Scenario	2 Cluster	3 Cluster	4 Cluster	5 Cluster
MODIS				
Reef Waters	0.78	0.7	0.68	0.67
Lagoonal	0.76	0.69	0.69	0.69
Coastal	0.6	0.65	0.59	0.61
Estuarine	No separation possible			
SeaWiFS				
Reef Waters	0.79	0.7	0.69	0.65
Lagoonal	0.77	0.65	0.65	0.63
Coastal	0.66	0.63	0.65	0.62
Estuarine	No separation possible			

3.3.3 Cluster analysis and intermediate classes

The silhouette plots (Figures 3–4 and 3–5) presented clustering based on 230 sample spectra of the 45 bottom classes used in this study. However, some of the bottom classes might have had individual sample spectra assigned to two clusters.

For example, of the five sample spectra for the rubble bottom class, some might have been assigned to C1 and some to C2 and therefore the bottom class could not clearly be identified as belonging to C1, the dark cluster, or C2, the light cluster. Tables 3–6 and 3–7 show the individual 45 bottom classes assigned to the two dominant clusters based on the two-cluster partitioning of their sample spectra. Using the silhouette plots, we assessed how well each bottom class fitted into C1 or C2 and, where there were bottom classes which could not unambiguously be assigned to either C1 or C2, placed them in an “intermediary” cluster. The intermediary cluster category included classes where more than two of the five bottom class spectral signatures were assigned to the opposite class, and therefore no clear placement of the bottom class into C1 or C2 could be made. For SeaWiFS bands, the cluster analysis of the remote-sensing reflectance signal produced a higher number of intermediary classes ($n = 13$) than for MODIS bands ($n = 5$), which allowed for a clearer assignment of each bottom class to either C1 or C2 for MODIS bands. For the radiative transfer scenarios for SeaWiFS bands, a large proportion (~60%) of sand and rubble classes could not be clearly assigned to C1 or C2. In addition, fewer bottom classes (19) were assigned to C1, the dark cluster, in the scenarios modeled for SeaWiFS bands compared to MODIS bands (21), where more sand mixture classes were assigned to C1.

Table 3-6: Bottom class partitioning for the two-cluster configuration for MODIS bands. For example, Rubble: Green algae (50:50) refers to 50% rubble and 50% green algae mixed linearly to calculate the bottom spectra for that class.

Cluster 1-DARK (<i>n</i> = 21)	Intermediary (<i>n</i> = 5)	Cluster 2-LIGHT (<i>n</i> = 19)
Endmembers		
Coral (100)		Light sand (100)
Green algae (100)		Rock (100)
Brown algae (100)		Rubble (100)
Seagrass (100)		Sand (100)
Mixed bottom classes		
Brown algae: Green algae (50:50, 25:75)	Rubble: Brown algae (75:25)	Light sand: Brown algae (50: 50, 75:25)
Brown algae: Coral (50:50, 75:25)		Light sand: Green algae (50: 50, 75:25)
Green algae: Coral (75:25)	Rubble: Coral (75:25)	Light sand: Rock (50:50, 75:25)
Rubble: Green algae (50:50)		Light sand: Rubble (50:50, 75:25)
Rubble: Brown algae (50:50, 75:25)	Rubble: Green algae (75:25)	Light sand: Seagrass (50:50, 75:25)
Sand: Brown algae (50:50, 75:25)		Light sand: Coral (75:25)
Sand: Green algae (50:50, 75:25)	Sand: Coral (75:25)	Sand: Rock (50:50, 75:25)
Sand: Seagrass (50:50, 75:25)		
Seagrass: Brown algae (75:25)		
Seagrass: Green algae (75:25)	Seagrass: Rubble (50:50)	Sand: Rubble (50:50, 75:25)
Seagrass: Rock (75:25)		
Seagrass: Rubble (75:25)		

Table 3-7: Bottom class partitioning for the two-cluster configuration for SeaWiFS bands.

Cluster 1-DARK (<i>n</i> = 19)	Intermediary (<i>n</i> = 13)	Cluster 2-LIGHT (<i>n</i> = 13)
Endmembers		
Coral (100)	Sand (100)	Light sand (100)
Green algae (100)	Rubble (100)	Rock (100)
Brown algae (100)		
Seagrass (100)		
Mixed bottom classes		
Brown algae: Green algae (50:50, 25:75)	Sand: Rock (50:50)	Light sand: Brown algae (50:50, 75:25)
Brown algae: Coral (50:50, 75: 25)	Sand: Rubble (50:50)	Light sand: Rock (50:50, 75:25)
Green algae: Coral (75:25)	Sand: Rock (75:25)	Light sand: Rubble (50:50, 75:25)
Rubble: Green algae (50:50)	Sand: Brown algae (75:25)	Light sand: Seagrass (50:50, 75:25)
Sand: Brown algae (50:50)	Sand: Coral (75:25)	Light sand: Coral (75:25)
Sand: Green algae (50:50, 75:25)	Seagrass: Rubble (50:50)	Light sand: Green algae (75:25)
Sand: Seagrass (50:50, 75:25)	Rubble: Green algae (75:25)	
Seagrass: Brown algae (75:25)	Light sand: Green algae (50:50)	Sand: Rubble (75:25)
Seagrass: Green algae (75:25)	Rubble: Brown algae (50:50,75:25)	
Seagrass: Rock (75:25)		
Seagrass: Rubble (75:25)	Rubble: Coral (75:25)	

3.3.4 Detectability of bottom cover

The maximum depth of bottom detectability was found to be 17 m for MODIS and 19 m for SeaWiFS for light sand (the most reflective bottom cover considered) in the clear Reef Waters optical scenario of the GBR. In this paper, we present results for the light sand and seagrass bottom covers only: light sand represents the bright spectral reflectance substrate with the highest reflectance averaged over 400–700 nm of all coral reef bottom classes considered. Seagrass was chosen to represent the dark spectral group since it has a low spectral reflectance and occurs over considerably larger spatial scales in the GBR relative to green algae, the darkest spectral class (Figure 3–3).

The maximum depths of bottom detectability were similar for both MODIS and SeaWiFS sensors for both bottom classes. For the clear Reef Water optical scenario, light sand was detected at slightly greater depth using SeaWiFS (19 m) than when using MODIS (17 m), while the opposite was true for seagrass, which was detected at greater depth for MODIS (15 m) than for SeaWiFS (11 m) (Figure 3–6). For the Lagoonal optical scenario, the maximum depth at which light sand bottom reflectance was detected was 9 m for both sensors (Figure 3–6), while seagrass was detectable up to 7 m for SeaWiFS and 5 m using MODIS. For the Coastal and Estuarine scenarios, no bottom contamination was recorded using a seagrass bottom cover for either MODIS or SeaWiFS bands. For the Coastal optical scenario light sand bottom contamination was detected up to 7 m depth for both MODIS and SeaWiFS bands, while no bottom contamination was recorded for Estuarine optical scenarios for either sensor.

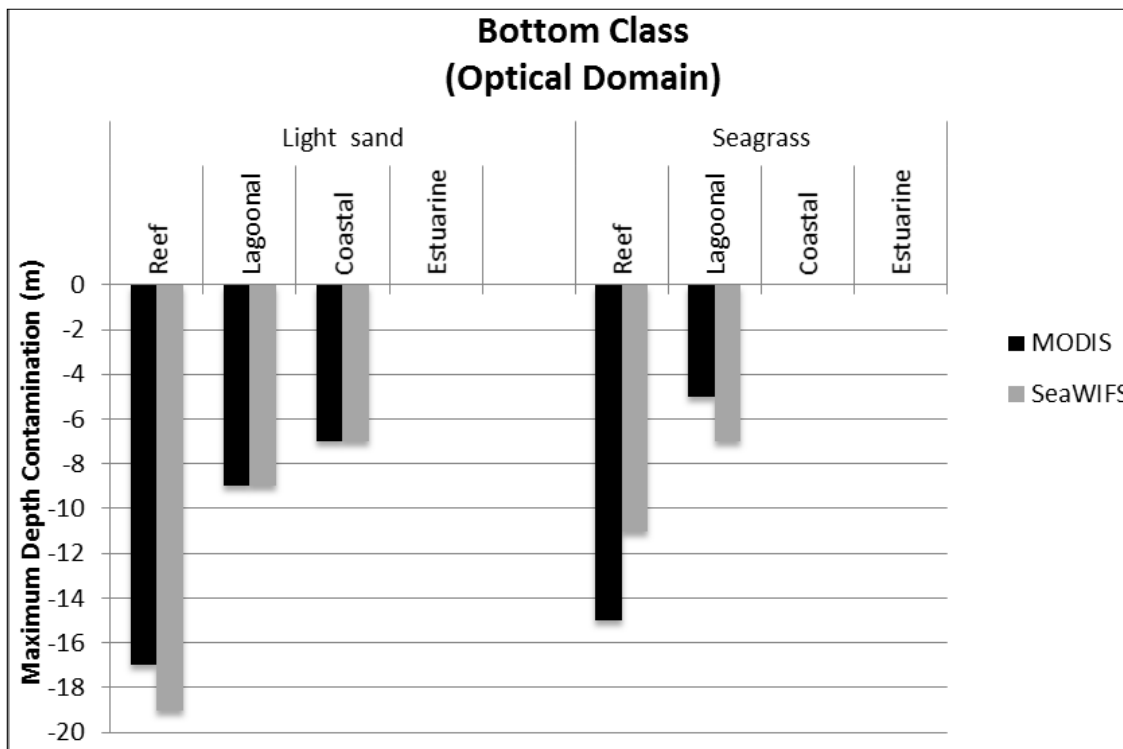


Figure 3-6: Maximum depth of detectability for light sand and seagrass under four different optical domain scenarios: Estuarine, Lagoonal, Coastal and Reef Waters for depths assessed between 5 m and 49 m.

The $R_{rs\text{corr}}$ values for MODIS and SeaWiFS are shown in Figure 3–7 for depths from 5 to 20 m for the four optical scenarios. The contribution of sand and seagrass bottom reflectance to the net remote-sensing reflectance was greatest for the Reef Waters optical scenario for both MODIS and SeaWiFS sensors. The $R_{rs\text{corr}}$ values for the Estuarine and Coastal optical scenarios were close to zero for light sand, even at shallow depths, as illustrated in Figure 3–7. For seagrass, the $R_{rs\text{corr}}$ values for the Estuarine, Coastal and also the Lagoonal optical scenarios were close to zero at all depths.

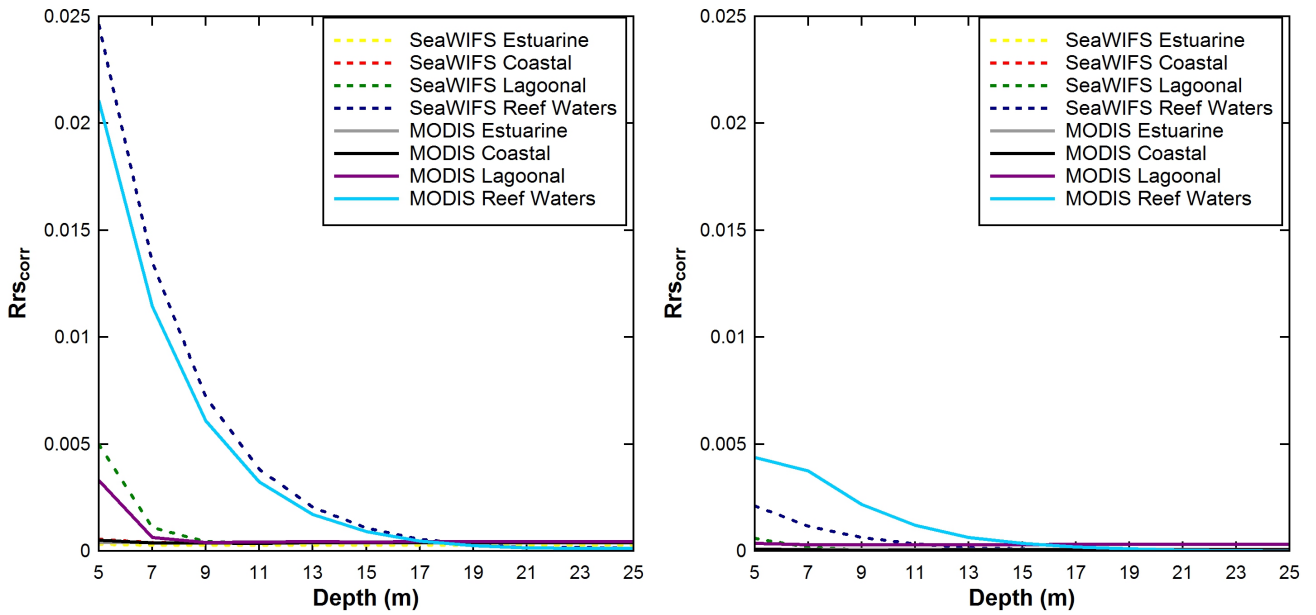


Figure 3-7: Water column-corrected (a black bottom scenario was subtracted from the model run), average surface reflectance signals for two extremes of substrate brightness: light sand (left panel) and seagrass (right panel) for the four optical water property scenarios for SeaWiFS and MODIS sensors. For light sand, the $R_{rs\text{corr}}$ values for the Estuarine and Coastal scenarios are close to zero even at shallow depths, while for seagrass, $R_{rs\text{corr}}$ values are close to zero at all depths for the Estuarine, Coastal and Lagoonal scenarios.

3.4 Discussion

This study assessed the influence of bottom reflectance on the spectrally-averaged R_{rs} signal measured by the moderate resolution SeaWiFS and MODIS sensors in optically shallow waters of coral reef environments. The results showed: (i) that there was no significant ($R_{rs\text{corr}} < 0.0005 \text{ sr}^{-1}$) influence of bottom reflectance on the R_{rs} signal for depths $>19 \text{ m}$ for either sensor; and (ii) that the assessed bottom cover classes can be amalgamated into two distinct functional groups, “light” and “dark”, based on the modeled R_{rs} surface reflectance signals. Only R_{rs} spectra dominated by light sand and its mixtures can be clearly discriminated from other bottom cover types typically found in coral reef waters.

SeaWiFS and MODIS R_{rs} data are routinely used to derive IOPs and a number of IOP-based geophysical products such as $chl-a$ and the diffuse attenuation coefficient (K_d). Light reflected off the seafloor in optically shallow waters contaminates the sensor-observed R_{rs} signal and subsequently causes errors in the derived IOPs. The recently-developed semi-analytical SWIM algorithm was specifically devised to improve IOP retrievals in optically shallow coral reef waters, such as the GBR.

An essential input component of the SWIM algorithm is a bottom reflectance map (McKinna et al., 2015). To construct a bottom reflectance map, it is essential to know the number of distinct spectral classes to be mapped and which spectra best represent these classes (McKinna et al., 2015). Further, it is useful to know in which geographic areas bottom reflectance is most likely to contaminate R_{rs} and therefore needs to be included in the bottom reflectance map. To address this, we determined the maximum geometric depth at which bottom reflectance may be detectable under different IOP/water clarity scenarios.

The maximum depth of bottom detectability for clear reefal waters of the GBR was determined to be 17 m and 19 m for spectrally-averaged MODIS band SeaWiFS bands, respectively. However, the depth of bottom detectability was reduced substantially in highly attenuating, inshore waters. Hence the SWIM algorithm may not need to account for bottom reflectance where the water column depth exceeds 19 m. We found bottom reflectance from seagrass, a relatively dark substrate, had no influence on spectrally-averaged R_{rs} at depths exceeding 15 m for MODIS bands and depths exceeding 11 m for SeaWiFS. Seagrass occurrence is prevalent in coral reef waters and has been recorded down to depths of 61 m in the GBR (Coles et al., 2009). In Estuarine waters, which are dominated by terrigenous runoff, particularly in the summer wet season, bottom reflectance contamination was found to be minimal and undetectable in waters >5 m. In Coastal water types, darker bottom covers such as seagrass were also undetectable at depths >5 m.

The minor differences in the maximum depth of bottom detectability between MODIS and SeaWiFS may be explained by the placement of their spectral bands. For example, for Reef Waters using the light sand bottom spectra, SeaWiFS provided a slightly deeper maximum depth than MODIS (19 m vs. 17 m), which is likely due to the placement and width of the assessed bands. The differences in the bands 490/488 (SeaWiFS band 3 and MODIS/Aqua band 10, respectively) and 555/551 (SeaWiFS band 5 and MODIS Aqua band 12, respectively) result in different radiance retrievals for these blue-green bands (Franz et al., 2005), which may have caused the minor differences in maximum depth of detectability. Further, the minor difference in maximum depth of bottom reflectance detectability might be due to band-averaging, as MODIS has two red bands compared to one for SeaWiFS.

In addition, our study used 2 m depth increments, thus the real difference in maximum depth of bottom reflectance detectability lies within a 0–2 m depth range. Even a 2 m depth difference in a 1 km × 1 km pixel is relatively minor and is not expected to make much difference to IOP retrievals using semi-analytical inversion algorithms.

We focused on the band-averaged maximum depth of bottom reflectance detectability to investigate to which depth MODIS and SeaWiFS satellite sensors could detect bottom signals affecting shallow water inversion models. We selected a cutoff threshold of 0.00005 sr^{-1} , which was 2% of the maximum, band-averaged, modeled remote sensing reflectance, 0.025 sr^{-1} . Anything below this threshold was considered noise. Therefore, one could argue that no signal from the bottom was recorded below this threshold. However, a minimal influence of benthic albedo was detected at the red bands ($>650 \text{ nm}$), where pure water absorption is high. The bottom reflectance contribution was primarily detected in bands at 488 nm, 531 nm and 551 nm for modeled MODIS R_{rs} and at 490 nm, 510 nm and 555 nm for modeled SeaWiFS R_{rs} .

The four optical environments used in this study are defined on the basis of chlorophyll, suspended matter and CDOM, rather than on the optical properties themselves. We acknowledge that the simulations of the optical properties are computed within HE5, using conversions to absorption, scattering and backscattering, and therefore may not be always appropriate in coastal waters. Further, it should be noted that at the resolution of MODIS and SeaWiFS, one would expect mixed depth pixels, as well as mixed bottom types. This might lead to increasing or decreasing detectability and separability of bottom types and thus lead to uncertainties in IOP retrievals.

However, to date there are no studies known to the authors that have ascertained the maximum depth at which MODIS or SeaWiFS-observed R_{rs} are contaminated by benthic reflectance despite these moderate resolution sensors being commonly used in near-coastal waters by the international scientific community. Some recently developed ocean color shallow water inversion models that retrieve IOPs, such as SWIM, require input of bottom reflectance parameters as model input. Hence, determining the maximum depth of bottom detection at moderate resolution sensor bands is essential to the implementation of shallow water inversion models to coral reef ecosystems.

Here, we presented the maximum depth of bottom reflectance contribution to spectrally-averaged R_{rs} for light sand and seagrass spectra only. We found these to represent two contrasting groups in coral reef waters, light *versus* dark substrates, based on their average spectral reflectance. Seagrass best represented the dark spectra group for the GBR as seagrass meadows can be thick and extensive there. Besides being the most common bottom cover of the dark spectral group in the GBR, seagrass is also closest to the average spectra of the dark spectral group. In the GBR, seagrass accounts for an estimated 40,000 km² of bottom cover (Schaffelke et al., 2005) compared to coral reef and algae cover of ~24,158 km² (Beaman, 2010), with the remaining ~280,242 km² (81%) of the GBR Marine Park comprising primarily sand and mud.

Clustering analysis showed that a two-cluster bottom reflectance input configuration, light and dark, is sufficient for parameterizing a shallow water inversion algorithm for MODIS and SeaWiFS sensors. Assessment of spectral uniqueness based on clustering showed that more clusters resulted in weak cluster structures and misclassified bottom types. Using several spectral samples for each bottom reflectance class allowed us to examine whether particular bottom classes might be ambiguously assigned to a specific cluster and hence misclassified. Modeled R_{rs} signals at MODIS bands assigned to two primary clusters allowed more consistent grouping of the individual bottom reflectances, with less bottom classes assigned to an “intermediary” cluster group, than at SeaWiFS bands. The intermediary cluster group contained bottom classes that could not be clearly assigned to C1 (dark) or C2 (light) because some of the five (ten for coral) spectral samples from one bottom class were assigned to C1 while others were assigned to C2. Using SeaWiFS bands, the majority of sand and rubble classes could not be clearly assigned to C1 or C2 as their spectral signatures lay between C1 and C2 (not as light as light sand but also not as dark as seagrass or similar). For either sensor, there was no bottom reflectance detected from seagrass for the Coastal or Estuarine optical scenarios, where the water is turbid, even at a shallow depth of 5 m. However, bottom contamination from light sand was still recorded in coastal waters by MODIS. The results provide insight into the optimal substrate clustering for bottom reflectance parameterization in shallow water models. The endmember and average spectra for the light and dark clusters are presented in the Appendix of this chapter.

To date, there have been no bottom cover spectral reflectance studies focusing on spectral separability or spectral uniqueness of bottom reflectance spectra at MODIS or SeaWiFS spectral and spatial resolutions known to the authors. Indeed, most comparative studies of bottom reflectance in shallow waters have focused on habitat classification mapping, (Example: Mumby et al., 1997, Kutser et al., 2003, Holden and LeDrew, 1998) that requires a greater level of spatial and spectral detail. At large, research on substrate spectral uniqueness has been undertaken using sensors with higher spatial resolution (pixel size <50 m and mostly <4 m) as they are commonly used to map benthic habitat or bathymetry at higher resolution (Example: Mishra et al., 2006, Stumpf et al., 2003, Kutser et al., 2006, Botha et al., 2013, Dekker et al., 2011, Brando et al., 2009). The spatial area imaged by these sensors is typically much smaller than the scale of larger coral reef ecosystems such as the GBR. Most high spatial resolution multi- and hyperspectral satellite-borne sensors do not have the temporal or spatial coverage provided by MODIS and SeaWiFS. Indeed, the broad swath and regular repeat orbits afforded by MODIS and SeaWiFS are needed to monitor and manage the ecosystem health of the GBR waters on a near-daily basis.

Higher resolution sensors are typically able to discern smaller objects, and image pixels often contain signals from a single substrate class. These smaller objects cannot be distinguished by MODIS or SeaWiFS satellite sensors, as image pixels frequently contain signals from a mixture of substrate types. In order for a homogeneous bottom cover to contribute to sensor-observed R_{rs} , its size has to be larger than several pixels in a specific satellite image. We made the assumption that, if the bottom cover extent was smaller than the pixel size, the signal detected represented the average brightness of all bottom covers in that pixel. Nevertheless, smaller percentages of particular types of bottom cover, such as small patches of sand between extensive seagrass beds, may be detectable if their reflectance signal dominates a particular pixel. MODIS and SeaWiFS have a coarser spatial resolution than most of the commonly used higher resolution satellite sensors (such as IKONOS, WorldView2, etc.). Thus, bottom covers considered in this study generally occur on spatial scales >1000 m and are not based on specific species per habitat classification, but rather classified into broader bottom classes, such as algae. A number of pure endmember bottom spectra were combined into mixed bottom types most commonly observed in the GBR at MODIS and SeaWiFS scales.

From an ocean color perspective, we may consider the GBR to be divided into three distinct zones based on water depth and geological features: (1) an inner shelf zone with a depth range of 0–20 m dominated by terrigenous sediment; (2) a middle shelf zone with a depth range of 20–40 m of mixed carbonate-siliciclastic sediment; and (3) an outer shelf zone with a depth range of 40–90 m of carbonate-dominated sediment (Belperio and Searle, 1988, Mathews et al., 2007). The maximum depth of bottom contamination of 19 m found in this study corresponds primarily to the inner shelf region of 0–20 m. This region, with a width of <60 km, is therefore of primary concern for benthic contamination in ocean color algorithms. Because of resuspension and other processes, this is also the zone where optically complex ocean color remote sensing challenges are the greatest. However, our results showed that the most significant bottom contamination is recorded from light (carbonate) sand, which is mainly found in the middle and outer shelf zones of the GBR (Belperio, 1983). Hence, this study suggests that the primary areas of concern for benthic contamination of the R_{rs} signal may be shallow waters adjacent to coral reefs on the mid- to outer shelf of the GBR, rather than the shallow inner shelf region.

3.5 Conclusions

This study has considered spectral separability or classification in the context of improving bottom cover benthic albedo (reflectance) parameterization in shallow water inversion models. To date ocean color algorithms have primarily been developed for moderate resolution sensors, such as MODIS or SeaWiFS, which are typically employed to provide data on the global oceans on a daily basis. It is well known by the research community that the frequency and placement of the current ocean color satellite sensor bands are inadequate and do not capture most of the variability of the remote sensing reflectance caused by differences in IOPs and bottom cover (Lee et al., 2007, Lee and Carder, 2002, Decker et al., 1992, Wernand et al., 1997). This study confirms that the separability of common bottom covers is limited using the existing set of visible bands of the MODIS and SeaWiFS satellite sensors. The only bottom cover group that could be confidently separated from other bottom cover classes was light sand and its mixtures. This separability deteriorated in Lagoonal and Coastal water optical scenarios. In Estuarine waters, no bottom cover class could be separated even though some bottom contamination was recorded up to 5 m depth. These findings are consistent with previous studies that noted that light and dark features can be separated, but finer class separability would require higher spectral resolution (Botha et al., 2013).

The results show that bottom reflectance in shallow water models only needs to be considered up to 19 m depth for MODIS and SeaWiFS based on spectrally averaged results. This would exclude a large area of the GBR, and similarly of other coral reef systems, which are deeper than 19 m and hence, not significantly affected by bottom reflectance. In addition, we can conclude that only two spectral signatures have to be considered in the parameterization of bottom reflectance in shallow water inversion algorithms when applied to sensors such as SeaWiFS and MODIS. A light and a dark spectral signature should provide sufficient detail to improve the IOP retrievals. The outcomes of this work will guide the development of improved bottom reflectance datasets required by shallow water ocean color inversion algorithms such as SWIM. Such improved parameterization will assist in better estimating how much light is reflected from the bottom, contaminating ocean color satellite imagery used for water clarity monitoring, and thus lead to improved retrievals of IOPs and water.

CHAPTER 4 : SENSITIVITY ANALYSIS OF BOTTOM REFLECTANCE PARAMETERIZATION IN SHALLOW WATER MODELS

The aim of this section was to assess how different bottom parameterization affects the IOP retrievals using SWIM. SWIM is a new shallow water inversion model, and it is not currently known how sensitive the IOP retrievals are to bottom reflectance parameterization. It is not intended to represent the actual IOPs in the GBR, but rather to demonstrate how differences in bottom parameterization affect IOP retrievals in time and space. To assess the sensitivity of IOP retrievals due to bottom reflectance under different water conditions experienced in the GBR study region, a time series of IOP retrievals was produced. Further, the sensitivity of IOP retrievals in different regions of the GBR was assessed.

Main findings:

- The sensitivity in IOP retrievals due to bottom reflectance parameterization was affected by water clarity conditions.
- IOP retrievals were affected by both the magnitude of the bottom type spectra and spectral shape.
- The influence of reflectance by different bottom types on SWIM retrievals of IOPs was greatest at depths shallower than 20 m.
- The differences in IOP retrievals due to changes in bottom reflectance parameterization showed both spatial and temporal variability.

4.1 Introduction

The usefulness of ocean color models depends on the accuracy and reliability of their output, yet all output values are subject to uncertainties and errors, because all models are abstractions of reality. Accurate input data are not always available. Inherent optical property (IOP) retrievals from remotely sensed ocean color data are frequently used or reported without well-researched or documented estimates of their uncertainties/sensitivities (Boss and Maritorena, 2006). Ideally, the uncertainties of ocean color products, such as IOPs should be determined through a comparison with sufficient *in situ* measurements (match-ups) (Werdell and Bailey, 2005). Match-ups are common for sea surface temperature products, where there are millions of match-up points available globally, as thousands of floats and buoys routinely measure sea surface temperature (Smith and Reynolds, 2004, Kilpatrick et al., 2001, Reynolds et al., 2002). However, there is no large database that would allow for a comprehensive match-up study using *in situ* IOPs in the GBR. Even though much effort has been directed into the generation of global databases used for validation of ocean color products (Fargion et al., 2002, Werdell and Bailey, 2005, Werdell et al., 2003), *in situ* IOP and chlorophyll data are expensive to collect and are usually not readily available (Werdell and Bailey, 2005). Thus, it is often not possible to conduct a comprehensive validation study to determine the level of uncertainty of an ocean color product.

Frequently, match-up analyses are only performed for a fraction of a sensor's records or spatial extent (Example: Antoine et al., 2008, Schroeder et al., 2007, Wang et al., 2009). Hence, ocean color match-ups often create only a snapshot, and generally do not account for spatial and temporal variability of the data (Boss and Maritorena, 2006). Additionally, there are uncertainties in input data, such as bottom reflectance, in shallow water environments. These uncertainties can vary both spatially and temporally. For example, input data might represent a dry period while the model is run for both dry and wet seasons. Spatial uncertainties can occur when input data is limited and is applied to a different region, such as when data from the northern Great Barrier Reef (GBR) is used for modeling the southern GBR. Thus, uncertainties of ocean color products, like IOP or chlorophyll retrievals, cannot be stated as a single global value, as they can change spatially and with time. It is important for the interpretation of ocean color products, to document uncertainties in IOP retrievals. None of the current shallow water ocean color inversion models, including the recently developed Shallow Water Inversion Model, SWIM

(McKinna et al., 2015), has published records of the uncertainties in bottom reflectance parameterization on the retrieval of IOPs.

In this chapter, a sensitivity analysis was undertaken to assess the potential uncertainty of water column IOP retrievals arising from uncertainties in bottom reflectance inputs in the SWIM algorithm. The GBR was used as the test region to assess the impact of bottom reflectance parameterization on IOP retrievals using the SWIM algorithm. Specific test regions have been described in Chapter 2 of this thesis. This sensitivity analysis does not address the accuracy of retrieved IOPs, but rather provides an insight into the potential effects of bottom reflectance parameterization on IOP retrievals. The results provide an overview of the complexity of bottom spectra and spatial resolution needed for the development of spatially explicit bottom reflectance maps, which are required as an input parameter to SWIM.

4.2 Data and methods

The aim of this study is to assess how different bottom spectral reflectance parameterization affects the IOP retrievals in SWIM. The researcher used *in situ* spectral reflectance data and SWIM modeling to assess the effect of bottom reflectance parameterization on IOP retrievals. The overall study design is shown schematically in Figure 4–1.

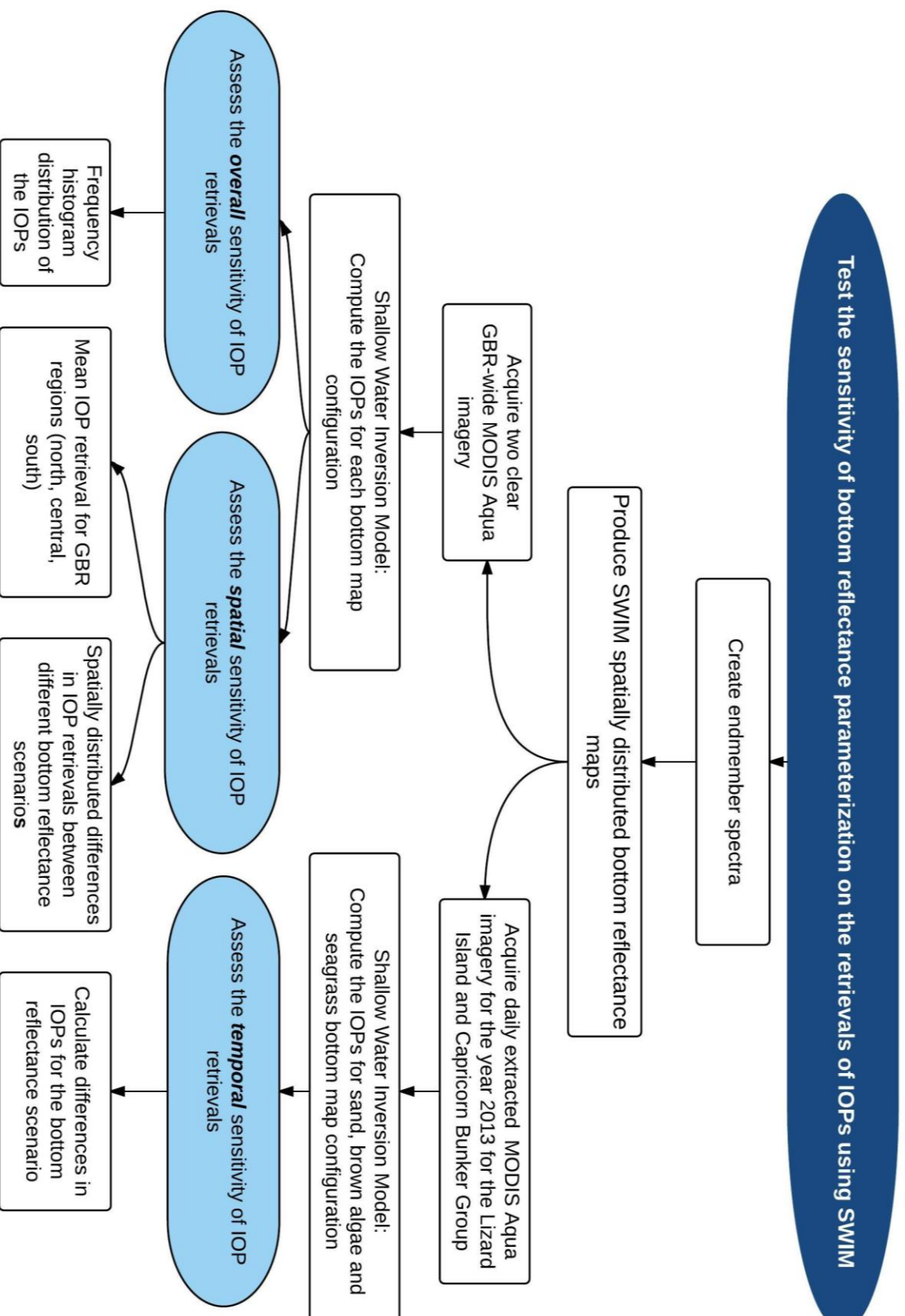


Figure 4-1 : Flowchart of the sensitivity analysis approach used in Chapter 4

4.2.1 Bottom reflectance scenarios

The SWIM algorithm (McKinna et al., 2015) is an implementation of the semi-analytical, non-linear search algorithm developed by Lee et al. (1998, 1999). SWIM has been incorporated into the NASA Ocean Biology Processing Group L2gen satellite data processing code (available as part of the SeaWiFS Data Analysis System (SeaDAS); <http://oceancolor.gsfc.nasa.gov>). The bottom reflectance parameterization in SWIM is defined as follows:

$$\rho(\lambda) = q_1\rho_1 + q_2\rho_2 + \dots + q_n\rho_n, \text{ where } q_1 + q_2 + \dots + q_n = 1 \quad (4.1)$$

where $\rho(\lambda)$ is the spectral bottom reflectance, n is the number of bottom types with unique reflectance spectra within the pixel, and q_n is the proportional area of bottom n within the pixel (McKinna et al., 2015). The researcher created bottom reflectance maps for the GBR to test the sensitivity of IOP retrievals from SWIM to changes in bottom reflectance parameterization. Each test map has a spatially-uniform bottom type coverage over the entire GBR. Seven scenarios were generated where 100% of the bottom type spectral signature was assigned to each pixel, while a further two scenarios were generated using mixed bottom types (sand and seagrass)(Table 4–1).

Table 4-1: Table of bottom reflectance scenarios

Bottom types	Percentage cover (%)
Sand (light)	100%
Seagrass	100%
Brown algae	100%
Green algae	100%
Coral	100%
Black	100%
White	100%
SandSeagrass1	Sand 75%, Seagrass 25%
SandSeagrass2	Sand 50%, Seagrass 50%

The black bottom reflectance scenario was selected to illustrate a completely non-reflective bottom type, while the white scenario shows a fully reflective bottom with the maximum possible spectral reflectance. The bottom reflectance spectra were derived from an average of *in situ* measurements from spectral libraries (Roelfsema, 2012b, Roelfsema and Phinn, 2013, Roelfsema, 2012a) for each bottom type, and are illustrated in Figure 4–2. The generated bottom reflectance scenarios were used as an auxiliary input dataset for the SWIM algorithm, using the SeaDAS L2gen processing code.

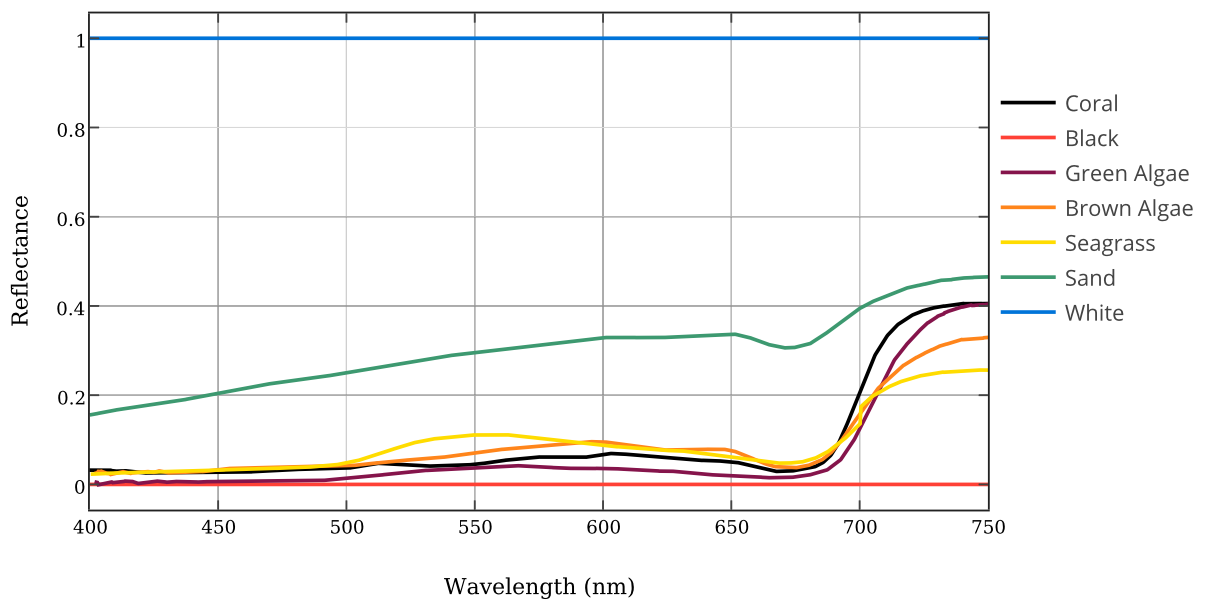


Figure 4-2: Spectral signatures used to generate the bottom reflectance scenarios in the sensitivity analysis

The data processing and analysis was divided into three parts: (a) **general** overview of the characteristic differences in IOP retrievals based on different bottom reflectance scenarios, (b) **spatial** differences in IOP retrievals using different bottom reflectance scenarios and (c) **temporal** differences in IOP retrievals under different bottom reflectance scenarios. The assessed IOP parameters of interest are presented in Table 4–2. The wavelength at 443 nm was chosen because it represents the chlorophyll absorption peak (Martin, 2014).

Table 4-2: Optical parameters derived from the SWIM algorithm using different bottom reflectance scenarios

Level-2 Products	Symbol	Units
Total absorption coefficient at 443 nm	a443	m ⁻¹
Backscattering coefficient of particulate matter at 443 nm	bbp443	m ⁻¹

4.2.2 Overview and spatial assessment of the sensitivity of IOP retrievals to bottom reflectance parameterization

4.2.2.1 Image processing

Two MODIS Aqua Scenes covering the entire GBR were selected for initial assessment. MODIS Aqua Level-1A data were downloaded for the 3 December 2005 (Scene 1) (Figure 4–3) and 09 August 2011 (Scene 2) (Figure 4–4) reflecting summer (wet) and winter (dry) conditions. These two images, in particular, were selected for their spatial coverage of the entire GBR with minimal cloud cover and apparent limited sensor noise. The scenes were processed using the SWIM algorithm within L2gen in its standard configuration. Different bottom reflectance scenarios were applied to each L2gen model run. A high-resolution digital elevation model for the GBR at a grid pixel resolution of 0.001-arc degree (about 100 m) (Beaman, 2012) was used as an auxiliary dataset required by the SWIM algorithm. The bathymetry dataset is described in Chapter 2 and is included in the SeaDAS software package. The generated Level-2 files were re-projected to WGS1984 for further analysis using the SeaDAS re-projection tool.

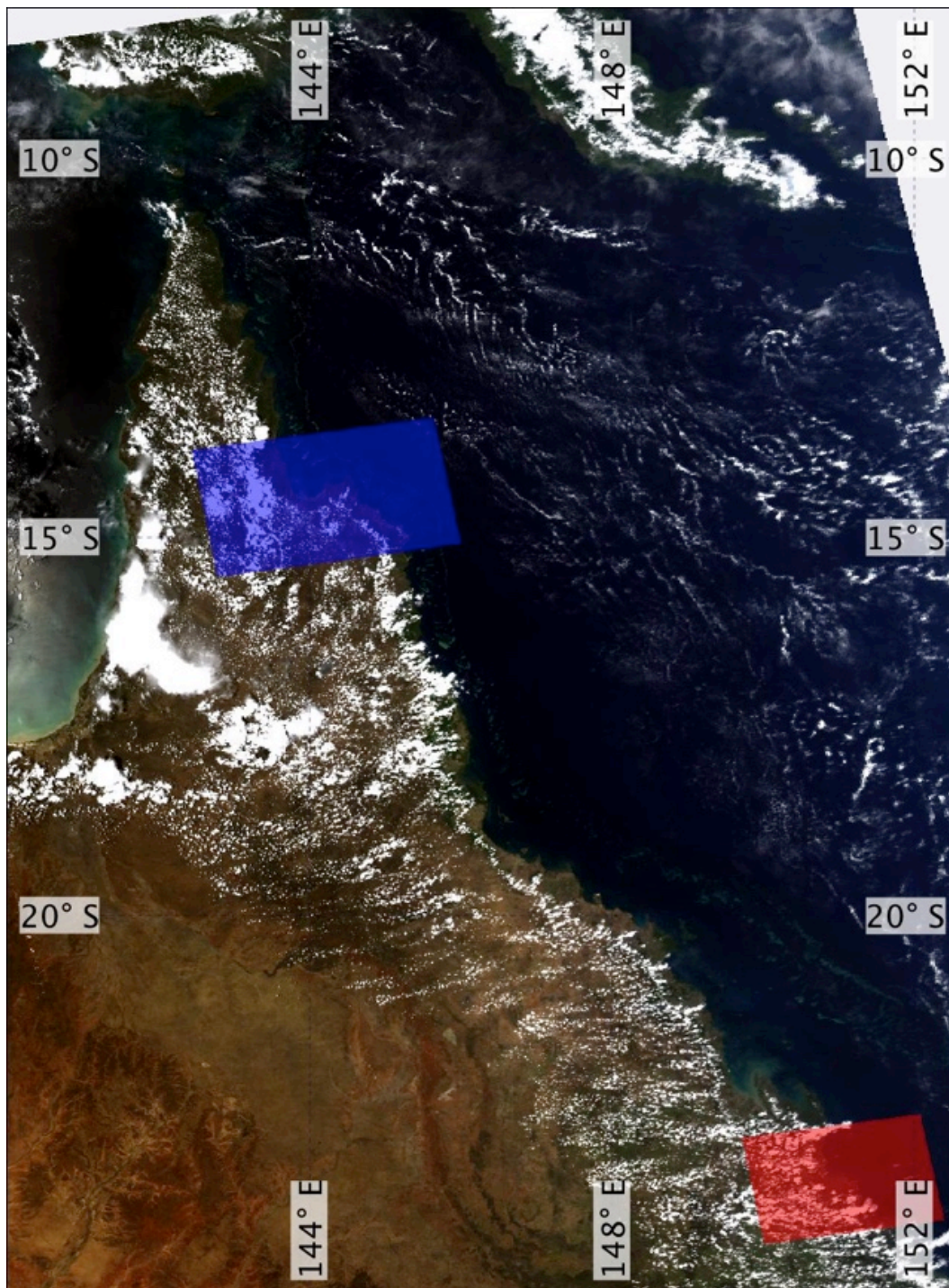


Figure 4-3: True color image of the selected MODIS Scene 1 (03 December 2005) processed using SeaDAS. The scene shows the Lizard Island (blue) and Capricorn Bunker (red) sub-regions used for time series analysis.

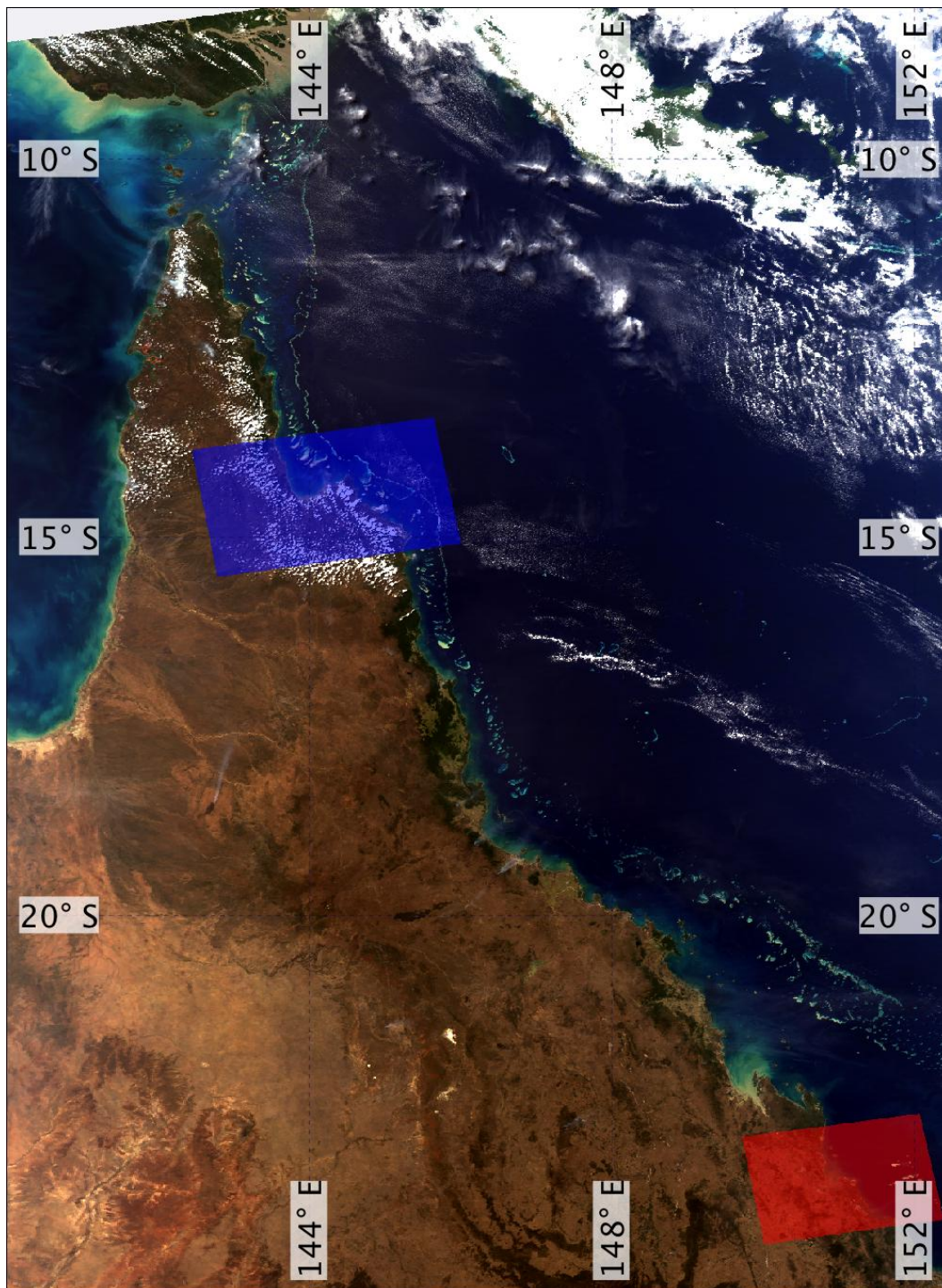


Figure 4-4: True color image of the selected MODIS Scene 2 (09 August 2009) processed using SeaDAS. The scene shows the Lizard Island (blue) and Capricorn Bunker (red) sub-regions used for time series analysis.

4.2.2.2 Data analysis

4.2.2.2.1 Analysis of overall sensitivity of IOP retrievals under different bottom reflectance scenarios

Frequency histograms were generated to assess the distribution and overall retrieved IOP values due to different bottom reflectance parameterization within the SWIM model. Frequency histograms of modeled a443 and bbp443 values, showing the number of pixels per scene at each different a443 and bbp443 value bins. The reprojected Level-2 scenes were collocated with the gbr100 bathymetry dataset to generate a region of interest (ROI) mask for the depths of interest, from 5 to 25 m. The histogram distribution of the number of pixels for the bottom reflectance scenarios was generated using the SeaDAS GUI histogram tool and the created ROI mask. To generate the histograms, the value ranges of a443 and bbp443 data within the region of interest for Scenes 1 and 2 were evenly divided into bins.

4.2.2.2.2 Spatial variability in IOP retrievals under different bottom reflectance scenarios

Analysis of mean IOP retrieval for GBR regions (north, central, south)

To assess the spatial differences in IOP retrievals under different bottom reflectance parameterizations, the GBR was divided into three sections: (1) the northern GBR (10 S to 15 S), (2) the central GBR (15 S to 20 S) and (3) the southern GBR (20 S to 25 S). Figure 4–5 shows the shallow water bathymetry (5 to 25 m) for the three GBR sections. First, the summary mean retrieved IOPs for pixels overlying five depth bins (5 to 8 m, 8 to 11 m, 11 to 14 m, 14 to 17 m and 17 to 20 m) for the generated Level-2 files for each of the bottom reflectance scenarios were computed (Table 4–1), using the zonal statistics Python code from the Supplementary Spatial Statistics Toolbox in the ArcGIS software (ArcGIS, 2011). Each depth in 3 m intervals was assigned to a zone using the raster depth mask created from the gbr100 bathymetry dataset. A one-way multivariate analysis of variance (one-way MANOVA) was conducted in SPSS to assess whether the mean retrieved IOPs were significantly different from each other (Field, 2009). A Tukey HSD test (Field, 2009) was also conducted to evaluate which of the mean retrieved IOPs were significantly different from the others.

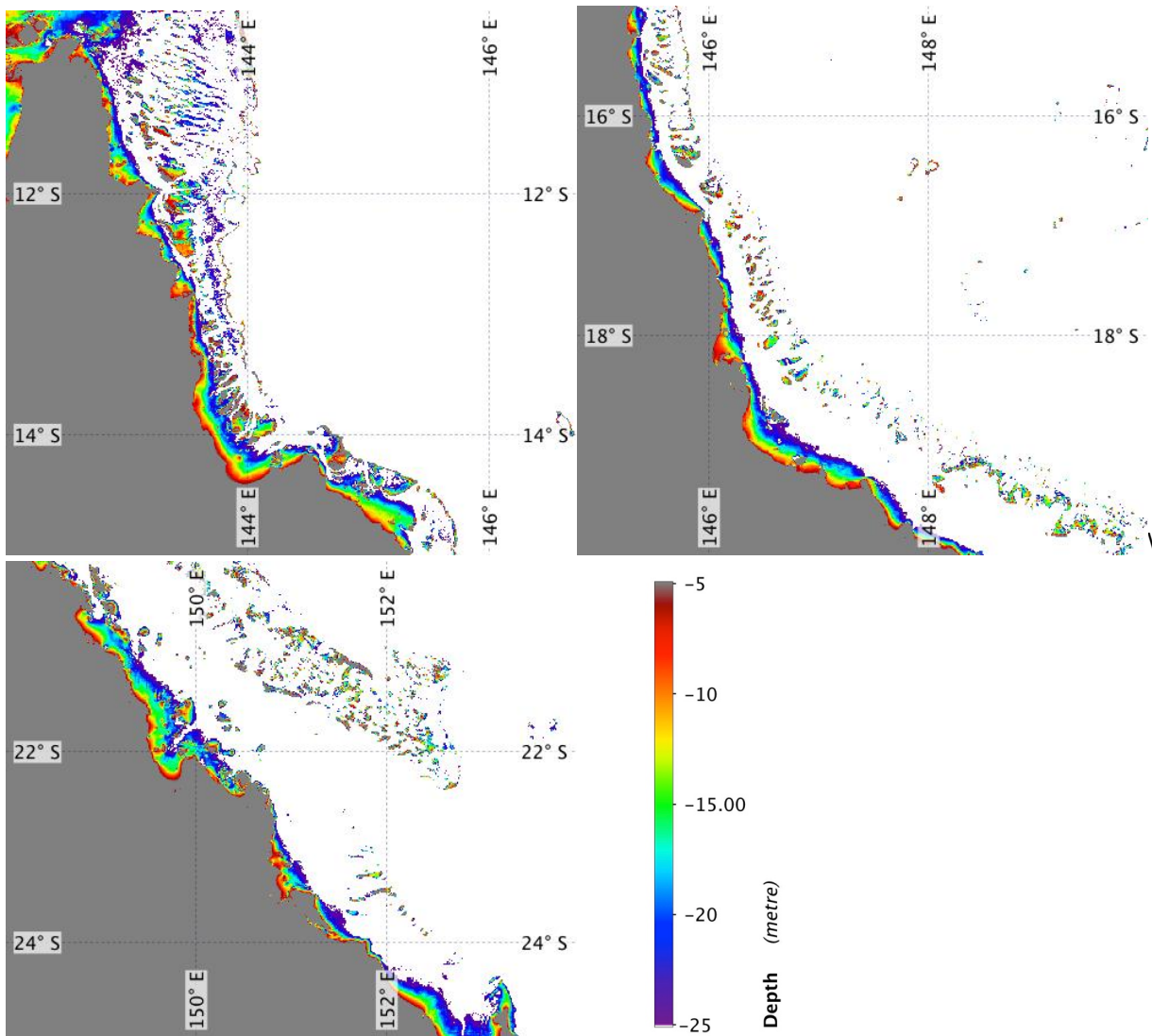


Figure 4-5: Shallow water bathymetry for the three sections of the Great Barrier Reef, the northern (top), central (center) and southern (bottom).

Analysis of spatially distributed differences in IOP retrievals between different bottom reflectance scenarios

To analyze the spatial differences in IOP retrievals due to bottom reflectance parameterization, two cases were considered. The first case compared the IOP retrievals from the black and white bottom reflectance scenarios with each other, subtracting the estimated IOPs of the black bottom reflectance scenario from that of the white bottom reflectance scenario, using the band math tool in the SeaDAS software (<http://seadas.gsfc.nasa.gov>). This provides the potential range in retrieved IOPs based on the differences between the brightest (maximum) and the darkest (minimum) bottom reflectance scenarios.

The second case was generated following the same procedure, but subtracting the IOPs generated from the seagrass bottom reflectance scenario from IOPs generated using reflectance from carbonate sand. Sand and seagrass are regularly used in ocean color algorithms for testing purposes (Example: Lee et al., 2001, Louchard et al., 2002).

4.2.3 Temporal assessment of the sensitivity of IOP retrievals to bottom reflectance parameterization

To assess the temporally-variable effect of bottom reflectance on IOP retrievals, time series analyses for two contrasting subregions were performed. Computational and time restraints precluded time series analyses of the entire GBR region. One of the test areas was located in the northern GBR, near Lizard Island (LI) [13.83°–15.06°S, 142.66°–145.78°E]. The second test region was located in the southern GBR and included the Capricorn Bunker Group of reefs (CB) [-22.82°–24.06°S, 149.74°–152.39°E] (Figure 4–3 and Figure 4–4). The time series test regions were chosen to illustrate the sensitivity of IOP retrievals under different oceanographic conditions (Steinberg, 2007, Burrage et al., 1996) and hence optical properties. Daily Level-1A MODIS Aqua data, from 01 January 2013 to 01 January 2014, were ordered from the NASA ocean color website (<http://oceancolour.gsfc.nasa.gov>) for the two test regions, LI and CB. The data were batch processed from Level-1A to Level-2 using SWIM within the SeaDAS L2gen processing code and its standard atmospheric correction (Ahmad et al., 2010, Bailey et al., 2010). The processed time series were then re-projected to WGS1984 and summary statistics were extracted in 1 m depth bins from 5 to 25 m, using the zonal statistics Python code from the Supplementary Spatial Statistics Toolbox in the ArcGIS software (ArcGIS, 2011).

4.3 Results

4.3.1 Overall sensitivity of IOP retrievals under different bottom reflectance scenarios

A total of 39,800 pixels for Scene 1 (03 December 2005) and 42,600 pixels for Scene 2 (09 August 2011) were included in the analyses of bbp443 and a443 pixel distributions. Overall, the distribution of the number of pixels in each bbp443 depth bin is very similar for all scenarios, except the white bottom reflectance scenario, in both scenes. However, the distribution of the number of pixels in each bbp443 depth bin is different between Scene 1 and 2. In Scene 1 there is a clear peak at $\sim 0.007 \text{ m}^{-1}$, while in Scene 2 the peak is less defined and broader (between $0.0003\text{-}0.01 \text{ m}^{-1}$) (Figure 4-6). Most of the pixels provided retrieved bbp443 values between 0 and 0.030 m^{-1} . In Scene 1, the highest number of pixels (4205) was recorded for the sand bottom reflectance scenario in the lowest bbp443 bin (0.00018 m^{-1}). The black bottom scenario only had 10 pixels in the 0.00018 m^{-1} bin. For the different bottom reflectance scenarios in Scene 2, sand also had the highest number of pixels (4425) in the lowest bbp443 bin (0.00018 m^{-1}) and the black bottom scenario had the lowest number (83) of pixels in the lowest bbp443 bin (0.00018 m^{-1}). The distribution of pixels to each bbp443 bin was nearly identical for the brown algae and seagrass scenarios for bbp443 values above 0.001 m^{-1} , in both scenes.

For Scene 1, the white bottom scenario contains 14220 pixels below 0.005 m^{-1} , while the black scenario only contains 4601 pixels, the seagrass scenario 8778 pixels and the sand scenario 14173 pixels below 0.005 m^{-1} . The brighter bottom reflectance scenarios (sand, sandseagrass1, sandseagrass2 and white) had a lower number of pixels falling in the bbp443 range between 0.005 and 0.016 m^{-1} (between 12389 and 21615 pixels), compared to the darker scenarios (between 23684 and 26593 pixels). Yet, the white bottom reflectance scenarios had about twice as many pixels (10917) in the bbp443 bins above 0.020 m^{-1} compared to the other scenarios, which all had between 4590 and 5302 pixels above 0.020 m^{-1} .

The mean bbp443 in Scene 1 was nearly equal at approximately 0.013 m^{-1} for the coral, seagrass and black, as well as brown and green algae bottom reflectance scenarios, while the sand and sand mixture bottom reflectance scenarios produced a lower mean bbp443 at approximately 0.012 m^{-1} .

For Scene 2, the white bottom reflectance scenario contained 13512 pixels below 0.005 m^{-1} , while the black scenario contained only 8381 pixels. The seagrass scenario contained 10340 pixels and the sand scenario, 15164 pixels below 0.005 m^{-1} . The brighter bottom reflectance scenarios (sand, sandseagrass1, sandseagrass2 and white) had a lower number of pixels falling in the bbp443 range between 0.005 and 0.016 m^{-1} (between 10359 and 17380 pixels), compared to the darker scenarios (between 19354 and 20732 pixels). The white bottom reflectance scenarios had about half as many pixels (10359) in the bbp443 bins between 0.005 and 0.016 m^{-1} , compared to the black bottom reflectance scenarios (20106 pixels). Yet, the white bottom reflectance scenarios had about 50% more pixels in the bbp443 bins above 0.020 m^{-1} compared to the other scenarios, which all had between 9003 and 10022 pixels above 0.020 m^{-1} . In Scene 2, the numbers of pixels per bbp443 bin were more similar than in Scene 1 through all the bottom reflectance scenarios. Scene 2 also had more pixels with a bbp443 value close to 0.00018 m^{-1} than Scene 1. Generally, the mean bbp443 values were higher for Scene 2 compared to Scene 1. The white bottom reflectance scenario produced the highest mean bbp443 value in both scenes. However, in Scene 2 most bottom types had close mean bbp443 values between approximately 0.017 - 0.018 m^{-1} . Seagrass had a higher mean bbp443 value (0.020 m^{-1}), compared to the algae coral, sand and sand mixtures scenarios.

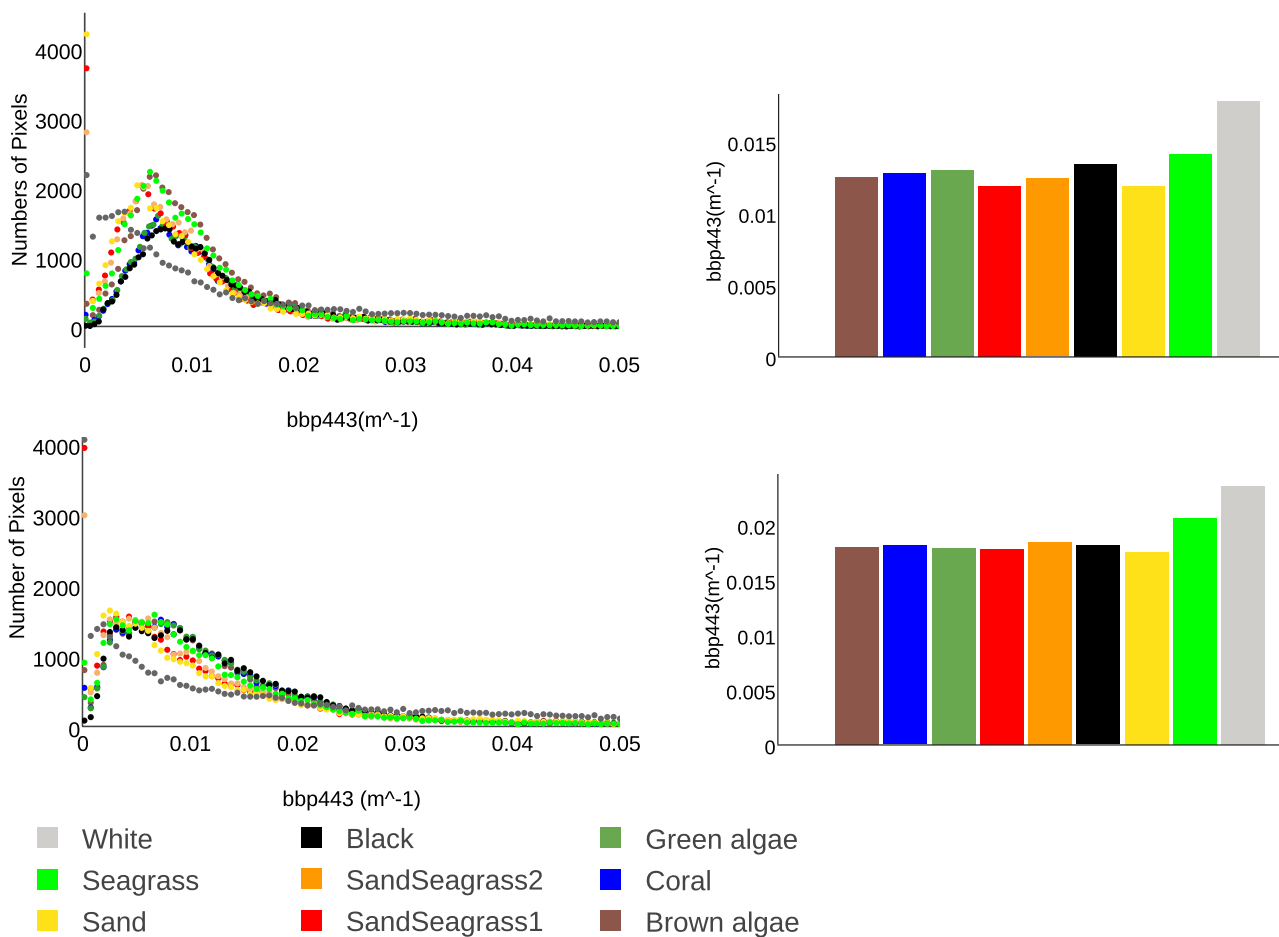


Figure 4-6: Region of interest (5 to 25 m depth) histogram distribution for backscatter coefficient at 443nm (bbp443) for Scene 1, (03 December 2005) (top), and for Scene 2, (09 August 2011) (bottom) and mean bbp443 values for each bottom scenario.

Considering absorption values from Scene 1, most pixels provided total absorption coefficient at 443 nm values between 0.02 to 0.180 m⁻¹, for all the assessed bottom scenarios (Figure 4–7). The white bottom spectra had the lowest number of pixels (71.46%) while the other scenarios had between 90.18% and 96.88% (between 0.020 and 0.180 m⁻¹). Yet, the white bottom scenario had the most pixels (7644) in the approximately 0.068 m⁻¹ a443 value bin. Only between 1% and 2% of the a443 pixels of the darker bottom scenarios (black, seagrass, coral, green and brown algae) were between 0.18 and 0.5 m⁻¹ in Scene 1. The white bottom scenarios had 16.05% of a443 pixels between 0.18 and 0.5 m⁻¹, while 4.31% of the a443 pixels of the sand bottom reflectance scenario were between 0.18 and 0.5 m⁻¹.

In Scene 2, the white bottom scenario also had the lowest number of pixels (63.95%) of total absorption coefficient at 443 nm values between 0.02 and 0.180 m^{-1} (Figure 4–7). The other bottom scenarios had between 83.02% and 89.38% of pixels with a_{443} values between 0.02 and 0.180 m^{-1} . In Scene 1, only between 3.57% and 6.19% of the a_{443} pixels of the darker bottom scenarios (black, seagrass, coral, green and brown algae) were between 0.18 and 0.5 m^{-1} . The white bottom scenarios had 16.57% of the a_{443} pixels between 0.18 and 0.5 m^{-1} , while 6.47% of the a_{443} pixels of the sand bottom reflectance scenario were between 0.18 and 0.5 m^{-1} .

Scene 2 had a slightly larger number of pixels towards the higher end of the a_{443} values (a_{443} between 0.180 and 0.500 m^{-1}) compared to Scene 1. Overall, while the peaks in the frequency of number of pixels for a_{443} under the different bottom scenarios were quite similar, the peaks in the frequency of number of pixels for the bbp_{443} values were less distinct and centered. The mean a_{443} was slightly higher in Scene 2 compared to Scene 1. Yet the distribution of the mean a_{443} was nearly equal for Scenes 1 and 2, with the white bottom reflectance scenario having the highest mean a_{443} value followed by sand, sand mixtures and seagrass. The black, coral and algae scenarios had nearly equal mean a_{443} values (approximately 0.100 for Scene 1 and 0.150 for Scene 2).

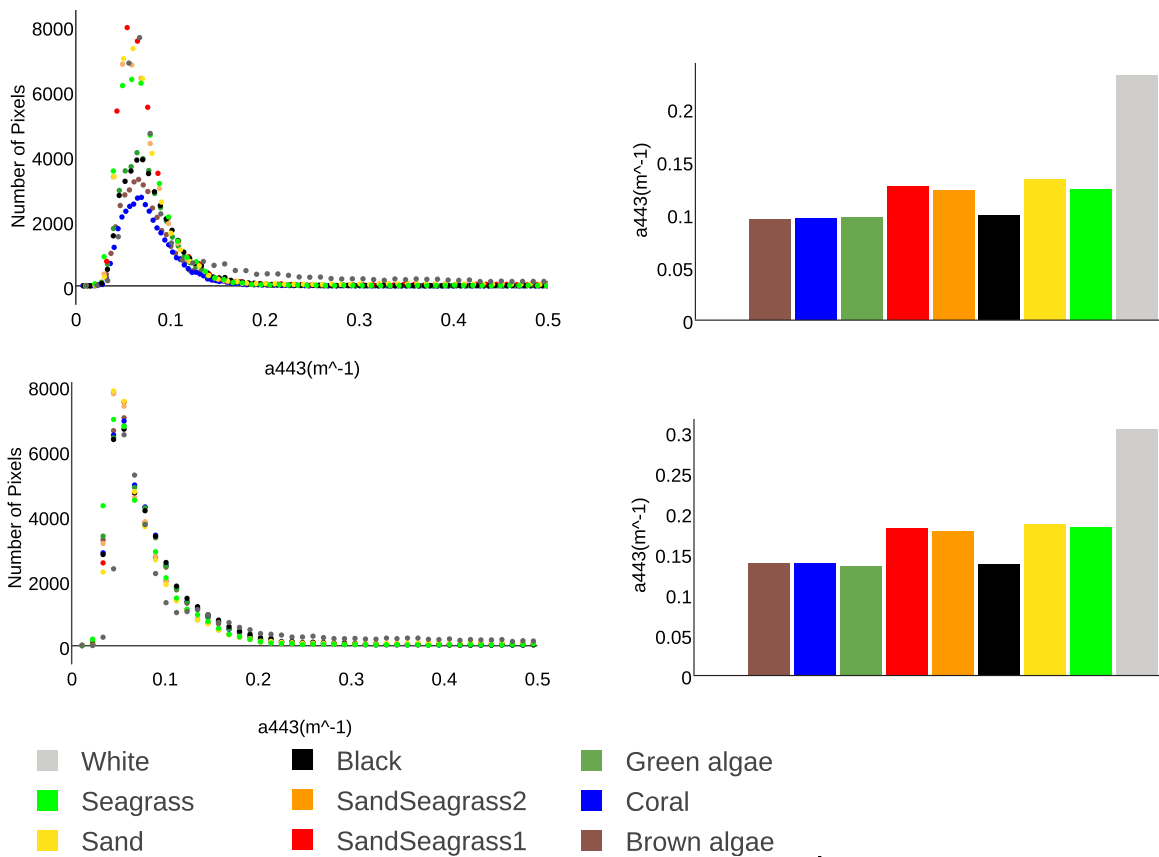


Figure 4-7: Region of interest (5 to 25 m depth) histogram distribution for absorption coefficient at 443nm (a_{443}) for Scene 1, (03 December 2005) (top), and for Scene 2, (09 August 2011) (bottom) and mean a_{443} values for each bottom scenario.

4.3.2 Spatial sensitivity of IOP retrievals under different bottom reflectance scenarios

4.3.2.1 Mean IOP retrieval for GBR regions (north, central, south)

Mean bbp_{443} was highest (0.04 - 0.068 m^{-1}) for the white bottom scenario for the shallowest depth range (5 to 8 m) (Figure 4–8). The mean retrieved IOPs are tabulated in Appendix A. Retrieved bbp_{443} decreased with increasing depth under all bottom reflectance scenarios. At depth 14 to 20 m retrieved bbp_{443} values become similar with a maximum difference of 0.003 m^{-1} in both scenarios and all regions. Only in Scene 2 in the northern GBR the white bottom reflectance scenario produces mean bbp_{443} value up to twice as high (0.015 m^{-1}) at 17 to 20 m depth compared to the other bottom reflectance scenarios. In Scene 1, significant differences between computed bbp_{443} between different bottom types were only observed in the 5-8 m and 8-11 m depth bins ($F(8, 18) = 7.703$; $p < 0.05$) and ($F(8, 18) = 8.433$; $p < 0.05$). The Tukey HSD test showed that the

mean bbp443 of the white bottom reflectance scenario was the only one that was significantly different ($p < 0.05$) from all the other tested bottom reflectance scenarios for the 5-8 m and 8-11 m depth bins only. The differences between mean retrieved bbp443 of all the other bottom reflectance scenarios were not significant ($p > 0.05$). There was a significant difference ($p < 0.05$) between the mean bbp443 of the regions (north, central and south) for the depth bins for 11-14 m ($F(2, 24) = 13.890$; $p < 0.05$), 14-17 m ($F(2, 24) = 97.293$; $p < 0.05$) and 17-20 m ($F(2, 24) = 142.600$; $p < 0.05$), in Scene 1. The Tukey HSD showed that there the south was significantly different from the north and central ($p < 0.05$), while the values for the central and north areas were not significantly different ($p > 0.05$).

In Scene 2, only the depth bin 5-8 m had a significant difference between bottom types ($F(8, 18) = 3.394$; $p < 0.05$). The Tukey HSD test showed that the mean bbp443 of the white bottom reflectance scenario was significantly different from the sand, sand mixtures and green algae bottom reflectance scenarios at depth 5-8 m ($p < 0.05$). The differences between all the other bottom reflectance scenarios were not significant ($p > 0.05$). There was a significant difference ($p < 0.05$) between the mean bbp443 of the regions (north, central and south) for all depth bins, in Scene 2. The Tukey HSD showed that there was no significant difference in the mean bbp443 ($p > 0.05$) between north and central in the 17-20 m depth bin, while significant differences were found between north and south and central and south ($p < 0.05$). For the 14-17 m and 8-11 m depth bins, there were significant differences between all the regions ($p < 0.05$). At depths between 11-14 m, on the other hand, there was no significant difference in mean bbp443 between central and south ($p > 0.05$), while significant differences were found between south and north and central and north ($p < 0.05$). For the 5-8 m depth bins, there was no significant difference in mean bbp443 between north and south ($p > 0.05$), while the differences were significant between south and central and north and central ($p < 0.05$). For both scenes and all regions, means of estimated bbp443 were very similar for the coral, brown algal and green algal bottom type scenarios across all depth ranges.

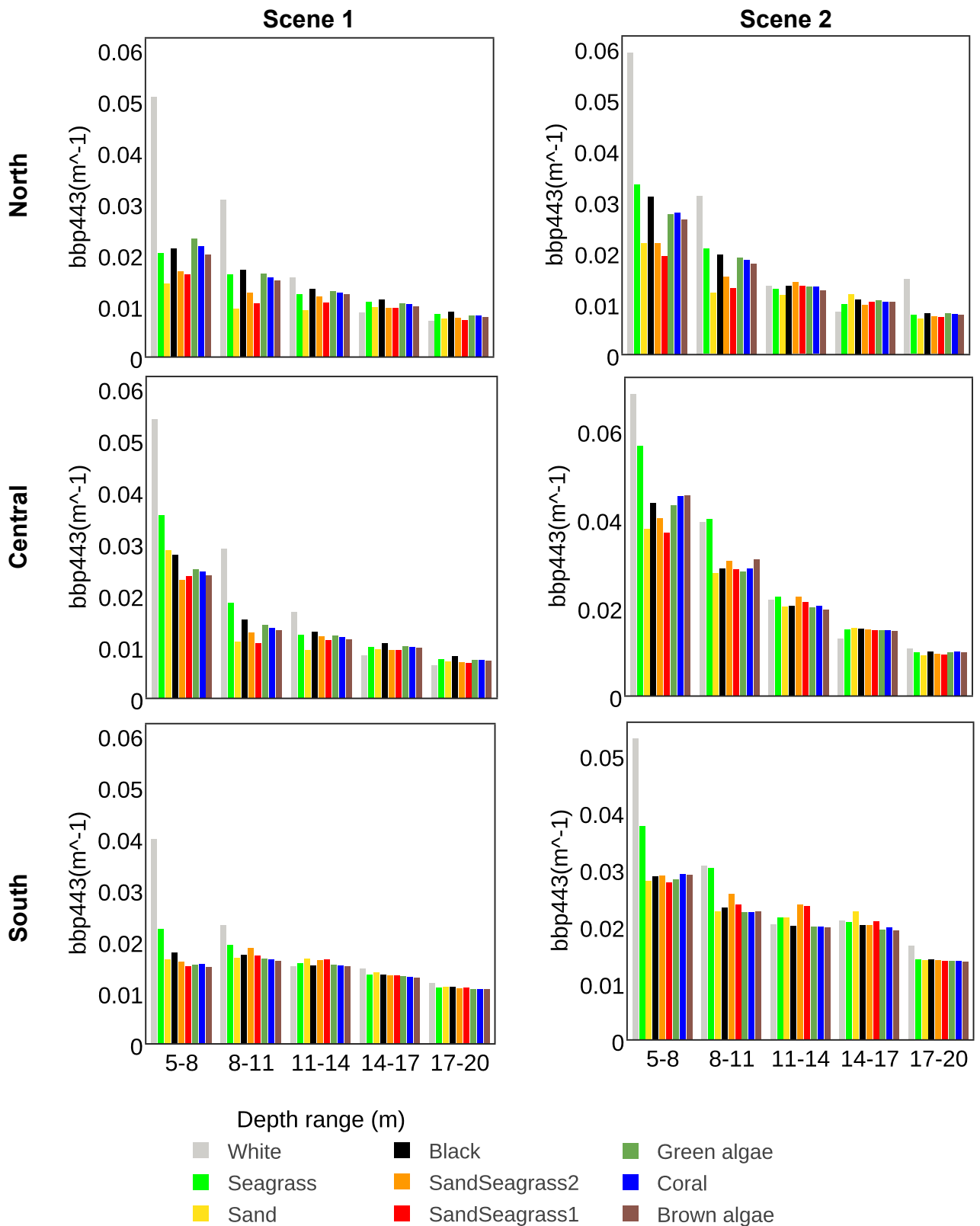


Figure 4-8: Mean backscatter retrievals (bbp443) for Scenes 1 (03 December 2005) and 2 (09 August 2011) for the northern, central and southern Great Barrier Reef under different bottom reflectance scenarios and depth ranges.

Retrieved a_{443} values were highest for the white bottom reflectance scenario for the two shallowest depth ranges (5 to 8 m and 8 to 11 m) for all three GBR regions and both Scenes 1 and 2. The highest mean a_{443} was recorded for the south GBR in Scene 2 (0.78 m^{-1}) (Figure 4–9). The differences in calculated mean a_{443} between the white scenario and the other bottom scenarios was greatest ($> 0.4 \text{ m}^{-1}$) in the northern GBR for both scenes for the depths between 5 and 8 m, although smaller in Scene 1 than in Scene 2. Minor differences in mean a_{443} values were recorded between the coral, black, as well as the brown and green algae scenarios for both scenes, all regions and all assessed depths. Higher mean a_{443} values were calculated using the brighter bottom reflectance scenarios (sand, sandseagrass1 and sandseagrass2) than those found in the darker bottom reflectance scenarios (brown algae, green algae, coral and black), except seagrass in Scene 1.

In Scene 1, only the depth bins 17-20 m had no significant differences between bottom types ($p > 0.05$), while all the other depth bins showed significant differences in mean a_{443} ($p < 0.05$). The Tukey HSD test showed that the mean a_{443} of the white bottom reflectance scenario was the only one that was significantly different from black, coral, seagrass, brown and green algae at 14-17 m depths ($p < 0.05$). Further, the white bottom scenario produced significant differences ($p < 0.05$) in mean a_{443} between all the other bottom types at depths 5-14 m. The differences between all the other bottom reflectance scenarios were not significant ($p > 0.05$).

In Scene 2, all the depth bins had significant differences between bottom types ($p < 0.05$). The Tukey HSD test showed that the mean a_{443} of the white bottom reflectance scenario was the only one that was significantly different from all the other tested bottom types at 17-20 and 5-8 m depth bins ($p < 0.05$). Yet, the mean a_{443} was not significantly different between any of the bottom types in the 14-17 m and 11-14 m depth bins according to the Tukey HSD test. There was a significant difference in mean a_{443} between the white bottom reflectance scenario and the coral and green algae scenario ($p < 0.05$) in the 8-11 m depth bin. In the 5-8 m depth bin, the mean a_{443} values of all bottom scenarios were significantly different ($p < 0.05$) from the mean a_{443} values in the white scenario in Scene 2. The differences between all the other bottom reflectance scenarios were not significant ($p > 0.05$). There were significant differences ($p > 0.05$) in mean a_{443} between the different regions of the GBR (north, south and central) for the

depth bins at 14-17 m, 11-14 m and 8-11 m. No significant differences ($p < 0.05$) in mean a443 between the GBR regions were found for depth bins 17-20 m and 5-8 m. The Tukey HSD test showed that only the north and south had a significant difference ($p < 0.05$) in mean a443 for the depth bins 14-17 m and 11-14 m, while in the 8-11 m depth bin the only significant difference ($p < 0.05$) was observed between the central and northern GBR. The other regions did not have significant differences ($p > 0.05$) in mean a443.

There were no significant differences ($p > 0.05$) in mean a443 between Scene 1 and Scene 2 in the northern part of the GBR at all depth bins. Yet, there were significant differences ($p < 0.05$) in mean a443 in the central GBR at all depth bins, except for the 5-8 m depth bin, which did not have a significant difference ($p > 0.05$) between Scene 1 and Scene 2. The mean a443 in the southern GBR showed significant differences between Scene 1 and Scene 2 ($p < 0.05$) at depths of 17-14 m and 14-11 m, but it was not significantly different for the other depth bins.

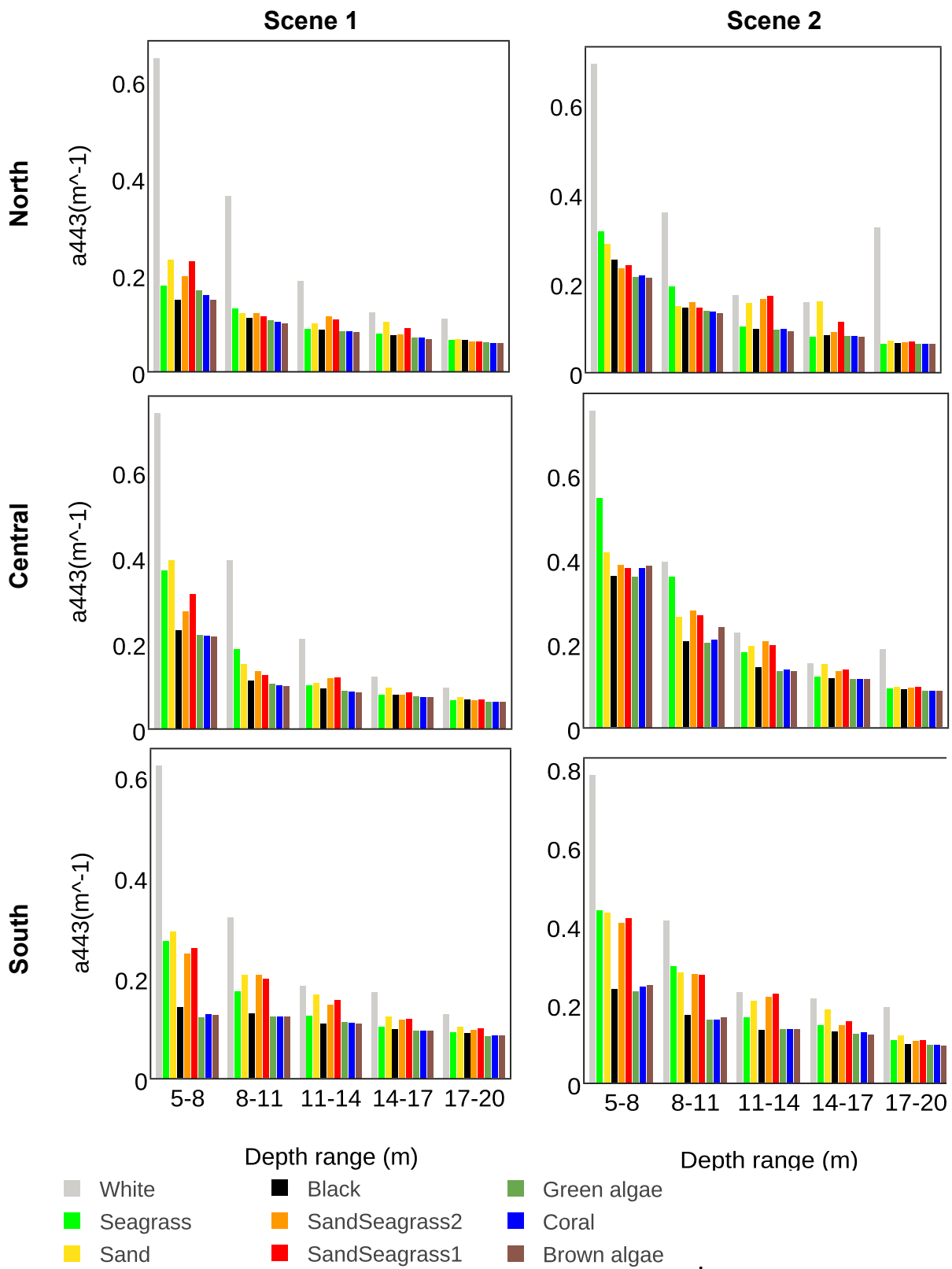


Figure 4-9: Mean absorption retrievals (a_{443}) for Scenes 1 (03 December 2005) and 2 (09 August 2011) for the northern, central and southern Great Barrier Reef under different bottom reflectance scenarios and depth ranges.

4.3.2.2 Spatially distributed differences in IOP retrievals between different bottom reflectance scenarios

Relative differences in bbp443 reached high levels (up to $> \pm 1000\%$), but most ranged between $\pm 200\%$ for the white and black (Figure 4–10) and between ± 100 for the sand and seagrass bottom reflectance scenarios (Figure 4–11). Most of the changes can be observed near the coast and the outer reef in both scenes, which corresponded to the shallow water areas (5 to 25 m). A large area of the northern GBR was affected by bottom reflectance parameterization in both assessed scenes. Interestingly, positive and negative changes can be observed within the same region for all GBR regions in both scenes. Near the coast, the white bottom reflectance case produced higher bbp443 values than the black bottom scenario. The differences in bbp443 retrievals of the black and white bottom reflectance scenarios showed which areas might be sensitive to bottom reflectance parameterization. The changes in retrieved bbp443 due to differences in bottom reflectance were highly spatially variable and did not follow a clear pattern. However, similar patterns in differences in retrieved bbp443 of the black and white bottom reflectance scenarios were observed between Scenes 1 and 2.

The changes in retrieved bbp443 between the sand and seagrass bottom types were considerably smaller than the changes in retrieved bbp443 from black and white bottom reflectance scenarios. Overall, higher bbp443 retrievals from the sand bottom reflectance scenario could be observed adjacent to the coast, where the change in retrieved bbp443 was positive. In Scene 2, there were more and larger areas where the seagrass bottom produced higher bbp443 values than the sand bottom in all GBR regions. Higher bbp443 values from the sand bottom reflectance scenarios were observed in small areas adjacent to the coast, where the change was positive. Most changes in retrieved bbp443 between bottom reflectance scenarios were observed near the coast and around the reefal areas for both Scene 1 and 2. The northern and central GBR had similar differences in bbp443 retrievals between Scenes 1 and 2. The southern GBR, on the other hand, had slightly higher changes in retrieved bbp443 in Scene 1 compared to Scene 2 in the coastal areas. However, like the differences in bbp443 from the black and white scenario, the changes in retrieved bbp443 between the sand and seagrass bottom reflectance scenarios provided similar spatial patterns between Scene 1 and 2.

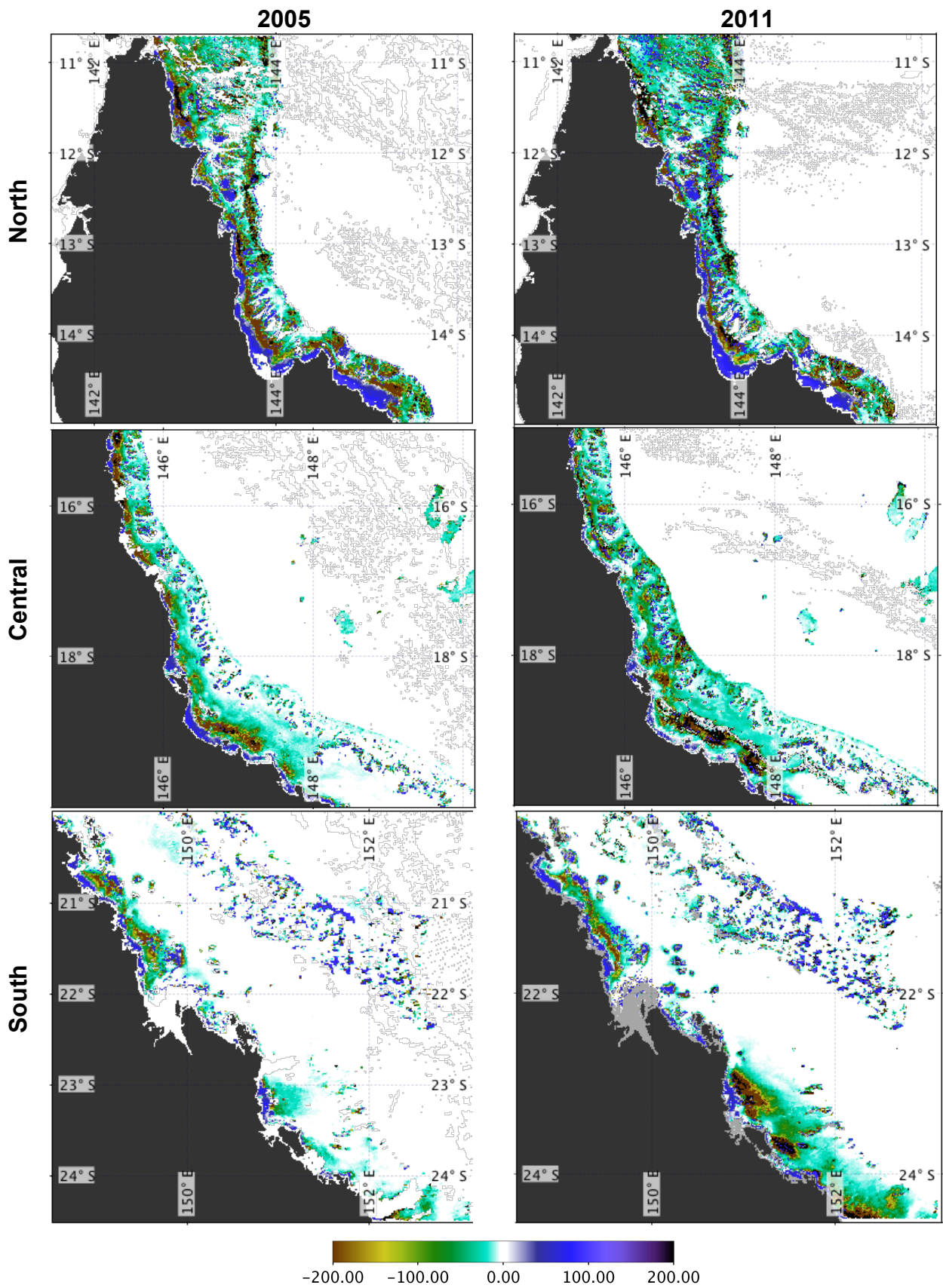


Figure 4-10: Relative differences in algorithm-derived bbp443 between the black and white bottom scenarios (1) Scene 1 northern GBR (top-left panel) (2) Scene 2 northern GBR (top-right panel) (3) Scene 1 central GBR (center-left panel) (4) Scene 2 central GBR (center-right panel) (5) Scene 1 southern GBR (bottom-left panel) (6) Scene 2 southern GBR (bottom-right panel)

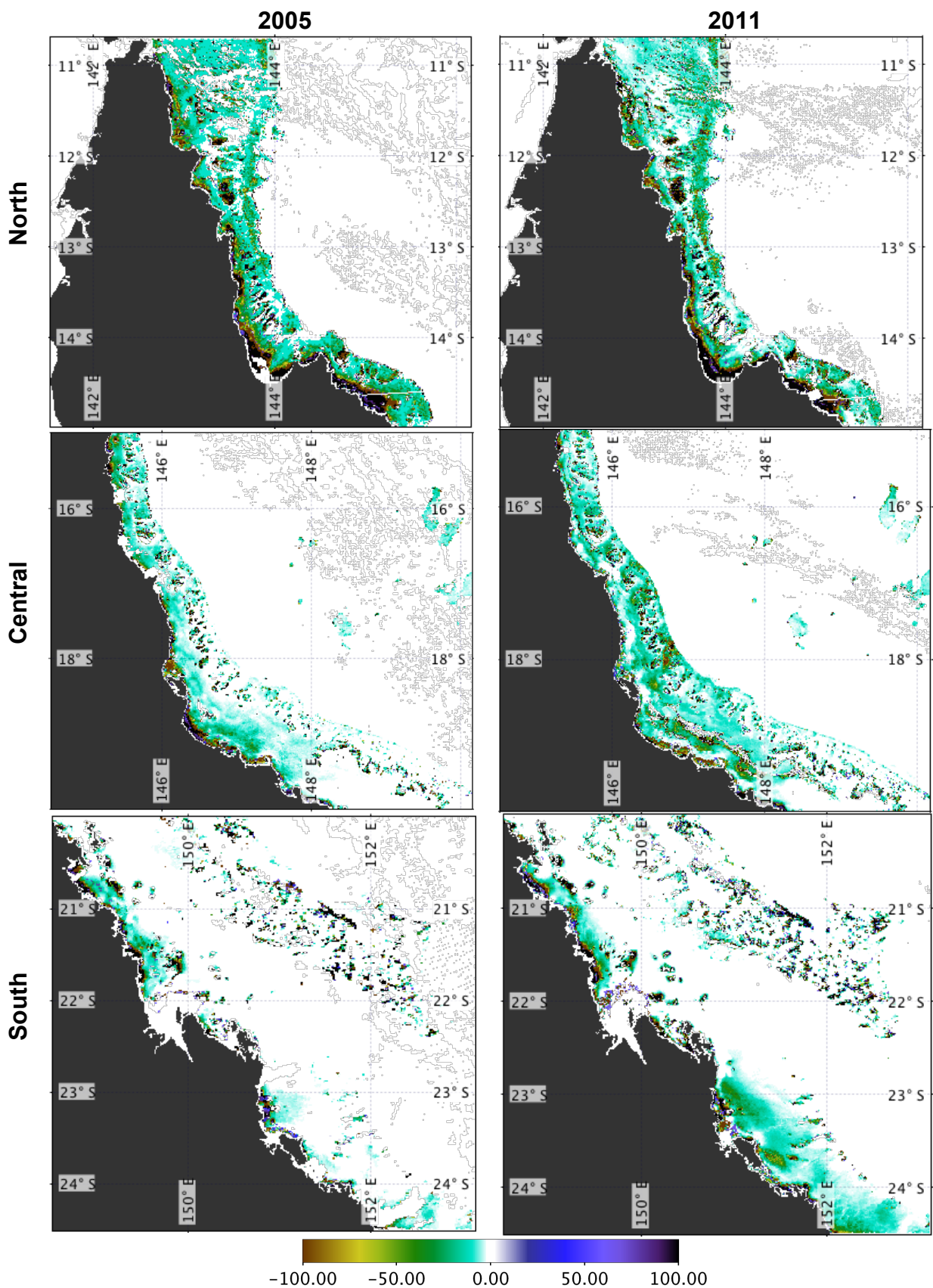


Figure 4-11: Relative differences in algorithm-derived bbp443 between the sand and seagrass bottom scenarios (1) Scene 1 northern GBR (top-left panel) (2) Scene 2 northern GBR (top-right panel) (3) Scene 1 central GBR (center-left panel) (4) Scene 2 central GBR (center-right panel) (5) Scene 1 southern GBR (bottom-left panel) (6) Scene 2 southern GBR (bottom-right panel)

The a443 retrievals were also assessed using percentage change. The percentage difference range in algorithm-calculated a443 for the black and white bottom reflectance scenarios was between -10 and 90% (Figure 4–12), and between -30 and 25% for the sand and seagrass scenarios (Figure 4–13). The changes in algorithm-calculated a443 were much higher between the black and white scenarios for Scene 2, compared to Scene 1. Bottom reflectance parameterization affected most of the northern GBR, with a higher percentage change observed in the coastal areas and around the reefs. The percentage difference in retrieved a443 between the black and white scenarios was lower for the outer reef areas, where it ranged between 13 and 35% for Scene 2. In the central GBR, Scene 1 provided a higher positive percentage change in the coastal areas, while Scene 2 had a higher percentage change in a443 values in the area between the coast and the outer reefs. In the southern GBR, the area between the coast and the Capricorn Bunker group showed a change in retrieved a443 values in Scene 2 but little change in Scene 1, for the black and white bottom scenarios.

The areas where a443 was affected by bottom reflectance parameterization of the sand and seagrass bottom types were much smaller compared to the areas affected by the black and white bottom reflectance scenarios (Figure 4–13). Both positive and negative percentage changes were observed along the coast, indicating that neither sand nor seagrass produced consistently higher a443 values. The differences between Scenes 1 and 2 were also smaller between the sand and seagrass bottom reflectance scenarios, compared to the black and white bottom reflectance scenarios.

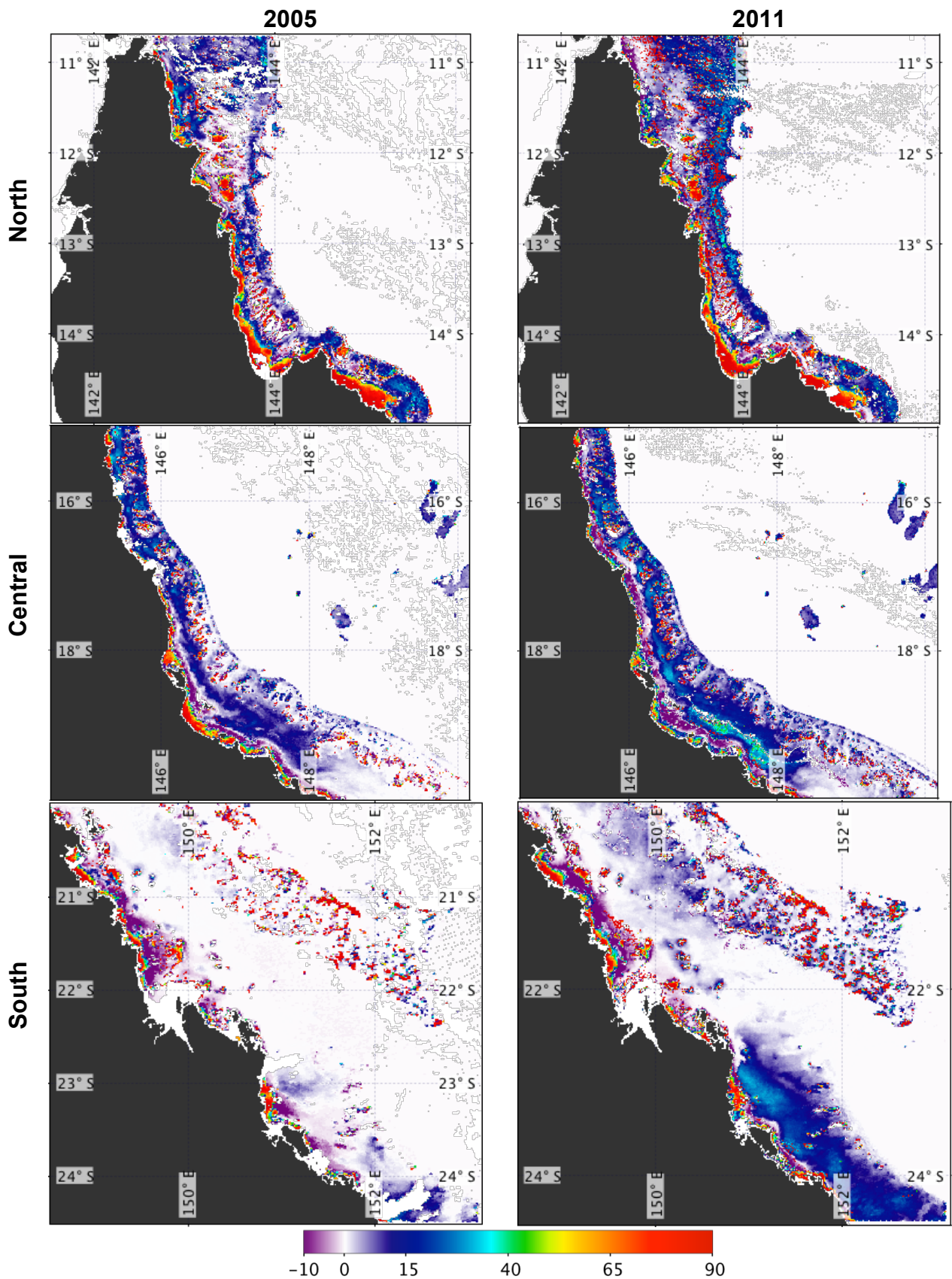


Figure 4-12: Relative differences in algorithm-derived a443 between the black and white bottom scenarios (1) Scene 1 northern GBR (top-left panel) (2) Scene 2 northern GBR (top-right panel) (3) Scene 1 central GBR (center-left panel) (4) Scene 2 central GBR (center-right panel) (5) Scene 1 southern GBR (bottom- left panel) (6) Scene 2 southern GBR (bottom-right panel)

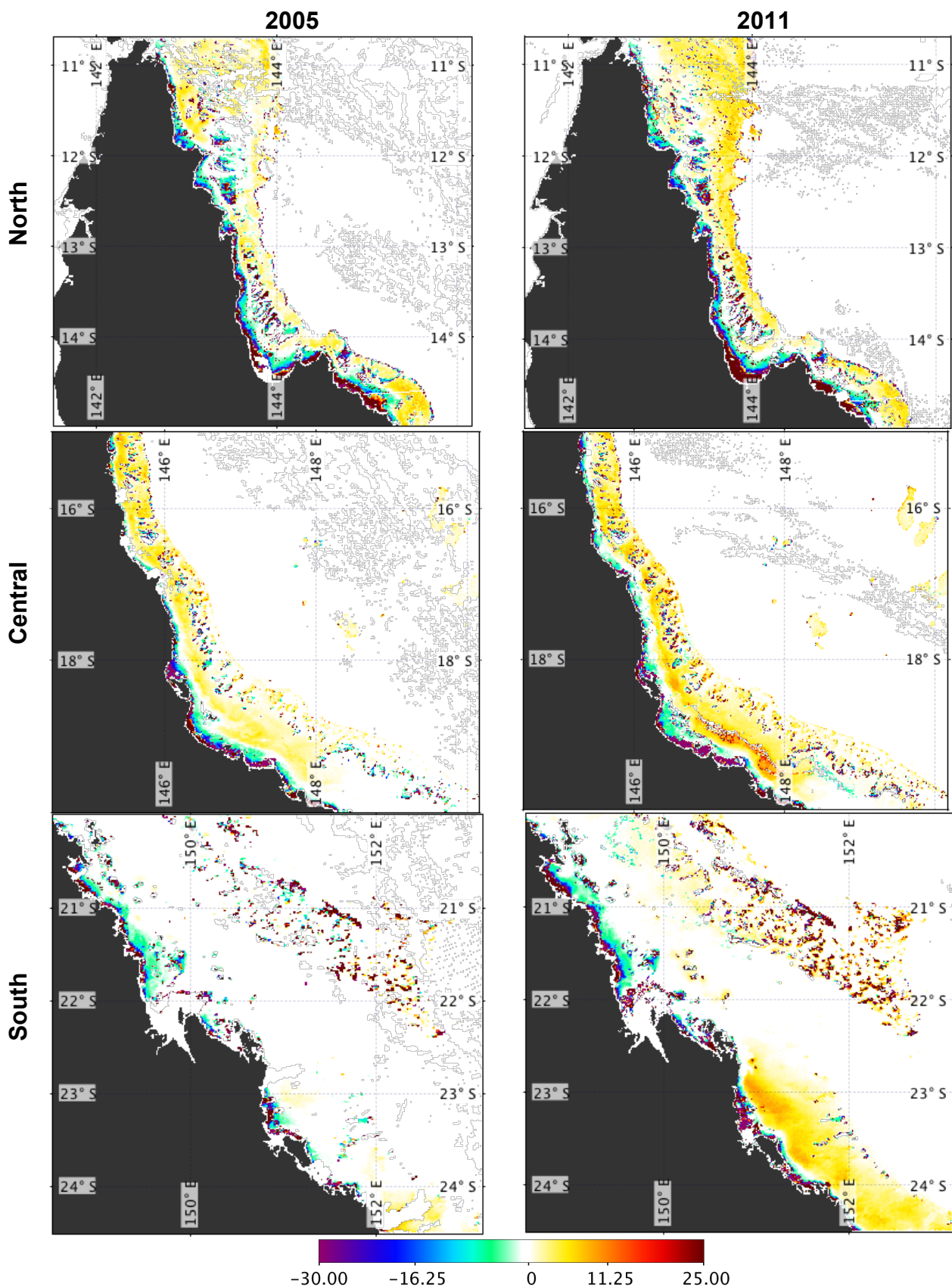


Figure 4-13: Relative differences in algorithm-derived a443 between the seagrass and sand bottom scenarios (1) Scene 1 northern GBR (top-left panel) (2) Scene 2 northern GBR (top-right panel) (3) Scene 1 central GBR (center-left panel) (4) Scene 2 central GBR (center-right panel) (5) Scene 1 southern GBR (bottom- left panel) (6) Scene 2 southern GBR (bottom-right panel)

4.3.2.3 Spatially distributed differences in IOP retrievals between Scenes 1 and 2

To get a better understanding of the differences between the bottom scenarios of the two scenes, the IOP retrievals for the sand bottom reflectance scenario were compared between the two scenes. The results show that differences in a_{443} values were slightly lower in Scene 1 compared to Scene 2 in the very top part of the GBR (10-12° S) (Figure 4–14), indicating that water quality was lower in that part in Scene 1. The differences between the bottom reflectance scenarios white and black, as well as sand and seagrass were slightly higher in Scene 2 compared to Scene 1 in the outer reefs. The retrieved bbp_{443} did not show large variations between Scenes 1 and 2 in the northern part of the GBR (10-15 ° S), but indicated that there were marginally lower bbp_{443} values calculated for the outer reef in the northern GBR (Figure 4–15). In the central GBR a_{443} was higher in Scene 2 compared to Scene 1 in parts along the coast, but higher in the outer reefal areas in Scene 1 than Scene 2. The same pattern could be observed in the bbp_{443} between the two scenes. The southern GBR displayed higher retrieved IOP values along the coast in Scene 2 while the outer reefs had higher retrieved IOP values in Scene 1.

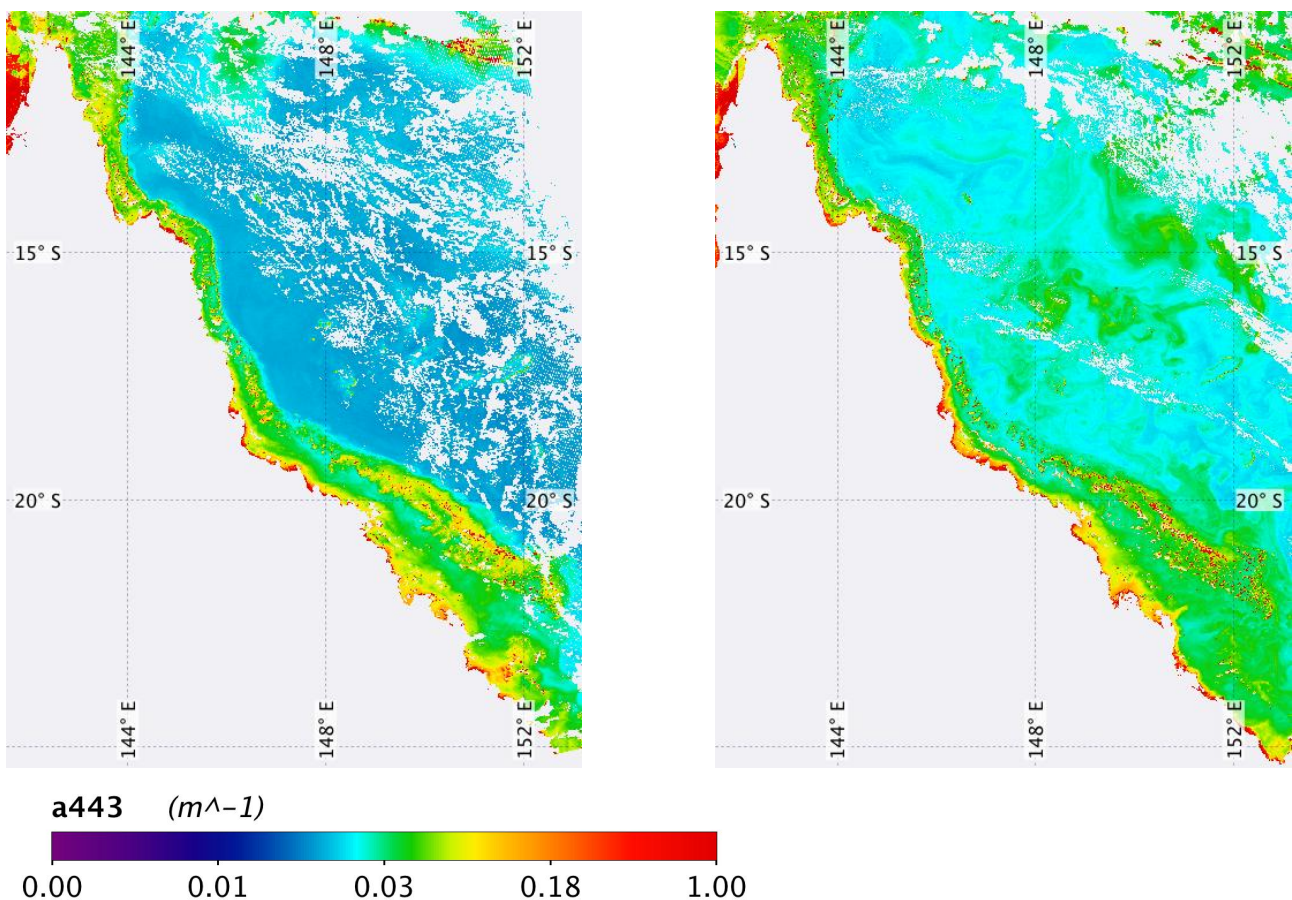


Figure 4-14: Retrieved a_{443} for Scene 1 (left) and Scene 2 (right) using the sand bottom reflectance scenario.

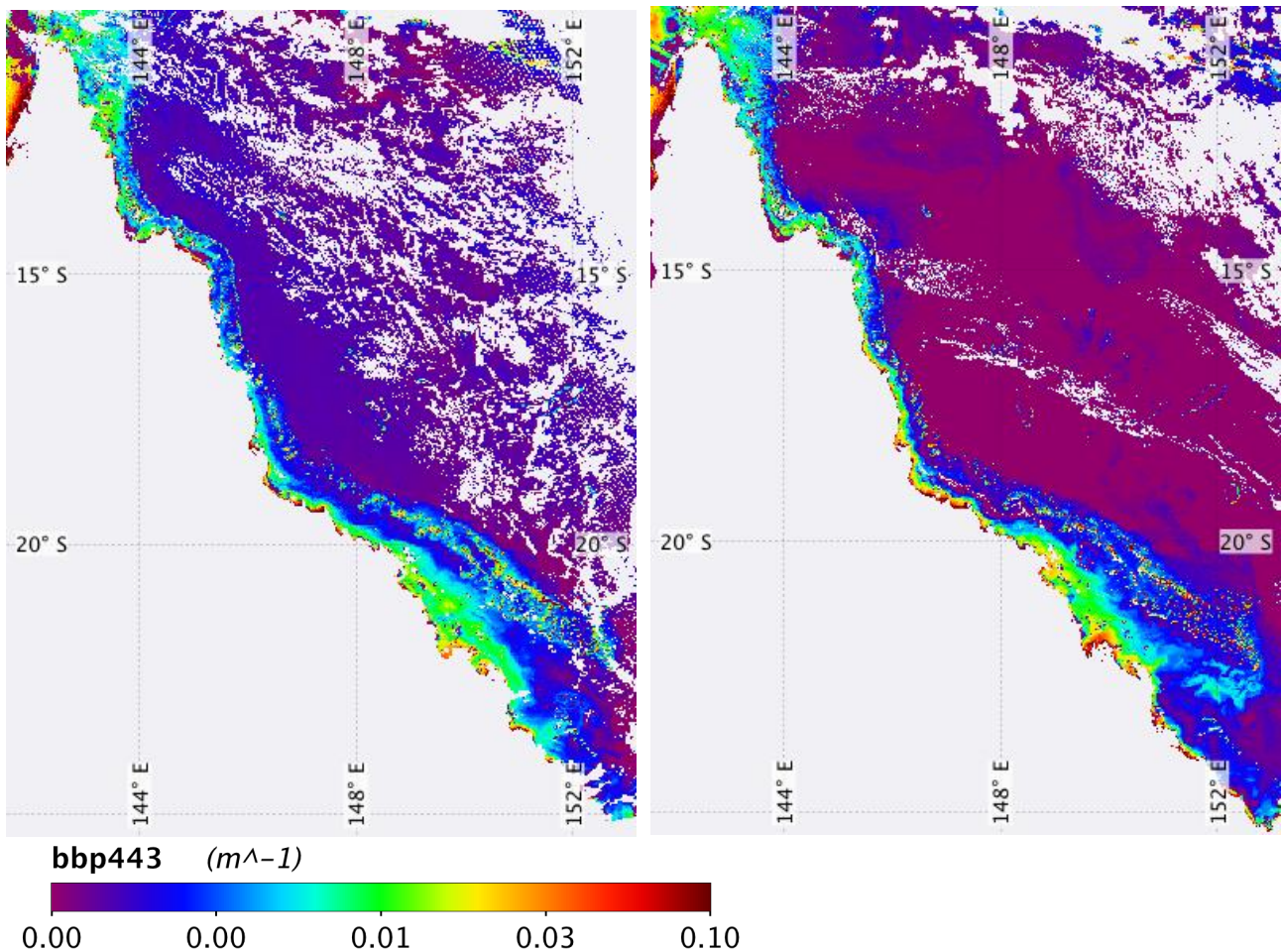


Figure 4-15: Retrieved bbp443 for Scene 1 (left) and Scene 2 (right) using the sand bottom reflectance scenario

The retrieved IOPs were compared to the secchi depth for the two scenes to get further understanding into the water clarity of the two scenes (Figure 4–16). The secchi depth algorithm from Weeks et al. (2012) used to generate the images does not correct for bottom reflectance. However, by comparing the IOPs and secchi depth one can gain insight into the effect of water clarity on differences in IOP retrievals. The secchi depth imagery from Scene 1 shows slightly lower water transparency in the northern and central GBR compared to Scene 2. In the southern GBR, the outer reefs also displayed poorer water transparency in Scene 1 compared to Scene 2. However, the area between the reefs and the coast in the southern GBR was slightly more transparent in Scene 1 compared to Scene 2. Overall, the secchi depth algorithm showed clearer waters in Scene 2 compared to Scene 1. This was not as clearly observed from the IOP retrievals, where higher IOP values were observed in Scene 2.

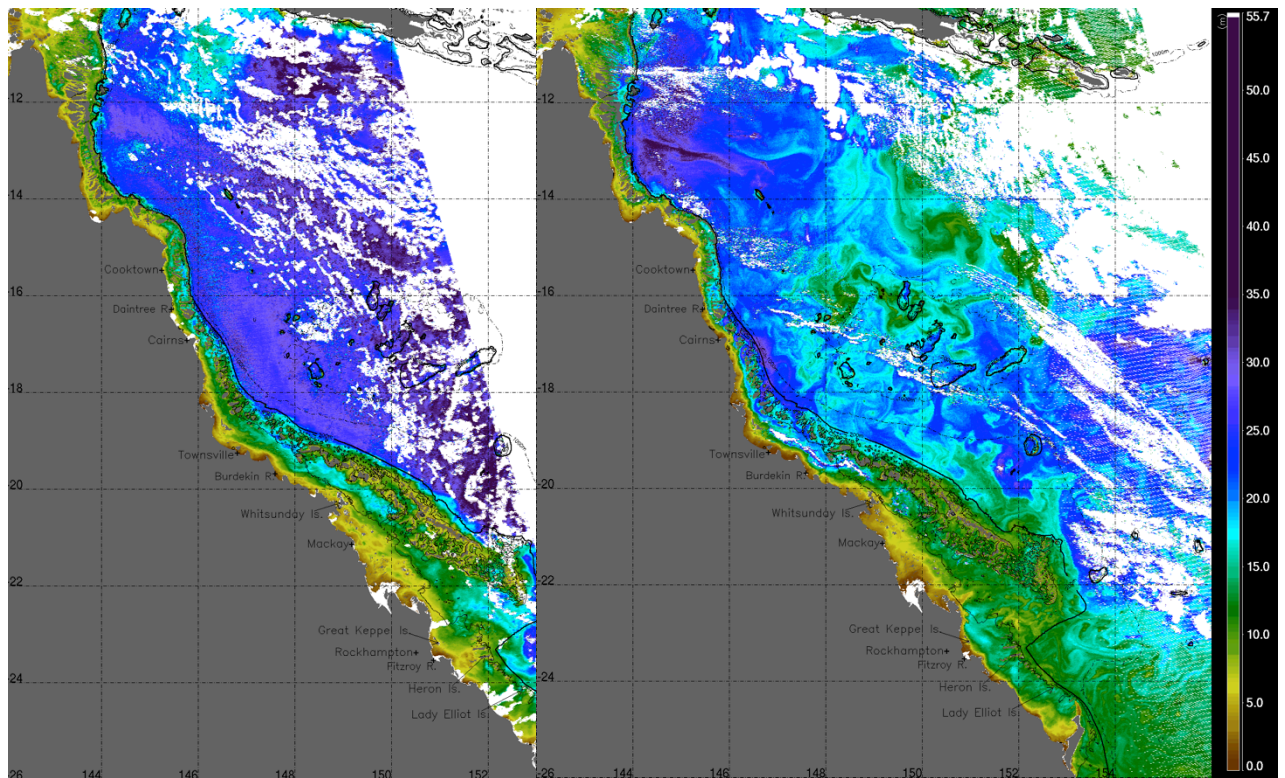


Figure 4-16: Secchi depth for Scene 1 (left) and Scene 2 (right) processed using the GBR-validated Secchi depth algorithm (Weeks et al., 2012)

4.1.1 Temporal sensitivity of IOP retrievals under different bottom reflectance scenarios

In this section, the researcher assessed the differences in water column a_{443} and bbp_{443} retrievals using bottom reflectance spectra from brown algae and sand, as well as the differences between retrievals using seagrass and sand reflectance spectra for the time period from 1 January 2013 to 1 January 2014. Differences were calculated by subtracting the mean daily a_{443} and bbp_{443} values of the sand bottom reflectance scenario from those of the brown algae scenario (BASA), and the sand bottom values from the seagrass bottom values (SESA). The results of the differences in retrieved bbp_{443} of the LI and CB time series are displayed in Figure 4–17.

The time series analysis for both the CB and LI study areas showed that IOP retrievals at depth ranges from 5 to 20 m were most sensitive to changes in bottom reflectance parameterization, for both a443 and bbp443, for both areas (CB and LI). For the assessed time period, smaller differences (± 0.05) in a443 retrievals were recorded at depths shallower than 20 m from May to July 2013 for both the study areas compared to the rest of the year. More frequent large positive differences in a443 retrievals ($0.1-0.15 \text{ m}^{-1}$) were observed in the CB area, compared to the LI area for both BASA and SESA scenarios at depths shallower than 12 m. In general, the changes in a443 retrievals were positive for the shallower depths (above 12 m) and negative for deeper depths (below 15 m). This means that retrieved a443 values were higher for the dark bottom types (brown algae and seagrass) than for the sand bottom reflectance scenario in shallower depths. The opposite was true for the deeper depth (below approximately 15 m), where retrieved a443 was higher for the sand bottom reflectance scenario compared to the darker bottom types. However, in the LI region, retrieved a443 values were higher for the sand bottom reflectance scenario in the months February to May 2013 in depths shallower than 10m, while for the remainder of the year, the brown algae and seagrass scenarios produced higher a443 values. Also, in the CB area, the months of August, September and November 2013 provided higher retrieved a443 values for the dark bottom reflectance scenarios compared to the sand bottom reflectance scenario, with differences in a443 between -0.15 and -0.05 m^{-1} for depths above 10 m. While most changes in a443 retrievals were observed at depths above 20 m, there were some changes observed between sand and dark bottom reflectance scenarios for depths below 20 m.

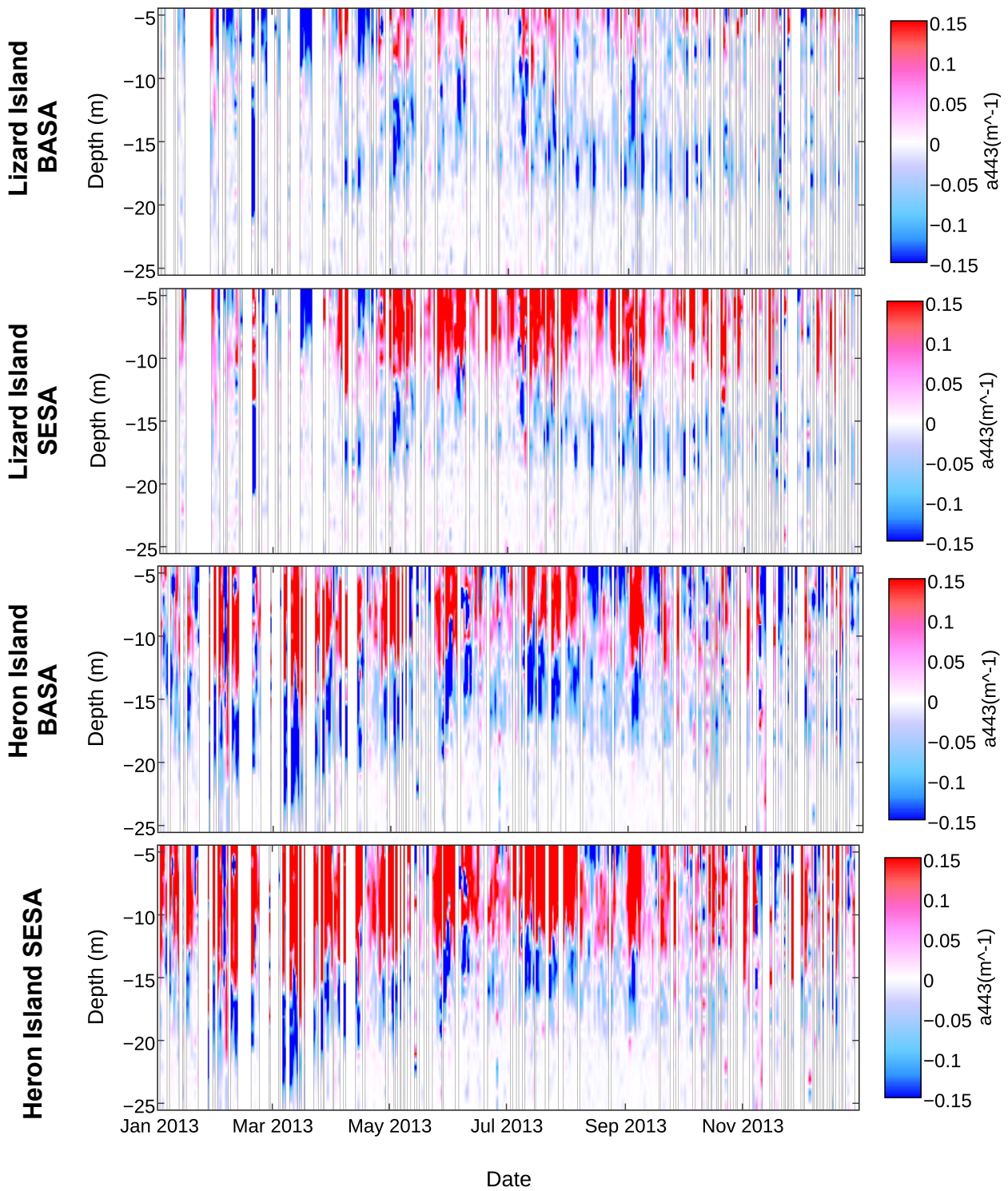


Figure 4-17: 12 –month time series differences in a443 retrievals for the SESA and BASA scenarios for the Lizard Island and Capricorn Bunker test regions

The results of the differences in retrieved bbp443 between the LI and CB time series are shown in Figure 4–18. Similar to the a443 retrievals, the bbp443 retrievals were larger for the dark bottom reflectance scenarios, compared to the sand in shallower (above 12 m) areas. This led to positive changes in bbp443 for these areas, while negative changes were observed in depths below approximately 15 m. Also similar to the a443 retrievals, the differences in bbp443 values were smaller in the LI area compared to the CB region. Again similar to the retrieved a443 values, the bbp443 values showed a slight variation across the year 2013, with negative differences recorded at shallower depths (above 12 m) during May to September 2013. In June 2013, the differences in bbp443 in the CB region showed the highest negative values for the year, in both BASA and SESA for depths from 7 to 20 m. In the LI region, the highest differences in retrieved bbp443 and a443 occurred from the end of April to early December 2013.

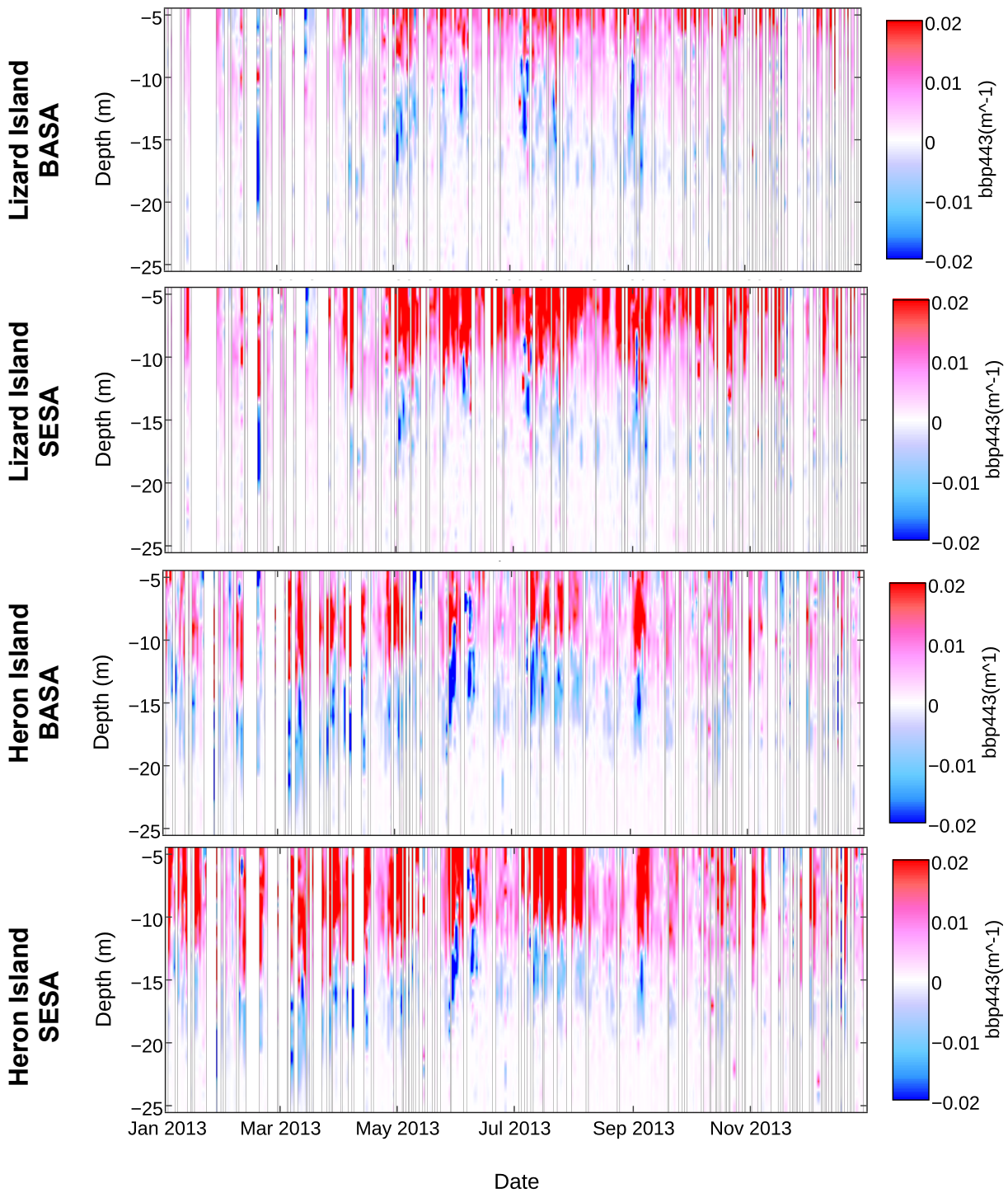


Figure 4-18: 12 -month time series of differences in bbp443 retrievals for the SESA and BASA scenarios for the Lizard Island and Capricorn Bunker test regions

To assess the median yearly trend in percentage change between the sand and seagrass, as well as the sand and brown algae scenario at different depths, the differences were converted to values. The median percentage change is highest at 5 to 10 m depth for both a443 (11-43%) and bbp443 (15-34%) in all assessed scenarios (Figure 4-19). The median percentage change is smallest at depth below 20 m for both a443 (2-7%) and bbp443 (2-6%). The CB had more differences in median retrieved IOPs for the SESA scenario. Yet, it had lower levels of median percentage change for a443 (2-25%) and bbp443 (6-23%), compared to LI areas, which had changes in a443 (7-34%) and bbp443 (6-43%).

The LI BASA scenarios had higher a443 (19%) median percentage change at very shallow depth (5m) compared to the CB BASA scenario (15%). However, at depths between 7 to 15 m the LI BASA scenario had a lower percentage change in median a443 values (11-16%), compared to the CB scenario that had changes of 16-21%. At depth below 15 m median percentage difference is lower for the CB BASA (2-16%) compared to the LI BASA scenario (7-16%).

The LI BASA scenarios had higher bbp443 (15-30%) median percentage change at very shallow depth 5-12 m compared to the CB BASA scenario (10-15%). At depth between 12-16 m median percentage difference in a443 is slightly higher for the CB BASA (7-12%) compared to the LI BASA scenario (7-11%). While at depth below 20m the median percentage difference in bbp443 is the same for the LI and CB BASA scenario.

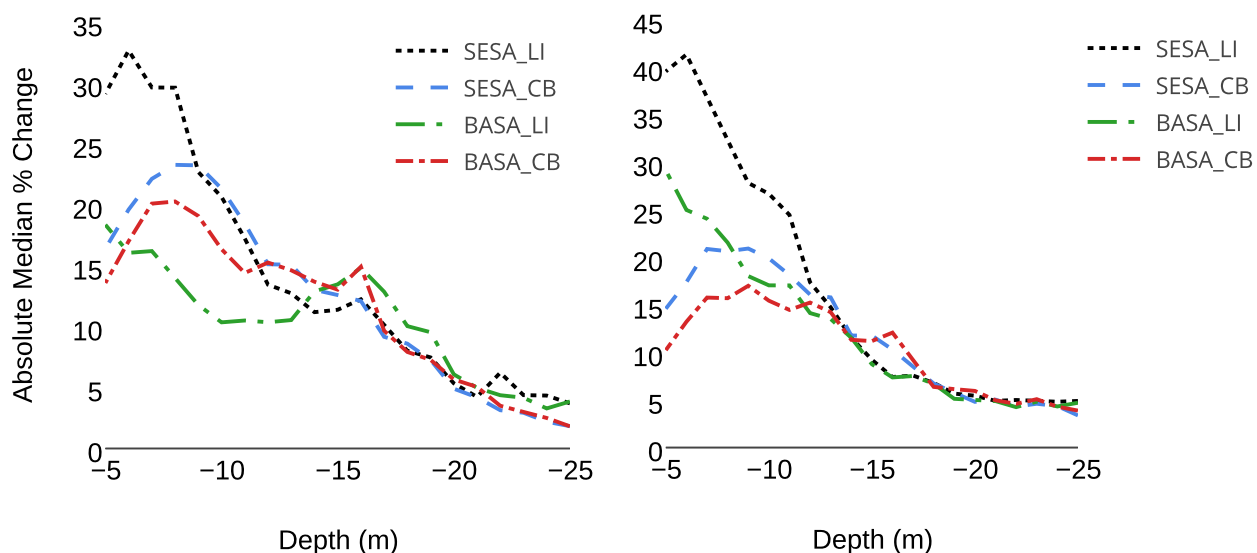


Figure 4-19: Yearly median percentage differences from 5 to 25 m in bbp443 (left panel) and a443 (right panel) for the SESA and BASA scenarios in the Capricorn Bunker Group (CB) and the Lizard Island area (LI)

4.4 Discussion

The objective of this research was to analyze the impact of bottom reflectance parameterization on IOP retrievals using SWIM. It has been demonstrated that IOP retrievals are clearly impacted by bottom reflectance parameterization in shallow waters. **The results of this chapter confirm that bbp443 retrievals can be highly sensitive to bottom reflectance parameterization.** Bottom reflectance contributions from different bottom types could cause up to 2-fold change in estimates of water column IOP values (a443a and bbp443) (Figure 4-10 and 4-11). Such large variations in retrieved IOPs were also observed by McKinna et al. (2015), where SWIM produced up to 400% lower retrieved IOP values compared to the deep water optimized models Quasi Analytical Algorithm (QAA) and Generalized IOP algorithm (GIOP) (McKinna et al., 2015). Even in the open ocean, where bottom reflectance does not contribute to IOP retrievals, bbp values can vary greatly. Ocean color models match-ups to *in situ* backscattering coefficients do not always produce satisfactory results even in deep ocean waters (Example: Mélin et al., 2005, Maritorena et al., 2010). Mélin et al. (2005) found that based on 17 match-ups, the comparison for the backscattering coefficient gives mean differences in the range of 31–53% for a study site in the Adriatic Sea. Maritorena et al. (2010) reported that there was a consistent difference observed throughout the assessed time-series between MODIS Aqua-derived bbp values and *in situ* match-ups. The results of this

chapter confirm that bbp443 retrievals can be highly sensitive to bottom reflectance parameterization.

For both scenes and all regions, means of estimated bbp443 were very similar for the coral, brown algal and green algal bottom type scenarios across all depth ranges with not significant differences. *Coral, brown algae and green algae have similar spectral shape and magnitude, thus IOP retrievals are expected to be more similar for these bottom types compared to sand or seagrass, which have different spectral shapes.* These results are consistent with the findings of Chapter 3 (Reichstetter, Fearn, et al., 2015), which found that most dark spectra, such as algae, coral and seagrass, can be clustered together into a “dark” cluster based on the modeled surface reflectance signals.

The results showed that the sensitivity in IOP retrievals due to bottom reflectance parameterization was different under different water clarity conditions (different scenes). *More light penetrates through the water column in clearer waters compared to more turbid waters. Therefore, the amount of light reaching the bottom is different in the two assessed scenes, resulting in different IOP retrievals. The black (non-reflective bottom) and white (completely reflective bottom) cases are extreme scenarios and the differences in IOP retrievals were expected to be greater than between other bottom types.* There were considerable variations between Scene 1, captured in December 2005, and Scene 2, in August 2011, in differences of IOP distributions, summary statistics and spatial differences. GBR waters are generally most transparent during September and most turbid during March (Weeks et al., 2012). In addition, the average monthly rainfall is lowest May to October (dry season) in the GBR, while from November to April (wet season), it is impacted by monsoonal winds (Furnas & Mitchell, 2001; Weeks et al., 2012) The wet season results in greater river outflow, hence lower clarity, especially inshore (Fabricius, Logan, Weeks, & Brodie, 2014; Weeks et al., 2012). The comparison between the two scenes using the sand bottom reflectance scenario showed that the differences in retrieved IOPs were not large and were mostly observed in the coastal areas and outer reefs. Yet, the percentage differences between the *IOP retrievals for the white and black and the sand and seagrass scenarios* were generally larger in Scene 2 compared to Scene 1. Scene 2 had slightly lower retrieved IOP values in areas where the percentage differences were higher between the retrieved IOPs of the

white and black, as well as the sand and seagrass bottom reflectance scenarios. Therefore, it can be concluded that small changes in water clarity can greatly affect the sensitivity of IOP retrievals due to bottom reflectance parameterization. These changes are local, do not usually occur GBR-wide, and are influenced by oceanographic patterns and river runoff, *typically being more significant in coastal turbid waters.*

Both spectral shape and magnitude affect IOP retrievals. This research showed that the magnitude of the bottom type spectra was not the only parameter determining the differences in IOP retrievals, but the spectral shape also influenced IOP retrievals. For example, the mean sand spectra was approximately 2.5 times higher than the spectra of the darker bottom types (coral, seagrass brown and green algae) but did not result in consistently higher mean retrieved IOPs. In addition, there was only an average 8% difference between brown algae and seagrass, yet the differences in IOP retrievals varied between the two bottom types. The influence of the spectral shape used in the bottom reflectance parameterization could also be observed in the mean IOP retrievals in Scenes 1 and 2, where the dark bottom types (coral, brown and green algae) generally had similar effects on IOP retrievals, while seagrass, which has a different spectral shape compared to the other dark bottom types—as illustrated in Figure 4–2 —had a different pattern in IOP retrievals. In contrast, white and black spectra, which have no spectral shape, but have the highest (white) and the lowest (black) spectral magnitude respectively did not consistently give the highest (white) and lowest (black) IOP retrievals.

The influence of reflectance by different bottom types on SWIM retrievals of a443 and bbp443 was greatest at depths shallower than 20 m. Most differences were observed in shallow waters (5 to 14 m) and only small differences were observed beyond 20 m. *More light reaches the seafloor in shallow water areas, compared to deeper areas. Thus, the differences in IOP retrievals for different bottom types are greater in shallow water areas due to the increased proportion of light reflected from the seafloor compared to light reflected from the water column.* However, the small differences that were observed at depths below 20 m were observed in the time series, where the sand bottom reflectance and the seagrass and algae bottom reflectance scenarios showed differences in IOP retrievals. This is contrary to other studies, which found that below 20 m, remote sensing reflectance or chlorophyll retrievals should not be impacted by bottom reflectance (Carder, Cannizzaro, & Lee, 2005; Reichstetter, Fearn, et al., 2015). Yet, none of these

studies were based on *in situ* data, but rather on modeled and synthetic data. The changes in retrieved IOPs were relatively minor ($\pm 0.05\text{m}^{-1}$ for a443 and $\pm 0.005\text{m}^{-1}$ for bbp443) and were observed between February and March 2013, when water clarity is generally more turbid compared to the May to October months (Weeks et al., 2012). Lower water clarity is often associated with higher IOP retrievals (Blondeau-Patissier et al., 2009), thus differences are higher between scenarios, while the percentage differences show little change. McKinna et al. (2015) found that SWIM, QAA and GIOP produced comparable IOP retrievals at depths greater than 30 m but showed some differences for depths less than 30 m, most likely directly due to bottom reflectance. The differences for waters shallower than 30 m were most likely associated with the SWIM model IOP configuration, which is still being optimized as noted in (McKinna et al., 2015).

The differences in IOP retrievals due to changes in bottom reflectance parameterization showed both spatial and temporal variability. Spatial and temporal variability in IOP retrievals based on different bottom reflectance scenarios were expected. The variability in changes of IOP retrievals due to changes in bottom reflectance parameterization may be partly associated with spatial and temporal variability of water clarity in the GBR (Fabricius et al., 2014, Weeks et al., 2012, McKinna et al., 2015). Figures 4–10 to 4–13 showed clear spatial variability within the GBR regions. It can be seen that uncertainties in IOP retrievals were highly variable spatially. The time series analysis showed that there was a slight seasonal trend in differences in IOP retrievals, most likely associated with the lower values in a443 and bbp443 during the May to September 2013 period, when waters are generally clearer in the GBR (Weeks et al., 2012). Previous *in situ* IOP studies have concluded that seasonal variability in IOPs occurs across the GBR regions (Furnas and Mitchell, 2001, Blondeau - Patissier et al., 2009). There are only a very few studies of *in situ* IOP measurements in the GBR, and these studies have found large bio-optical variability between and within regions (Blondeau - Patissier et al., 2009, Oubelkheir et al., 2006). This high variability in retrieved IOPs might also explain the high variability in changes in retrieved IOPs from the SWIM algorithms due to differences in bottom reflectance parameterization. The large variation in optical properties in the GBR would be likely to lead to large variations of uncertainties in modeled IOPs under different bottom reflectance scenarios. In general, the central GBR produced slightly higher mean IOP retrievals for both assessed MODIS scenes, compared to the northern and southern GBR at shallower depth (5-8 m) as evident in Figure 4–8 and 4–9.

To increase confidence in shallow water ocean color products, it is therefore essential to assess retrieved IOP uncertainties due to bottom reflectance parameterization on a subregional scale. General uncertainty guidelines cannot be provided for the whole of the GBR.

The median yearly percentage difference between the retrieved IOPs of the sand and brown algae, as well as the sand and seagrass scenarios for the Capricorn Bunker Group and the Lizard Island area, decreases with increasing depth for the analyzed time period from 01 January 2013 to 31 December 2013 (Figure 4-19). The percentage change in median IOP retrievals is only 2-7% at depth below 20 m between the sand and seagrass, as well as the sand and brown algae scenarios. Yet, the percentage different in mean IOP retrievals is between 11-43% for shallower depths (5-10 m). These findings are consistent with findings in Chapter 3, where bottom reflectance impacts on the remote sensing signal decrease with increasing depth (Reichstetter et al., 2015a). Carder et al. (2005) also concluded that bottom reflectance contributions decrease with increasing depth and become negligible at 20 m depth.

Overall, the distribution of the number of pixels in each bbp443 depth bin is very similar for all scenarios, except the white bottom reflectance scenario, in both MODIS scenes. The white bottom reflectance scenario is the only one that produced significantly different mean IOP retrievals ($p < 0.05$). Scene 1 had significant differences ($p < 0.05$) in retrieved a443 between the white bottom type and any of the others bottom types for all depth bins except the 17-20 m depth bin. In Scene 2, all the depth bins showed significant differences ($p < 0.05$) between retrieved a443 of the white and all the other bottom types. The retrieved bbp443 were only significantly different ($p < 0.05$) between the white bottom scenario and the other bottom scenarios at depth 5-11 m in Scene 1 and 5-8 m in Scene 2. The white bottom reflectance scenario is an extreme case with a fully reflective bottom, which is not realistic in real life applications. However, it highlights where bottom reflectances are likely to occur. It highlights that bottom reflectance becomes negligible in depth below 17 m in Scene 1, as no significant differences between bottom reflectance scenarios were observed, even considering a fully reflecting bottom scenario. It has to be noted that the retrieved IOPs have been averaged over a large area and thus differences in retrieved IOPs are small. Larger differences might be observed in individual pixels or over a smaller area. The reported differences in mean IOP retrievals give an indication of the expected sensitivities for GBR –wide or

regional (north, central and south) applications. It is common in ocean color remote sensing that large areas are assessed for water clarity or quality indicators (Petus et al., 2014, Weeks et al., 2012). However, if SWIM-derived IOPs in shallow water areas are assessed using a small study area, differences in IOP retrievals between the individual bottom reflectance scenarios might be larger.

Yearly median percentage differences in IOP retrievals were highest (a443=28-34% and bbp443=20-43%) between sand and seagrass at shallow depths (5- 10 m) in the Lizard Island study area. The percentage differences were higher in the Lizard Island area, compared to the Capricorn Bunker area. McKinna et al. (2015) noted that the Lizard Island area is sensitive to bottom reflectance with SWIM producing lower a443 and bbp443 values compared to QAA and GIOP, which do not account for bottom reflectance at depths shallower than 30 m. The Lizard Island area contains extensive seagrass areas (McKenzie et al., 2014a, McKenzie et al., 2001). The seagrass areas might explain the large differences in retrieved IOPs between seagrass and sand.

4.5 Conclusion and recommendation

The aim of this study was to demonstrate the effects of bottom reflectance parameterization on IOP retrievals. The results provided a detailed assessment of GBR-wide and regional uncertainties in IOP retrieval due to bottom reflectance parameterization. The study concluded that bottom reflectance contributions from different bottom types could cause up to a two-fold change in estimates of water column IOP retrieval values. However, this was found to be significant only at depths shallower than 20 m.

Differences in IOP retrievals due to changes in bottom reflectance parameterization showed both spatial and temporal variability across the GBR. However, differences in retrieved IOPs might be greater in individual pixels or in smaller subregions. Further research should be undertaken to investigate subregional sensitivities in IOP retrievals due to differences in bottom reflectance parameterization.

This research focused on the GBR only. Further research should be directed towards the assessment of bottom reflectance parameterization in different regions in the world under different environmental conditions. Ideally, *in situ*, rather than modeled, IOP

measurements should be used to fully understand the impact of changes in bottom reflectance parameterization on IOP retrievals. This is the first detailed study of the impact of bottom reflectance parameterization on IOP retrievals in SWIM for the GBR.

CHAPTER 5 BOTTOM REFLECTANCE PARAMETERIZATION IN SHALLOW WATER OCEAN COLOR MODELS

This chapter uses different methods and types of datasets to assess the applicability and suitability to improve IOP retrievals in SWIM. The results provide a basis for generating spatially explicit bottom reflectance parameterization in SWIM and its impact on IOP retrievals.

Associated publications

REICHSTETTER, M., MCKINNA, L., FEARN, P., WEEKS, S. J., ROELFSEMA, C. M. & FURNAS, M. 2015b. Seafloor brightness map of the Great Barrier Reef, Australia, derived from biodiversity data.

MCKINNA, L. I. W., FEARN, P. R. C., WEEKS, S. J., WERDELL, P. J., **REICHSTETTER, M.**, FRANZ, B. A., SHEA, D. M. & FELDMAN, G. C. 2015. A semianalytical ocean color inversion algorithm with explicit water column depth and substrate reflectance parameterization. *Journal of Geophysical Research: Oceans*, 120, 1741-1770.

Main findings

- All four bottom reflectance maps (Lyzenga graded, Lyzenga classified, Bierwirth, and biodiversity) produce comparable IOP retrievals with little differences for most of the areas in the Capricorn Bunker Group.
- Field data compared poorly to retrieved bbp555, but compared well to retrieved a443 for all four assessed bottom reflectance maps.
- Landsat 8-based mapping approaches require more user expertise and are more time intensive compared to *in situ* based approaches.

5.1 Introduction

This chapter describes and compares four different methods to develop spatially explicit bottom reflectance maps to improve IOP retrievals in SWIM using two different types of data. To generate ocean color products from analytical ocean color models such as SWIM, a spatially explicit bottom reflectance map is needed. Currently, there is no such map of the GBR available that is suitable to be used in the bottom reflectance parameterization of SWIM. The need for spatially explicit bottom reflectance maps has only arisen in the past few years with the advance of shallow water ocean color inversion models, where it was shown that accounting for bottom reflectance can potentially improve IOP retrievals (McKinna et al., 2015). Previously, most ocean color algorithms that are applied to shallow water environments are either parameterized using a single bottom cover or they use a look-up table (Dekker et al., 2011). Typically, shallow water algorithms include bottom reflectance parameters, but may also derive some aspect of the bottom reflectance, such as classification of bottom types, where the algorithm selects a reflectance signature from a library of signatures. This is different to SWIM, which uses a pre-defined and explicit parameterization of the reflectance at each pixel. SWIM is currently the only operational shallow water algorithm and has been included in the NASA SeaDAS processing code.

Applications of remote sensing that use bottom reflectance mapping include monitoring coral reef health, water column correction for substrate mapping or deriving seafloor bathymetry (Example: Andréfouët et al., 2003, Mumby et al., 2004b, Stumpf et al., 2003, Vahtmäe et al., 2006, Purkis and Pasterkamp, 2004). At large, these studies used remote sensing to derive bottom cover. There are many different approaches to map seafloor cover or benthic reflectance using remote sensing imagery (Example: Lyzenga, 1981, Lyzenga et al., 2006, Bierwirth et al., 1993). Remote sensing presents a valuable tool for mapping the bottom of the shallow ocean. Yet, extracting the reflectance spectrum from the data of satellite sensors is complex. Visual inspection of moderate or high spatial resolution images (<1000 m) of reef systems can reveal valuable information of reef extent and reef configuration, as well as distribution of cover types. But, bottom cover often cannot be accurately identified by just visual inspection, as a dark-colored pixel can represent different bottom types, such as algae, seagrass or coral (Reichstetter et al., 2015a). Water depth further influences visual bottom classification as lighter, more reflective, bottom covers in deeper depth can resemble darker covers at shallower depths.

Many remote sensing algorithms that apply a water column correction to derive bottom reflectance, or bottom classifications, require remote sensing data that has been atmospherically corrected and masked for land and clouds (Zoffoli et al., 2014). At large, water column correction algorithms consider the bottom as a Lambertian reflector (Zoffoli et al., 2014). In addition, the remote sensing signal measured at the surface, R_{rs} , is usually separated into two components: the water column and the ocean bottom. Water column correction algorithms used for estimating bottom cover or bottom reflectance can be broadly divided into band combination algorithms, model-based algebraic and optimization algorithms or spectral matching algorithms (Zoffoli et al., 2014).

Band combination algorithms are mostly applied to multispectral data, such as imagery from Landsat (Zoffoli et al., 2014). They assume that bottom radiance in band i ($L_{B,i}$) is an exponential function of depth and the vertical attenuation coefficient in band i ($K_{D,i}$) (Zoffoli et al., 2014, Lyzenga, 1978, Lyzenga, 1981, Lyzenga et al., 2006). Band combination algorithms attempt to linearize the relationship between radiance or reflectance in two bands, i and j , and water depth. The models run under the assumption that the water column is vertically and horizontally homogeneous and the variability in bottom reflectance for the same bottom type is small. While some band combination algorithms have been developed for waters with lower transparency, such as coastal environments, generally, these algorithms are only accurate for waters with high transparency. Lyzenga developed the most commonly used band combination algorithm (Zoffoli et al., 2014, Lyzenga, 1978, Lyzenga, 1981, Lyzenga et al., 2006).

Model-based algebraic algorithms use *in situ* measurements of water column parameters – for example, absorption and scattering coefficients – to define the behavior of light within a water column (Zoffoli et al., 2014). Most of these models require measurements of depth as an input parameter. Some of the most common model-based algebraic algorithms include those by Lee et al. (1999) and Bierwirth et al. (1993).

Optimization or matching approaches are commonly classified as radiative transfer based algorithms using spectral matching. They can be divided into semi-analytical and database search algorithms. Semi-analytical algorithms start with radiative transfer theory to derive an approximate analytical model functionally relating R_{rs} to water column depth and reflectance. They then estimate best-fit values of model parameters using non-linear optimization from the image R_{rs} . Database search algorithms use a radiative transfer based algorithm to create a database of R_{rs} spectra for all possible combinations of water absorption and scattering properties, water depths, and bottom reflectance that might be found in the study area. They then match the database spectra to the image spectra to create a bottom cover map.

The aim of this chapter is to assess which types of datasets and mapping approaches can be used to potentially improve IOP retrievals. To achieve this aim, four different approaches have been used to generate bottom cover maps for use in SWIM. Three bottom cover maps are based on Landsat 8 imagery. Two of these maps were created using the band combination method of Lyzenga (1978). For the first map, the researcher used the Lyzenga depth-invariant index as input for unsupervised classification processing to derive a light and dark classified map. The second map was generated by converting the Lyzenga depth-invariant index into graded percentages of light bottom cover. The light bottom cover is indicative for sand cover and relates to the “light” bottom cover category from Chapter 3. The third map is based on the model-based algebraic method of Bierwirth et al. (1993) to derive a map of percentage light cover. An additional bottom cover map was created, which is not based on remote sensing data, but rather on *in situ* biodiversity data. There are no studies known to the author that have converted *in situ* biodiversity data into bottom cover maps for the use in shallow water inversion models.

Differences in IOP retrievals using bottom reflectance corrections based on the different mapping methods are presented. The approaches to bottom reflectance mapping presented here illustrate how different types of datasets can be used to create bottom reflectance maps that can be applied to ocean color shallow water inversion models to improve IOP retrievals. While the datasets used in this study are GBR specific, the methods are applicable to other parts of the world. Importantly, the study demonstrates that bottom reflectance can be mapped using different datasets, depending on availability and user expertise.

5.2 Methods

The methods for this chapter can be divided into two stages. First, the researcher produced four different bottom reflectance maps using two different types of datasets (Landsat 8 and biodiversity). Second, the effect of the four different bottom reflectance maps on IOP retrievals was assessed. An outline of data processing and analysis is presented in Figure 5-1 and summarized in the following sections.

Assess and test different approaches to create a spatially explicit bottom reflectance map for areas deeper than 5 m using different types of datasets

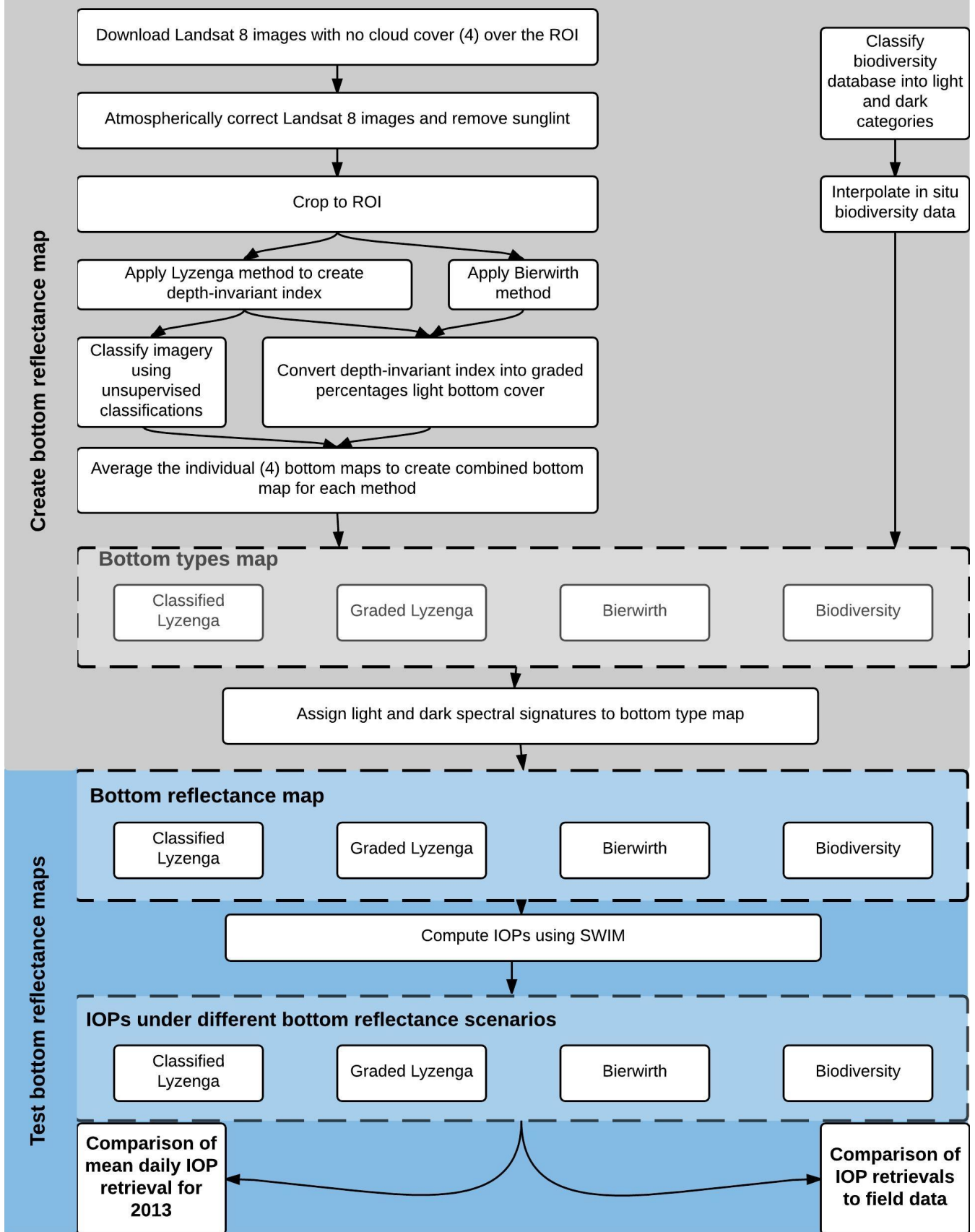


Figure 5-1: Flowchart of methods used in this study

5.2.1 Study area

This study provides an approach to mapping light and dark bottom cover in the southern part of the Great Barrier Reef of Australia. The study site includes the Capricorn Bunker Group (23.2 S –23.7 S, 151.6 E –152.1 E) (Figure 5-2). The study area was selected due to the availability of field data and the researcher’s knowledge of the area. The region of interest (ROI) is the shallow water area between 5 m and 25 m depth, which lie mostly between shallow reefs and islands.

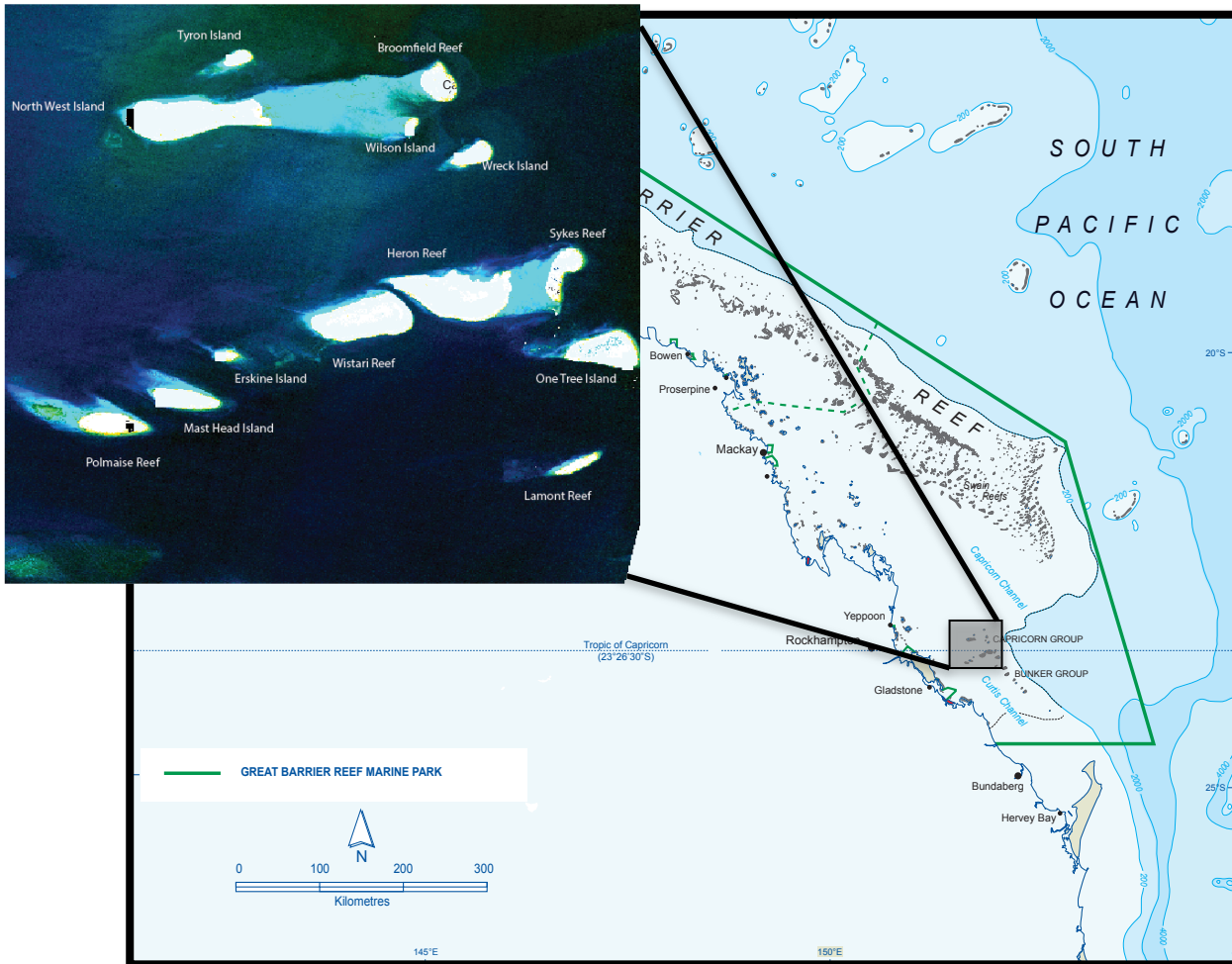


Figure 5-2: Atmospherically corrected Landsat 8 (LC80910762014198LGN00) (17 July 2014) image for the study area: the Capricorn Bunker Group and the southern GBR and map of the Great Barrier Reef with the green line on the GBR map indicates the boundaries of the Great Barrier Reef Marine Park area

5.2.2 Mapping process

The seafloor brightness maps were developed primarily as an input parameter for the SWIM algorithm as implemented in the NASA SeaDAS software package (<http://oceancolor.gsfc.nasa.gov>) to improve IOP retrievals. The current SWIM model for the GBR is parameterized as follows:

$$\rho_{net}(\lambda) = c_L \rho_L(\lambda) + c_D \rho_D(\lambda) \quad (5.1)$$

where $\rho_{net}(\lambda)$ is the net benthic reflectance per pixel and C_L representing relative proportion of light and C_D presenting the relative proportion of dark bottom cover (McKinna et al., 2015). The “light” spectrum was generated from average sand spectra and the “dark” spectrum was generated from an average of dark substrate spectra (green and brown algae, coral and seagrass) as presented in McKinna et al. (2015) (Figure 5-3).

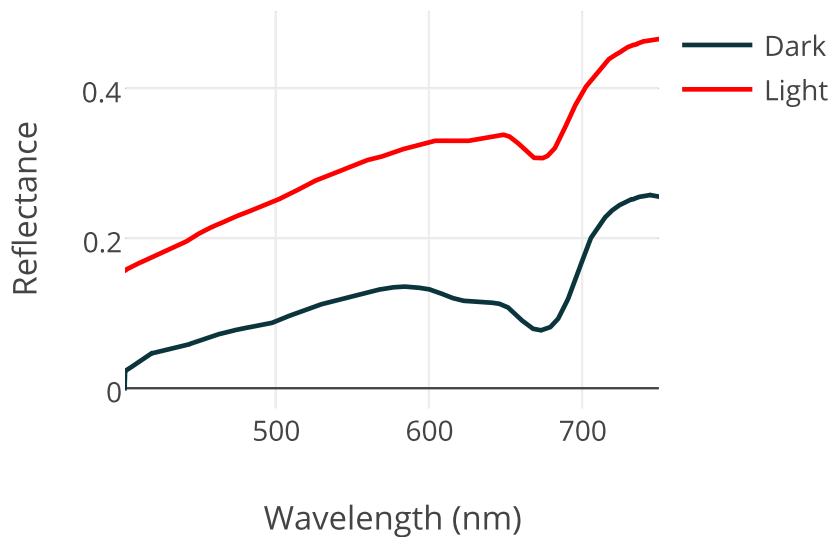


Figure 5-3 Light and dark spectra used in the SWIM bottom reflectance parameterization

This section outlines how to create a bottom reflectance map, which is based on two different types of datasets: biodiversity and satellite imagery.

The following four benthic reflectance maps were created:

Graded percentage light maps:

1. Biodiversity data (BIO)
2. Lyzenga depth-invariant index (LZ)
3. Bierwirth approach (BR)

and a classified map:

4. Lyzenga depth-invariant index (CL)

5.2.2.1 Bottom reflectance map from biodiversity data (BIO)

Quantitative bottom community structure and cover density data were used to create a bottom reflectance map. The dataset is based on the Reef CRC Great Barrier Reef Seabed Biodiversity Project (hereafter referred to as the CRC Biodiversity Project), which produced the most comprehensive characterization of living and non-living bottom cover throughout the GBR. The \$9 million project was a collaboration between four research partners – the Australian Institute of Marine Science (AIMS), the Commonwealth Scientific and Industrial Research Organisation (CSIRO), Queensland Department of Primary Industries and Fisheries (QDPI&F), and the Queensland Museum (Pitcher, 2007). The aim of the CRC Biodiversity Project was to map non-reef habitats and their biodiversity throughout the Great Barrier Reef Marine Park (Pitcher, 2007). The map produced by the CRC Biodiversity Project was based on samples collected at 1210 locations throughout the GBR at depths between 10 m and 150 m, which is unique as most previous reef biological surveys focused on shallow reef habitats (<5 m deep) (Pitcher, 2007). At each sampling site, several devices, including towed video and digital cameras, baited remote underwater video stations (BRUVS), a digital echo-sounder, an epibottom sled and research trawls trawlers were deployed to collect samples of sediment, benthic plants, invertebrates and fish on the seabed.

Twenty-three (23) of the sampling sites fell within the study area examined in detail in this chapter (Figure 5-4). The data from the 23 specific locations were used to generate a bottom reflectance map of light and dark features.

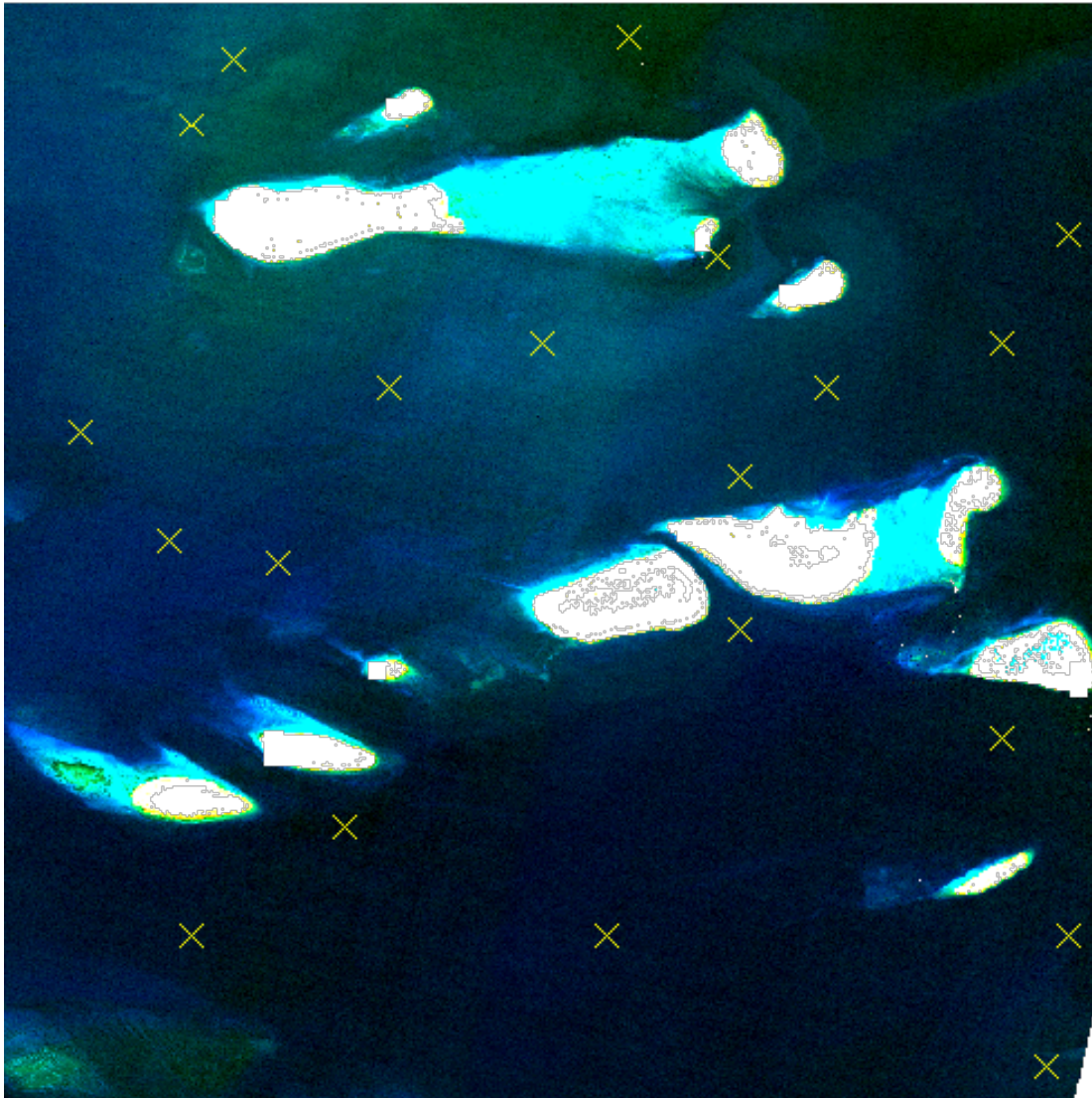


Figure 5-4: RGB Landsat 8 image (17 July 2014) and sample points map showing the 23 sites sampled during the CRC seabed biodiversity survey in the study region (Data from: Pitcher, 2007).

The original benthic cover type classifications listed in Table 5-1 were converted into optically light and dark categories, based on the spectral separability criteria defined in Chapter 3 (Reichstetter et al., 2015). Photographic and written descriptions of each biodiversity class were used to gain an understanding of their likely optical characteristics.

The assumption was made that sparse and medium cover categories mainly contain sand or carbonate sand and, at the spatial scale of MODIS satellite resolution (1 km), the light spectra dominate; hence, these categories were assigned to the light class.

Table 5-1: Light and dark feature classification based on the CSIRO seabed biodiversity

Light feature	Dark feature
No Biohabitat	Alcyonarians Dense
Bioturbated	Whip Garden Dense
Alcyonarians Sparse	Gorgonian Garden
Alcyonarians Medium	Sponge Garden
Whip Garden Sparse	Hard Coral Garden
Whip Garden Medium	Live Reef Corals
Gorgonian Garden	Flora
Gorgonian Garden	Algae
Sponge Garden Sparse	Halimeda
Sponge Garden	Caulerpa
Hard Coral Garden	Seagrass
Hard Coral Garden	
Bivalve Shell Beds	
Squid Eggs	
Tube Polychaete Beds	

For each benthic sampling site, the relative proportion from the entries in Table 5-1 were used to calculate light and dark bottom cover contribution, which resulted in two maps: (i) percentage of light substrate and (ii) percentage of dark substrate. The light and dark sample point maps were interpolated to a raster using ArcGIS geospatial software (ArcGIS, 2011) with (a) an inverse distance weighted interpolator, (b) a cell size set to be of 0.0009999 decimal degrees (dd) (~ 100 m), and (c) a maximum number of surrounding points (extrapolation distance) of 12. The resulting grids were represented in stretched values along a color ramp for display and analysis purposes. The spatially distributed bottom reflectance map was assigned the light and dark spectra as presented in Figure 5-3.

5.2.2.2 Bottom reflectance map from Landsat data

Three shallow water bottom reflectance maps using Landsat 8 data were produced. The approach adopted here was to classify light and dark bottom covers based on color. Four Level 1 images from the Operational Land Imager (OLI) on Landsat 8 were obtained in GeoTIFF format from EarthExplorer (<http://earthexplorer.usgs.gov/>), covering the southern GBR area (Path 91/Row 76) with less than 10% cloud cover over the study area (Table 5-2). The images were cropped to cover the study area. The four quasi-true color images of the study area are displayed in Figure 5-5.

Table 5-2: Landsat 8 images used for the remote-sensing based bottom reflectance maps

Landsat Image	Date	Symbol
LC80910762013211LGN00	30 July 2013	Image A
LC80910762014198LGN00	17 July 2014	Image B
LC80910762014230LGN00	18 August 2014	Image C
LC80910762015217LGN00	05 August 2015	Image D

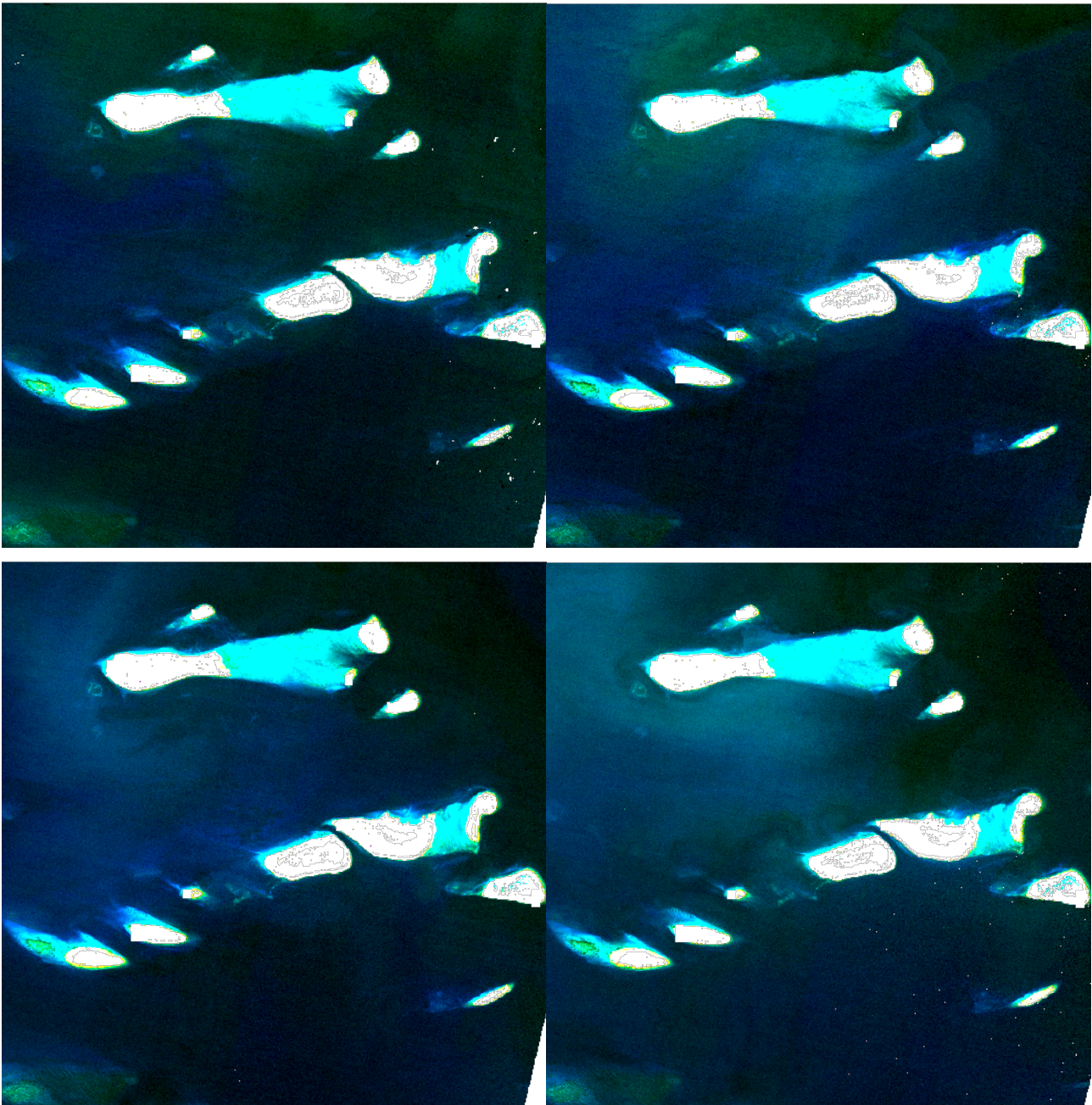


Figure 5-5: RGB Landsat 8 images used to generate the bottom reflectance maps: Image A (July 2013) (top left panel), image B (July 2014) (top right panel), image C (August 2014) (bottom left panel) and image D (July 2015) (bottom right panel).

The images were atmospherically corrected to at-surface reflectance using the SeaDAS L2gen processing code (Vanhellemont et al., 2014). The images were projected to a horizontal datum of WGS84 and collocated with the gbr100 bathymetry dataset (Beaman, 2012) using the SeaDAS GPT toolkit. The image analysis and processing for all images was carried out using ENVI, ArcGIS and SeaDAS. The four images were then pre-processed prior to the image analysis to mask out land and deep-water areas (deeper than 25 m).

Land was masked out during the atmospheric correction using the SeaDAS L2gen processing code. The deep waters were masked out using the bathymetry dataset by applying a mask to each Landsat 8 band. Two different approaches, Lyzenga (1978, 1981) and Bierwirth et al. (1993), were used to correct the effects of the water column on bottom reflectance. The following sections describe the individual approaches to generate light and dark bottom cover maps using remote sensing techniques.

5.2.2.2.1 Lyzenga approach

Lyzenga (1978, 1981) developed a band-ratio-based approach to create a depth-invariant index for multiband satellite imagery, which compensates for variation in depth. The Lyzenga method makes two main assumptions: (i) waters are clear and (ii) light intensity decreases exponentially with increasing depth. The Lyzenga method creates a single depth-invariant band for each pair of spectral bands (for further details, readers are directed to Lyzenga (1978), Lyzenga (1981)). The researcher calculated the ratio of attenuation coefficients k_i/k_j and produced depth-invariant bands for Landsat 8 bands 1 and 2, 1 and 3, as well as 2 and 3. Band 4 contained relatively little information in areas corresponding to the study area as the water column absorbed the majority of red light. For each of the four assessed Landsat scenes, the coastal blue (Rrs443), blue (Rrs482) and green (Rrs561) Landsat 8 bands yielded three usable depth-invariant bands for subsequent classification.

Classification map

An unsupervised classification approach using k-Means (Canty, 2014), which does not require any initial inputs of spectral training data to classify the Landsat 8 imagery, was considered to be adequate for distinguishing the differences in spectral signatures between spectrally light and dark bottom covers. Upon visual examination of each band, it was decided that all the depth-corrected bands using the Lyzenga method – coastal blue_blue (Rrs443_Rrs482), coastal blue_green (Rrs443_Rrs561) and blue_green (Rrs482_Rrs561) – would be used for classification of bottom covers. The atmospherically corrected and depth-invariant Landsat 8 satellite images were subjected to k-Means clustering using ENVI, an unsupervised classification method which organized each pixel into the assigned number of classes (eight classes in the present study) during 10 iterations.

The resultant classification was examined visually against the satellite imagery to assess if any classes could be grouped – for example, if any were clearly representing the same bottom types – and to highlight any areas that had obviously been misclassified. The eight classes were then amalgamated into three classes. Each of the three classes was assigned a symbol to discriminate pixels related to masked (M), light (L), or dark (D) areas.

To assess the consistency of the mapping approach, pairwise change detection maps of light and dark features were produced. Further, the classified Landsat 8 satellite images containing the three classes (M, L and D) were then combined to produce a synthesized raster image containing the class codes – 100% light, 75% light 25% dark, 50% light 50% dark, 75% dark 25% light and 100% dark.

Percentage light graded map based on the Lyzenga depth-invariant index

Input maps into the SWIM model are continuous and not classified because, in reality, areas are neither 100% dark nor 100% light, but contain a mixture of light and dark spectra. Therefore, a graded percentage light cover map was generated using Landsat 8 imagery. The principal researcher used the depth-invariant layer produced as described in the previous section, from Landsat 8 bands 2 and 3 only, to generate a graded percentage light cover map. The first step was to extract the area between depth of 5 m and 25 m. The images were then adjusted to set the minimum value to 0. The resulting raster was divided by the maximum raster value and multiplied by 100 for all the assessed images. The resulting four percentage light images – A, B, C and D – were then added together and divided by four to get the average image. The resulting percentage light cover was then adjusted to eliminate outliers.

5.2.2.2 Graded bottom reflectance map based on Bierwirth et al. (1993) method

The same imagery as used in the previous sections was used to create a graded map with percentages of light and dark bottom cover. However, whereas in the previous section the Lyzenga (1978) approach was applied to correct for water column effects, in this section the Bierwirth et al. (1993) water column correction algorithm was applied to the Landsat 8 images. In addition, K_d Lee (Lee et al., 2005) was calculated using the L2gen processing code in SeaDAS. Since K_d cannot be calculated successfully in shallow water

areas, the principal researcher used the average K_d Lee values of the deep water area (25–200 m) within the Landsat 8 scenes. K_d Lee values are different in deep water areas compared to shallow water areas. Yet, band ratios, such as proposed in some studies (Zoffoli et al., 2014, Bierwirth et al., 1993, Lyzenga, 1978, Lyzenga, 1981), are also not entirely accurate. Using this approach, the researcher tried to establish if different methods of applying K_d would lead to different IOP retrieval results. Band ratios often do not work in coastal areas, whereas K_d Lee values could potentially improve the water column correction. Table 5-3 shows the K_d Lee values used during the water column correction process.

Table 5-3: Mean K_d Lee values used in the Bierwirth et al. (1993) water column correction

Wavelength (nm)	Image A	Image B	Image C	Image D
443	0.0613	0.0575	0.0495	0.0619
482	0.0493	0.0456	0.0384	0.0476
561	0.0907	0.0911	0.0865	0.0908

The researcher used the gbr100 bathymetry as the known input depth and did not calculate the bottom depth using the approach stated in Bierwirth et al. (1993). The researcher considered the gbr100 bathymetry dataset values more accurate than the depth values calculated from the Landsat 8 Imagery using the Bierwirth method. Knowing the water depth (Z) and the attenuation coefficient (K_d), the researcher used the following formula to calculate the bottom reflectance:

$$R_{B_i} = R_{E_i} e^{(2K_d i Z)} \quad (5.2)$$

where R_{E_i} is the atmospherically corrected surface reflectance and R_{B_i} is the derived estimate of true bottom reflectance for band i . The R_B for each wavelength (443, 483 and 561) was averaged to generate the band-averaged bottom reflectance. A linear peak-clipped histogram function was applied using the Sentinel Application Platform (SNAP) data-processing software (ESA, 2016) to eliminate extreme values and adjust the data so it can be converted to a percentage light bottom cover map.

The linear peak-clipped histogram function redistributed the pixel values based on linear scaling between minimum and maximum pixels around the peak so that extreme low and high values do not influence the overall distribution. The data was then normalized from 0–100 to generate the 100% light map, where the 100% light means 100% sand cover and 0% light means no sand cover. This image processing procedure was applied to all four Landsat 8 images (A, B, C and D). The resulting four band-averaged bottom reflectance images were then averaged to produce the final bottom reflectance map (BR) of the Capricorn Bunker region.

5.2.3 SWIM modeling

The SWIM (Shallow Water Inversion Model) method used in this study is an implementation of the semi-analytical, non-linear search algorithm developed by Lee et al. (1998, 1999). SWIM is part of the NASA Ocean Biology Processing Group L2gen satellite data processing code (available as part of the SeaWiFS Data Analysis System (SeaDAS); <http://oceancolour.gsfc.nasa.gov>). SWIM does account for bottom reflectance heterogeneity, whereas the original model from Lee et al. (1998, 1999) did not. A high-resolution digital elevation model (DEM) for the GBR and adjoining Coral Sea at a grid pixel resolution of 0.001-arc degree (about 100 m) was used in this project and is further described in Chapter 2. The bathymetry dataset (gbr100) is included in the SeaDAS software package.

Extracted L1A MODIS Aqua time series data for the test region, from 1 January 2013 to 31 December 2013, was obtained from the NASA ocean color website (<http://oceancolour.gsfc.nasa.gov>). The data was batch processed from Level-1A to Level-2 using the L2gen implementation of SWIM to produce retrieved a443 and bbp443.

5.2.4 Field data

For testing the bottom reflectance parameterization, a field campaign was conducted in the Capricorn Bunker area. Water column attenuation and backscattering were measured during the period 23–25 April 2013. Only four data points out of 18 were selected to be useful and appropriate for a match-up analysis, as the other data points did not fall within valid MODIS pixels (Figure 5-6).

Absorption and beam attenuation measurements are made using WET Labs ac-9 or ac-s instruments. The ac-9 instrument utilizes two dual-flow tubes – attenuation (c) and absorption (a) tubes – a collimated source lamp, and spectral bandpass filters on a rotating wheel to record absorption and attenuation in the visible to near infrared electromagnetic spectrum at multiple wavelengths (Slade et al., 2010, Moore et al., 1997). Absorption is recorded using a reflective tube and a wide-angle detector, which includes a diffuser, while attenuation is recorded using a non-reflective tube and collimated detector (Slade et al., 2010). The ac-9 instrument records attenuation and absorption at nine wavelengths at a rate of 6 Hz (Slade et al., 2010).

In this study, a 25-centimeter path length WetLabs ac-9 was used to measure the absorption coefficient (a) and beam attenuation coefficient (c) of materials other than water at nine wave bands at 10 nm FWHM across the visible spectrum. Absorption and attenuation signals at 715 nm were corrected for temperature-dependent water absorption (Pegau et al., 1997) and the data was averaged over one-meter depth intervals. Daily field calibrations were undertaken to detect instrument drift (Moore et al., 1997). Total backscattering (b_b) was measured using a Hydroscat-2 HobiLabs (www.hobilabs.com). Since calibration of this instrument was not possible during the project durations, it was assumed that the manufacturer's calibration remained valid.

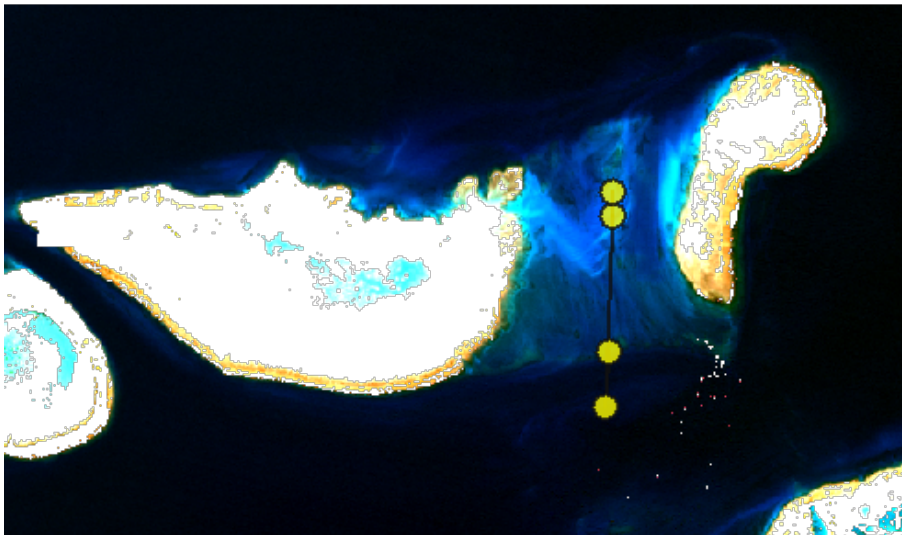


Figure 5-6: RGB Landsat 8 image (17 July 2014) displaying the field data point used in this study

5.2.5 Comparison of IOP retrieval

The daily mean IOP retrievals for pixels overlying four depth bins (5–10 m, 10–15 m, 15–20 m and 20–25 m) (Figure 5-7) were extracted from the generated L2 files for each of the different bottom reflectance maps, using the zonal statistics Python code from the Supplementary Spatial Statistics Toolbox in the ArcGIS software (ArcGIS, 2011). Each depth in 5-meter intervals was assigned to a zone using the raster depth mask created from the gbr100 bathymetry dataset. Only scenes with valid pixels in each depth range were considered, which resulted in the processing of 244 scenes out of a possible 365. A regression analysis (Type I) was conducted to compare the IOP retrievals in each depth zone and under different bottom reflectance scenarios. Type I regression was considered appropriate due to the high correlation of the retrieved IOPs. Histogram distribution and scatterplots were also generated to assess the distribution of the mean daily IOP retrievals from the different bottom reflectance scenarios.

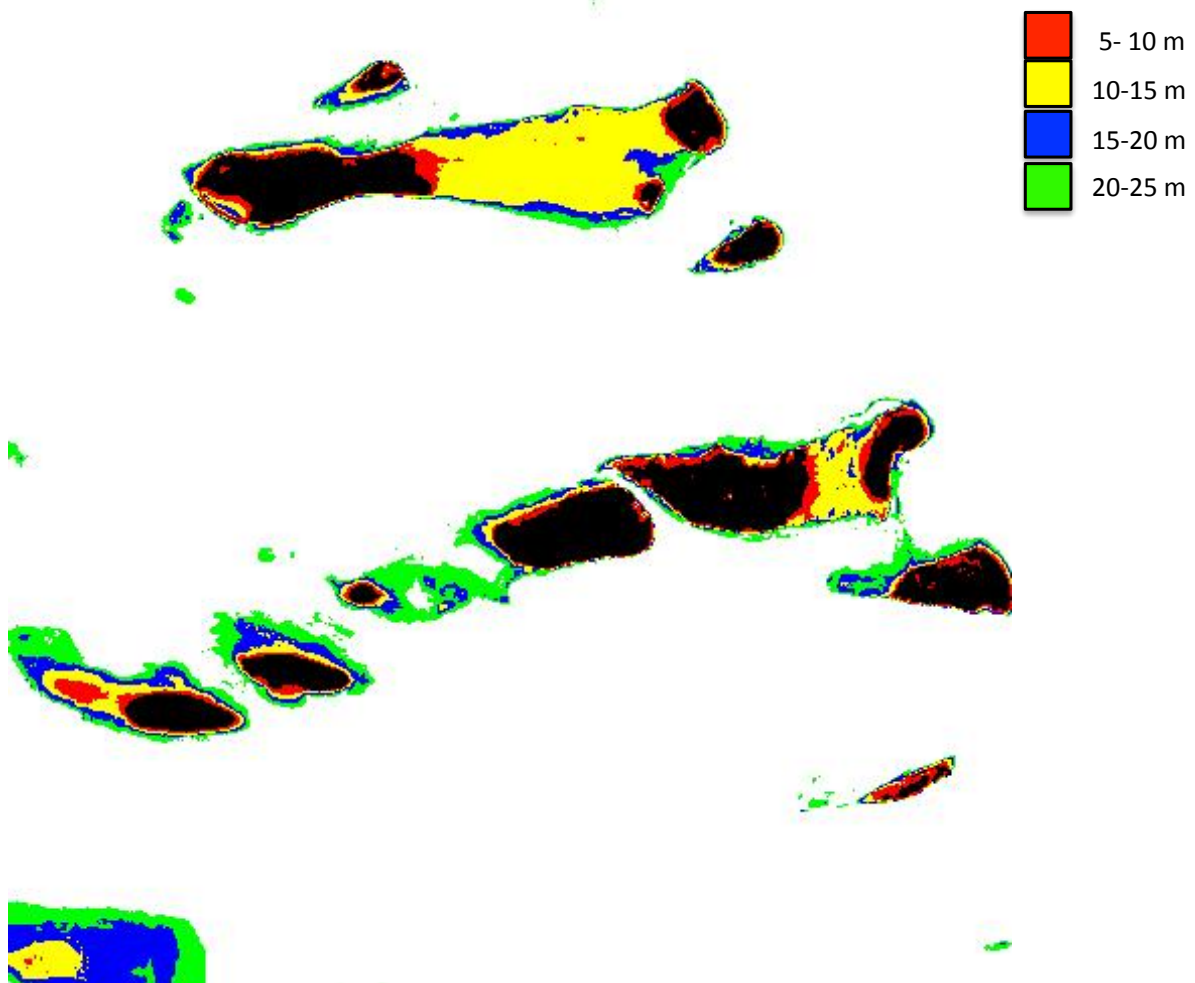


Figure 5-7: Depth bins used to derive mean daily IOPs

5.2.6 Comparison of IOP retrievals to field data

MODIS Aqua data for the ROI for 24 April 2013 was downloaded and processed to Level 2 using SWIM in L2gen for each of the four different bottom reflectance maps. An additional scenario was generated using the QAA model to compare the differences of SWIM-derived and QAA-derived IOPs when compared to *in situ* data. In the present study, a match-up was considered valid if a match-up point fell within the latitude and longitude of a valid (non-zero) pixel within a 3X3-pixel window. The average retrieved IOPs were extracted using a 3X3-pixel window for each of the four field data points. The average retrieved IOPs were then compared to the *in situ* data.

5.3 Results

5.3.1 Comparison of bottom reflectance maps

5.3.1.1 Percentage light bottom reflectance maps

This section displays the percentage light maps only. The percentage dark bottom cover is calculated as follows within the current SWIM format:

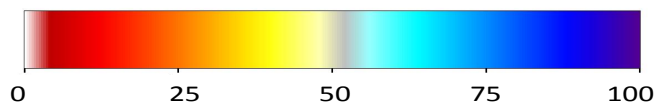
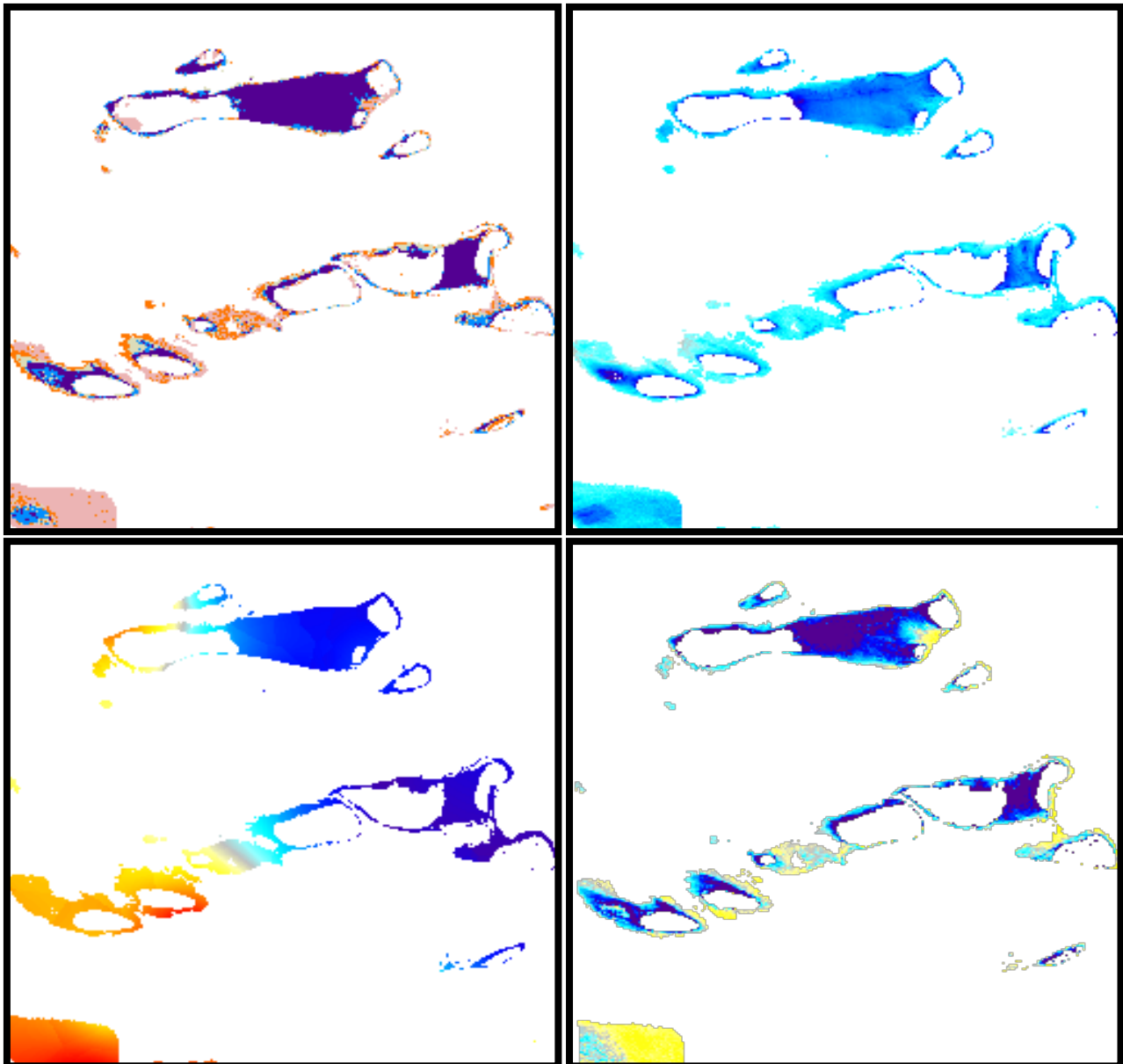
Percentage (%) dark bottom cover= 100% - percentage (%) light bottom cover

For example, if a pixel in the light bottom cover map has a value of 80% the dark bottom cover pixel will contain 20%, meaning that 20% of the dark spectral signature gets mixed with 80% of the light spectral signatures within SWIM.

The bottom reflectance maps, which are based on Landsat 8 imagery, have a 30-meter resolution, while the bottom reflectance map based on the biodiversity dataset was interpolated at a 100-meter resolution to match the gbr100 bathymetry dataset (Figure 5-8). However, all the maps are interpolated to MODIS resolution (1 km) within SWIM and thus are missing some information around reefs and land. The percentage light bottom cover in the biodiversity map (BIO) is not affected by the locations of reefs, islands and bathymetry features, but shows an increase in percentage light bottom cover from the southwest to the northeast. There are only 23 biodiversity sample sites (Figure 5-4) within the assessed region and thus the southwest to northeast increase in percentage light bottom cover is most likely due to interpolation.

The graded Lyzenga (LZ) and the Bierwirth (BR) maps look similar in terms of resolution, relationship to islands and shallow reefs, as well as bathymetry features. Yet, the BR map has more dark (less light) pixels compared to the LZ map. The classified Lyzenga (CL) has five distinct classes, while all the other presented bottom maps are graded. The CL map is the only map that has areas with no light (0%) bottom cover, thus 100% of the dark spectra will be used within SWIM when computing IOPs. All the other bottom reflectance maps have at least 25% light bottom reflectance cover. The CL map has areas ranging from 0%–100% light bottom reflectance. The Lyzenga-graded (LZ) bottom reflectance map has between 50% and 100% light bottom reflectance cover in each pixel. The biodiversity (BIO) bottom reflectance map has between 25% and 100% light bottom reflectance in each pixel – similar to the Bierwirth (BR) map, which has between 30% and 100% light bottom reflectance in each pixel.

There are differences in the percentage of light bottom cover of up to 90% in a pixel between the CL map and the other maps (BIO, LZ and BR). The differences between the graded light bottom reflectance maps (LZ, BIO and BR) are smaller and are generally below 50%. Most of the areas with lower percentages of light bottom reflectance cover were observed west of 151°50' E. Most of the inter-reefal area between North West Island and Broomfield Reef was classified with high percentages of light bottom cover (above 50%). The area between Broomfield Reef and Wilson Island has a lower percentage of light bottom cover (below 50%) in the BR map, while it is classified as having 0% light bottom cover in the classified map. The same area has higher percentages of light bottom cover (50–90%) in the BIO and LZ maps. The area between Heron Reef and Sykes Reef contains a high level of percentage light bottom reflectance (above 75%) except for the LZ map, which displays areas with light bottom reflectance cover below 75%.



Percentage light cover (%)

Figure 5-8: Maps of percentage light cover at original resolution using the following methods: Lyzenga classified (CL) (top left), Lyzenga graded (LZ) (top right), biodiversity (BIO) (bottom left) and the Bierwirth approach (BR) (bottom right). The white pixels are not of interest to this study and either represent land or deep areas.

5.3.1.1 Differences in percentage light bottom cover of individual Landsat 8 scenes using the Lyzenga method

The three (3) Landsat 8-based bottom reflectance maps (LZ, CL and BR) were generated using four individual Landsat 8 images as listed in Table 5-2. The brightness of Landsat 8 images changes between different acquisition dates. Thus, the percentage light spectra assigned to each pixel may differ between Landsat 8 images from different acquisition dates. To illustrate the differences in percentage light bottom cover derived from single Landsat 8 images, a pairwise percentage change analysis was performed for the graded Lyzenga-based approach only (Figure 5-9). As mentioned previously each of the four individual Landsat 8 images was processed into a graded percentage light cover map using the Lyzenga method and then combined in an average map. This section assessed the four individual graded Landsat 8 maps, before they were combined in the final map. Most changes occurred within a range of $\pm 25\%$. The greatest change was observed in the very bright areas between North West Island and Broomfield Reef, and between Heron Reef and Sykes Reef. In addition, larger changes in the percentage of light bottom cover tend to be more evident closer to land or shallow reef areas. Very few differences were observed between images B (17 July 2014) and C (18 August 2014) ($\pm 15\%$), with the majority of pixels differing by $\pm 5\%$. Larger areas containing higher differences ($\pm 20\%$ – 25%) in the percentage of light bottom cover per pixel were observed between images A (30 July 2013) and B, A and C, B and D (05 August 2015), as well as C and D compared to A and D or B and C.

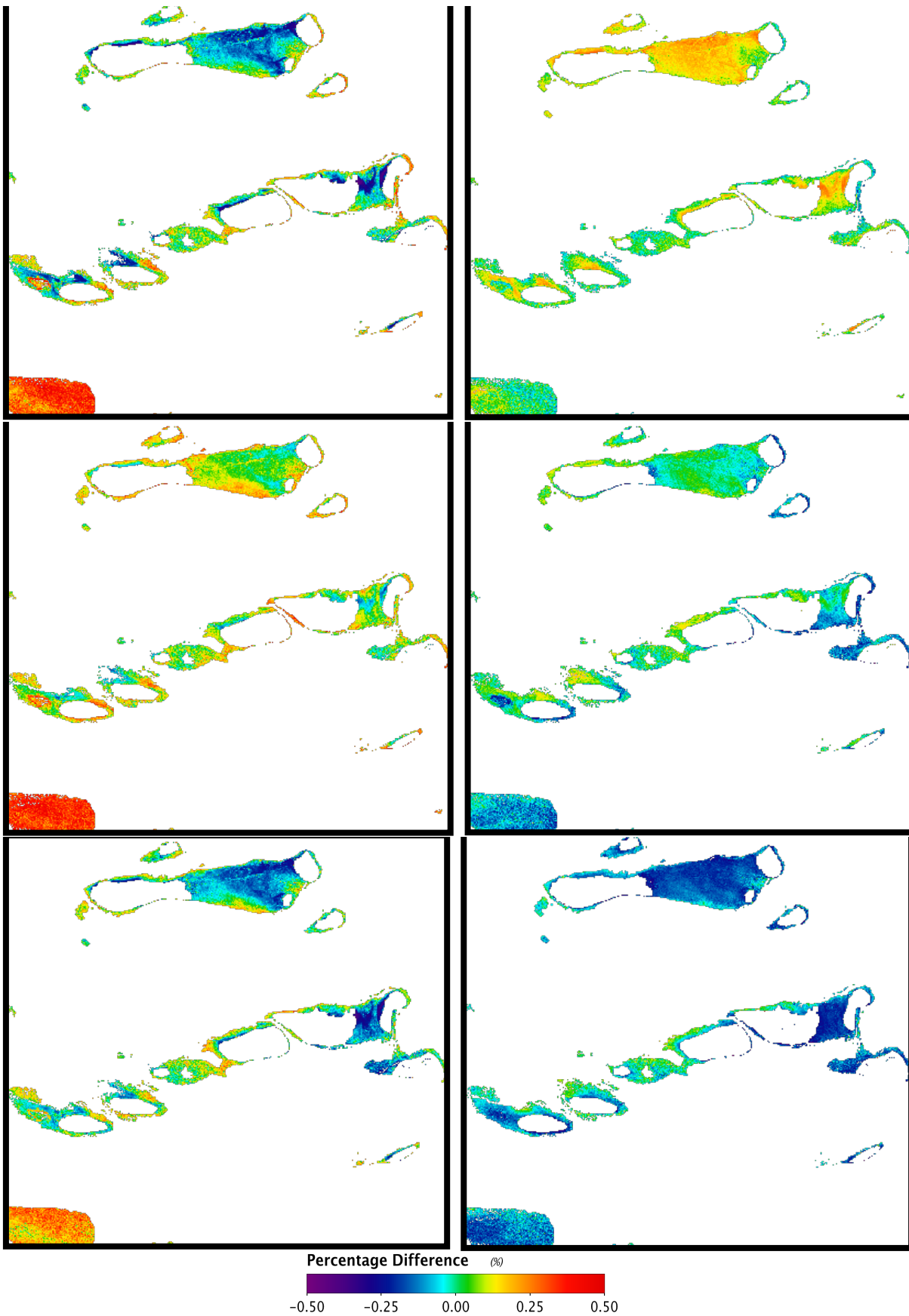


Figure 5-9: Pairwise percentage differences in Lyzenga graded light bottom cover maps between the four Landsat 8 images: images, A (July 2013) and B (July 2014) (top left), B (July 2014) and D (August 2015) (top right), A (July 2013) and D (August 2015) (center left), B (July 2014) and C (August 2014) (center right), A (July 2013) and C (August 2014) (bottom left), C (August 2014) and D (August 2015) (bottom right).

5.3.2 Comparison of IOP retrievals under different bottom reflectance scenarios

The SWIM-based IOP retrievals (a443 and bbp443) were compared for the four different bottom maps (BR, CL, BIO and LZ) for mean daily MODIS data from 01 January 2013 to 31 December 2013 using regression analysis. Figures 5-10 and 5-11 show the comparisons of IOP retrieval data for each of the bottom reflectance maps (BR, CL, BIO and LZ). Each of the four panels shows data for depth bins (5-10 m, 10-15 m, 15-20 m and 20-25 m). Within each panel are IOP retrievals distribution histograms for each of the four bottom reflectance maps, and scatter plots of IOP retrieval data comparing pairs of bottom reflectance maps. Also included in the figures are coefficient of determination (r^2), intercept (A), slope (b) and the root mean square error (E) of retrieved a443 and bbp443.

There is a good agreement ($r^2 > 0.710$) between the retrieved daily a443 values under the different bottom reflectance scenarios (BR, CL, BIO and LZ) (Figure 5-10). At depths greater than 20 m, the agreement between the a443 values is evident as shown in Figure 5-10 (bottom right panel) by the coefficient of determination ($r^2 > 0.987$), the slopes (b) being close to 1.0, the intercept (A) < 0.001 and the root mean square error (E) < 0.012 . Better results were achieved for the retrieved a443 values at depths of 5–10 m (Figure 5-10 top left panel) and 10–15 m (Figure 5-10 top right panel) with both r^2 and slope values close to 1.0 and $E < 0.04$, compared to 15–20 m (Figure 5-10 bottom left panel) with a minimum r^2 of 0.71, slopes between 0.78 and 1.117 and $E < 0.062$. The poorest agreement in retrieved a443 values was observed between the CL and BIO bottom reflectance comparison ($r^2 > 0.710$, $b = 1.118$, $A = -0.013$, $E = 0.062$) at 15–20 m depths. Generally, the slopes were between 0.78 and 1.17 for the 15–20 m depth ranges, while the r^2 values remained high (0.710–1.00). This indicates that the impact of differences in the bottom reflectance parameterization may lead to biases resulting in differences of retrieval retrieval between –22% to +17% per one m^{-1} change by using different substrate reflectance maps.

The CL bottom reflectance scenario has the greatest range of mean daily-retrieved a443 values at 10–15 m depths compared to the other bottom reflectance scenarios. The BIO bottom reflectance scenario had the smallest spread as evident in the histograms in Figure 5-10 (bottom left panel) in mean daily-retrieved a443 values. At depths of 5–10 m, as well

as from 10–15 m, the mean daily-retrieved a_{443} value for all bottom reflectance scenarios was between an r^2 value of 0.964 and 0.991.

However, the distribution of IOP retrieval values is greatest in the shallowest depth bin (5–10 m), compared to the other assessed depths, as shown by the histograms of retrieved s in Figure 5-10.

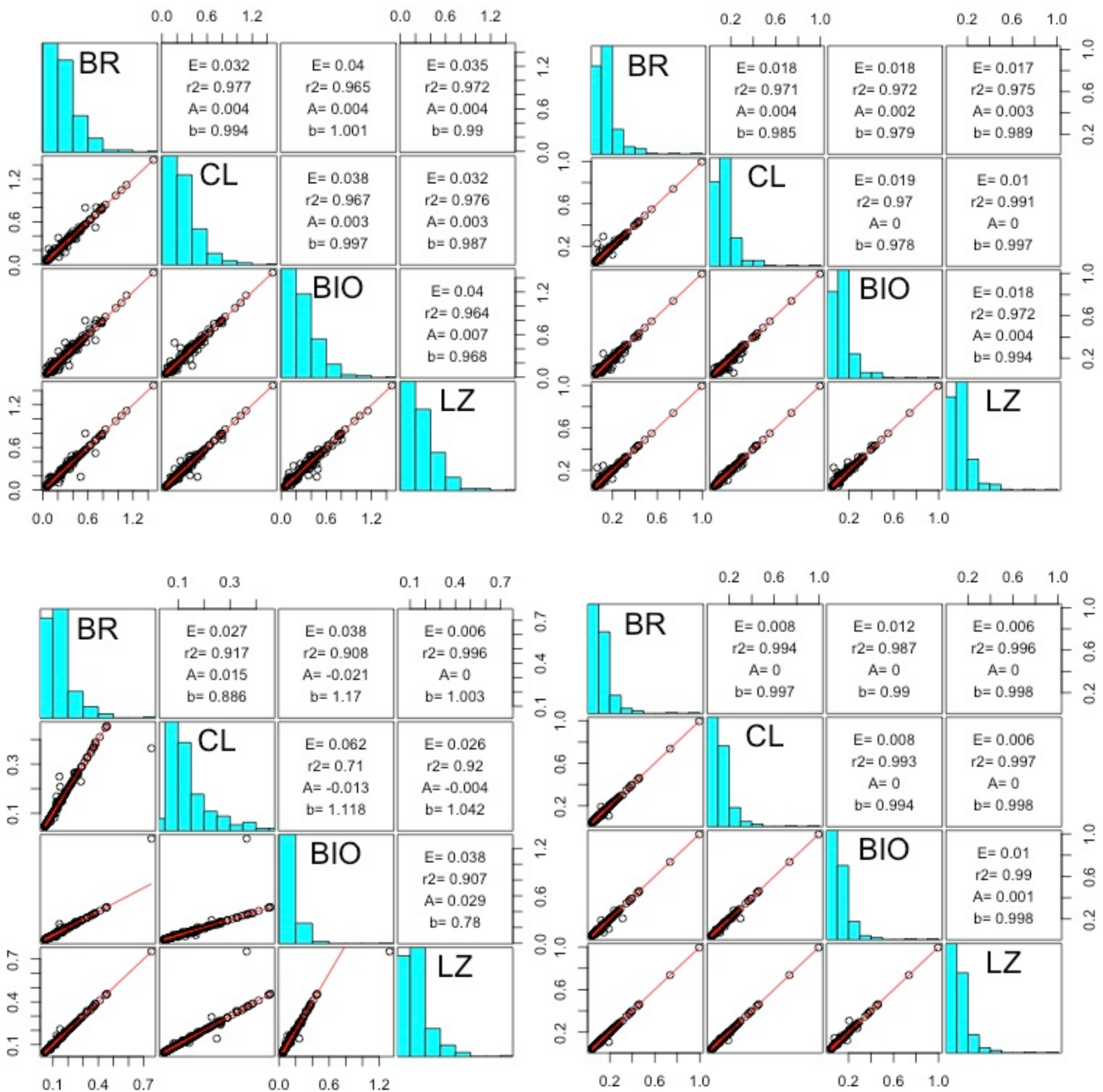


Figure 5-10: Scatterplots displaying pairwise comparison (column to row) between mean daily SWIM-derived a_{443} values of the four different bottom reflectance maps (BR, CL, BIO and LZ) from 1 January 2013 to 31 December 2013 grouped within the following 5-meter depth bins: 5–10 m (top left panel), 10–15 m (top right panel) 15–20 m (bottom left panel) and 20–25 m (bottom right panel).

There is good agreement ($r^2 > 0.832$) between the retrieved daily bbp443 values under the different bottom reflectance scenarios (BR, CL, BIO and LZ) (Figure 5-11). At depths greater than 20 m, the agreement between the retrieved bbp443 values is evident as shown in Figure 5-11 (bottom right panel) by the coefficient of determination (r^2) > 0.982 , the slopes (b) being close to 1.0, the intercept (A) equal to 0 and the root mean square error (E) < 0.001 .

Better results were achieved for the retrieved bbp443 values at depth bins of 5–10 m (Figure 5-11 top left panel) and 10–15 m (Figure 5-11 top right panel), with both r^2 , slope (b) values close to 1.0, intercept (a) close to 0 and root mean square error (E) < 0.005 , compared to those for the depth bin of 15–20 m minimum r^2 of 0.832, slopes between 0.702 and 1.68 and $E < 0.008$ (Figure 5-11 bottom left panel). The largest difference in retrieved bbp443 values was observed between the CL and the BIO bottom reflectance scenario ($r^2 > 0.832$, $b = 1.68$ and $A = -0.007$, $E = 0.008$) for the 15–20 m depth range. The slopes were between 0.702 and 1.68 for the 15–20 m depth range, while the r^2 values remained high (0.832–1.00). This indicates that the variation in retrieved IOPs due to changes in bottom reflectance parameterization (different maps) is not equal, resulting in differences of IOP retrieval between –29.8% to +68% per one m^{-1} change.

The histogram distribution of bbp443 is also greatest in the shallowest depth bin (5–10 m) compared with the other assessed depth bins. The BR bottom reflectance map produced the greatest range of bbp443 values as shown in Figure 5-11 top left panel.

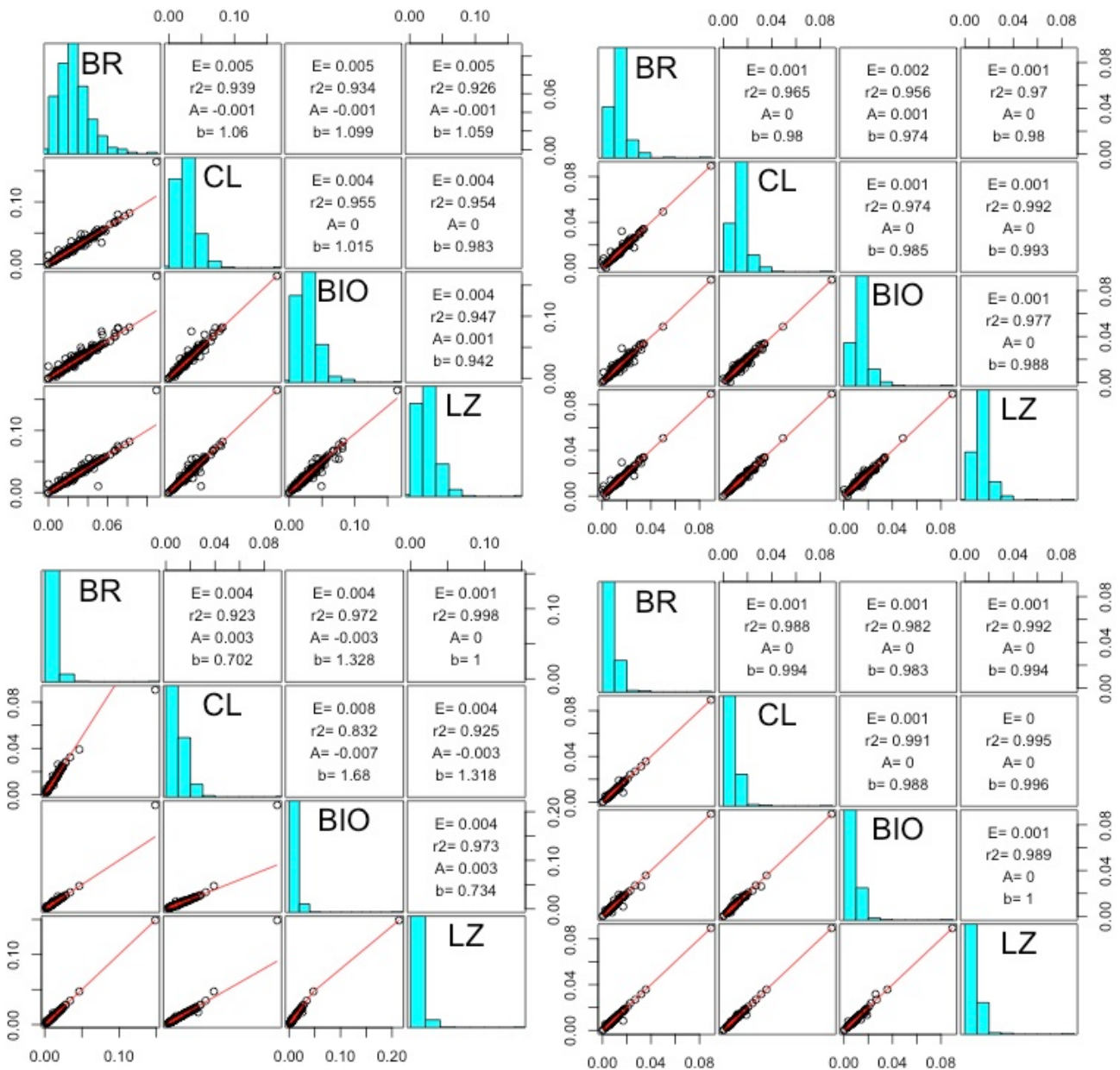


Figure 5-11: Scatterplots displaying pairwise comparison (column to row) between mean daily SWIM-derived bbp443 values of the four different bottom reflectance maps (BR, CL, BIO and LZ) from 1 January 2013 to 31 December 2013 grouped within the following 5-meter depth bins: 5–10 m (top left panel), 10–15 m (top right panel) 15–20 m (bottom left panel) and 20–25 m (bottom right panel). Comparison of IOP retrievals to field data.

The retrieved IOP values were compared to a very limited amount of *in situ* data (4 data points). Table B-1 in Appendix B provides some more detail of the individual field data points used in this section. The retrievals of average a_{443} values from a 3x3 window size for each *in situ* data point were comparable to the *in situ* data (maximum difference of -0.0016 m^{-1}) and were closer than the average QAA a_{443} values (difference of $+0.0204$) (Table 5-4). The BIO bottom reflectance scenario produced a higher average a_{443} value,

which resulted in a smaller difference in the *in situ* data compared to the other SWIM-derived a443 values, as well as the QAA-derived a443 value. The average retrieved a443 values of the BR and CL bottom reflectance scenarios were the same (0.0726 m^{-1}), while the average retrieved a443 value of the LZ bottom reflectance scenario was slightly higher at 0.0727 m^{-1} . The average retrieved a443 value for QAA is considerably higher at 0.0946 m^{-1} compared to the SWIM-derived average a443 values, and is also higher than the average *in situ* value (0.0024 m^{-1}).

The average bbp555 retrieval values from SWIM were approximately 3.5 times higher than the *in situ* data value, while the average retrieved bbp555 QAA value was only just over two times higher than the *in situ* value. The BIO bottom reflectance scenario produced a higher average bbp555 value compared with those of the other bottom reflectance scenarios (BR, CL and LZ) and thus produced a larger difference to the *in situ* data value (almost 3.5 times). The average retrieved bbp555 values of the BR and CL bottom reflectance scenarios are very close, with only 0.0001 m^{-1} difference between them, while the average retrieved bbp555 value of the LZ bottom reflectance scenario sits approximately in the middle of the range of the four SWIM-derived bbp555 values at 0.0075 m^{-1} . The average retrieved bbp555 value for QAA is considerably lower (0.0053 m^{-1}) compared to the SWIM-derived average bbp555 values, but also higher than the average *in situ* value (0.0742 m^{-1}).

Table 5-4: Average retrieved IOP values using SWIM with different bottom reflectance scenarios, QAA and *in situ* data

	Average bbp555 (m ⁻¹)	Average a443 (m ⁻¹)
SWIM_BR	0.0071	0.0726
SWIM_CL	0.0070	0.0726
SWIM_BIO	0.0083	0.0730
SWIM_LZ	0.0075	0.0727
QAA	0.0053	0.0946
<i>In situ</i>	0.0024	0.0742

5.4 Discussion

In this chapter, the researcher assessed four approaches to generating bottom reflectance maps (BR, CL, BIO, LZ) for use in SWIM. The retrieved IOPs using the four bottom reflectance map scenarios were compared over a one-year period (1 January 2013 to 31 December 2013). **The results showed that there were minor differences in IOP retrieval between the four maps, with $r^2 > 0.9$, slopes close to 1 and intercepts close to 0 for the 5–10 m, 10–15 m and 20–25 m depth bins.** Only the 15–20 m depth bin showed some differences in IOP retrievals with slopes between 0.78 and 1.17 for a443 retrievals and between 0.70 and 1.68 for bbp443 retrievals. Most of the 15–20 m pixels are located in the southwestern part of the assessed ROI (Figure 5-7). As seen in Figure 5-7, this area's contribution to light bottom cover ranges from 0% in the CL map to 75% in the LZ map. It is an area that produced a great range of differences in the individual Landsat 8-based maps (Figure 5-9), with differences in light bottom cover of up to 50% between the four different individual Landsat 8 images.

The BR and LZ maps showed very little differences in retrieved IOPs, with differences of 0.04% in mean daily retrieved a443 values and 0-6% in retrieved bbp443 values. This is likely due to the same source dataset and similar processing method. Even though the CL map is also based on the Landsat 8 dataset it shows slightly larger differences in retrieved IOPs, compared to the BR (a443= 0.03-11.4% and bbp443=0.06-29.8%) and LZ (a443= 0.02-4% and bbp443=0.04-31.8%) maps. The BIO map is based on a different datasets (biodiversity) compared to the LZ, CL and BR maps, which are based on Landsat 8. This resulted in larger differences between the BIO map compared to the LZ, CL and BR maps.

The CL bottom reflectance map produced the largest range of differences in IOP retrievals, with a minimum r^2 of 0.71, when compared to the BIO scenario at depths between 15 m and 20 m. This difference is most likely explained by the dark areas, with 0% light bottom cover present in the CL map, while none of the other bottom cover maps has areas with 0% light bottom cover as evidenced in Figure 5-8. The results in the previous chapter showed that there is no significant difference in mean retrieved IOPs between the 75% sand and 25% seagrass bottom cover class and the 50% sand and 50% seagrass bottom cover class. This finding indicates that IOP retrievals are not greatly affected by differences in $\pm 25\%$ light bottom cover under the current SWIM model configuration. This is supported by the current results, where bottom reflectance maps have different percentages in light bottom cover, yet the retrieved IOPs show good agreement. Yet, the comparison was based on mean daily retrieval values over several pixels, which resulted in good agreement between the retrieved IOPs. However, individual pixels or small areas in a scene where the individual bottom maps show large differences in percentage light spectra, might still lead to considerable differences in retrieved IOPs.

All the methods presented here could potentially be utilized to produce bottom reflectance parameters for use in SWIM and are likely to improve IOP retrievals. Unfortunately, not enough validation data was available to determine which bottom reflectance scenario produced retrieval values that compared best with the *in situ* data. McKinna et al. (2015) used a GBR-wide version of the BIO map described in this thesis (Reichstetter, McKinna, et al., 2015) to test the applicability of SWIM in shallow water environments. They found that, in general, the retrieval of IOPs is more sensitive to water column depth than benthic reflectance. Further, the study concluded that the BIO light and dark map, as described in this thesis, could be used successfully in SWIM (McKinna et al., 2015). Further, the results of spectral separability described in Reichstetter, Fearn, et al. (2015) found that at MODIS bands no more than two bottom classes could be separated based on at-surface spectral reflectance. Therefore, for MODIS sensor data, a light and dark bottom reflectance map as described in this chapter should be sufficient as input into SWIM. Yet, the principal researcher agrees with the conclusion of McKinna et al. (2015) that for past, existing or planned sensors with higher spectral resolution such as the Hyperspectral Imager for Coastal Ocean (HICO), Ocean and Color Imager (OCI) or the Ocean and Land Color instrument (OLCI), more bottom cover classes might need to be considered.

Also, the choice of methods to create a bottom reflectance map depends not only on data availability, but also on water clarity, if remote sensing methods are to be employed. In less clear water the possibility of miss-classification due to water column impact is greater in satellite imagery. Thus, *in situ* measurements, if available, may be more appropriate.

Landsat 8-based bottom reflectance mapping approaches require more user expertise and are more time intensive than *in situ* point-based approaches. Most of the focus for creating bottom reflectance maps is based on high-resolution satellite imagery or a combination of satellite and LIDAR data (Park et al., 2010, Macon et al., 2008, Gao, 2009, Islam et al., 2004, Blakey et al., 2015, Bierwirth et al., 1993). However, without some user expertise and knowledge of the applicability of water column and atmospheric correction to satellite images, products can become unreliable (Bierwirth et al., 1993, Lyzenga, 1978, Lyzenga, 1981, Zoffoli et al., 2014). As demonstrated on the Lyzenga graded map here, different Landsat 8 scenes produced up to a 50% difference in percentage light spectra in some pixels in parts of the ROI. A single Landsat 8 scene might not necessarily be representative of a region, as brightness can change between acquisition dates. Thus, it is essential that several Landsat 8 scenes are processed and averaged or compared to derive a more accurate bottom cover representation. If the objective was to derive a GBR-wide bottom reflectance map based on Landsat 8 data this would be a time-consuming process. Approximately 25 Landsat 8 scenes would need to be processed to cover all the shallow water areas within the GBR (<http://earthexplorer.usgs.gov/>). If the approaches presented in this thesis were used, each of the 25 scenes would need four images, which would result in the processing of 100 Landsat images. Unfortunately, it is not easy to automate the presented methods due differences in band ratios and image brightness from scene to scene (Bierwirth et al., 1993, Lyzenga, 1978, Lyzenga, 1981, Lyzenga et al., 2006, Sagawa et al., 2010). In addition, the methods used in this thesis to correct for water column effects are not accurate in waters with low transparency, such as coastal areas (Sagawa et al., 2010, Bierwirth et al., 1993, Lyzenga, 1978, Lyzenga, 1981, Lyzenga et al., 2006).

Producing a spatially interpolated bottom cover map from *in situ* data is relatively easy and quick compared to satellite image processing. Little user expertise is needed and spatial interpolation methods are well documented and integrated in spatial software, such

as ArcGIS (ArcGIS, 2011, Mathews et al., 2007). The advantage of creating bottom reflectance maps from *in situ* data is that the water column – hence, the geometric depth – does not affect the classification of light and dark. There has been no previous research undertaken which compared different methods to generate bottom reflectance maps for the use in SWIM prior to the work undertaken for this thesis.

Landsat imagery has recurrent spatial coverage over the entire GBR region, while *in situ* data on benthic community composition and water column IOPs is often sparse and might not be available for remote locations. Landsat 8 covers the entire GBR at 30 m x 30 m pixel resolution (Roy et al., 2014), while the *in situ* data points are often very sparse and one point might be used to represent hundreds of kilometers. For example, the seabed biodiversity dataset used herein is the most complete and spatially dense GBR-wide biodiversity survey, but it took several years to complete (Pitcher, 2007). The data were collected using an elaborate statistical sample and fieldwork design (Pitcher, 2007). Yet, only 23 sample sites are located within the test region used in the research undertaken for this thesis. All of the *in situ* points located in waters deeper than 25 m are not in the focus depth range of this thesis. Currently, SWIM uses MODIS satellite imagery at a 1 km resolution (McKinna et al., 2015). Hence, the bottom maps were resampled within SWIM to match MODIS pixels and resolutions smaller than 1 km are not necessary and are not likely to improve IOP retrievals.

Data availability is also a major factor when deciding on the mapping approach to be used. Landsat data are freely available and easy to access (<http://earthexplorer.usgs.gov/>), which makes it a tool that can be used by anyone worldwide and is not region specific. While this thesis demonstrated that *in situ* biodiversity data could be used successfully to generate a bottom reflectance map for use in SWIM, such a detailed and comprehensive dataset might not be available in many other regions in the world.

Field data compared poorly with bbp555 values, but compared well with a443 values for all four bottom reflectance maps. The limited amount of field data available makes a comparison to the SWIM-derived data difficult. The SWIM bbp555 values are much higher (approximately 3.5 times as much) than the *in situ* data. However, considering that most bbp values range from 0.0001 to 0.1 m⁻¹ in the GBR, a difference of 0.0059 m⁻¹ between the SWIM-derived bbp and the *in situ* data is relatively small. This is

also true for the average QAA-derived bbp555, which is 0.0029 m^{-1} higher than the average *in situ* bbp555. Whether the differences are due to bottom reflectance parameterization alone cannot be determined with the limited amount of *in situ* data. As noted in Chapter 4, bbp retrievals are highly sensitive to bottom parameterization. It is known that any inversion algorithm suffers from the non-uniqueness of the solution, meaning that multiple combinations of IOP values can lead to a unique reflectance spectrum (Defoin-Platel & Chami, 2007). Even in the open ocean, where bottom reflectance does not contribute to the IOP retrievals, ocean color model match-ups to *in situ* backscattering coefficients do not always produce satisfactory results (Example: Maritorena, d'Andon, Mangin, & Siegel, 2010; Mélin, Berthon, & Zibordi, 2005). Mélin et al. (2005) found that based on 17 match-ups, the comparison for the backscattering coefficient gives mean differences in the range of 31–53% for a study site in the Adriatic Sea. Maritorena et al. (2010) reported that there was a consistent difference observed throughout the assessed time-series between MODIS Aqua-derived bbp values and *in situ* match-ups.

The three main reasons for uncertainties in IOP retrievals are: (i) uncertainties in $r_{rs}(\lambda)$ measurements, (ii) uncertainties in shapes of IOPs and (iii) uncertainties in the IOP– $r_{rs}(\lambda)$ relationship (Wang et al., 2005). Any of these uncertainties could affect the IOP retrievals within SWIM and thus explain the differences between SWIM-derived IOPs and *in situ* data. SWIM is a relatively new semi-analytical inversion model and efforts are still being made to improve the IOP model within SWIM (McKinna et al., 2015). Further, there are uncertainties with the *in situ* data. For example, the spatial extent where the match-up field data usually characterizes an area of around 1–10 m, while the satellite spatial scale – MODIS in this study – is 1000 m. The difference in scales introduces an uncertainty that is often hard to quantify (Boss and Maritorena, 2006).

5.5 Concluding remarks

This chapter discussed and assessed four methods to generate bottom reflectance maps for the application in SWIM from *in situ* biodiversity and Landsat 8 data. The results show that all the presented bottom reflectance maps have comparable IOP retrievals when used in SWIM in the presented study region. The addition of the generated bottom reflectance maps to the SWIM algorithm has the potential to improve ocean color retrievals of IOPs and subsequent IOP-centered product, which are commonly used by the research

community to assess water clarity variability and trends in the GBR. The GBR-wide BIO bottom reflectance map has been provided to the NASA Ocean Color Group for implementation in the SeaDAS software program. The BIO bottom reflectance map has since been used to test the performance of the newly implemented Shallow Water Inversion Model (SWIM), as developed by the Australian Research Council Project LP100100342: Improved tools for comprehensive monitoring of water-clarity and light availability in coral reef ecosystems

CHAPTER 6 : CONCLUSIONS, SIGNIFICANCE AND FUTURE RESEARCH

This chapter revisits the main findings of this thesis and discusses their specific contribution to the field of satellite remote sensing of ocean color. Limitations of the studies are presented and the directions for future works are suggested.

6.1 Summary

The Great Barrier Reef (GBR) has a wide range of ecological, economic and social values. In recent decades, the water quality of the GBR has been under pressure from anthropogenic and natural disturbances (Example: De'ath and Fabricius, 2010, Fabricius et al., 2013, Fabricius et al., 2014, Furnas and Mitchell, 2001) Water clarity is one measure of water quality (Fabricius et al., 2014, Weeks et al., 2012). There is a significant need to accurately monitor the changes in water clarity for management of the GBR ecosystem health. Ocean color remote sensing provides a means for spatially extensive, repeatable, multi-scale and multi-temporal assessment of water clarity conditions on the GBR. Advances in ocean color imagery processing algorithms over the past decade have allowed the generation of reliable ocean color products for deep water environments. However, in shallow water environments, these ocean color products often fail, partly due to bottom reflectance contamination (McKinna et al., 2015). Recently, efforts have been made to generate shallow water ocean color algorithms, which correct for bottom reflectance (McKinna et al., 2015, Lee, 1999, Dekker et al., 2011, Wettle and Brando, 2006). To date, there have been only a limited number of studies and no detailed assessment to address the question of “how bottom reflectance parameterization can be optimized in shallow water inversion models”.

This thesis outlines the development of a detailed and transferable method that sets a sound foundation for developing bottom reflectance parameters in shallow water inversion models in coral reef environments using the GBR as a test case. This was achieved by: (1) examining the separability and detectability of bottom covers at MODIS and SeaWiFS bands to find the appropriate classification in bottom reflectance, (2) testing the sensitivity of bottom reflectance in the newly-developed Shallow Water Inversion Model (SWIM) (McKinna et al., 2015) to determine the most appropriate spectral signature to use in bottom reflectance parameterization, and (3) generating and testing the applicability of spatially explicit bottom reflectance maps using different datasets for the retrieval of Inherent Optical Properties (IOPs) in SWIM.

6.2 Main findings and outcomes

Objective 1: To assess the spectral separability and detectability of bottom reflectance in coral reef environments.

The spectral separability and detectability of bottom cover types at spectral resolution provided by MODIS and SeaWiFS sensor bands were assessed. The results showed: (i) no significant contamination ($R_{\text{rs corr}} < 0.0005$) of bottom reflectance on the spectrally-averaged remote sensing reflectance signal at depths >17 m for MODIS and >19 m for SeaWiFS for the brightest spectral reflectance substrate (light sand) in clear reef waters; and (ii) all bottom cover classes can be combined into two distinct groups, “light” and “dark”, based on the modelled surface reflectance signals. This study establishes that it is possible to efficiently improve parameterization of bottom reflectance and water column IOP retrievals in shallow water ocean color models for coral reef environments.

Objective 2: To test the sensitivity of bottom reflectance parameterization on the retrieval of IOPs using SWIM.

The impact of bottom reflectance parameterization on IOP retrievals in SWIM was assessed. The results showed that there is no clear spatial pattern in mean IOP retrievals under different bottom reflectance scenarios. A GBR-wide assessment showed that IOP values are highly variable across the GBR, and thus the sensitivity of IOP retrievals due to bottom reflectance parameterization also vary throughout the GBR. Further, the results suggested that water clarity influences the differences in IOP retrievals between different bottom types. Analysis showed that most of the differences in SWIM water column IOP retrievals varied between sand and seagrass, as well as between the sand and algae bottom reflectance scenarios, are observed at depths above -20 m. The results suggested that magnitude of the bottom reflectance spectra is not the only factor influencing the retrievals of IOPs—they are also influenced by the spectral shape. It was concluded that a subregional assessment of the impact of bottom reflectance parameterization on IOP retrievals is necessary to increase confidence in shallow water ocean color products.

Objective 3: Assess and test different approaches to create a spatially explicit bottom reflectance map for areas deeper than 5 m, using different datasets.

Four different bottom reflectance maps were generated based on different datasets. Three maps were generated using Landsat 8 data applying different methods to derive bottom reflectance for the Capricorn Bunker area. The fourth map was based on a biodiversity *in situ* dataset. A visual inspection of the different bottom reflectance maps showed that Lyzenga classified has the largest difference in percentage light bottom cover from the other bottom reflectance maps (90%), while the differences between the graded bottom reflectance maps (biodiversity, Lyzenga graded, Bierwirth graded) were generally smaller than 50%. The maps were used in the bottom reflectance parameterization within SWIM to create bottom reflectance scenarios. The mean daily retrieved IOPs from the different bottom reflectance scenario were compared. The results showed that all maps produced comparable results (r^2 0.71- 1.00) for depth from 5-25 m. Only for depth at 15-20 m the IOP retrievals did not agree well with a minimum r^2 of 0.71, slopes ranging from 0.70 to 1.68. This study establishes that all four methods used to generate bottom reflectance maps produce comparable IOP retrievals and thus can be used for bottom reflectance parameterization in SWIM.

6.3 Limitations and future research

As is often the case with scientific research, this thesis has led to more questions than answers. Research undertaken during this study has shown that the impacts of bottom reflectance on IOP retrievals are complex and difficult to assess for an area as large as the GBR. Future research should focus on six key areas to optimize parameterization of bottom reflectance in shallow water inversion models.

In this thesis, bottom cover maps were presented at a certain point in time. Yet, bottom cover is not static and changes over time. Some bottom covers, such as algae, might also change within seasons. Seasonal or temporal changes were not considered in this study due to data limitations. However, should new bottom cover data become accessible, the bottom reflectance maps created as part of this thesis could be updated. Also, if information on seasonal trends of bottom cover distribution becomes available, the inclusion of seasonal bottom maps in SWIM might be warranted.

The bottom cover maps generated in this thesis were only rigorously tested on one section of the GBR, the Capricorn Bunker group (23.2 S –23.7 S, 151.6 E –152.1 E). While the bottom reflectance maps based on biodiversity and sediment data cover the entire

GBR, the Landsat based maps only cover the Capricorn Bunker area. Hence, for comparative purposes, testing was only undertaken for that area. Further research should be directed to generating bottom reflectance maps for the entire GBR and testing their impact on IOP retrievals across the system.

The gbr100 bathymetry (Beaman, 2012) was used both to generate the bottom reflectance maps and to generate the IOP retrievals using SWIM, without accounting for tidal influences. In the GBR, tidal influences over shallow waters can be high and, if not accounted for, might lead to errors both in bottom map classifications and IOP retrievals. Currently there is no option to account for tidal influences in SWIM.

To generate bottom reflectance maps from remote sensing data, the researcher chose to use Landsat data, as it is free and readily available. Yet, newer satellites with higher spectral and spatial resolution, such as WorldView-2, might improve the accuracy of bottom reflectance maps. Future research should focus on methods to produce bottom reflectance maps from other data sources such as high-resolution satellite sensors.

SWIM has not been tested on regions other than the GBR; and therefore it was not possible to test the impact of bottom reflectance parameterization on IOP retrievals for other locations in this study. It is essential to test the impact of bottom reflectance parameterization in other locations around the world to determine wider applicability of the presented bottom reflectance parameterization methods.

This thesis assessed bottom reflectance parameterization for use in SWIM (McKinna et al., 2015). Future research into the applicability of the presented bottom reflectance parameterization for other shallow water inversion algorithms should be prioritized.

6.4 Contribution to knowledge

The methods and products presented in this thesis provide a fundamental basis for bottom reflectance parameterization in shallow water inversion models. This study has successfully demonstrated ways to optimise bottom reflectance parameterization in SWIM. Guidelines for selecting the most appropriate methods were developed to produce bottom reflectance input parameterizations based on different available datasets. This study has substantially increased knowledge on how bottom reflectance parameterization affects IOP retrievals. The contributions of this thesis to the body of scientific knowledge are:

- The first ever study to develop an optimal number of bottom types for bottom reflectance parameterization;
- First attempt to determine a bottom reflectance contamination depth limit;
- Identification of the relationships between bottom reflectance parameterization in SWIM and IOP retrievals;
- Provision of a fundamental basis for spatially explicit bottom reflectance maps for use in SWIM based on different datasets.

REFERENCES

- ACKLESON, S. G. 2003. Light in shallow waters: A brief research review. *Limnology and Oceanography*, 48, 323-328.
- ADLER-GOLDEN, S. M., ACHARYA, P. K., BERK, A., MATTHEW, M. W. & GORODETZKY, D. 2005. Remote bathymetry of the littoral zone from AVIRIS, LASH, and QuickBird imagery. *Geoscience and Remote Sensing, IEEE Transactions on*, 43, 337-347.
- AHMAD, W. & NEIL, D. 1994. An evaluation of Landsat Thematic Mapper (TM) digital data for discriminating coral reef zonation: Heron Reef (GBR). *International Journal of Remote Sensing*, 15, 2583-2597.
- AHMAD, Z., FRANZ, B. A., MCCLAIN, C. R., KWIATKOWSKA, E. J., WERDELL, J., SHETTLE, E. P. & HOLBEN, B. N. 2010. New aerosol models for the retrieval of aerosol optical thickness and normalized water-leaving radiances from the SeaWiFS and MODIS sensors over coastal regions and open oceans. *Applied optics*, 49, 5545-5560.
- ANDRÉFOUËT, S., BERKELMANS, R., ODRIOZOLA, L., DONE, T., OLIVER, J. & MÜLLER-KARGER, F. 2002. Choosing the appropriate spatial resolution for monitoring coral bleaching events using remote sensing. *Coral Reefs*, 21, 147-154.
- ANDRÉFOUËT, S., KRAMER, P., TORRES-PULLIZA, D., JOYCE, K. E., HOCHBERG, E. J., GARZA-PÉREZ, R., MUMBY, P. J., RIEGL, B., YAMANO, H. & WHITE, W. H. 2003. Multi-site evaluation of IKONOS data for classification of tropical coral reef environments. *Remote Sensing of Environment*, 88, 128-143.
- ANDRÉFOUËT, S., MULLER-KARGER, F. E., HOCHBERG, E. J., HU, C. & CARDER, K. L. 2001. Change detection in shallow coral reef environments using Landsat 7 ETM+ data. *Remote Sensing of Environment*, 78, 150-162.
- ANDRÉFOUËT, S. & RIEGL, B. 2004. Remote sensing: a key tool for interdisciplinary assessment of coral reef processes. *Coral Reefs*, 23, 1-4.
- ANTOINE, D., D'ORTENZIO, F., HOOKER, S. B., BÉCU, G., GENTILI, B., TAILLIEZ, D. & SCOTT, A. J. 2008. Assessment of uncertainty in the ocean reflectance determined by three satellite ocean color sensors (MERIS, SeaWiFS and MODIS - A) at an offshore site in the Mediterranean Sea (BOUSSOLE project). *Journal of Geophysical Research: Oceans (1978–2012)*, 113.
- ANTOINE, D., MOREL, A., GORDON, H. R., BANZON, V. F. & EVANS, R. H. 2005. Bridging ocean color observations of the 1980s and 2000s in search of long - term trends. *Journal of Geophysical Research: Oceans*, 110.
- ARCGIS, E. 2011. Release 10. *Redlands, CA: Environmental Systems Research Institute*.
- BAILEY, S. W., FRANZ, B. A. & WERDELL, P. J. 2010. Estimation of near-infrared water-leaving reflectance for satellite ocean color data processing. *Optics Express*, 18, 7521-7527.
- BARNES, B. B., HU, C., CANNIZZARO, J. P., CRAIG, S. E., HALLOCK, P., JONES, D. L., LEHRTER, J. C., MELO, N., SCHAEFFER, B. A. & ZEPP, R. 2014. Estimation of

diffuse attenuation of ultraviolet light in optically shallow Florida Keys waters from MODIS measurements. *Remote Sensing of Environment*, 140, 519-532.

- BARNES, B. B., HU, C., SCHAEFFER, B. A., LEE, Z., PALANDRO, D. A. & LEHRTER, J. C. 2013. MODIS-derived spatiotemporal water clarity patterns in optically shallow Florida Keys waters: A new approach to remove bottom contamination. *Remote Sensing of Environment*, 134, 377-391.
- BATAGELJ, V. 1988. Generalized Ward and related clustering problems. *Classification and related methods of data analysis*, 67-74.
- BEAMAN, R. 2012. Great Barrier Reef and Coral Sea bathymetry. In: JAMES COOK UNIVERSITY, S. O. E. A. E. S. (ed.). <http://deepreef.org>: <http://deepreef.org>.
- BEAMAN, R. J. 2010. 3DGBR: A high-resolution depth model for the Great Barrier Reef and Coral Sea. *Marine and Tropical Sciences Facility (MTSRF) Project*, 2.
- BEIJBOM, O., EDMUNDS, P. J., KLINE, D. I., MITCHELL, B. G. & KRIEGMAN, D. Automated annotation of coral reef survey images. Computer Vision and Pattern Recognition (CVPR), 2012 IEEE Conference on, 2012. IEEE, 1170-1177.
- BELPERIO, A. 1983. Terrigenous sedimentation in the central Great Barrier Reef lagoon: a model from the Burdekin region. *BMR Journal of Australian Geology and Geophysics*, 8, 179-190.
- BELPERIO, A. & SEARLE, D. 1988. Terrigenous and carbonate sedimentation in the Great Barrier Reef province. *Developments in Sedimentology*, 42, 143-174.
- BIERWIRTH, P., LEE, T. & BURNE, R. 1993. Shallow sea-floor reflectance and water depth derived by unmixing multispectral imagery. *Photogrammetric Engineering and Remote Sensing*, 59, 331-338.
- BISSETT, W. P., ARNONE, R., DEBRA, S., DIETERLE, D. A., DYE, D., KIRKPATRICK, G. J., SCHOFIELD, O. M. & VARGO, G. A. 2005. Predicting the optical properties of the West Florida Shelf: resolving the potential impacts of a terrestrial boundary condition on the distribution of colored dissolved and particulate matter. *Marine chemistry*, 95, 199-233.
- BLAKEY, T., MELESSE, A. & HALL, M. O. 2015. Supervised Classification of Benthic Reflectance in Shallow Subtropical Waters Using a Generalized Pixel-Based Classifier across a Time Series. *Remote Sensing*, 7, 5098-5116.
- BLONDEAU - PATISSIER, D., BRANDO, V. E., OUBELKHEIR, K., DEKKER, A. G., CLEMENTSON, L. A. & DANIEL, P. 2009. Bio - optical variability of the absorption and scattering properties of the Queensland inshore and reef waters, Australia. *Journal of Geophysical Research: Oceans (1978–2012)*, 114.
- BOSS, E. S. & MARITORENA, S. 2006. Uncertainties in the products of ocean-colour remote sensing. IOCCG.
- BOTHA, E. J., BRANDO, V. E., ANSTEE, J. M., DEKKER, A. G. & SAGAR, S. 2013. Increased spectral resolution enhances coral detection under varying water conditions. *Remote Sensing of Environment*, 131, 247-261.
- BRANDO, V. E., ANSTEE, J. M., WETTLE, M., DEKKER, A. G., PHINN, S. R. & ROELFSEMA, C. 2009. A physics based retrieval and quality assessment of bathymetry from suboptimal hyperspectral data. *Remote Sensing of Environment*, 113, 755-770.

- BRANDO, V. E., DEKKER, A. G., PARK, Y. J. & SCHROEDER, T. 2012. Adaptive semianalytical inversion of ocean color radiometry in optically complex waters. *Applied Optics*, 51, 2808-2833.
- BRICAUD, A., MOREL, A., BABIN, M., ALLALI, K. & CLAUSTRE, H. 1998. Variations of light absorption by suspended particles with chlorophyll a concentration in oceanic (case 1) waters: Analysis and implications for bio - optical models. *Journal of Geophysical Research: Oceans (1978-2012)*, 103, 31033-31044.
- BURRAGE, D. M., STEINBERG, C. R., SKIRVING, W. J. & KLEYPAST, J. A. 1996. Mesoscale circulation features of the Great Barrier Reef region inferred from NOAA satellite imagery. *Remote Sensing of Environment*, 56, 21-41.
- CALL, K. A., HARDY, J. T. & WALLIN, D. O. 2003. Coral reef habitat discrimination using multivariate spectral analysis and satellite remote sensing. *International Journal of Remote Sensing*, 24, 2627-2639.
- CAMPBELL, J. B. 2002. *Introduction to remote sensing*, Guilford Press.
- CAMPBELL, J. B. & WYNNE, R. H. 2011. *Introduction to remote sensing*, Guilford Press.
- CANNIZZARO, J. P. & CARDER, K. L. 2006. Estimating chlorophyll a concentrations from remote-sensing reflectance in optically shallow waters. *Remote Sensing of Environment*, 101, 13-24.
- CANTY, M. J. 2014. *Image analysis, classification and change detection in remote sensing: with algorithms for ENVI/IDL and Python*, CRC Press.
- CAPOLSINI, P., ANDRÉFOUËT, S., RION, C. & PAYRI, C. 2003. A comparison of Landsat ETM+, SPOT HRV, Ikonos, ASTER, and airborne MASTER data for coral reef habitat mapping in South Pacific islands. *Canadian Journal of Remote Sensing*, 29, 187-200.
- CARDER, K. L., CANNIZZARO, J. P. & LEE, Z. Ocean color algorithms in optically shallow waters: Limitations and improvements. 2005.
- CASAL, G., KUTSER, T., DOMÍNGUEZ-GÓMEZ, J., SÁNCHEZ-CARNERO, N. & FREIRE, J. 2011. Mapping benthic macroalgal communities in the coastal zone using CHRIS-PROBA mode 2 images. *Estuarine, Coastal and Shelf Science*, 94, 281-290.
- COLES, R., MCKENZIE, L., DE'ATH, G., ROELOFS, A. & LEE LONG, W. 2009. Spatial distribution of deepwater seagrass in the inter-reef lagoon of the Great Barrier Reef World Heritage Area. *Mar Ecol Prog Ser*, 392, 57-68.
- DE'ATH, G. & FABRICIUS, K. 2010. Water quality as a regional driver of coral biodiversity and macroalgae on the Great Barrier Reef. *Ecological Applications*, 20, 840-850.
- DECKER, A., MALTHUS, T., WIJNEN, M. & SEYHAN, E. 1992. The effect of spectral bandwidth and positioning on the spectral signature analysis of inland waters. *Remote Sensing of Environment*, 41, 211-225.
- DEFOIN - PLATEL, M. & CHAMI, M. 2007. How ambiguous is the inverse problem of ocean color in coastal waters? *Journal of Geophysical Research: Oceans*, 112.
- DEKKER, A. G. 1993. Detection of optical water quality parameters for eutrophic waters by high resolution remote sensing.
- DEKKER, A. G., PHINN, S. R., ANSTEE, J., BISSETT, P., BRANDO, V. E., CASEY, B., FEARN, P., HEDLEY, J., KLONOWSKI, W. & LEE, Z. P. 2011. Intercomparison of

shallow water bathymetry, hydro-optics, and benthos mapping techniques in Australian and Caribbean coastal environments. *Limnol. Oceanogr.: Methods*, 9, 396-425.

- DIAZ-PULIDO, G., MCCOOK, L. & GREAT BARRIER REEF MARINE PARK, A. 2008. State of the Reef Report 2008: Macroalgae. Townsville: Great Barrier Reef Marine Park Authority.
- DIERSSEN, H. M. 2010. Perspectives on empirical approaches for ocean color remote sensing of chlorophyll in a changing climate. *Proceedings of the National Academy of Sciences*, 107, 17073-17078.
- DIERSSEN, H. M., ZIMMERMAN, R. C., LEATHERS, R. A., DOWNES, T. V. & DAVIS, C. O. 2003. Ocean color remote sensing of seagrass and bathymetry in the Bahamas Banks by high-resolution airborne imagery. DTIC Document.
- DOBSON, E. L. & DUSTAN, P. The use of satellite imagery for detection of shifts in coral reef communities. 2000. 22-26.
- DOXARAN, D., BABIN, M. & LEYMARIE, E. 2007. Near-infrared light scattering by particles in coastal waters. *Optics express*, 15, 12834-12849.
- ESA, E. S. A. 2016. SNAP [Online]. European Space Agency. Available: <http://step.esa.int/main/toolboxes/snap/> [Accessed 02/01/2016 2016].
- EUGENIO, F., MARCELLO, J. & MARTIN, J. 2015. High-Resolution Maps of Bathymetry and Benthic Habitats in Shallow-Water Environments Using Multispectral Remote Sensing Imagery. *Geoscience and Remote Sensing, IEEE Transactions on*, 53, 3539-3549.
- FABRICIUS, K. E. 2005. Effects of terrestrial runoff on the ecology of corals and coral reefs: review and synthesis. *Marine Pollution Bulletin*, 50, 125-146.
- FABRICIUS, K. E., DE'ATH, G., HUMPHREY, C., ZAGORSKIS, I. & SCHAFFELKE, B. 2013. Intra-annual variation in turbidity in response to terrestrial runoff on near-shore coral reefs of the Great Barrier Reef. *Estuarine, Coastal and Shelf Science*, 116, 57-65.
- FABRICIUS, K. E., LOGAN, M., WEEKS, S. & BRODIE, J. 2014. The effects of river runoff on water clarity across the central Great Barrier Reef. *Marine pollution bulletin*, 84, 191-200.
- FAIR, N., CHAVE, A. D., FREITAG, L., PREISIG, J., WHITE, S. N., YOERGER, D. & SONNICHSEN, F. Optical modem technology for seafloor observatories. *Oceans 2006*, 2006. IEEE, 1-6.
- FARGION, G. S., MCCLAIN, C. R., WERDELL, P. J. & BAILEY, S. W. 2002. *The SeaWiFS bio-optical archive and storage system (SeaBASS): Current architecture and implementation*, Goddard Space Flight Center.
- FEARNS, P., KLONOWSKI, W., BABCOCK, R., ENGLAND, P. & PHILLIPS, J. 2011. Shallow water substrate mapping using hyperspectral remote sensing. *Continental Shelf Research*.
- FELDMAN, G. C. 2015. *Ocean Color Web* [Online]. NASA. Available: <http://oceancolor.gsfc.nasa.gov/> [Accessed October 07 2014].
- FENG, H. 2004. *Ocean Color Modeling: Parameterization and Interpretation*.
- FIELD, A. 2009. *Discovering statistics using SPSS*, Sage publications.

- FRANKLIN, S. E. 2001. *Remote sensing for sustainable forest management*, CRC.
- FRANZ, B. A., WERDELL, P. J., MEISTER, G., BAILEY, S. W., EPLEEJR, R. E., FELDMAN, G. C., KWIATKOWSKAA, E., MCCLAIN, C. R., PATT, F. S. & THOMAS, D. The continuity of ocean color measurements from SeaWiFS to MODIS. *Optics & Photonics 2005*, 2005. International Society for Optics and Photonics, 58820W-58820W-13.
- FURNAS, M. & MITCHELL, A. 2001. *Runoff of terrestrial sediment and nutrients into the Great Barrier Reef World Heritage Area*, CRC Press, Boca Raton.
- FURNAS, M., MITCHELL, A., SKUZA, M. & BRODIE, J. 2005. In the other 90%: phytoplankton responses to enhanced nutrient availability in the Great Barrier Reef Lagoon. *Marine Pollution Bulletin*, 51, 253-265.
- GAO, J. 2009. Bathymetric mapping by means of remote sensing: methods, accuracy and limitations. *Progress in Physical Geography*, 33, 103-116.
- GARDNER, W. 1986. Measurement of spectral correlation. *Acoustics, Speech and Signal Processing, IEEE Transactions on*, 34, 1111-1123.
- GBRMPA. 2002. *Great Barrier Reef general reference map*. Townsville, Qld.: Great Barrier Reef Marine Park Authority.
- GBRMPA 2009. *Great Barrier Reef outlook report 2009: in brief*, Townsville, Qld., Great Barrier Reef Marine Park Authority.
- GBRMPA 2014. *Great barrier reef outlook report 2014*. Townsville, Qld.
- GOODMAN, J. & USTIN, S. L. 2007. Classification of benthic composition in a coral reef environment using spectral unmixing. *Journal of Applied Remote Sensing*, 1, 011501.
- GOODMAN, J. A., PURKIS, S. J. & PHINN, S. R. 2013. *Coral reef remote sensing: A guide for mapping, monitoring and management*, Springer Science & Business Media.
- GREEN, E. P., CLARK, C. D., MUMBY, P. J., EDWARDS, A. J. & ELLIS, A. 1998. Remote sensing techniques for mangrove mapping. *International Journal of Remote Sensing*, 19, 935-956.
- HEDLEY, J., ROELFSEMA, C. & PHINN, S. R. 2009. Efficient radiative transfer model inversion for remote sensing applications. *Remote Sensing of Environment*, 113, 2527-2532.
- HEDLEY, J. D. & MUMBY, P. J. 2002. Biological and remote sensing perspectives of pigmentation in coral reef organisms. *Advances in Marine Biology*, 43, 277-317.
- HEDLEY, J. D., MUMBY, P. J., JOYCE, K. E. & PHINN, S. R. 2004. Spectral unmixing of coral reef benthos under ideal conditions. *Coral Reefs*, 23, 60-73.
- HEDLEY, J. D., ROELFSEMA, C. M., PHINN, S. R. & MUMBY, P. J. 2012. Environmental and Sensor Limitations in Optical Remote Sensing of Coral Reefs: Implications for Monitoring and Sensor Design. *Remote Sensing*, 4, 271-302.
- HOCHBERG, E. J., ATKINSON, M. J. & ANDRÉFOUËT, S. 2003. Spectral reflectance of coral reef bottom-types worldwide and implications for coral reef remote sensing. *Remote Sensing of Environment*, 85, 159-173.
- HOCHBERG, E. J., ATKINSON, M. J., APPRILL, A. & ANDREFOUËT, S. 2004. Spectral reflectance of coral. *Coral Reefs*, 23, 84-95.

- HOLDEN, H. & LEDREW, E. 1998. Spectral discrimination of healthy and non-healthy corals based on cluster analysis, principal components analysis, and derivative spectroscopy. *Remote Sensing of Environment*, 65, 217-224.
- HOLDEN, H. & LEDREW, E. 1999. Hyperspectral identification of coral reef features. *International Journal of Remote Sensing*, 20, 2545-2563.
- HOPLEY, D., MCLEAN, R., MARSHALL, J. & SMITH, A. 1978. Holocene-Pleistocene boundary in a fringing reef: Hayman Island, north Queensland. *Search*, 9, 323-325.
- HU, C., CARDER, K. L. & MULLER-KARGER, F. E. 2000. Atmospheric correction of SeaWiFS imagery over turbid coastal waters: a practical method. *Remote Sensing of Environment*, 74, 195-206.
- ISLAM, A., GAO, J., AHMAD, W., NEIL, D. & BELL, P. 2004. A composite DOP approach to excluding bottom reflectance in mapping water parameters of shallow coastal zones from TM imagery. *Remote sensing of environment*, 92, 40-51.
- JERLOV, N. G. 1976. *Marine optics*, Elsevier Science Ltd.
- JOYCE, K., PHINN, S., ROELFSEMA, C., NEIL, D. & DENNISON, W. 2004. Combining Landsat ETM+ and Reef Check classifications for mapping coral reefs: a critical assessment from the southern Great Barrier Reef, Australia. *Coral Reefs*, 23, 21-25.
- JUPP, D. L. B., MAYO, K. K., KUCHLER, D. A., CLAASEN, D. V. R., KENCHINGTON, R. A. & GUERIN, P. R. 1985. Remote sensing for planning and managing the Great Barrier Reef of Australia. *Photogrammetria*, 40, 21-42.
- KARPOUZLI, E., MALTHUS, T. & PLACE, C. 2004. Hyperspectral discrimination of coral reef benthic communities in the western Caribbean. *Coral Reefs*, 23, 141-151.
- KAUFMAN, L. & ROUSSEEUW, P. J. 2009. *Finding groups in data: an introduction to cluster analysis*, John Wiley & Sons.
- KESHAVA, N. 2004. Distance metrics and band selection in hyperspectral processing with applications to material identification and spectral libraries. *Geoscience and Remote Sensing, IEEE Transactions on*, 42, 1552-1565.
- KILPATRICK, K. A., PODESTA, G. P. & EVANS, R. 2001. Overview of the NOAA/NASA advanced very high resolution radiometer Pathfinder algorithm for sea surface temperature and associated matchup database. *Journal of Geophysical Research: Oceans (1978–2012)*, 106, 9179-9197.
- KIRK, J. T. O. 1984. Dependence of relationship between inherent and apparent optical properties of water on solar altitude. *Limnology and Oceanography*, 29, 350-356.
- KIRK, J. T. O. 1994. *Light and photosynthesis in aquatic ecosystems*, Cambridge university press.
- KLONOWSKI, W. M., FEARN, P. R. & LYNCH, M. J. 2007. Retrieving key benthic cover types and bathymetry from hyperspectral imagery. *Journal of Applied Remote Sensing*, 1, 011505-011505-21.
- KRUSE, F. A., BOARDMAN, J. W. & HUNTINGTON, J. F. 2003. Comparison of airborne hyperspectral data and EO-1 Hyperion for mineral mapping. *Geoscience and Remote Sensing, IEEE Transactions on*, 41, 1388-1400.

- KUTSER, T., DEKKER, A. G. & SKIRVING, W. 2003. Modeling spectral discrimination of Great Barrier Reef benthic communities by remote sensing instruments. *Limnology and Oceanography*, 48, 497-510.
- KUTSER, T. & JUPP, D. L. 2006. On the possibility of mapping living corals to the species level based on their optical signatures. *Estuarine, Coastal and Shelf Science*, 69, 607-614.
- KUTSER, T., MILLER, I. & JUPP, D. L. B. 2006. Mapping coral reef benthic substrates using hyperspectral space-borne images and spectral libraries. *Estuarine, Coastal and Shelf Science*, 70, 449-460.
- LABS, H. 2015. *HydroScat-6P Backscattering Sensor - Fluorometer* [Online]. HOBI Labs. Available: <http://www.hobilabs.com> [Accessed January 28 2015].
- LASS, L. W., THILL, D. C., SHAFII, B. & PRATHER, T. S. 2002. Detecting Spotted Knapweed (*Centaurea maculosa*) with Hyperspectral Remote Sensing Technology 1. *Weed Technology*, 16, 426-432.
- LEE, Z. 1999. Hyperspectral Remote Sensing for Shallow Waters. 2. Deriving Bottom Depths and Water Properties by Optimization. *Applied Optics*, 38, 3831.
- LEE, Z., CARDER, K., ARNONE, R. & HE, M. 2007. Determination of primary spectral bands for remote sensing of aquatic environments. *Sensors*, 7, 3428-3441.
- LEE, Z. & CARDER, K. L. 2002. Effect of Spectral Band Numbers on the Retrieval of Water Column and Bottom Properties from Ocean Color Data. *Applied Optics*, 41, 2191-2201.
- LEE, Z., CARDER, K. L. & ARNONE, R. A. 2002. Deriving inherent optical properties from water color: a multiband quasi-analytical algorithm for optically deep waters. *Applied Optics*, 41, 5755-5772.
- LEE, Z., CARDER, K. L., CHEN, R. F. & PEACOCK, T. G. 2001. Properties of the water column and bottom derived from Airborne Visible Infrared Imaging Spectrometer (AVIRIS) data. *J. Geophys. Res.*, 106, 11639-11651.
- LEE, Z., CARDER, K. L., MOBLEY, C. D., STEWARD, R. G. & PATCH, J. S. 1998. Hyperspectral remote sensing for shallow waters. I. A semianalytical model. *Applied Optics*, 37, 6329-6338.
- LEE, Z., HU, C., CASEY, B., SHANG, S., DIERSSEN, H. & ARNONE, R. 2010. Global Shallow Water Bathymetry From Satellite Ocean Color Data. *Eos, Transactions American Geophysical Union*, 91, 429-430.
- LEE, Z. P., DU, K. P. & ARNONE, R. 2005. A model for the diffuse attenuation coefficient of downwelling irradiance. *Journal of Geophysical Research: Oceans*, 110.
- LEIPER, I., PHINN, S. & DEKKER, A. G. 2011. Spectral reflectance of coral reef benthos and substrate assemblages on Heron Reef, Australia. *International Journal of Remote Sensing*, 33, 3946-3965.
- LEIPER, I. A., SIEBECK, U. E., MARSHALL, N. J. & PHINN, S. R. 2009. Coral health monitoring: linking coral colour and remote sensing techniques. *Canadian Journal of Remote Sensing*, 35, 276-286.
- LESSER, M. & MOBLEY, C. 2007. Bathymetry, water optical properties, and benthic classification of coral reefs using hyperspectral remote sensing imagery. *Coral Reefs*, 26, 819-829.

- LIRMAN, D., GRACIAS, N. R., GINTERT, B. E., GLEASON, A. C. R., REID, R. P., NEGAHDARIPOUR, S. & KRAMER, P. 2007. Development and application of a video-mosaic survey technology to document the status of coral reef communities. *Environmental Monitoring and Assessment*, 125, 59-73.
- LOISEL, H., VANTREPOTTE, V., JAMET, C. & DAT, D. N. 2013. Challenges and New Advances in Ocean Color Remote Sensing of Coastal Waters.
- LOUCHARD, E. M., REID, R. P., STEPHENS, F. C., DAVIS, C. O., LEATHERS, R. A. & DOWNES, T. V. 2002. Optical remote sensing of benthic habitats and bathymetry in coastal environments at Lee Stocking Island, Bahamas: A comparative spectral classification approach. DTIC Document.
- LOVELOCK, C. E. & ELLISON, J. 2007. Vulnerability of mangroves and tidal wetlands of the Great Barrier Reef to climate change.
- LYZENGA, D. R. 1978. Passive remote sensing techniques for mapping water depth and bottom features. *Applied optics*, 17, 379-383.
- LYZENGA, D. R. 1981. Remote sensing of bottom reflectance and water attenuation parameters in shallow water using aircraft and Landsat data. *International Journal of Remote Sensing*, 2, 71-82.
- LYZENGA, D. R., MALINAS, N. P. & TANIS, F. J. 2006. Multispectral bathymetry using a simple physically based algorithm. *Geoscience and Remote Sensing, IEEE Transactions on*, 44, 2251-2259.
- MACON, C., WOZENCRAFT, J., PARK, J. Y. & TUELL, G. Seafloor and land cover classification through airborne LIDAR and hyperspectral data fusion. Geoscience and Remote Sensing Symposium, 2008. IGARSS 2008. IEEE International, 2008. IEEE, II-77-II-80.
- MALENOVSKÝ, Z., ROTT, H., CIHLAR, J., SCHAEPMAN, M. E., GARCÍA-SANTOS, G., FERNANDES, R. & BERGER, M. 2012. Sentinels for science: Potential of Sentinel-1,-2, and-3 missions for scientific observations of ocean, cryosphere, and land. *Remote Sensing of Environment*, 120, 91-101.
- MARITORENA, S., D'ANDON, O. H. F., MANGIN, A. & SIEGEL, D. A. 2010. Merged satellite ocean color data products using a bio-optical model: Characteristics, benefits and issues. *Remote Sensing of Environment*, 114, 1791-1804.
- MARITORENA, S., SIEGEL, D. A. & PETERSON, A. R. 2002. Optimization of a semianalytical ocean color model for global-scale applications. *Applied Optics*, 41, 2705-2714.
- MARTIN, S. 2014. *An introduction to ocean remote sensing*, Cambridge University Press.
- MATHEWS, E., HEAP, A. & WOODS, M. 2007. Inter-reefal seabed sediments and geomorphology of the Great Barrier Reef: A spatial analysis, Vol. 2007/09. *Geoscience Australia, Canberra, Australia*.
- MCKENZIE, L., SMITH, N., JOHNS, L., YOSHIDA, R. & COLES, R. 2014a. seagrass monitoring.
- MCKENZIE, L. J., FINKBEINER, M. A. & KIRKMAN, H. 2001. Methods for mapping seagrass distribution. *Global Seagrass Research Methods. Elsevier Science BV, Amsterdam*, 101-121.
- MCKENZIE, L. J., YOSHIDA, R. L., GRECH, A. & COLES, R. 2014b. Composite of coastal seagrass meadows in Queensland, Australia - November 1984 to June 2010.

Supplement to: McKenzie, Len J; Yoshida, Rudolf L; Grech, Alana; Coles, Robert (2010): Queensland seagrasses. Status 2010 - Torres Strait and East Coast. Fisheries Queensland (DEEDI), Cairns, 6 pp, hdl:10013/epic.42902.d001. PANGAEA.

- MCKINNA, L. I. W., FEARN, P. R. C., WEEKS, S. J., WERDELL, P. J., REICHSTETTER, M., FRANZ, B. A., SHEA, D. M. & FELDMAN, G. C. 2015. A semianalytical ocean color inversion algorithm with explicit water column depth and substrate reflectance parameterization. *Journal of Geophysical Research: Oceans*, 120, 1741-1770.
- MÉLIN, F., BERTHON, J.-F. & ZIBORDI, G. 2005. Assessment of apparent and inherent optical properties derived from SeaWiFS with field data. *Remote sensing of environment*, 97, 540-553.
- MINGHELLI-ROMAN, A., CHISHOLM, J. R., MARCHIORETTI, M. & JAUBERT, J. M. 2002. Discrimination of coral reflectance spectra in the Red Sea. *Coral Reefs*, 21, 307-314.
- MISHRA, D., NARUMALANI, S., RUNDQUIST, D. & LAWSON, M. 2006. Benthic habitat mapping in tropical marine environments using QuickBird multispectral data. *Photogrammetric Engineering and Remote Sensing*, 72, 1037.
- MOBERG, F. & FOLKE, C. 1999. Ecological goods and services of coral reef ecosystems. *Ecological economics*, 29, 215-233.
- MOBLEY, C., BOSS, E. & ROESLER, C. 2010. Ocean optics web book.
- MOBLEY, C. D. 1994. *Light and water: Radiative transfer in natural waters*, Academic press San Diego, CA.
- MOBLEY, C. D., GENTILI, B., GORDON, H. R., JIN, Z., KATTAWAR, G. W., MOREL, A., REINERSMAN, P., STAMNES, K. & STAVN, R. H. 1993. Comparison of numerical models for computing underwater light fields. *Applied Optics*, 32, 7484-7504.
- MOBLEY, C. D. & MOBLEY, C. D. 1994. *Light and water: Radiative transfer in natural waters*, Academic press San Diego.
- MOBLEY, C. D. & SUNDMAN, L. K. 2008a. Hydrolight 5 Ecolight 5 technical documentation. *Sequoia Scientific, Incorporated, Bellevue, WA, 98005, 95.*
- MOBLEY, C. D. & SUNDMAN, L. K. 2008b. *Hydrolight 5 Ecolight 5 Users' Guide*, Bellvue, WA, USA, Sequoia Scientific Inc.
- MOBLEY, C. D., SUNDMAN, L. K. & BOSS, E. 2002. Phase function effects on oceanic light fields. *Applied Optics*, 41, 1035-1050.
- MOBLEY, C. D., SUNDMAN, L. K., DAVIS, C. O., BOWLES, J. H., DOWNES, T. V., LEATHERS, R. A., MONTES, M. J., BISSETT, W. P., KOHLER, D. D. R. & REID, R. P. 2005. Interpretation of hyperspectral remote-sensing imagery by spectrum matching and look-up tables. *Applied Optics*, 44, 3576-3592.
- MOORE, C. C., BRUCE, E. J., PEGAU, W. S. & WEIDEMANN, A. D. WET Labs ac-9: Field calibration protocol, deployment techniques, data processing, and design improvements. *Ocean Optics XIII*, 1997. 725-730.
- MUMBY, P., CLARK, C., GREEN, E. & EDWARDS, A. 1998. Benefits of water column correction and contextual editing for mapping coral reefs. *International Journal of Remote Sensing*, 19, 203-210.

- MUMBY, P., GREEN, E., EDWARDS, A. & CLARK, C. 1997. Coral reef habitat mapping: how much detail can remote sensing provide? *Marine Biology*, 130, 193-202.
- MUMBY, P. J. & EDWARDS, A. J. 2002. Mapping marine environments with IKONOS imagery: enhanced spatial resolution can deliver greater thematic accuracy. *Remote Sensing of Environment*, 82, 248-257.
- MUMBY, P. J., GREEN, E. P., EDWARDS, A. J. & CLARK, C. D. 1999. The cost-effectiveness of remote sensing for tropical coastal resources assessment and management. *Journal of Environmental Management*, 55, 157-166.
- MUMBY, P. J., HEDLEY, J., CHISHOLM, J., CLARK, C., RIPLEY, H. & JAUBERT, J. 2004a. The cover of living and dead corals from airborne remote sensing. *Coral Reefs*, 23, 171-183.
- MUMBY, P. J., SKIRVING, W., STRONG, A. E., HARDY, J. T., LEDREW, E. F., HOCHBERG, E. J., STUMPF, R. P. & DAVID, L. T. 2004b. Remote sensing of coral reefs and their physical environment. *Marine Pollution Bulletin*, 48, 219-228.
- MYERS, M., HARDY, J., MAZEL, C. & DUSTAN, P. 1999. Optical spectra and pigmentation of Caribbean reef corals and macroalgae. *Coral Reefs*, 18, 179-186.
- O'REILLY, J. E., MARITORENA, S., MITCHELL, B. G., SIEGEL, D. A., CARDER, K. L., GARVER, S. A., KAHRU, M. & MCCLAIN, C. 1998. Ocean color chlorophyll algorithms for SeaWiFS. *Journal of Geophysical Research: Oceans (1978–2012)*, 103, 24937-24953.
- ORCUTT, J. 2013. Earth System Monitoring. *Earth System Monitoring: Selected Entries from the Encyclopedia of Sustainability Science and Technology*, ISBN 978-1-4614-5683-4. Springer Science+ Business Media New York, 2013, 1.
- OUBELKHEIR, K., CLEMENTSON, L. A., WEBSTER, I. T., FORD, P. W., DEKKER, A. G., RADKE, L. C. & DANIEL, P. 2006. Using inherent optical properties to investigate biogeochemical dynamics in a tropical macrotidal coastal system. *Journal of Geophysical Research: Oceans (1978–2012)*, 111.
- PANIGRAHI, N. 2014. *Computing in Geographic Information Systems*, CRC Press.
- PARK, J. Y., RAMNATH, V., FEYGELS, V., KIM, M., MATHUR, A., AITKEN, J. & TUELL, G. Active-passive data fusion algorithms for seafloor imaging and classification from CZMIL data. SPIE Defense, Security, and Sensing, 2010. International Society for Optics and Photonics, 769515-769515-10.
- PEGAU, W. S., GRAY, D. & ZANEVELD, J. R. V. 1997. Absorption and attenuation of visible and near-infrared light in water: dependence on temperature and salinity. *Applied optics*, 36, 6035-6046.
- PERRY, M. J. Optical sensors. 2003.
- PETUS, C., DA SILVA, E. T., DEVLIN, M., WENGER, A. S. & ÁLVAREZ-ROMERO, J. G. 2014. Using MODIS data for mapping of water types within river plumes in the Great Barrier Reef, Australia: Towards the production of river plume risk maps for reef and seagrass ecosystems. *Journal of environmental management*, 137, 163-177.
- PHINN, S., ROELFSEMA, C., DEKKER, A., BRANDO, V. & ANSTEE, J. 2008. Mapping seagrass species, cover and biomass in shallow waters: An assessment of satellite multi-spectral and airborne hyper-spectral imaging systems in Moreton Bay (Australia). *Remote Sensing of Environment*, 112, 3413-3425.

- PINNEL, N., HEEGE, T. & ZIMMERMANN, S. 2004. Spectral discrimination of submerged macrophytes in lakes using hyperspectral remote sensing data. *SPIE Proceedings on Ocean Optics XVII*, 1, 1-16.
- PITCHER, C. R., DOHERTY, P., ARNOLD, P., HOOPER, J., GRIBBLE, N., BARTLETT, C., BROWNE, M., CAMPBELL, N., CANNARD, T., CAPPO, M., CARINI, G., CHALMERS, S., CHEERS, S., CHETWYND, D., COLEFAX, A., COLES, R., COOK, S., DAVIE, P., DE'ATH, G., DEVEREUX, D., DONE, B., DONOVAN, T., EHRKE, B., ELLIS, N., ERICSON, G., FELLEGERA, I., FORCEY, K., FUREY, M., GLEDHILL, D., GOOD, N., GORDON, S., HAYWOOD, M., HENDRIKS, P., JACOBSEN, I., JOHNSON, J., JONES, M., KINNINMOTH, S., KISTLE, S., LAST, P., LEITE, A., MARKS, S., MCLEOD, I., OCZKOWICZ, S., ROBINSON, M., ROSE, C., SEABRIGHT, D., SHEILS, J., SHERLOCK, M., SKELTON, P., SMITH, D., SMITH, G., SPEARE, P., STOWAR, M., STRICKLAND, C., VAN DER GEEST, C., VENABLES, W., WALSH, C., WASSENBERG, T., WELNA, A., YEARSLEY, G. 2007. *Seabed biodiversity on the continental shelf of the Great Barrier Reef World Heritage Area*, CSIRO Marine and Atmospheric Research.
- PLATT, T. 2008. *Why Ocean Colour?: The Societal Benefits of Ocean-colour Technology*, International Ocean-Colour Coordinating Group.
- POINER, I., STAPLES, D. & KENYON, R. 1987. Seagrass communities of the Gulf of Carpentaria, Australia. *Marine and Freshwater Research*, 38, 121-131.
- PULLIZA, D. T. 2004. *A multi-sensor comparison for coral reef habitat mapping: a case study using a tropical patch reef environment in Biscayne National Park, Florida*. University OF Puerto Rico.
- PURKIS, S. & PASTERKAMP, R. 2004. Integrating in situ reef-top reflectance spectra with Landsat TM imagery to aid shallow-tropical benthic habitat mapping. *Coral Reefs*, 23, 5-20.
- QIN, Y., BRANDO, V. E., DEKKER, A. G. & BLONDEAU - PATISSIER, D. 2007. Validity of SeaDAS water constituents retrieval algorithms in Australian tropical coastal waters. *Geophysical Research Letters*, 34.
- REICHSTETTER, M., FEARNES, P. R. C. S., WEEKS, S. J., MCKINNA, L. I. W., ROELFSEMA, C. & FURNAS, M. 2015a. Bottom Reflectance in Ocean Color Satellite Remote Sensing for Coral Reef Environments. *Remote Sensing*, 7, 16756-16777.
- REICHSTETTER, M., MCKINNA, L., FEARNES, P., WEEKS, S. J., ROELFSEMA, C. M. & FURNAS, M. 2015b. Seafloor brightness map of the Great Barrier Reef, Australia, derived from biodiversity data.
- REYNOLDS, R. W., RAYNER, N. A., SMITH, T. M., STOKES, D. C. & WANG, W. 2002. An improved in situ and satellite SST analysis for climate. *Journal of climate*, 15, 1609-1625.
- ROELFSEMA, C. 2012a. Spectral reflectance library. *In: QUEENSLAND, U. O. (ed.)*. University of Queensland.
- ROELFSEMA C.M., S. R. P., D. TRACEY, J. SPEIRS, M. HEWSON AND K. JOHANSEN. 2010. *A Web Based Toolkit for Using Remote Sensing to Map and Monitor Terrestrial* [Online]. The University of Queensland. Available: <http://www.gpem.uq.edu.au/brg-rstoolkit/> [Accessed December 5 2015].

- ROELFSEMA, C. M. & PHINN, S. R. 2012. Spectral reflectance library of selected biotic and abiotic coral reef features In Heron Reef. PANGAEA.
- ROELFSEMA, C. M. & PHINN, S. R. 2013. Spectral reflectance library of selected biotic and abiotic coral reef features in Glovers Reef, Belize.
- ROELFSEMA, C. M., PHINN, S. R. & JOYCE, K. E. Evaluating benthic survey techniques for validating maps of coral reefs derived from remotely sensed images. Proc 10th Int Coral Reef Symp, 2006. 1771-1780.
- ROELFSEMA, C. M. P., STUART R 2012b. Spectral reflectance library of selected biotic and abiotic coral reef features In Heron Reef. *In: CENTRE FOR REMOTE SENSING & SPATIAL INFORMATION SCIENCE, S. O. G., PLANNING & ENVIRONMENTAL MANAGEMENT (ed.)*. Brisbane, Australia: The University of Queensland.
- ROUSSEEUW, P. J. 1987. Silhouettes: a graphical aid to the interpretation and validation of cluster analysis. *Journal of computational and applied mathematics*, 20, 53-65.
- ROY, D. P., WULDER, M. A., LOVELAND, T. R., WOODCOCK, C. E., ALLEN, R. G., ANDERSON, M. C., HELDER, D., IRONS, J. R., JOHNSON, D. M. & KENNEDY, R. 2014. Landsat-8: Science and product vision for terrestrial global change research. *Remote Sensing of Environment*, 145, 154-172.
- SAGAWA, T., BOISNIER, E., KOMATSU, T., MUSTAPHA, K. B., HATTOUR, A., KOSAKA, N. & MIYAZAKI, S. 2010. Using bottom surface reflectance to map coastal marine areas: a new application method for Lyzenga's model. *International Journal of Remote Sensing*, 31, 3051-3064.
- SATHYENDRANATH, S. 2000. Reports of the International Ocean-Colour Coordinating Group. *IOCCG, Dartmouth, Canada*, 3, 140.
- SCHAFFELKE, B., CARLETON, J., SKUZA, M., ZAGORSKIS, I. & FURNAS, M. J. 2012. Water quality in the inshore Great Barrier Reef lagoon: Implications for long-term monitoring and management. *Marine Pollution Bulletin*, 65, 249-260.
- SCHAFFELKE, B., MELLORS, J. & DUKE, N. C. 2005. Water quality in the Great Barrier Reef region: responses of mangrove, seagrass and macroalgal communities. *Marine Pollution Bulletin*, 51, 279-296.
- SCHOWENGERDT, R. A. 2006. *Remote sensing: models and methods for image processing*, Academic press.
- SCHROEDER, T., SCHAAL, M. & FISCHER, J. 2007. Retrieval of atmospheric and oceanic properties from MERIS measurements: A new Case - 2 water processor for BEAM. *International Journal of Remote Sensing*, 28, 5627-5632.
- SCOFFIN, T. P. & TUDHOPE, A. W. 1985. Sedimentary environments of the central region of the Great Barrier Reef of Australia. *Coral Reefs*, 4, 81-93.
- SLADE, W. H., BOSS, E., DALL'OLMO, G., LANGNER, M. R., LOFTIN, J., BEHRENFELD, M. J., ROESLER, C. & WESTBERRY, T. K. 2010. Underway and moored methods for improving accuracy in measurement of spectral particulate absorption and attenuation. *Journal of Atmospheric and Oceanic Technology*, 27, 1733-1746.
- SMITH, T. M. & REYNOLDS, R. W. 2004. Improved extended reconstruction of SST (1854-1997). *Journal of Climate*, 17, 2466-2477.

- SOHN, Y., MORAN, E. & GURRI, F. 1999. Deforestation in North-Central Yucatan(1985-1995)- Mapping secondary succession of forest and agricultural land use in Sotuta using the cosine of the angle concept. *Photogrammetric engineering and remote sensing*, 65, 947-958.
- SOHN, Y. & REBELLO, N. S. 2002. Supervised and unsupervised spectral angle classifiers. *Photogrammetric Engineering and Remote Sensing*, 68, 1271-1282.
- SPALDING, M. D., RAVILIOUS, C. & GREEN, E. P. 2001. *World atlas of coral reefs*, Univ of California Press.
- SPURGEON, J. P. G. 1992. The economic valuation of coral reefs. *Marine Pollution Bulletin*, 24, 529-536.
- STEINBERG, C. 2007. Impacts of climate change on the physical oceanography of the Great Barrier Reef.
- STUMPF, R. P., HOLDERIED, K. & SINCLAIR, M. 2003. Determination of water depth with high-resolution satellite imagery over variable bottom types. *Limnology and Oceanography*, 48, 547-556.
- STUMPF, R. P. & PENNOCK, J. R. 1989. Calibration of a general optical equation for remote sensing of suspended sediments in a moderately turbid estuary. *Journal of Geophysical Research: Oceans*, 94, 14363-14371.
- TUELL, G., BARBOR, K. & WOZENCRAFT, J. Overview of the coastal zone mapping and imaging lidar (CZMIL): a new multisensor airborne mapping system for the US Army Corps of Engineers. SPIE Defense, Security, and Sensing, 2010. International Society for Optics and Photonics, 76950R-76950R-8.
- TUELL, G. H., FEYGELS, V., KOPILEVICH, Y., WEIDEMANN, A. D., CUNNINGHAM, A. G., MANI, R., PODOBA, V., RAMNATH, V., PARK, J. Y. & AITKEN, J. Measurement of ocean water optical properties and seafloor reflectance with Scanning Hydrographic Operational Airborne Lidar Survey (SHOALS): II. Practical results and comparison with independent data. Optics & Photonics 2005, 2005. International Society for Optics and Photonics, 58850E-58850E-13.
- TZORTZIOU, M., SUBRAMANIAM, A., HERMAN, J. R., GALLEGOS, C. L., NEAL, P. J. & HARDING JR, L. W. 2006. Remote Sensing Reflectance and Inherent Optical Properties in the Mid-mesohaline Chesapeake Bay.
- UDY, J., GALL, M., LONGSTAFF, B., MOORE, K., ROELFSEMA, C., SPOONER, D. R. & ALBERT, S. 2005. Water quality monitoring: a combined approach to investigate gradients of change in the Great Barrier Reef, Australia. *Marine Pollution Bulletin*, 51, 224-238.
- USGS. 2015. *EarthExplorer* [Online]. USGS. Available: <http://earthexplorer.usgs.gov/> [Accessed July 01 2014].
- VAHTMÄE, E., KUTSER, T., MARTIN, G. & KOTTA, J. 2006. Feasibility of hyperspectral remote sensing for mapping benthic macroalgal cover in turbid coastal waters—a Baltic Sea case study. *Remote Sensing of Environment*, 101, 342-351.
- VAN DER MEER, F. 1999. Iterative spectral unmixing (ISU). *International Journal of Remote Sensing*, 20, 3431-3436.
- VANHELLEMONT, Q., BAILEY, S., FRANZ, B. & SHEA, D. Atmospheric correction of Landsat-8 imagery using SeaDAS. ESA Special Publication SP-726. Presented at

- the 2014 European Space Agency Sentinel-2 for Science Workshop, Frascati, 2014.
- VERON, J., HOEGH-GULDBERG, O., LENTON, T., LOUGH, J., OBURA, D., PEARCE-KELLY, P. & SHEPPARD, C. 2009. The coral reef crisis: The critical importance of < 350 ppm CO₂. *Marine Pollution Bulletin*, 58, 1428-1436.
- WALLING, D. 2006. Human impact on land–ocean sediment transfer by the world's rivers. *Geomorphology*, 79, 192-216.
- WANG, M., SON, S. & HARDING, L. W. 2009. Retrieval of diffuse attenuation coefficient in the Chesapeake Bay and turbid ocean regions for satellite ocean color applications. *Journal of Geophysical Research: Oceans (1978–2012)*, 114.
- WANG, P., BOSS, E. S. & ROESLER, C. 2005. Uncertainties of inherent optical properties obtained from semianalytical inversions of ocean color. *Applied Optics*, 44, 4074-4085.
- WEEKS, S., WERDELL, P. J., SCHAFFELKE, B., CANTO, M., LEE, Z., WILDING, J. G. & FELDMAN, G. C. 2012. Satellite-derived photic depth on the great barrier reef: spatio-temporal patterns of water clarity. *Remote Sensing*, 4, 3781-3795.
- WERDELL, P. J. & BAILEY, S. W. 2005. An improved in-situ bio-optical data set for ocean color algorithm development and satellite data product validation. *Remote Sensing of Environment*, 98, 122-140.
- WERDELL, P. J., BAILEY, S. W., FARGION, G., PIETRAS, C., KNOBELSPIESSE, K., FELDMAN, G. & MCCLAIN, C. 2003. Unique data repository facilitates ocean color satellite validation. *EOS Trans. Am. Geophys. Union*, 84.
- WERDELL, P. J., FRANZ, B. A., BAILEY, S. W., FELDMAN, G. C., BOSS, E., BRANDO, V. E., DOWELL, M., HIRATA, T., LAVENDER, S. J. & LEE, Z. 2013. Generalized ocean color inversion model for retrieving marine inherent optical properties. *Applied Optics*, 52, 2019-2037.
- WERDELL, P. J. & ROESLER, C. S. 2003. Remote assessment of benthic substrate composition in shallow waters using multispectral reflectance. *Limnology and Oceanography*, 48, 557-567.
- WERNAND, M., SHIMWELL, S. & DE MUNCK, J. 1997. A simple method of full spectrum reconstruction by a five-band approach for ocean colour applications. *International Journal of Remote Sensing*, 18, 1977-1986.
- WETTLE, M. & BRANDO, V. E. 2006. *Sambuca: Semi-analytical model for bathymetry, un-mixing and concentration assessment*, CSIRO Land and Water.
- WHITEWAY, T. 2009. *Australian bathymetry and topography grid, June 2009*, Geoscience Australia, Department of Industry, Tourism and Resources.
- WILKINSON, C. 2004. Status of coral reefs of the World: 2004. Volume 2. *Status of coral reefs of the World*.
- WULDER, M. A., MASEK, J. G., COHEN, W. B., LOVELAND, T. R. & WOODCOCK, C. E. 2012. Opening the archive: How free data has enabled the science and monitoring promise of Landsat. *Remote Sensing of Environment*, 122, 2-10.
- ZHAO, J., BARNES, B., MELO, N., ENGLISH, D., LAPOINTE, B., MULLER-KARGER, F., SCHAEFFER, B. & HU, C. 2013. Assessment of satellite-derived diffuse attenuation coefficients and euphotic depths in south Florida coastal waters. *Remote Sensing of Environment*, 131, 38-50.

- ZHAO, M., HEINSCH, F. A., NEMANI, R. R. & RUNNING, S. W. 2005. Improvements of the MODIS terrestrial gross and net primary production global data set. *Remote sensing of Environment*, 95, 164-176.
- ZOFFOLI, M. L., FROUIN, R. & KAMPEL, M. 2014. Water column correction for coral reef studies by remote sensing. *Sensors*, 14, 16881-16931.

Appendix A

Table A- 1 : Mean retrieved bhp443 under different bottom reflectance scenarios and GBR regions for 2005

2005										
North										
	Brown Algae	Coral	Green Algae	SandSeagrass1	SandSeagrass2	Black	Sand	Seagrass	White	
17-20 m	0.008	0.008	0.008	0.007	0.007	0.009	0.007	0.008	0.007	
14-17 m	0.010	0.010	0.010	0.010	0.009	0.011	0.010	0.011	0.009	
11-14 m	0.012	0.012	0.013	0.010	0.012	0.013	0.009	0.012	0.015	
8-11 m	0.015	0.015	0.016	0.010	0.012	0.017	0.009	0.016	0.031	
5-8 m	0.020	0.021	0.023	0.016	0.017	0.021	0.014	0.020	0.051	
Central										
	Brown Algae	Coral	Green Algae	SandSeagrass1	SandSeagrass2	Black	Sand	Seagrass	White	
17-20 m	0.007	0.007	0.007	0.007	0.007	0.008	0.007	0.007	0.006	
14-17 m	0.010	0.010	0.010	0.009	0.009	0.010	0.009	0.010	0.008	
11-14 m	0.011	0.012	0.012	0.011	0.012	0.013	0.009	0.012	0.017	
8-11 m	0.013	0.014	0.014	0.011	0.013	0.015	0.011	0.018	0.029	
5-8 m	0.024	0.024	0.025	0.023	0.023	0.028	0.029	0.035	0.054	
South										
	Brown Algae	Coral	Green Algae	SandSeagrass1	SandSeagrass2	Black	Sand	Seagrass	White	
17-20 m	0.010	0.010	0.011	0.011	0.011	0.011	0.011	0.011	0.012	
14-17 m	0.013	0.013	0.013	0.013	0.013	0.013	0.014	0.013	0.015	
11-14 m	0.015	0.015	0.015	0.016	0.016	0.015	0.016	0.016	0.015	
8-11 m	0.016	0.016	0.016	0.017	0.018	0.017	0.017	0.019	0.023	
5-8 m	0.015	0.015	0.015	0.015	0.016	0.018	0.016	0.022	0.040	

Table A-2: Mean retrieved bbp443 under different bottom reflectance scenarios and GBR regions for 2011

2011										
North										
	Brown Algae	Coral	Green Algae	SandSeagrass1	SandSeagrass2	Black Sand	Sand Seagrass	White		
17-20 m	0.008	0.008	0.008	0.007	0.007	0.008	0.007	0.008	0.015	
14-17 m	0.010	0.010	0.010	0.010	0.010	0.011	0.012	0.010	0.008	
11-14 m	0.012	0.013	0.013	0.013	0.014	0.013	0.012	0.013	0.013	
8-11 m	0.018	0.018	0.019	0.013	0.015	0.019	0.012	0.021	0.031	
5-8 m	0.026	0.028	0.027	0.019	0.022	0.031	0.022	0.033	0.059	
Central										
	Brown Algae	Coral	Green Algae	SandSeagrass1	SandSeagrass2	Black Sand	Sand Seagrass	White		
17-20 m	0.010	0.010	0.010	0.009	0.009	0.010	0.009	0.010	0.011	
14-17 m	0.015	0.015	0.015	0.015	0.015	0.015	0.015	0.015	0.013	
11-14 m	0.019	0.020	0.020	0.021	0.022	0.020	0.020	0.022	0.022	
8-11 m	0.031	0.029	0.028	0.029	0.030	0.029	0.028	0.040	0.039	
5-8 m	0.045	0.045	0.043	0.037	0.040	0.043	0.038	0.056	0.068	
South										
	Brown Algae	Coral	Green Algae	SandSeagrass1	SandSeagrass2	Black Sand	Sand Seagrass	White		
17-20 m	0.014	0.014	0.014	0.014	0.014	0.014	0.014	0.014	0.016	
14-17 m	0.019	0.020	0.019	0.021	0.020	0.020	0.022	0.021	0.021	
11-14 m	0.020	0.020	0.020	0.023	0.024	0.020	0.021	0.021	0.020	
8-11 m	0.022	0.022	0.022	0.024	0.026	0.023	0.022	0.030	0.030	
5-8 m	0.029	0.029	0.028	0.027	0.029	0.029	0.028	0.037	0.053	

Table A-3: Mean retrieved a443 under different bottom reflectance scenarios and GBR regions for 2005

2005										
North										
	Brown Algae	Coral	Green Algae	SandSeagrass1	SandSeagrass2	Black Sand	Sand Seagrass	White		
17-20 m	0.06	0.06	0.06	0.06	0.06	0.06	0.07	0.06	0.11	
14-17 m	0.07	0.07	0.07	0.09	0.08	0.07	0.10	0.08	0.12	
11-14 m	0.08	0.08	0.08	0.11	0.11	0.08	0.10	0.09	0.19	
8-11 m	0.10	0.10	0.11	0.11	0.12	0.11	0.12	0.13	0.36	
5-8 m	0.15	0.16	0.17	0.23	0.20	0.15	0.23	0.18	0.65	
Centre										
	Brown Algae	Coral	Green Algae	SandSeagrass1	SandSeagrass2	Black Sand	Sand Seagrass	White		
17-20 m	0.06	0.06	0.06	0.07	0.07	0.07	0.07	0.07	0.10	
14-17 m	0.07	0.07	0.07	0.08	0.08	0.08	0.10	0.08	0.12	
11-14 m	0.08	0.08	0.09	0.12	0.12	0.09	0.11	0.10	0.21	
8-11 m	0.10	0.10	0.10	0.12	0.13	0.11	0.15	0.18	0.39	
5-8 m	0.21	0.22	0.22	0.31	0.27	0.23	0.39	0.37	0.74	
South										
	Brown Algae	Coral	Green Algae	SandSeagrass1	SandSeagrass2	Black Sand	Sand Seagrass	White		
17-20 m	0.08	0.08	0.08	0.10	0.09	0.09	0.10	0.09	0.13	
14-17 m	0.09	0.09	0.09	0.12	0.12	0.10	0.12	0.10	0.17	
11-14 m	0.11	0.11	0.11	0.15	0.15	0.11	0.17	0.12	0.18	
8-11 m	0.12	0.12	0.12	0.20	0.21	0.13	0.21	0.17	0.32	
5-8 m	0.13	0.13	0.12	0.26	0.25	0.14	0.29	0.27	0.62	





Table A-4: Mean retrieved a443 under different bottom reflectance scenarios and GBR regions for 2011

2011										
North										
	Brown Algae	Coral	Green Algae	SandSeagrass1	SandSeagrass2	Black Sand	Sand Seagrass	White		
17-20 m	0.08	0.08	0.08	0.10	0.09	0.09	0.10	0.09	0.13	
14-17 m	0.09	0.09	0.09	0.12	0.12	0.10	0.12	0.10	0.17	
11-14 m	0.11	0.11	0.11	0.15	0.15	0.11	0.17	0.12	0.18	
8-11 m	0.12	0.12	0.12	0.20	0.21	0.13	0.21	0.17	0.32	
5-8 m	0.13	0.13	0.12	0.26	0.25	0.14	0.29	0.27	0.62	

17-20 m	0.06	0.06	0.06	0.07	0.07	0.06	0.07	0.06	0.32
14-17 m	0.08	0.08	0.08	0.11	0.09	0.08	0.09	0.16	0.16
11-14 m	0.09	0.10	0.09	0.17	0.16	0.10	0.15	0.10	0.17
8-11 m	0.13	0.13	0.14	0.14	0.16	0.14	0.15	0.19	0.36
5-8 m	0.21	0.22	0.21	0.24	0.23	0.25	0.29	0.31	0.69
Centre									
	Brown Algae	Coral	Green Algae	SandSeagrass1	SandSeagrass2	Black Sand	Seagrass	White	
17-20 m	0.09	0.09	0.09	0.10	0.09	0.09	0.10	0.09	0.19
14-17 m	0.11	0.11	0.11	0.14	0.13	0.12	0.15	0.12	0.15
11-14 m	0.13	0.14	0.13	0.20	0.20	0.14	0.19	0.18	0.23
8-11 m	0.24	0.21	0.20	0.27	0.28	0.20	0.26	0.36	0.39
5-8 m	0.38	0.38	0.36	0.38	0.39	0.36	0.41	0.54	0.75
South									
	Brown Algae	Coral	Green Algae	SandSeagrass1	SandSeagrass2	Black Sand	Seagrass	White	
17-20 m	0.09	0.10	0.09	0.11	0.11	0.10	0.12	0.11	0.19
14-17 m	0.12	0.13	0.12	0.16	0.15	0.13	0.19	0.15	0.21
11-14 m	0.13	0.14	0.14	0.23	0.22	0.13	0.21	0.17	0.23
8-11 m	0.16	0.16	0.16	0.27	0.28	0.17	0.28	0.29	0.41
5-8 m	0.25	0.24	0.23	0.42	0.41	0.24	0.43	0.44	0.78

Appendix B

Table B- 1: Detailed of match-up *in situ* data used in this thesis

	Latitude	Longitude	Depth	a440	bbp550	Bottom cover
Point 1	23.465	152.013	12.4	0.05	0.0027	
Point 2	23.475	152.012	10.1	0.16	0.0025	
Point 3	23.439	152.014	7.5	0.05	0.0021	
Point 4	23.435	152.014	21	0.03	0.0025	
Average				0.074	0.0024	